Functionalized Fluorescent Polystyrene Nanobeads For Sensing And Bio-imaging Applications

Thesis Submitted to AcSIR For the Award of
the Degree of
DOCTOR OF PHILOSOPHY
In Chemical Science

By
Sarabjot Kaur Makkad
10CC14J26011

Under the guidance of
Dr. Asha S. K.

CSIR-National Chemical Laboratory

Dedicated to
Guru Gobind Singh Ji...

He is not only important; He is everything.....

सीएसआईआर - राष्ट्रीय रासायनिक प्रयोगशाला
(वैज्ञानिक तथा औद्योगिक अनुसंधान परिषद)
डॉ. होमी भाभा मार्ग, पुणे - 411 008, भारत
CSIR - NATIONAL CHEMICAL LABORATORY
(Council of Scientific & Industrial Research)
Dr. Homi Bhabha Road, Pune - 411 008, India

24.08.2018

Certificate

This is to certify that the work incorporated in this Ph.D. thesis entitled ***Functionalized Fluorescent Polystyrene Nanobeads For Sensing And Bio-imaging Applications*** *submitted by* ***Ms. Sarabjot Kaur Makkad*** *to* ***Academy of Scientific and Innovative Research (AcSIR)*** *in fulfilment of the requirements for the award of the Degree of Doctor of Philosophy, embodies original research work under my supervision. We further certify that this work has not been submitted to any other University or Institution in part or full for the award of any degree or diploma. Research material obtained from other sources has been duly acknowledged in the thesis. Any text, illustration, table etc., used in the thesis from other sources, have been duly cited and acknowledged.*

Ms. Sarabjot Kaur (Student)

Dr. Asha S. K. (Supervisor)

Communication Channels
NCL Level DID : 2590
NCL Board No. : +91-20-25902000
EPABX : +91-20-25893300
: +91-20-25893400
FAX
Director's Office : +91-20-25902601
COA's Office : +91-20-25902660
SPO's Office : +91-20-25902664
WEBSITE
www.ncl-india.org

DECLARATION

I hereby declare that the matter embodied in this thesis entitled ***"Functionalized Fluorescent Polystyrene Nanobeads For Sensing And Bio-imaging Applications"*** *is the result of investigations carried out by me at Polymer Science and Engineering Chemistry Division, CSIR-National Chemical Laboratory, Pune, India under the supervision of Dr. Asha S. K.*

In keeping with the general practice of reporting scientific observations due acknowledgements have been made wherever the work described is based on the findings of other investigators.

August, 2018 ***Sarabjot Kaur***

Pune, India

ACKNOWLEDGEMENT

O' Lord ! When you are on my side, what do I owe to anyone else?

You entrusted everything to me , when I became yours.

- Guru Granth Sahib Ji

By grace of almighty, I would be able to complete the work that has been initiated years ago. I thank Him with all my heart to let me follow my passion and completing my work within given timeframe. Starting few years were a bit horrific. It seemed like somebody made me watch "Conjuring 2" all alone on a big screen. But gradually it turned out to be fun. Although Ph.D degree is awarded to an individual; it is in reality, a hidden efforts from so many people who combinely work for a cause.

Firstly, I want to seize this opportunity to express my deepest gratitude to my research supervisor Dr. Asha Syamakumari. These five years of association, with a person like her, has been truly amazing. The past year has not been so easy for me, but she made me learn to fight against all odds. She consistently concentrated on moving ahead instead of lamenting over the challenges. She has foresight of widening our horizons and guiding us to think straight. Her evergreen smile; her ready to start a new day spirit; her positive soul and her charisma gave me the strength to persevere. She has helped me in more ways than simply enriching my basic knowledge and I feel extremely privileged and fortunate to receive guidance from her.

I would like to extend my sincere gratitude to Professor M. Jayakannan (IISER, Pune) for helping me cultivate my basic knowledge about polymer chemistry during his coursework classes. Also, there was a phase when our lab was entering into cellular research and inspite of his busy schedule, he managed his time and facilities for understanding our work. We couldn't have completed that project without his supervision and active collaboration. It has been a great learning experience and an absolute pleasure working with him. I would also like to thank Nilesh, Mehak and Sonashree for carrying out the cell imaging studies.

I acknowledge Dr. Mahesh Kulkarni for helping me in bilirubin sensing studies by providing me with human blood serum. I would also like to thank his students especially Rajeshwari and Arvind for assisting me in handling the same.

I owe special thanks to my DAC members- Dr. Ashutoosh Ambade, Dr. Guruswamy, Dr. Naina Wavhal, Dr. Banerjee (Former DAC member) for their timely discussions and valuable suggestions during my DAC sessions.

I would like to acknowledge Dr. Ashwini Kumar Nangia (Director, CSIR-NCL) and Dr. Sourav Pal (Former Director, CSIR-NCL) for providing me with fine infrastructure and adequate instrumentation facilities. I extend my thanks to Council of Scientific and Industrial Research (CSIR), New Delhi for prestigious Shyama Prasad Mukherjee (SPM) fellowship and financial aid.

I extend my appreciation to Student Academic Office (SAO) staff for their persistent and prompt co-operation during the entire tenure.

I would like to acknowledge Mr. Shamal K Menon, Mrs. Santhakumari, Mr. Venkatesh Thogiti, Mrs. Sheetal, Mr. Pankaj Raj for helping me immensely in various characterization techniques.

I am grateful to all seniors Dr. Kaushlendra Kumar, Dr. Nagesh B. Kolhe, Dr. Chinmay G. Nardele, Dr. Rekha Narayan, Dr. T. Senthil kumar, Dr. Swapnil Sonawane, Dr. Prajitha K.P., Dr. Saibal Bhaumik, Dr. Shekhar Shinde, Dr. Suresh, Dr. Nisha (especially for my working table), Dr. Ravi Jangir, Dr. Narsimha, Dr. Pramod, Dr. Smita, Dr. Bapu, Dr. Ananthraj, Dr. Rajendra for everything that I learnt from them. I appreciate their time, co-operation and support.

I wish to thank my labmates from CSIR-NCL and IISER Pune, Sandeep, Shrikant, Moumita, Navnath, Aryan, Ganesh, Akhil, Sharath, Nilesh, Mehak, Bhagyashree, Sonashree, Mishika, Rooma, Dilna , Anjali, Anju, Haritha, Agnus, Devendra, Sharanya, Durga, Shreya, Priyanka, Harish, Vikash, Akshata for their help and support.

"Friends are light when we walk in dark, they are shoulder when we need support, they are hope at time of disappointment" these were a few couple of lines that I used to write for exams during my schooling. But I never realized it, until I met them. I am honoured and blessed to have Jayshri di and Bikash Garai as my friends. I never felt the difficulties that difficult because the support I got from them was always on dominating side. When I count the things I should be grateful for, our friendship is there at the top. I extend my warmest appreciation to Preeti Jain, Ekta Sangtani, Yogesh Nevare, Durgaprasad, Monika Mathur, Meghana, Monica Malik, Shubhra jyotsana, Ashwini, Pravin, Bittu, Basudeb, Arun Dadwal, Prabhanjan, Yogita, Sapna, Madhuri, Pratibha, Swechcha, Bhagyashri for their endless support and motivation.

Mere words could never express my gratitude to my Daddy (Dr. B.S. Makkad), Mumma (Dr. M.K. Makkad) and brother (Jagpreet Singh) who has been truly caring and being there for me, who support me in my decisions, and whose presence can even lift the burden of a thorny day. They are the anchor that hold me through life's storm. I also want to thank my grandparents (Mr. Jodh Singh, Mr. Charanjeet Singh, Mrs. Lajwanti Kaur and Mrs. Ranjeet Kaur) for their endless support and love. I spent most of my childhood with them; my parents being working. They hold my tiny hands for just a little while, but my heart forever. I thank my amazing masi Mrs. Mohanjeet Kaur, Mrs. Ravinder Kaur and bua Mrs. Ajit Kaur, Mrs. Amrit Kaur for their unconditional love. I thank my cousins Kundan, Gurditt, Nandan, Jaspreet and Kamalpreet for enriching my life with several memorable moments.

Last but not the least, I am thankful to unknown reviewers of my thesis for investing their precious time and knowledge for reviewing my work.

- Sarabjot Kaur

PREFACE

Fluorescent materials have been known for a wide range of applications such as multicolor emitting materials, security markers, fluorescent probes in bio-imaging, standards in flow cytometry and cell sorting, photonic crystals, chemical and bio-sensors *etc*. Several polymerization methods such as suspension, dispersion, emulsion and miniemulsion *etc.* have been developed to synthesize fluorescent polymer beads in the desired size range depending on the requirement. Among them, miniemulsion polymerization is popular because one can have a one to one copy of monomer droplet transformed to polymer particle. The nanoparticles formed are highly monodisperse and in the size range of 50-500 nm. Unlike other methods, a hydrophobe is used in this approach to prevent molecular diffusion by Ostwald Ripening - one of the main drawbacks of emulsion polymerization. This enables the encapsulation of a large variety of materials like dyes, metal complex, small organic molecule *etc.* into the polymer matrix.

Although there are quite a number of reports on the physical encapsulation of fluorophores into the polymer matrix, it is very well known that physical encapsulation often leads to dye leakage. Leaching of dyes from the polymer backbone is highly unwanted for any application including bio-imaging and sensing. Any dye leakage into cell environment leads to cell toxicity if used as cell marker or might hamper reproducibility and performance of sensor in case of sensing applications. Thus covalent attachment of the fluorophores into the polymer matrix is greatly desired.

Covalently stitched fluorescent nanoparticles are promising candidates to be used as cell markers as well as sensors. The prime objective of the work is to synthesize fluorescent polymer nanobeads for bio-imaging and sensing applications. Oligo(*p*-phenylenevinylene) (OPV) and perylene bisimide (PBI) were chosen as the fluorophores because of their strong absorption, high fluorescence quantum yield and outstanding thermal, chemical and photostability. Polystyrene was chosen as polymer matrix because of its proven biocompatibility and reduced aggregation induced self-quenching of fluorescence of dyes.

Throughout the thesis, miniemulsion polymerization method was made use of to develop the polystyrene nanoparticles in the size range of 100-300 nm. The particle size and surface charge of nanoparticles were determined using Dynamic Light Scatterig (DLS) while their spherical morphology was confirmed by Field Emission Scanning

Electron Microscopy (FESEM), Transmission Electron Microscopy (TEM). As the nanoparticles were fluorescent; their photophysical studies were carried out using absorption and emission spectroscopy.

The thesis has been arranged into five chapters.

Chapter 1 gives a glance on the introduction of fluorescent materials, different approaches to synthesize fluorescent polymeric nanoparticles and their applications thereof. A brief comparison in the later section highlights the advantages of polystyrene nanoparticles over other luminescent particles.

Chapter 2 presents covalent incorporation of fluorophores based on PBI OPV in the form of cross-linkers into the backbone of polystyrene. Fluorescent Polystyrene (PS) nanobeads in the size range ~70 – 120 nm incorporating perylene bisimide (PBI-PS) and/or oligo (*p*-phenylenevinylene) (OPV-PS) was developed by miniemulsion polymerization technique. OPV- PS exhibited blue emission with ϕ_{FL} = 26%, PBI-PS showed orange yellow emission with ϕ_{FL} = 9.7% in 1X PBS buffer, while OPV(PBI)-PS nanobeads incorporating both the fluorophores exhibited multicolor emission capabilities (λ_{ex} from 350 nm to 490 nm).

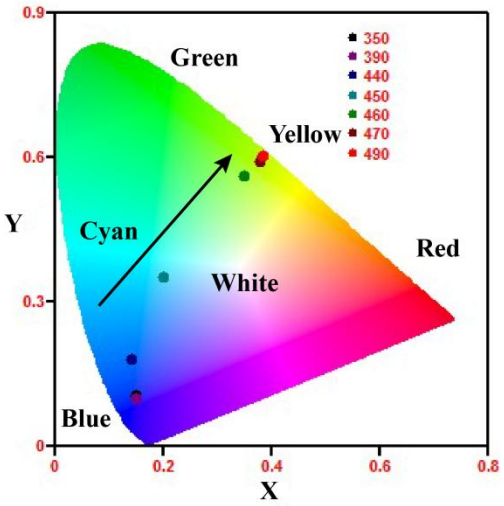

Chapter 3 elaborates application of multicolor emitting fluorescent PS nanobeads (developed in chapter-2) for bio-imaging in HeLa and MCF-7 cells. Cell viability analysis was carried out to assure their biocompatibility. Cellular uptake of the nanoparticles was confirmed by flow cytometry analysis and confocal laser scanning microscopy (CLSM) images. The subcellular localization of the nanoparticles in the cytoplasm and perinuclear region could be precisely established by their simultaneous multicolor emission. The PS based single optical agent presented here can thus function

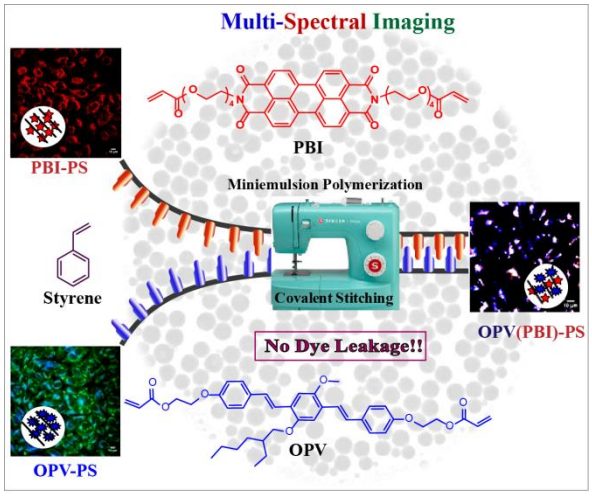

as three-channel fluorescent probe to meet the requirements for multicolor bio-imaging. The ability for multicolor imaging has the potential to overcome the cellular autofluorescence and to enhance the resolution contrast of the image. Additionally, their emission was found to remain unaffected by external triggers such as pH, temperature that could be present in the cellular environment.

In ***Chapter 4A***, solid state emitting, distinctly dual vapor sensors with high quantum yield were developed for detection of volatile organic compounds. Selective functionalization with carboxy and amine functionality was used to decorate the resulting polystyrene nanobeads having both PBI and OPV fluorophores. White light emitting nanobeads on coming in contact with vapors of electron deficient nitroaromatics quenched OPV emission and exhibited yellow under UV lamp while exposure to amine vapours quashed PBI emission selectively, resulting in blue emission . Such a wide range of color alteration from white to either blue or yellow from the same sensor makes it a true dual analyte sensor with two distinct outputs. Control of surface functionality (-COOH, -NH2 and neutral) on the nanobeads further enhanced the sensing efficiency. Real time, device based application has been demonstrated using free standing film. The fabricated film is capable for efficient detection of fast analyte exchange from dilute solution and it can be reused upto 8 cycles.

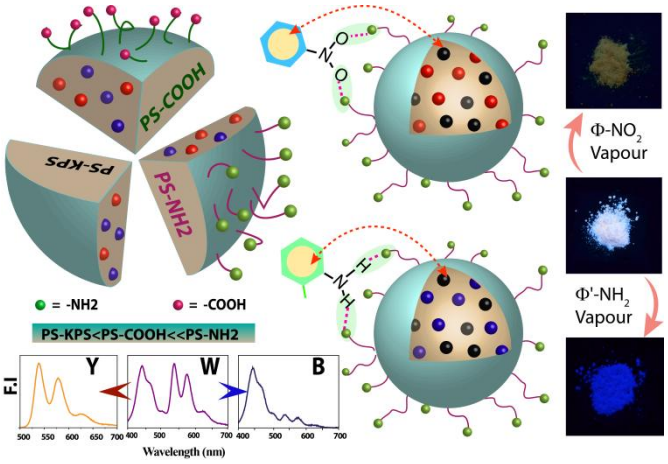

Along the same line, solution state PS based sensor was showcased in ***Chapter 4B***, to promptly detect the presence of picric acid in water. Its surface was decorated with -NH_2 group with the aim to boost analyte-sensor interaction. The excellent selectivity of the sensor among the library of other nitro-organics was attributed to combined effect of energy transfer, inner filter effect and

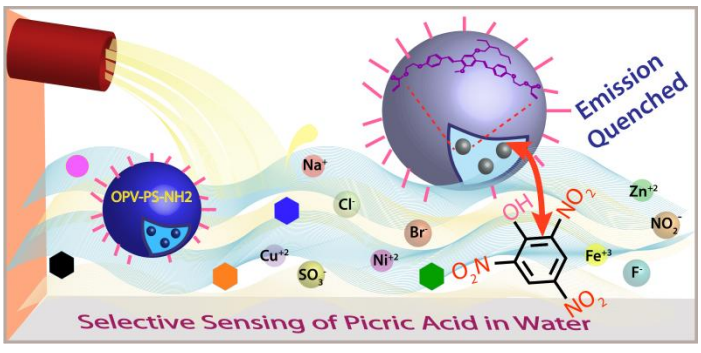

electron transfer. PA concentration, as low as 58 nM in water could be efficiently detected by the sensor. Additionally, zero interference from more than 30 different organic contaminants, cations and anions that might be present in water makes the sensor highly efficient for real water based analysis.

Finally, in ***Chapter 5***, a tailor made water soluble glucuronic acid bearing polystyrene polymer (PS-DGlu) was developed and utilized as polymeric surfactant in styrene miniemulsion polymerization to prepare glucuronic acid functionalized PS nanobeads covalent incorporating OPV. This functionalized fluorescent PS nanobeads was then applied for selective sensing of bilirubin in human blood serum containing other active interferences such as glucose, sucrose, metal ions, cholesterol *etc*. The limit of detection was found to be as low as 20 nM which is found to be in clinically applicable range of <25 to >50 µmol/L. Instant visual detection of bilirubin under UV lamp could be possible where blue emission of polymer turned bluish green instantly after bilirubin addition. This could be explained on the basis of energy transfer from OPV to bilirubin which is further supported by its emission spectra as well as CIE co-ordinate diagram.

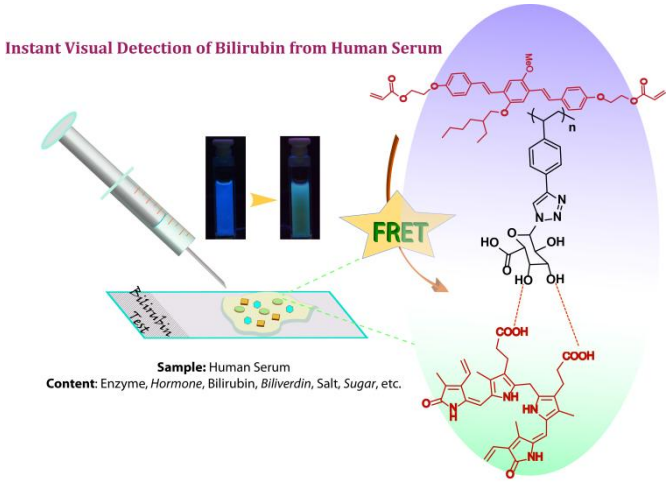

Chapter 6 summarizes the detailed discussion in the previous chapters and highlights the possibility of the facts for future applications.

Sarabjot Kaur Makkad

ABBREVIATIONS AND SYMBOLS

Abbreviations	Full form
Đ	Polydispersity index
AIBN	Azobisisobutyronitrile
CIE	Commission Internationale de l'Eclairage (International Commission on Illumination)
Φ	Quantum yield
Et_3N	Triethylamine
DAPI	4' 6-Diamidino-2-phenylindole
DCM	Dichloromethane
EA	Ethyl acetate
DMSO	Dimethylsulfoxide
DMAP	Dimethyl amino pyridine
FTIR	Fourier transform Infra Red
DLS	Dynamic light scattering
GPC	Gel permeation chromatography
TEM	Transmission electron microscopy
FESEM	Field emission scanning electron microscopy
CLSM	Confocal laser scanning microscopy
SEC	Size exclusion chromatography
ESI	Electron spray ionization
GC-MS	Gas chromatography-mass spectrometer
TLC	Thin layer chromatography
AIE	Aggregration induced emission
Mn	Number average molecular weight
Mw	Weight average molecular weight

DLC	Dye loading content
DLE	Dye loading efficiency
CMC	Critical micellar concentration
RT	Room temperature
CFL	Compact fluorescent lamp
LED	Light emitting diode
NMR	Nuclear magnetic resonance
K-t-OBu	Potassium tertiary butoxide
h	Hour
g	Gram
mg	Milligram
mL	Millilitre
PS	Polystyrene
OPV	Oligo (*p*-pheneylenevinylene)
PBI	Perylenebisimide
PTCDA	Perylenetetracarboxylicbisanhydride
HD	Hexadecane
ACVA	4-4’-Azobis(4-cyanovaleric acid)
St	Styrene
AA	Acrylic acid
AEMH	2-Aminoethyl methacrylatehydrochloride
MMA	Methyl methacrylate
OLED	Organic light-emitting diode
THF	Tetrahydrofuran
mmol	Millimole
mol	Mole
nM	nanomolar
nm	Nanometer
µm	micrometer

ppm	Parts per million
pH	Power of hydrogen
OD	Optical density
λ	wavelength
λ_{ex}	Excitation wavelength
λ_{em}	Emission wavelength
PMMA	Polymethyl methacrylate
TGA	Thermogravimetric analysis
MTT	3-(4,5-dimethylthiazol-2-yl)-2,5-diphenyltetrazolium bromide
UV	Ultraviolet
UV-Vis	Ultraviolet-visible
PET	Photoinduced electron transfer
FRET	Förster resonance electron transfer
IFE	Inner filter effect
KPS	Potassium per sulfate
SDS	Sodium dodecyl sulfate
PBS	Phosphate-buffered saline
NB	Nitrobenzene
o-TD	*o*-Toluidine
PA	Picric acid
TNP	Trinitrophenol
NP	Nanoparticle
UCNP	Upconverting nanoparticle
QD	Quantum dot
MOF	Metal-organic framework
COF	Covalent organic framework
EDTA	Ethylenediamine tetracarboxylic acid
NIR	Near infrared

S/N	Signal to noise ratio
Δ	Heat
*	Solvent signal (in NMR spectrum)

Table of Content

CHAPTER-1

General Introduction and Literature

Abstract: *This chapter introduces different classes of fluorescent nanoparticles and their importance in modern life. Various synthetic approaches for polymeric fluorescent nanoparticles and their advantages have been showcased in the subsequent discussions. Through the discussion, the current status of such nanoparticles have been highlighted in terms of synthetic protocol and applications. Illustrative examples have been presented to showcase the advantage and limitation of polymeric NPs and thus the scope of the current work. Finally some of the limitations of other luminescent particles are highlighted that could potentially be addressed through use of polystyrene NPs as demonstrated in the subsequent chapters.*

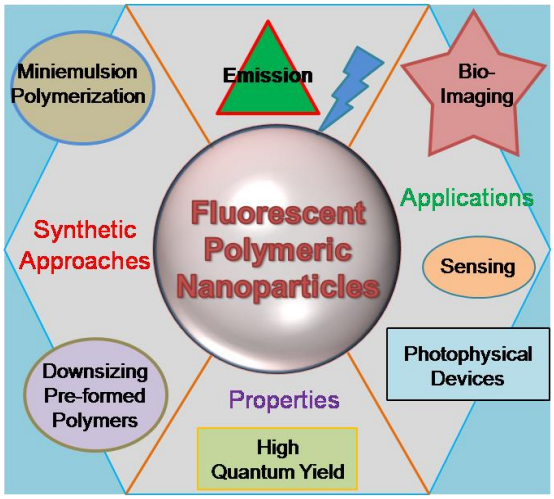

1.1 Fluorescence and the basic concept: Fluorescence is the phenomenon of photon emission by a molecule or material, immediately (in the time scale of 10^{-8} s) after absorbing photons of suitable higher energy. This difference in (wavelength or frequency units) between positions of band maxima of absorption and emission spectra of same electronic transition is termed as Stokes Shift[1] of the spectrum. The origin of fluorescence can be best described from Jablonski diagram[1] (***Figure 1.1***). On absorbing photon of suitable energy, the ground level electron is excited to a higher level, as the first phase of any energy absorption process. During the relaxation step, this electron releases energy while returning to its ground state through several photophysical phenomenon which includes both non-radiative (internal conversion, inter-system crossing) and radiative (fluorescence, phosphorescence) processes.

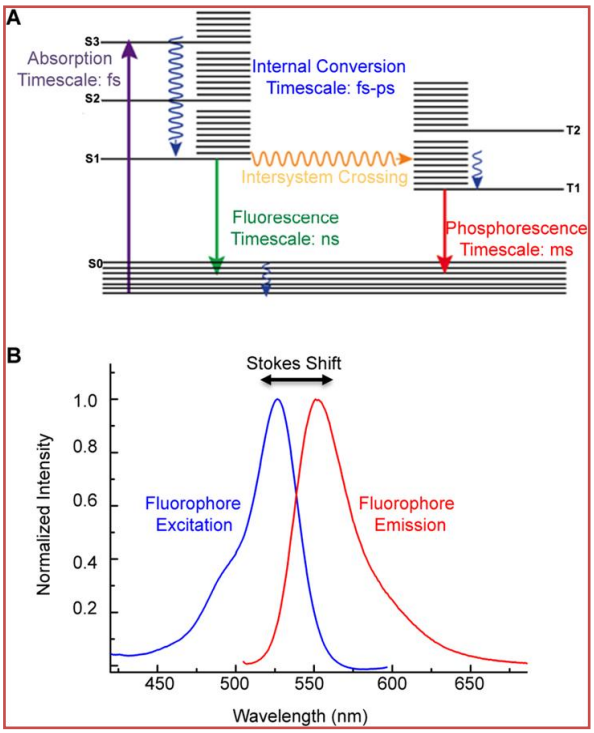

Figure 1.1: A) Jablonski Diagram explaining different non-radiative and radiative pathways illustrating the origin of fluorescence and B) illustration of Stokes' shift from the spectra. Adopted with permission from ***Ref 1***. Copyright 2015, American Chemical Society.

Nature has provided a huge library of fluorescent materials ranging from minerals such as rubies to pigments like chlorophyll to fluorescence observed in jellyfish, dragon fish, spiders *etc*. Apart from nature, fluorescence is ubiquitous phenomenon which has become a part of our day to day life *eg.* CFL lamps, credit cards, currency notes, warning signage, security markers, food additives, medicines *etc*. Fluorescent materials have drawn tremendous interest of the researches owing to their high sensitivity, efficiency, resolution, versatility and promptness in the various fields of biological sciences and analytical chemistry. They have been known for a wide range of applications such as multi-color emitting materials[2-5], molecular logic gates[6-10], fluorescent probes in bio-imaging[11-15], standards in flow cytometry and cell sorting[16-17], photonic crystals[18-19], chemical[20-22] and bio-sensors[23-25], display devices[26-27] and many other innumerable instances.

Polymers are always considered as preferred choice for synthetic luminescent material because of their easy tunability, processability and moreover scope for endless design. The basic phenomenon behind such luminescent polymers lies in their chemical structure where the extended conjugation provides suitable excitation and subsequent pathway for emission. This emission often resulted either from the conjugated backbone of the polymer[28-29] or the insertion of some conjugated molecules into the polymeric backbone.[30-31] In general, the luminescence property is brought into the polymers through careful selection of the monomer units which are then polymerized through various suitable approaches. Use of fluorescence as assay for any application mainly rely on the fluorophore's photophysical properties such as quantum yield, photostability, Stokes' shift, lifetime *etc*. In this respect, small organic fluorophores are rigid aromatic system, often insoluble in water[32-36] and mostly suffers from limitation such as low absorptivity, short fluorescence lifetime, photobleaching, toxicity, poor stability in physiological environment.[37-40]

Of late, fluorescent nanoparticles (NPs) are emerging as a tool in modern research, owing to their several interesting properties. Such fluorescent NPs are profoundly tested in multiple applications like optoelectronics[41-43], chemical and bio-sensing, [44-47] bio-imaging [35,37, 38,40,48-50] *etc*. The emissive material in all such cases comprises of various chemical entities like metal NPs, upconverting nanoparticles (UCNPs), polymeric NPs, quantum dots (QDs) *etc*. Each of such classes of fluorescent NPs has different synthetic approaches and properties, which has proven advantageous for one or more type(s) of properties. Polymeric NPs are an interesting class of materials that offers a high control on the emission property through suitable chemical approaches, making it one of the highly discussed materials of its class. Such fluorescent particles are often superior to organic fluorophores with respect to these properties such as improved brightness and photostability, inertness to their microenvironment, non-cytoxicity, scope for surface modification *etc*.[35,37,40] Additionally, two or more fluorophores could be taken together into a single particle to achieve multi-color emission tuning. Apart from these there are numerous structure defining attributes of particles *eg.* shape, size, high surface area and distinctive emission properties that will enhance versatility and sensitivity of fluorescence based technique.[37] Several polymerization techniques have been developed to synthesize these fluorescent particles in the desired size range depending on the requirement basically using two different strategies: i) Direct polymerization which yields in-situ NPs

during polymerization process and ii) Post-modification using preformed polymers.[2,35,50,51]

1.2 Strategies for the Development of Fluorescent Polymeric Particles:

1.2.1 Direct Polymerization Based Techniques:

Radical polymerization is one of the best approaches for synthesis of luminescent polymers. Here, suitable luminescent monomers are subjected to reaction with a free radical, typically generated from a second component, the initiator. Once the generated radical from the initiator is transferred to a monomer, it initiates a chain reaction to link the available neighbouring molecules, thus forming a polymer. Free radical polymerization can be carried out either in bulk or in solution of the suitable monomer (capable of generating a free radical in the propagation step).[52] Bulk polymerization does not involve use of any solvent and therefore is one of simplest method of polymerization where oil soluble initiator is added to monomer in its liquid state. Final polymer formed from this approach is highly pure because of the involved chain reaction. However formation of localized hot spots leads to auto acceleration where the rate of propagation becomes much higher than the rate of termination (Gel effect), making it difficult for the efficient removal of heat. Although this approach is beneficial for small scale polymerizations, high exothermic nature of the polymerization method makes it difficult for the heat removal and subsequently becomes unsuitable for industrial application. The problem of heat removal can be controlled to some degree for the case of solution polymerization; although the use of organic solvent then raises concern about environmental and economic aspects, which are not convenient to commercial applications.

A modified approach to solve this problem resulted in **Dispersed Phase Polymerization** where the liquid monomer is dispersed into another second continuous phase, typically water. However, unlike the former solution based polymerization, water is cheap and abundant, and also benign to environment. The added water plays a crucial role in regulating temperature, eliminating the hot spot generation in the reaction medium. The high thermal conductivity of water (0.61 W/m.K) effectively aids in removing heat of polymerization through the continuous phase and provides a smooth condition to the polymerization process. During the polymerization process, viscosity of the medium remain close to that of pure water, owing to the generation of less thermal gradient in the

medium; thus molecular weight of the formed polymer remains unaffected from any change in viscosity. The continuous phase of water also moderates any extreme change in the reaction mixture due to high latent heat of vaporization and specific heat, thus making the temperature change in the reaction mixture gradual rather than sudden. Also one can get high polymer content at considerable viscosity. All these features make the process industrially favourable and commercially fascinating.

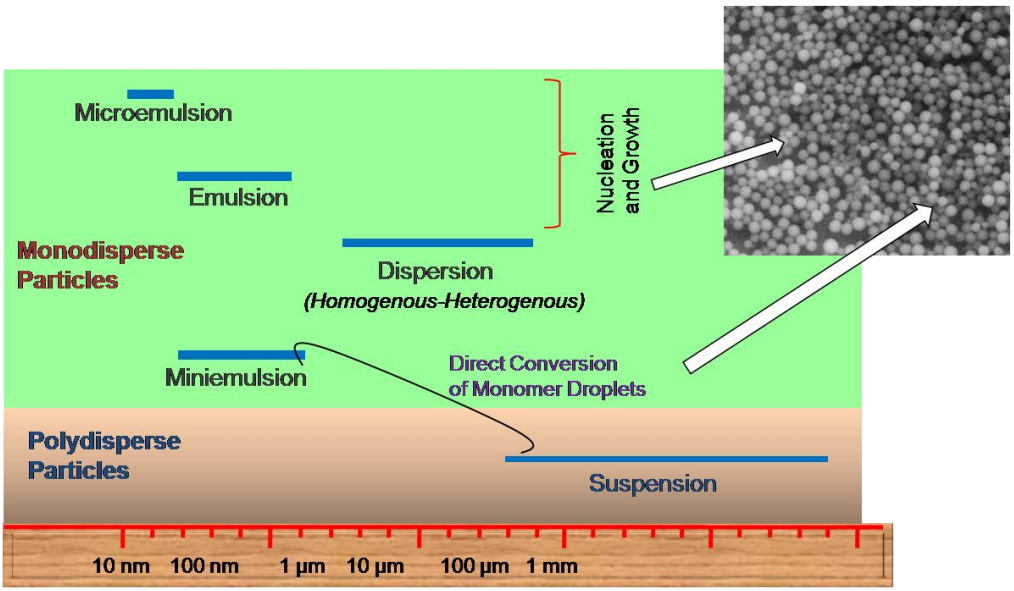

Figure 1.2: Schematics of particle size obtained by various dispersed phase polymerization and their nucleation mechanism.

Polymer dispersions possess remarkable properties which is capable of fulfilling today's market needs. They play key a role in the field of paper and textile industry, paints, synthetic rubber, adhesives, coatings as well as in biomedical and drug delivery applications. These can be synthesized by variety of techniques such as precipitation, suspension, dispersion, emulsion, microemulsion, miniemulsion (***Figure 1.2***). These techniques can be distinguished by the parameters like particle size, initial state of reaction mixture, mechanism of nucleation and kinetics involved *etc*.[53,54]

Suspension Polymerization[55] is used to synthesize large sized polymeric particles from the polymerization reaction. The monomer is usually taken as droplet inside a second continuous phase. The polymerization process is started with an oil-soluble initiator that initiates polymerization in the monomer droplet, resulting in the direct conversion of droplets into polymer particles. The resultant polymeric particles are large in size, within the observed range of 20 µm - 2 mm. These large particles are

sedimented from the reaction medium and can be easily collected through filtration. From the reaction kinetics, it is identical to that of the previously discussed bulk phase polymerization.

For the particles of size range smaller than suspension polymerization, **dispersion polymerization**[56] is used. Here the polymerization medium is chosen such that it can act as good solvent for both monomer and initiator but weakly solubilising solvent for the forming polymer. As the polymerization proceeds by the influence of the initiator, medium does not remain homogenous any longer and the generated polymer particles then become the locus of polymerization where more of the monomer molecules can be added throughout the reaction. This results in smaller sized polymer particles in the form of suspension. The typical particle size obtained by such polymerization lies in the range of 0.1 - 10 μm.

However, dispersion based polymerization approaches are not sufficient to bring down the particle size in the nanoscale regime. To achieve this target, the size of the polymerizing droplet need to be further reduced. In practice, this is achieved by using surfactant in the polymerization media. Use of surfactant causes the generation of very small size droplets of the monomer, in the form of emulsion. Thus, **Emulsion polymerization**[57,58] is a chemical process which comprises of monomer, initiator, water as continuous phase and a suitable surfactant (***Figure 1.3 (1)***). It accounts for the world's most widely applied polymer latex. Unlike suspension polymerization process, water-soluble initiator is used in this approach to keep it available throughout the whole reaction medium. The polymer NPs synthesized by this technique still have large size and are typically larger than 500 nm. As the surface area of micelle is much larger than the surface area of monomer droplet; polymerization mostly takes place inside the micelle. This technique gained popularity over the other process due to the advantage of having both molecular weight as well as high reaction rate simultaneously unlike other non-dispersed methods where the molecular weight is inversely proportional to the polymerization rate. However this method of preparing NPs mainly suffers from two drawbacks: One is Ostwald ripening[54,59,60] and other is Coalescence.[59,60] Ostwald ripening causes the formation of larger particles over time from the smaller particles, however it cannot be avoided for such system. Coalescence is mainly caused by collision of droplets that are in random Brownian motion and can be compromised to some extent through selection of appropriate surfactant system.

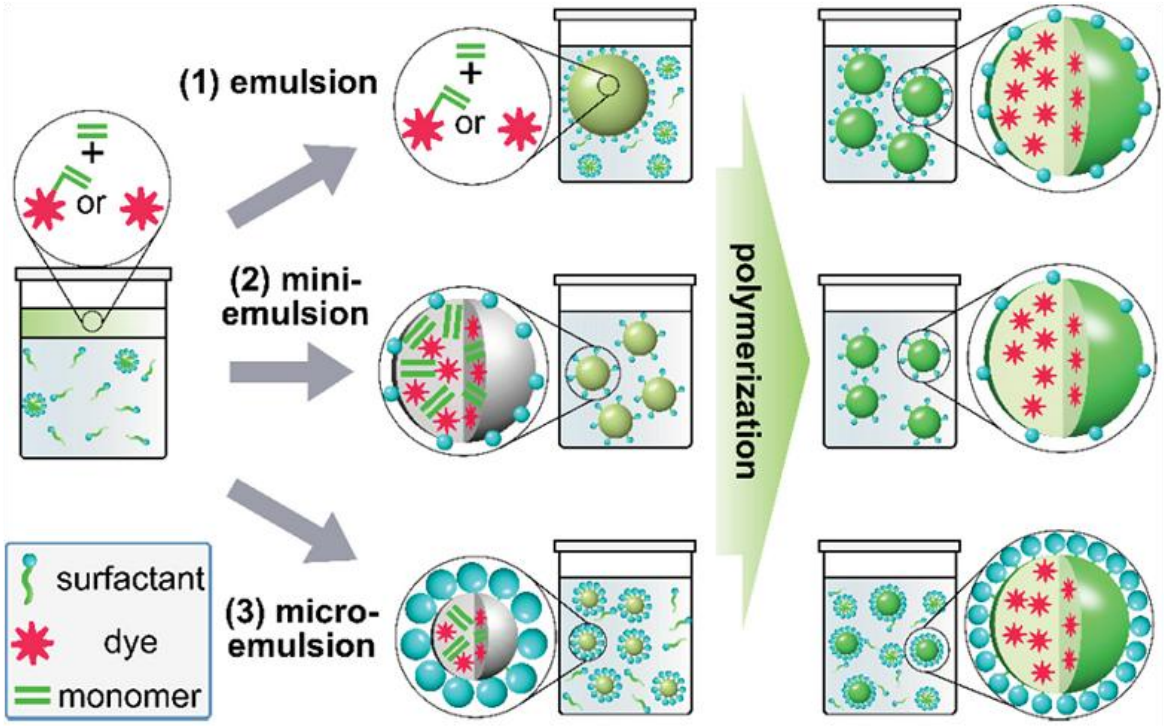

Figure 1.3: Synthesis of dye loaded NPs via emulsion, miniemulsion and microemulsion polymerization. Adopted with permission from ***Ref 35***. Copyright 2016**,** Wiley-VCH Verlag GmbH & Co. KGaA, Weinheim.

Although emulsion polymerization is a good technique for radical homopolymerization of oil soluble monomers, it faces a limitation for radical co-polymerization. The reason lies in its mechanism which is mainly kinetically driven and often results in the lack of homogeneity and thus restriction in desired composition range. Additionally, insertion of other molecules such as conjugated dyes is not possible as they might not diffuse through the aqueous phase due to its low water solubility which is required for its homogeneous incorporation into particles.

Thus there was a need of heterogeneous polymerization which could generate nano sized small, homogeneous, stable and narrowly distributed particles. This led to the development of **Miniemulsion polymerization**[61] (***Figure 1.3 (2)***). It was first proposed by Chou *et al.*[62] to describe stable emulsion with droplet size varying typically from 30 - 200 nm. It is formed by the application of high shear in a system containing monomer, water, surfactant, co-stabilizer. Unlike emulsion polymerization here the polymerization take place in monomer droplet where dispersion medium will only act as transporter for initiator, heat and side products *i.e.* every single monomer droplet will act as independent reactor and there is no exchange of materials between beads. This is possible only when surface area of monomer droplet is larger than that of micelle. Polymerization takes place

in highly parallel fashion in 10^{18}-10^{19} nano compartments per litre that are separated by continuous phase. Generally, the surfactant concentration is kept below its critical micellar concentration (CMC) resulting in absence of micelles and incomplete coverage of the NPs. Here the size of NPs is controlled either by surfactant concentration or by homogenization leading to smaller particle size as compared to those obtained by emulsion polymerization.

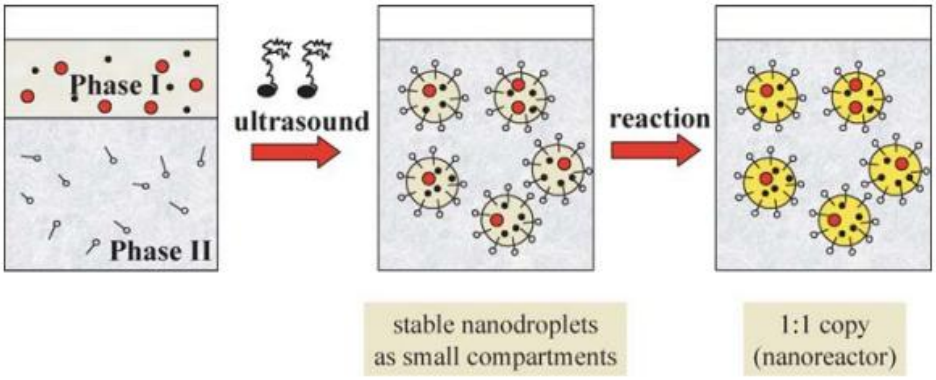

Figure 1.4: Principle of miniemulsion polymerization. Adopted with permission from ***Ref 61***. Copyright 2006, Annual Reviews.

Preparation of Miniemulsion:

For the preparation of miniemulsion, the surfactant (functional monomers if any) is first dissolved in continuous phase *i.e.* water and the co-stabilizer (or fluorophores if any) is dissolved in monomer. Then monomer is slowly added to water phase under stirring. And the mixture is kept under stirring condition at room temperature for an hour. This is termed as Pre-emulsification step. This is then subjected to high shear treatment either by ultrasonication or homogenization to produce miniemulsion and polymerized afterwards to get polymer NPs [61] (***Figure 1.4, 1.5***). There was a big debate regarding the order of mixing of component of formulation but that was finally ended in 1994 by Miller *et al.*who clearly demonstrated that order of mixing of component had no effect unless the efficient shearing treatment is given to the formulation.[63]

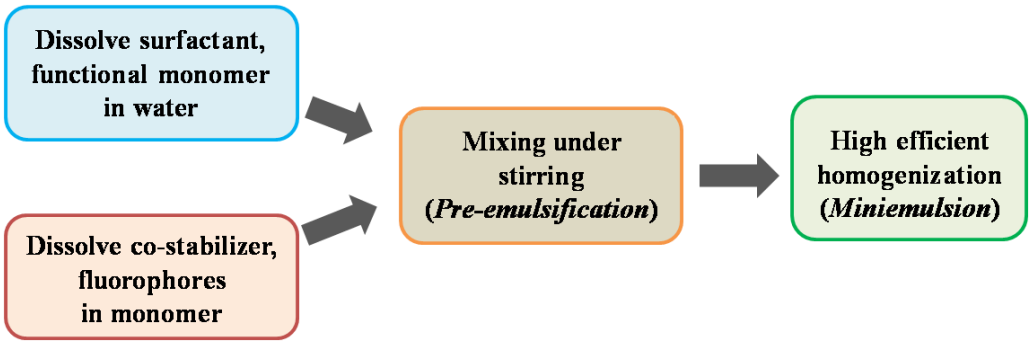

Figure 1.5: Schematics of steps involved in preparation of miniemulsion.

The other method by which one can have even smaller particle size than miniemulsion polymerization is **Microemulsion** (***Figure 1.3 (3)***) where size of monomer droplets were reduced by using higher amount of surfactant (above its CMC) and low shear leading to particle size in range of 5-50 nm. However the use of excess surfactant and size in 50 nm range often limits the application of such method in biomedical research.

Comparative table for various Emulsion based polymerizations.

Table of comparison among different types of emulsion based polymerization techniques is given below. These polymerization techniques differs mainly in terms of surfactant concentration, particle size, shear treatment, mechanism of nucleation, polymerization site *etc*. [54-55]

Properties	Emulsion	Miniemulsion	Microemulsion
Mechanism	Micellar Nucleation	Droplet Nucleation	Droplet Nucleation
Thermodynamic stability	Non-stable	Stable	Stable
Size Range	1-10 μm	20 -200 nm	10 nm
PDI	Low	Very low	Very low
Ostwald Ripening	Present	Absent	Absent
High Shear	Not required	Required	Not required
Polymerization Site	Micelle	Monomer droplet	Monomer droplet
Optical Property	Opaque	Opaque	Transparent
Spontaneity	Energy input is required.	Energy input is required.	Spontaneous ; No energy input is required.
Surfactant concentration	1-3 wt %	5 wt %	15-30 wt %

1.2.2 Techniques based on preformed polymers:

Polymeric NPs can also be prepared even after the synthesis of polymers in other phase. In this approach, mainly three basic strategies are applied to prepare NPs based on preformed polymers,[2,35,51,52,64] namely i) Emulsion solvent evaporation, ii) Nanoprecipitation and iii) Self-assembly.

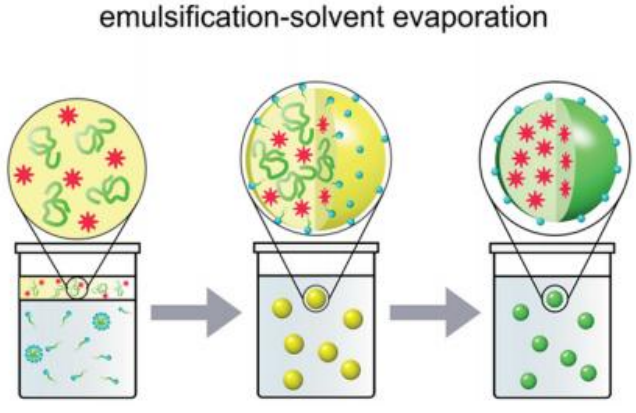

Figure 1.6: Dye loaded NPs via emulsion solvent evaporation method. Adopted with permission from ***Ref 35***. Copyright 2016**,** Wiley-VCH Verlag GmbH & Co. KGaA, Weinheim.

(i) **Emulsion solvent evaporation**: In this approach, the polymer is dissolved in a water-immiscible volatile solvent [typically dichloromethane (DCM) or ethyl acetate (EA)] followed by its dispersion into aqueous phase using high shear and a stabilizer (*eg.* polyvinyl alcohol (PVA)). The evaporation of solvent results in polymeric NPs in the size range of

200 nm. But it is often possible to decrease its particle size to less than 100 nm by varying the amount of stabilizer (***Figure 1.6***). Geng *et al.*[65] has successfully applied this method to prepare dye loaded polymeric NPs, where an aggregation induced emission (AIE) based dye (2,3-bis(4-(phenyl(4-(1,2,2-triphenylvinyl)-phenyl)amino)- phenyl)-fumaronitrile (TPETPAFN)) was loaded into poly (DL-lactide- co -glycolide) (PLGA). DCM solution of the polymer was added into aqueous solution having PVA as emulsifier and then DCM was allowed to evaporate to form stable nanoparticle emulsion.

(ii) **Nanoprecipitation:** In nanoprecipitation or solvent displacement method, the polymer is first made to dissolve in a water-miscible solvent such as dimethylsulfoxide (DMSO), tetrahydrofuran (THF), acetonitrile, dimethylformamide (DMF). The prompt diffusion of solvent into water upon addition of the above solvent resulted in the supersaturation of polymer followed by formation of NPs in the wide size range of <10 nm to more than 100 nm (***Figure 1.7***). One advantage of this approach is amphiphilic polymer coprecipitation method which made use of functional amphiphilic polymer to co-precipitate with any conjugated polymer in single step to form surface functionalized NPs. For example, amphiphilic comb polymer, PS-PEG-COOH was used to surface functionalize fluorescent conjugated polymer NPs, poly[9,9-dioctylfluorenyl-2,7-diyl)-co-1,4-benzo-{2,1′-3}-thiadiazole) (PFBT) having diameter 15 nm.[66] Additionally such NPs contain both PEG and COOH on the surface which assured both good colloidal stability and appreciable reactivity for conjugation to biomolecules such as streptavidin and antibodies *eg.* immunoglobin-G.

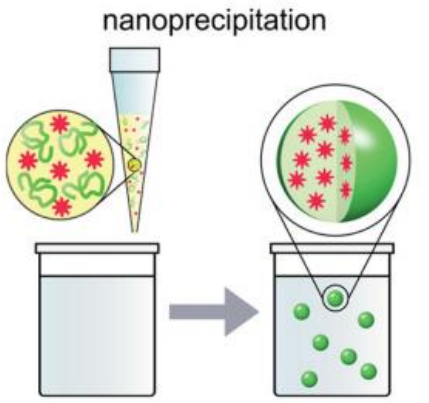

Figure 1.7: Dye loaded NPs via nanoprecipitation approach. Adopted with permission from ***Ref 35***. Copyright 2016**,** Wiley-VCH Verlag GmbH & Co. KGaA, Weinheim.

(iii) **Self-assembly:** Certain block copolymers being amphiphilic in nature have ability to self-assemble into NPs in micelle form. It consists of two components: i) hydrophobic block that encapsulates fluorophores ii) hydrophilic block that imparts water solubility and biocompatibility (***Figure 1.8***). Most often the hydrophilic block consist of polymers like polyethylene glycol (PEG), poly(meth) acrylic acid (PMA) and hydrophobic block of polymers such as PS, PMMA, polycaprolactone (PCL) *etc.* For such method, polymer solution in organic solvent is mixed with water and when its concentration exceeds CMC,

aggregation of polymer in aqueous phase leads to formation of NPs. For example, Yang *et al.*[67] reported amphiphilic diblock copolymer of poly(perylene diimide acrylate)–block–poly(poly(ethylene glycol) methacrylate) (PPDA–b–P(PEGMA)) prepared using reversible addition fragmentation transfer polymerization (RAFT) polymerization. They showed the self assembly of this polymer into polymeric NPs through hydrophobic interaction in average size of 60 nm in water for cellular imaging. The research group of Jayakannan *et al.*[68] reported OPV based initiator for ring opening polymerization (ROP) of substituted caprolactone and its further self assembly into spherical NPs of 150 nm in water. They encapsulated drug within these NPs for bio-imaging and drug delivery application simultaneously. Wurthner *et al.*[69] reported self assembly of wedge shaped amphiphile of PDI into 4-6 nm micellar NPs. Self assembly was marked by characteristic change in emission color from green (monomeric) to weak red (excimer).

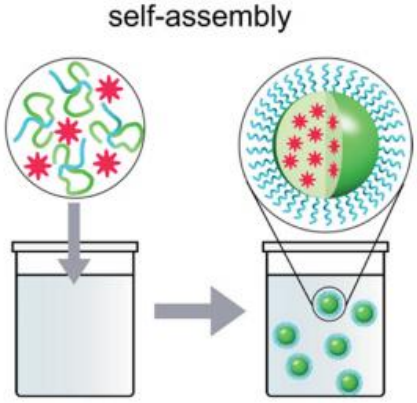

Figure 1.8: Dye loaded NPs via self assembly. Adopted with permission from ***Ref 35***. Copyright 2016**,** Wiley-VCH Verlag GmbH & Co. KGaA, Weinheim.

In this approach, no additional surfactant is required; amphiphilic polymer being used will itself act as surfactant. However, it is a thermodynamically governed process unlike nanoprecipitation, thus micelle can undergo rapid exchange making the stability of such self assembled structures uncertain on dilution.[70,71]

1.3 Dye Encapsulation Strategies for fluorescent polymeric NPs:

Apart from the use of inherently fluorescent polymer for the preparation of fluorescent polymeric NPs, fluorescence can be included for the polymeric NPs via a second approach, loading of fluorescent dye into the polymeric NPs. There are two basic approaches by which dye molecules can be introduced into the polymer backbone (i) Non-covalent approach (ii) Covalent approach. The former often suffers from leaching of dye from polymer backbone which is highly unwanted for any biomedical application. The leached dye not only renders toxicity to the biological cells but it also leads to decreased fluorescence intensity from dye thereby decreasing its signal to noise ratio. This is indeed undesirable for any sensing or bio-sensing applications.

1.3.1 Non-covalent approach:

It is the simplest approach where appreciably non polar dye is required which can be firmly encapsulated inside the hydrophobic polymer core. This can be achieved either (i) staining of already synthesized NPs, (ii) physically encapsulating dye during NPs preparation, (***Figure 1.9A***) (iii) supramolecular interaction (figure 1.9B). In the first method, the conventional dyes are loaded in the commercially available NPs using swelling procedures. In this approach, the dye loading efficiency (DLE) depends on the hydrophobicity of dye. For example, Nile Red was encapsulated into 100 nm polystyrene (PS) NPs using swelling technique by the group of Resch-Genger[72] where they achieved highest brightness for dye loading at 0.8 wt%. However, at this loading, the quantum yield (QY= 22%) was remarkably reduced as compared to lowest dye loading of 0.05 wt% (76%). In the second approach the dyes are encapsulated physically during NPs preparation. For instance, indocyanine green (ICG) was encapsulated into 100-300 nm PLGA NPs during their preparation with maximum dye loading at 0.2 wt%[73]; however much smaller size of 30 nm with ICG could be achieved using the block copolymer of poly((styrene-*alt*-maleic anhydride)-block-styrene).[74] The third approach deals with the preparation of fluorescent polymer NPs *via* supramolecular interaction such as hydrogen bonding where low molecular weight monomers are held together by non-covalent interactions to form a supramolecular polymer (SP).

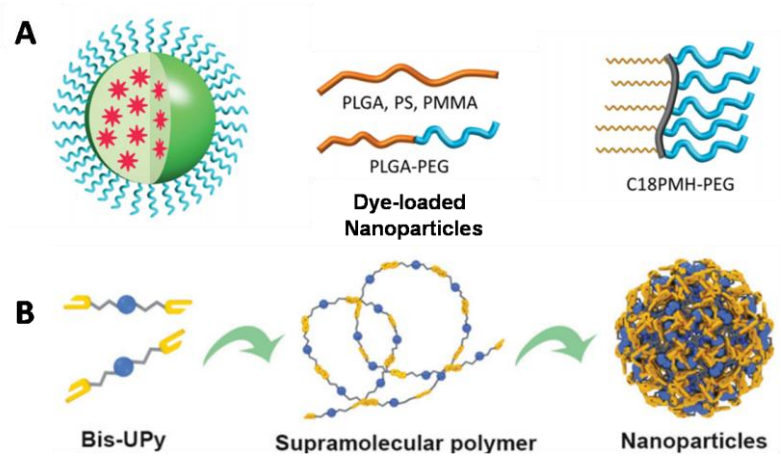

Figure 1.9: A) Physical encapsulation of dyes into polymer NPs. Adopted with permission from ***Ref 35***. B) Schematics of fluorescent supramolecular NPs preparation via hydrogen bonding interaction. Adopted with permission from ***Ref 75***. Copyright 2016**,** Wiley-VCH Verlag GmbH & Co. KGaA, Weinheim.

One such approach was demonstrated by Peng *et al.*[75] who was the first to report the water dispersible nanobeads of hydrogen-bonded SP via miniemulsion. Bis-

ureidopyrimidinone (Bis-UPy) based monomers containing chromophore were polymerized via quadruple hydrogen bonding to prepare supramolecular polymer which was further assembled into nanobeads using miniemulsion technique.

1.3.2 Covalent approach:

This approach includes use of polymerizable dye monomer to incorporate the dye covalently into polymer nanoparticle either through co-polymerization during polymerization. Generally, the monomers such as styrene, *n*-isopropylacrylamide (NIPAM), acrylamide and methyl methacrylate (MMA) are co-polymerized with the dyes having polymerizable acrylate group to prepare fluorescent beads. For example, the group of Katharina Landfester[76] reported fluorescent surface labelled nanoparticle by covalently attaching the BODIPY based surfmer (surfactant + monomer) into polystyrene nanoparticle (***Figure 1.10A***). Dossi *et al.*[77] reported rhodamine based polymerizable acrylate to co-polymerize with MMA using emulsion free radical polymerization to prepare fluorescent NPs for cell imaging. A photoswitchable dual color NPs were developed by adopting BODIPY and spiropyran based monomer together with MMA using miniemulsion polymerization for rewritable patterning and cell imaging application (***Figure 1.10B***).[78] Likewise, Li *et al.*[79] presented facile synthesis of highly fluorescent NPs by covalently incorporating twisted perylene diimide (PDI) into core-shell type polymeric NPs using modified emulsion polymerization (***Figure 1.10C***). Similarily, the chromophores could also be attached covalently using click chemistry to make fluorescent NPs. In one such case, Mackiewicz *et al.*[80] reported synthesis of multifunctional polyester NPs having targeting ligands as well as fluorescent dye on the surface using combination of ROP and click chemistry. The covalent linkage ensured complete absence of any dye leakage thereby enhancing signal to noise ratio and thus higher resolution contrast from the fluorophore. It also restricts fluorophore mobility thereby dispersing it uniformly within the NPs and thus minimizes fluorescence quenching of dyes by self aggregation.[33,35,37,76,81,82]

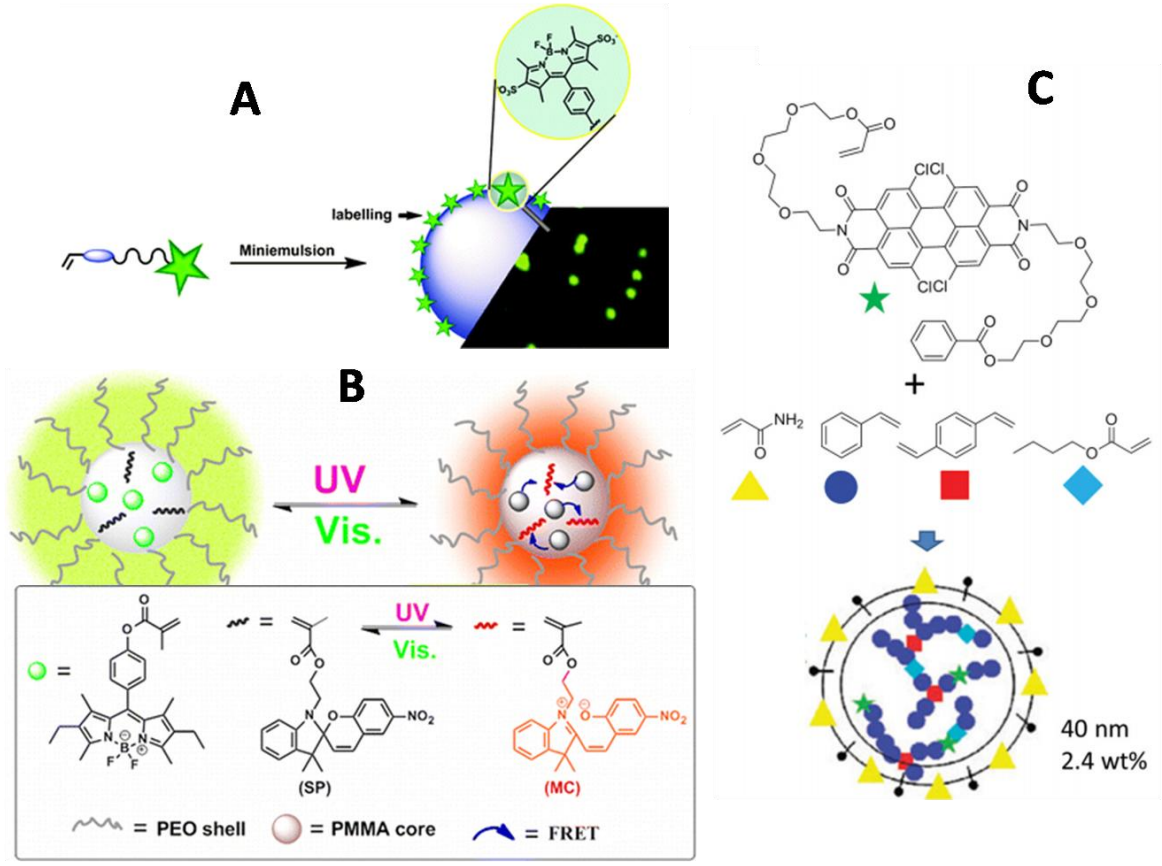

Figure 1.10: Illustration of different fluorescent monomers and their covalent incorporation into polymer NPs. Panel A adopted with permission from ***Ref 76***. Copyright 2012, American Chemical Society. Panel B adopted with permission from ***Ref 78***. Copyright 2015, American Chemical Society. Panel C adopted with permission ***Ref 79***. Copyright 2009, The Royal Society Of Chemistry.

1.4 Surface Functionalization Strategies:

The surface functionalization of particles play pivotal role in the variety of applications such as bio-imaging, drug delivery, chemical and bio-sensing *etc.* because of their large surface to volume ratio when compared to bulk material. The surface functionalization with ligands appreciably attributes to the combined properties of such NPs since surface atoms play an important role in determining such properties. The hydrophilic groups on the surface not only impart water solubility or colloidal stability to the NPs but also provides proper interaction site with the molecule of interest.

Polymers impart macromolecular property to the particle surface. For instance, coating NPs surface with polymer such as PEG provide stealth feature to NPs thereby preventing adsorption of serum protein; resulting in the increased circulation time and thus facilitating passive targeting *via* Enhanced Permeation and Retention (EPR) effect. For example, Landfester *et al.*[83] reported series of highly fluorescent carboxyl and amine

functionalized polystyrene (PS) NPs for bio-imaging application. Functional monomers (acrylic acid for carboxyl and 2-aminoethyl methacrylate hydrochloride (AEMH) for amine functionality) were co-polymerized with styrene encapsulating N-(2,6-diisopropylphenyl)-perylene-3,4-dicarboximide (PMI) dye using miniemulsion polymerization to synthesize PS NPs to be utilized as fluorescent probe in HeLa cells. And it was found that in case of carboxyl group, uptake increases with increasing amount of carboxyl group on the surface upto 10 wt% of monomer and decreases afterwards, however uptake increases with increasing surface charge in case of amine functionality. Wu *et al.* presented poly(styrene-co-maleic anhydride) (PSMA) polymer to surface functionalize fluorescent semiconducting polymer PFBT. Maleic anhydride was then hydrolyzed to generate free carboxyl group on the surface to enable further surface conjugation for bio-orthogonal labelling (***Figure 1.11A***).[84]

Malik *et al.* reported cationic polyfluorene (poly(3,3'-((2-phenyl-9H-fluorene-9,9-diyl)bis(hexane-6,1-diyl))bis(1-methyl-1H-imidazol-3-ium)bromide) (PFMI)) based polymer nanoparticles. They utilized this imidazolium surface functionalized NPs for the ultrasensitive detection of picric acid (PA) on multiple platforms (***Figure 1.11B***).[85] Thus, specific groups on the surface of NPs could augment the internalization ability, impart non-toxicity which are important criteria for biomedical application while provides specific analyte interaction site in case of sensing and bio-sensing applications.

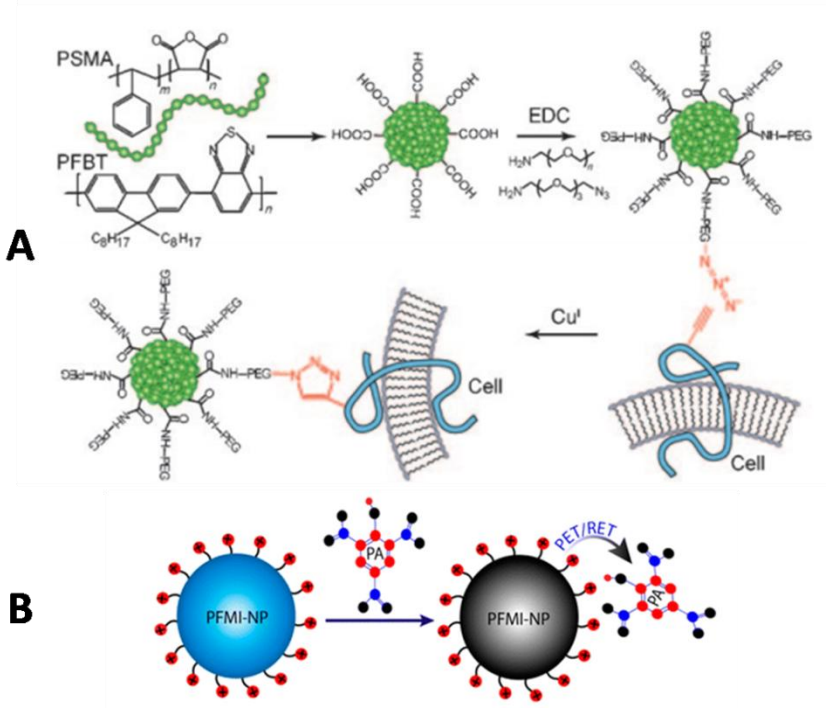

Figure 1.11: Schematics of surface functionalization of NPs with polymers either for (A) facile bioconjugation. Adopted with permission from ***Ref 84***. Copyright 2010**,** Wiley-VCH Verlag GmbH & Co. KGaA, Weinheim or (B) analyte interaction. Adopted with permission from ***Ref 85***. Copyright 2006, American Chemical Society.

1.5 Applications of Fluorescent Polymeric Particles:

1.5.1 Bio-imaging:

Fluorescent polymeric NPs have been employed in various biomedical applications such as fluorescent probes for cell and *in vivo* imaging, drug targeting, sustained release, gene delivery *etc*. The fluorescent property of such NPs made them useful for additional purposes such as visualizing pathways, mechanisms, and parameters that rules the NPs' entry into the cellular system. Studies *eg.* using PLGA NPs by Reisch *et al.*[86] have shown that the uptake of such fluorescent NPs into the cells mostly takes place *via* endocytosis.

Further studies were reported to get an insight about the effect of particle size on cellular uptake process, thereby establishing a relationship between the two. For instance, Vollrath *et al.*[87] investigated cellular uptake of fluorescent PMMA NPs in the size range of >100 (small), 100-200 (medium), <300 nm (large) and found that 100-200 nm particles showed the fastest uptake while NPs either smaller or larger than these size

range showed sluggish uptake by the cells. The imaging study with the fluorescent NPs demonstrated that smaller and medium sized NPs were co-localized in lysosomes and endosomes and were uptaken by clartharin dependent endocytosis, while the larger ones were not detected in either lysosomes or endosomes and were found to enter the cells by macropinocytosis.

Not only size of the NPs, but their surface charge also played a crucial role in cellular uptake, in terms of biodistribution, intracellular bioavailability and *in vivo* circulation of NPs. In one such attempt, Dausend *et al.*[88] have investigated the role of surface charge on the cellular uptake thereby improving the imaging efficacy and mechanism of uptake. Amine and carboxyl functionalized fluorescent PS NPs were used to impart positive and negative charge on the surface and were incubated into HeLa cells. Interestingly, they found that positively charged NPs showed enhanced cellular internalization as compared to the negative ones (***Figure 1.12***). Although the positive charge was found to enhance the cell uptake, some reports have shown marked disruption of plasma membrane and lysosomal damage, thus imparting strong cytotoxicity.

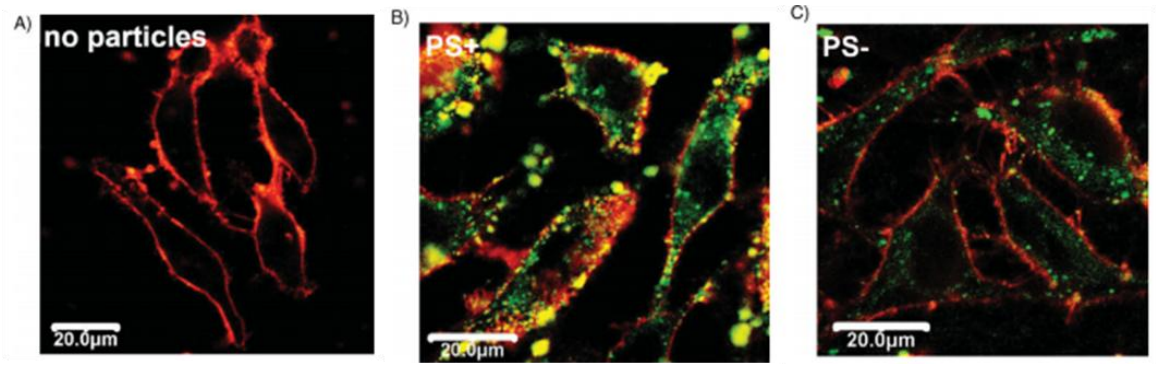

Figure 1.12: Cellular uptake of serum depleted HeLa cells after incubated with a) control, b) amine functionalized PS NPs, c) carboxy functionalized PS NPs for 1 h. The cell membrane stained with R414 (red) and NPs in green. Adopted with permission from ***Ref 88*** . Copyright 2008**,** Wiley-VCH Verlag GmbH & Co. KGaA, Weinheim.

Holzapfel *et al.*[89] presented dual reporter particles with both fluorescent dye and magnetite NPs (10-12 nm) encapsulated into poly(styrene-co-acrylic acid) using three step miniemulsion polymerization. Fluorescent dye and magnetite NPs were incorporated together for *in vitro* as well as magnetic resonance imaging. Their uptake was found to be dependent on surface -COOH group and increase in the uptake was observed by increasing -COOH groups (***Figure 1.13***).

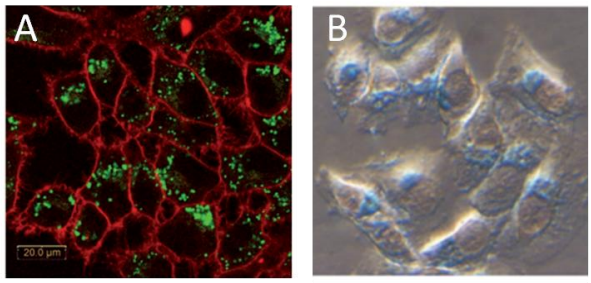

Figure 1.13: Cellular uptake of dual-marker PS NPs into HeLa cells, a) fluorescent NPs in green with cell membrane stained with R414 (red). b) prussian blue staining of NPs due to magnetite by magnetic resonance tomography. Adopted with permission from ***Ref 89***. Copyright 2006, IOP Publishing Ltd.

Large numbers of reports have focused on multicolor imaging to meet the demand for multiplexed bio-imaging and detection. Multicolor emission in cell imaging is particularly important for preventing any chaos in imaging due to cell autofluorescence caused in presence of water, oxygen *etc.*, especially during *in-vivo* studies . At the same time, it also increases the resolution contrast of image by accessing multiple excitation wavelengths for imaging application. For instance, research from group of McNeil[90], presented multicolor conjugated polymer dots (CP dots) for fluorescence imaging of live cells. The confocal laser scanning microscopy (CLSM) images assuredly demonstrate the uptake of these CP dots into perinuclear region. Exceptional photostability and high quantum yield makes them good candidate for cellular imaging applications (***Figure 1.14***). Bao *et al.*[91] prepared ultra small sized conjugated NPs which is highly preferable for multispectral sub cellular imaging. Full emission spectra from blue to red could be achieved by simply varying solvent or giving heat treatments.

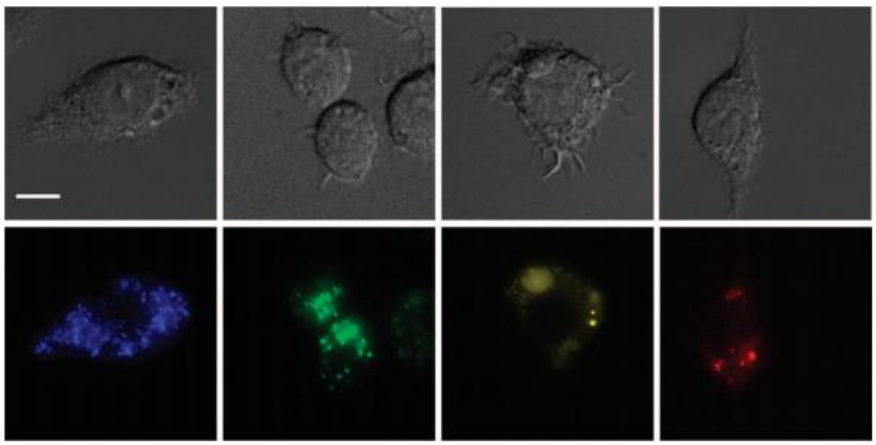

Figure 1.14: Differential interference contrast (DIC), top and fluorescence images, bottom of multicolor conjugated polymer dots into macrophage cells. Scale bar : 10 µm. Adopted with permission. Copyright 2008, American Chemical Society.

1.5.2 Multi-color tuning material:

If a picture describes thousand words then colored one should describe a million. This is because visual perception is capable of conveying far more information than any other senses in human beings. Therefore, multicolor tuning in fluorescent material offers tremendous advantage in applications such as organic light emitting diodes (OLEDs), anti counterfeiting, information encryption and storage, inkjet printing *etc.*

Color tuning plays a very crucial role in OLEDs for display devices such as television, computer monitors, mobile phones *etc*. Polymer based LEDs are particularly appealing due to their outstanding film forming ability and ability to cover large surfaces. One such example was presented by Baier and co-workers.[92] They synthesized multicolor emitting poly(arylene diethynylene) NPs of 20-30 nm diameter by co-polymerizing with either PBI or fluorenone through miniemulsion polymerization. Efficient energy transfer from conjugated polymer backbone to the incorporated dye moieties resulted in multicolor emission, which could be seen clearly under UV lamp (Figure 1.15).

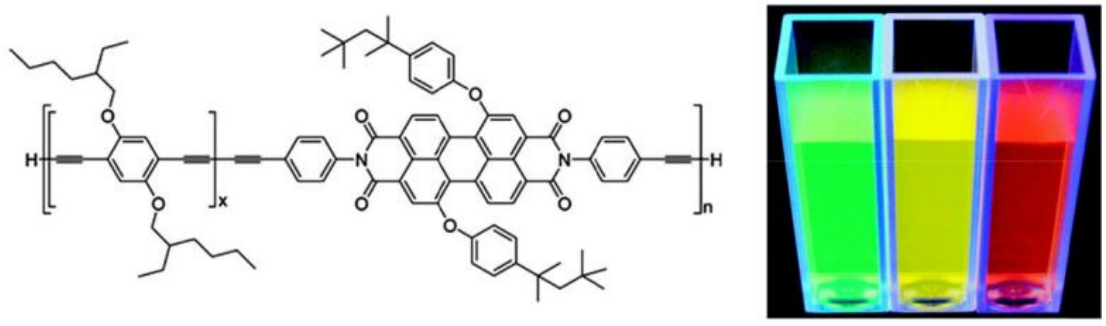

Figure 1.15: Co-polymerization of arylene diethynylene with PBI using miniemulsion polymerization (left). NPs dipersions for different monomer loadings under UV lamp. (right). . Adopted with permission. Copyright 2009, American Chemical Society.

Chen *et al.*[93] have developed FRET based multicolor, photoswitchable fluorescent polymer NPs by copolymerizing full form (MMA) with three polymerizable dyes namely spiropyran-linked methacrylate (SPMA), allyl-(7-nitro-benzo-[1,2,5]oxadiazol-4-yl)-amine (NBDAA), 4-ethoxy-9-allyl-1,8-naphthalimide (EANI). Recent years have seen another crucial importance of fluorescent NPs in OLED application, for energy efficient lighting system, replacing conventional lighting appliances. In this regard, white emitting OLEDs are particularly essential because of their high efficiency at the cost of low energy consumption. This has brought significant interest to multiple companies like Philiphs, Mitsuishi, NEC, General Electrics, Osram *etc.*[94,95] and they are developing different

approaches to make white emitting OLEDs in bulk scale including roll to roll printed LEDs (a) and wave light OLED (b) (***Figure 1.16***), curved LED , foldable smartphones. In this context, recently Park *et al.*[96] have reported white light emitting polyfluorene based conjugated polymer NPs for color conversion LED applications.

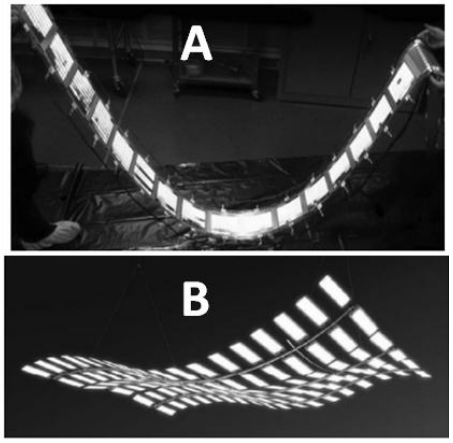

Figure 1.16: a) roll to roll printed OLED by General Electric (GE), b) Wave light by Osram, Figure reprinted with permission from ***Ref 94***. Copyright 2010**,** Wiley-VCH Verlag GmbH & Co. KGaA, Weinheim.

Another important application of fluorescent NPs is seen in protection of confidential information due to security purposes. Numerous fluorescent polymeric materials have been developed for encrypting information, *eg.* in anti-counterfeiting. For instance, Chang *et al.*[97] generated vast array of colors using aqueous polymer dots for creating full color fluorescence patterning which can print almost anything including logos, multi-color bar codes or any other custom patterns (***Figure 1.17*** Left). Pham *et al.*[98] reported fabrication of a recording medium with a polymer obtained *via* emulsion polymerization of MMA with three different dyes (with complete absence of overlap among their emission and absorption spectra). The multi-color emissive nature of the prepared polymer NPs thus allowed any biometric feature such as signature, photograph or signature to be printed on the surface by irradiating sample at specific wavelength (***Figure 1.20*** middle). Other emerging technology in print media is to develop rewritable patterning in order to prevent wastage of paper and environmental pollution caused due to deforestation associated with paper manufacturing. In this context, Zhong *et al*.[99] have reported AIE and spiropyran based photoswitchable polymeric NPs for rewritable fluorescence patterning. Thus dual color reversible emission could be consequently developed and erased using photomask by altering UV-Visible light source. As depicted

in ***Figure 1.17*** right, a pattern "AIE" was recorded by covering the paper with pattern "A" and subsequently erased by removing the same under UV light. Similarily a pattern "NP" was recorded by covering the paper with pattern "B" and subsequently erased by removing the same under visible light.

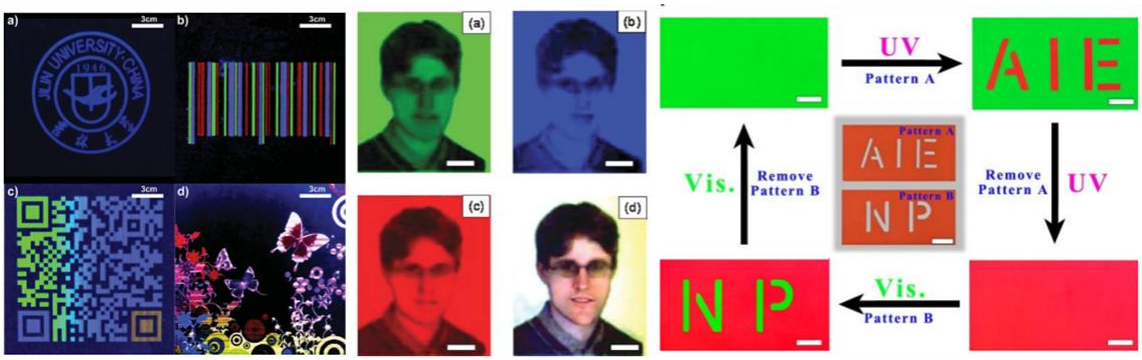

Figure 1.17: Full color photograph of (a) a logo, (b,c) 1D and 2D barcodes (d) any pattern (eg. upright butterfly) printed using P-dot inks under UV light. Scale bar: 3 cm. Adopted with permission from ***Ref 97***. Copyright 2008**,** Wiley-VCH Verlag GmbH & Co. KGaA, Weinheim (left panel). Image obtained by photobleaching, a) NBD, b) anthracene, c) Nile blue, d) full image by overlaying a, b, c images. Scale bar: 10 µm. Adopted with permission ***Ref 98***. Copyright 2007, The Royal Society of Chemistry (middle panel). Rewritable photoswitchable fluorescence patterning obtained by irradiating the sample alternatively under UV and visible light (right panel); Scale bar: 1 cm. Adopted with permission ***Ref 99***. Copyright 2017, The Royal Society of Chemistry (right panel).

1.5.3 Chemical Sensing:

Now a day, more and more emphasis is being highlighted to develop fluorescence based sensors for the sensing of various analytes including cations, anions, explosives, biomolecules, organic pollutants, pH, temperature *etc.* to attain better response time and ultra-selectivity. For example, Childress *et al.*[100] presented rhodamine doped polymer NPs for ratiometric detection of Hg^{+2} ions in water. The conjugated NPs served as FRET donor to rhodamine-B spirolactum derivative only when it encountered Hg^{+2} ions; switching the emission from green to orange red. Similarly, Chan *et al.*[101] developed ultra bright polymer NPs by incorporated pH sensitive fluorescein isothiocyanate (FITC) into poly(2,5-di(3',7'-dimethyloctyl)phenylene-1,4-ethynylene) (PPE) dots to be used as pH sensor. On increasing the pH in range of 5 to 8, emission of pH sensitive FITC increased while the emission from pH inert PPE dots remained unchanged, thereby providing a ratiometric pH sensor (***Figure 1.18 A)***. Moreover, Zhao *et al.*[102] developed dual emissive polymer dots for the prompt detection of fluoride (F^-) ions in water. The polymer dots

comprised of dual emissive conjugated polyelectrolyte with iridium (III) complex having red emission. As F^- ion from solution interacted with the polymer dots, red emission from iridium complex got quenched, leaving the blue emission from the conjugated polyelectrolyte (***Figure 1.18 B***).

Many sensing platforms have been developed in recent years based on surface functionalization strategy to augment analyte-sensor interaction as well as specificity among the sensors. One such example is presented by Chan *et al.*[103] who utilized PSMA for PS-COOH functionalized PFBT dots for efficient dual sensing of Cu^{+2} and Fe^{+2} in water (***Figure 1.18 C***). Mechanism of sensing is based on aggregation induced emission (AIE) quenching of PFBT dots selectively for Cu^{+2} and Fe^{+2}. The emission of two ions would differ on the addition of ethylenediaminetetraacetic acid (EDTA); recovery of emission in case of Cu^{+2} was observed upon addition of EDTA, while not for Fe^{+2}. Detection of nitroaromatics as another class of explosives and hazardous analytes has been thoroughly investigated over time by different research groups around the globe. In one such example, Gole *et al.* [104,105] have described the role of hydrogen bonding on the sensitivity of solid state sensors. The one having hydrogen bonded interaction would be able to efficiently sense the analyte among the library of analytes. Likewise, Zhang *et al.*[106,107] have demonstrated the formation of charge transfer complex between amine functionalized NPs and electron deficient aromatic compounds such as trinitophenol

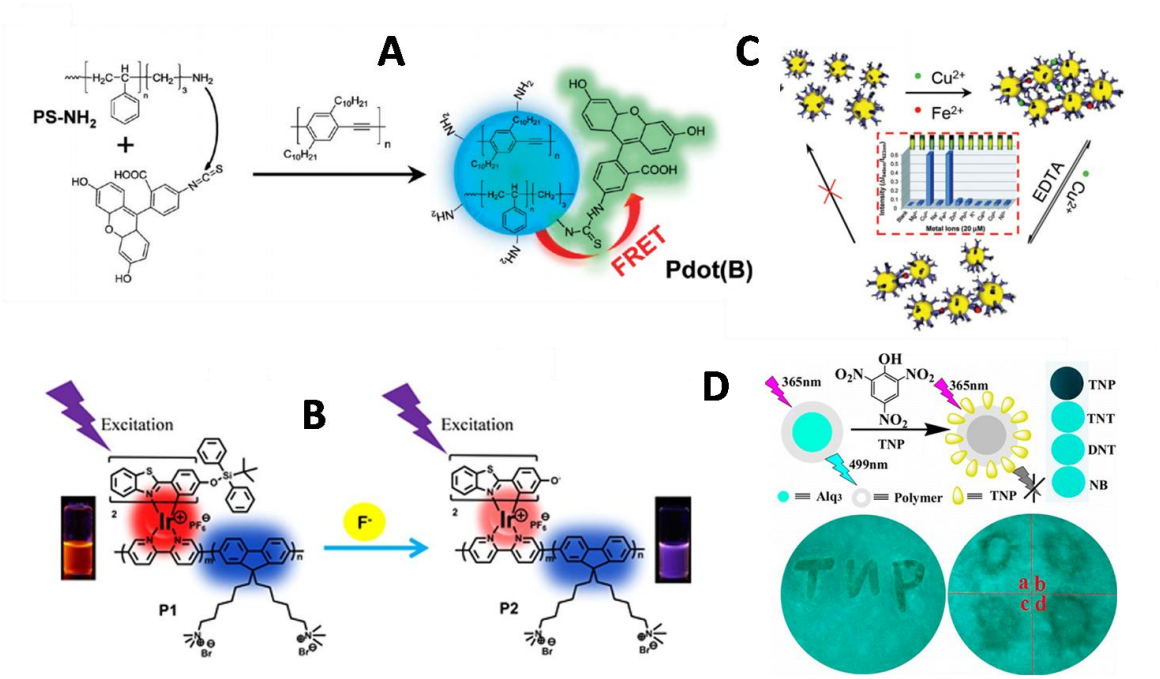

Figure 1.18: Schematics depicting a) preparation of PS-NH_2 functionalized Pdots for intracellular pH measurement. Adopted with permission from ***Ref 101***. Copyright 2011, American Chemical Society. b) fluoride detection in water using dual-emissive Pdots. c) dual sensing of Cu^{+2} and Fe^{+2} ions in water using PS-COOH functionalized PFBT Pdots. Inset is effect of different metal ions on the emission intensity of Pdots. Adopted with permission from ***Ref 103***. Copyright 2011, The Royal Society Of Chemistry. d) Paper based sensor prepared using colloidal solution of nanocomposite and its application for PA sensing. Adopted with permission from ***Ref 108***. Copyright 2012, American Chemical Society.

(TNP), trinitrotoulene (TNT) in water to strongly quench the emission of donor. Apart from solution based studies, Ma *et al.*[108] reported a paper based sensor where hydroxyquinoline aluminium (AlQ_3) coated with hydrophilic polymer. The resulting paper sensor was used to detect TNP from solution with a limiting concentration as low as 32.3 ng/mL of TNP. They have also demonstrated that TNP could be used as ink to write on coated paper resulting in instant quenching of blue emission (***Figure 1.18 D***).

1.5.4 Biosensing:

Apart from chemical sensing, scientists also have employed these polymeric NPs to detect the presence of various biological species such as enzyme, protein, nucleic acid, biomolecules *etc*. For instance, Jang *et al.*[109] utilized fluorescent NPs of borate modified poly acrylonitrile (BPAN) to detect intracellular H_2O_2 from the living cells *via* photo-induced energy transfer (PET). The detection is observed from the peak shift after the reaction of BPAN with H_2O_2 and is highly specific over other reactive oxygen species (ROS) present in the cells (***Figure 1.19 A***). Similarly, Rao *et al.*[110] reported dual emission

based polymer NPs for selective sensing of reactive oxygen and nitro species (RONS) in living mice. Increased RONS is indicative of some pathological process including bacterial infection to diseases such as cardiovascular diseases and even cancer. They prepared Pdots consisting of RONS insensitive polymer covered by RONS sensitive cyanine dyes. In absence of RONS there would be efficient energy transfer from polymer to dye; however, presence of RONS would decompose dye and enhanced the emission from Pdots (***Figure 1.19 B***).

Research from the group of Seeberger[111] highlighted the detection of bacteria using water soluble carbohydrate functionalized fluorescent poly(*p*-phenylene ethynylene) (PPE) based polymer. The carbohydrate surfactants on the surface of the particles are able to interact with carbohydrate binding site from the surface of bacteria specifically *E-coli*, resulting in bright fluorescent aggregates, making their detection possible at lower limit. Likewise many carbohydrates were tested to detect different strains of bacteria (***Figure 1.19 C***). Furthermore, Zhou *et al.*[112] reported nanospheres with (4-carboxybutyl) triphenylphosphonium bromide (TPP) and Pluronic F127 for intracellular imaging of calcium ions simultaneously in lysosomes and mitochondria. Also, there exist a numbers of reports in the literature for the detection of nucleic acid. One such report was presented by Wang *et al.*[113] who developed self assembly based turn-on detection of nucleic acid where interaction of nucleic acid as anlayte enhances the emission property of the polymeric NPs. Initially, the cationic polymer existed in aggregated state, causing a complete quenching of the emission from negatively charged PBI. However, on the addition of single stranded DNA (poly anion), PBI became free and its emission was restored to show the 'Turn-On' detection.

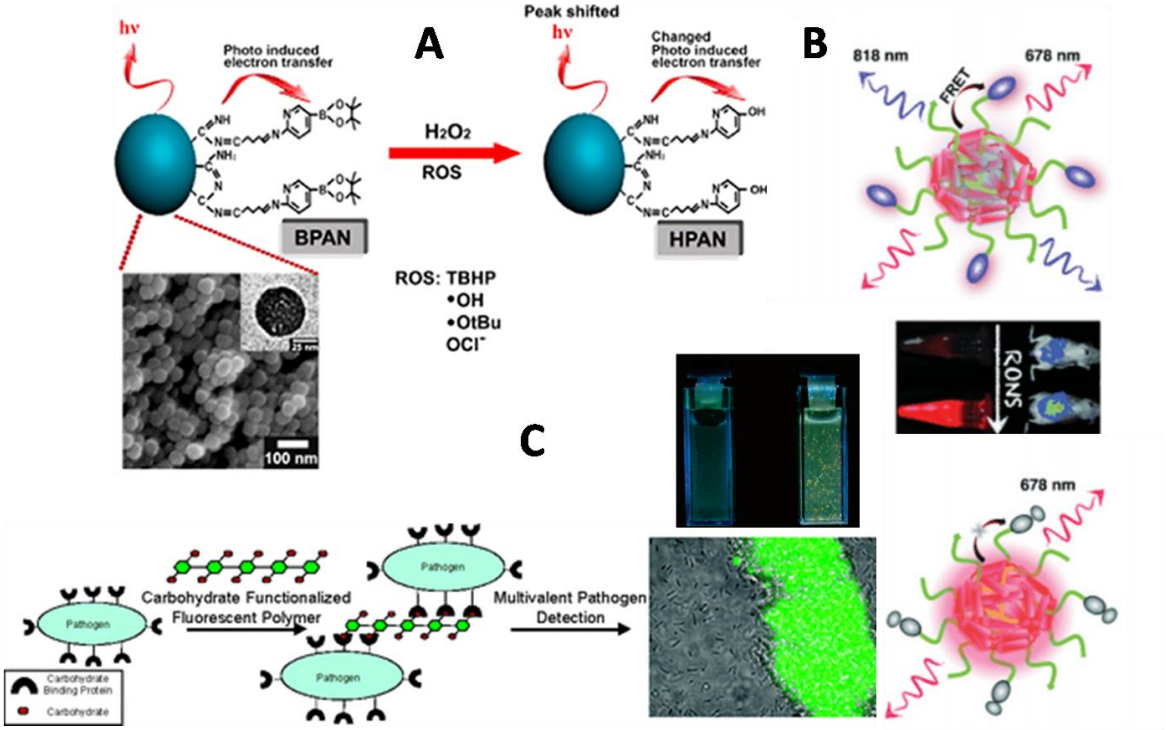

Figure 1.19: Schematic representation of A) selective sensing of intracellular H_2O_2 using fluorescent BPAN NPs among other ROS. Adopted with permission from ***Ref 109***, Copyright 2012, American Chemical Society. B) FRET based *in vivo* imaging of RONS using polymer NPs. Adopted with permission ***Ref 110***. Copyright 2013**,** Wiley-VCH Verlag GmbH & Co. KGaA, Weinheim. C) Detection of bacteria using water soluble carbohydrate functionalized fluorescent polymer (green emission of E-coli cluster after binding with polymer). Adopted with permission ***Ref 111***. Copyright 2004, American Chemical Society

1.6 Comparison among various well known NPs:

There are several well-studied and commercially available fluorescent NPs such as quantum dots, upconverting NPs, self-assembled conjugated NPs and polymeric NPs *etc.*

Quantum dots have got unmatched success in imaging and sensing application because of high quantum yield, good photostability, long lifetime *etc.* But despite of such listed advantages, they often suffered from leakage of heavy toxic metals like cadmium, selenium into the biological system.[38,40] They also impart interminable toxicity issues including cytotoxicity, induced apoptosis, peroxidative stress *etc.*[35,38,40,114]Also, their emission properties vary largely with temperature[37] and pH.[38] In fact their use in biomedical application is still a question of debate.

The next important candidate is upconverting NPs which are nanocrystals of sodium ytterbium fluoride and sodium gadolinium fluoride doped with Er(III), Yb(III) and Tm(III). They possess advantage like multicolor emission, size tunability *etc.* but have

relatively low quantum yield in water that hardly go beyond 0.5% [40,115,116] Also, their fluorescence properties changes with temperature and quenched non-selectively by several heavy metal ions.[40] Almost all the reported synthesis results in water-insoluble NPs which need to be surface modified to impart water dispersibility prior to any biological and sensing application.[40,130] But, these surface modifications cause change in their emission properties, and often left them unsuitable for imaging studies.[40,116] And similar to quantum dots their potential toxicity is still a matter of concern.[38,40,115] In present situation, no proper instrumentation facilities have been standardized or established to measure the optical signals from these materials in a concurrent and globally acceptable manner.[115]

Conjugated polymer NPs are often considered ideal candidate for bio-imaging and sensing being intrinsically fluorescent. But as water dispersibility is major requirement for the application, they occassionally need to be structurally modified with the insertion of functional groups, which is tiresome and tedious job to perform.[35,116,117] Also, they undergo rapid exchange and the stability of such self assembled conjugated polymer NPs remain unclear on dilution.[35,70,71] Biocompatibilty[35,40] , size tunability[117] further aids complications in this field.

Along this note, fluorescent Polystyrene (PS) based nanoparticles have ability to overcome the above mentioned limitations associated with the conventional NPs. As compared to other NPs, PS nanobeads can be easily synthesized in monodisperse form with narrow particle size distribution.[118] Also, their particle size can be easily tuned.[119] Additionally, fluorophore can be incorporated into PS beads following which they can be traced in the biological systems over prolong time period.[89,118] Moreover, surface modification of these beads with variety of functional groups can be achieved with ease which play a crucial role in various biological and sensing applications.[89] Also, PS is cost effective, easily scalable, bio-compatible, commercial polymer that are produced and consumed in large quantities. [118-120]

1.7 Aim of thesis:

The above discussion showcased a thorough literature survey on fluorescent polymeric NPs, their preparations using different approaches and their applications in various disciplines. The prime objective of the work is to synthesize fluorescent polymer nanobeads for bio-imaging and sensing applications. Detailed literature survey indicated that combination of multicolor emitting, covalently stitched, surface functionalized fluorescent PS nanobeads with high quantum yield (both solid as well as solution state) was lacking in the literature.

Although there are plenty of reports on the physical encapsulation of fluorophores into the polymer matrix, it is very well known that physical encapsulation often leads to dye leakage. Leaching of dyes from the polymer backbone is detrimental to both biomedical and sensing applications. Dye leakage might lead to cell toxicity if used as cell marker or might hamper reproducibility and performance of sensor in sensing applications. Thus covalent attachment of the fluorophores into the polymer matrix is desired. Keeping the advantage of PS nanobeads in mind, we planned to develop polymerizable fluorophores for their covalent incorporation into beads to prepare fluorescent PS nanobeads. Oligo(p-phenylenevinylene) (OPV) and perylene bisimide (PBI) were chosen as the fluorophores because of their higher molar extinction coefficients, high fluorescence quantum yield and outstanding thermal, chemical and photostability. Additionally, polystyrene also reduced aggregation induced self-quenching of emission of dyes.

The key features of currently synthesized fluorescent PS nanobeads are highlighted below:

a) Simple, easy and scalable approach for developing fluorescent NPs of narrow size distribution suitable for cell imaging as well as sensing application, b) Covalent attachment of dyes to the polymer backbone not only prevents dye leakage but also enhances signal to noise ratio, c) Multiple fluorophores can inserted into the single bead without significantly affecting its size to obtain multicolor emission from the beads , d) Ease of color tuning ranging from blue to green to red to white, e) Exceptionally high quantum yield and good photostability of NPs dispersion in water as well as in solid states, f) Possess exceptional stability in physiological environment (in case of bio-imaging), g) Non-dependence of emission properties of PS NPs over wide range of

temperature and pH unlike quantum dots and upconverting NPs, h) Ease of surface modification.

The thesis mainly emphasized the following mentioned aspects:

1. Development of covalently stitched fluorescent PS NPs in the size range of 100-150 nm via miniemulsion polymerization.

2. Application of these water dispersible multicolor emitting PS nanobeads as Single Optical Agent for Three-Channel Fluorescent Probe in bio-imaging of cancer cells.

3. Development of amine and carboxy surface functionalized PS based solid state sensor for dual-distinct sensing of volatile organic compounds.

4. Designing and synthesis of new polystyrene bearing glucuronic acid to act as surfactant in miniemulsion polymerization for preparing glucuronic acid functionalized fluorescent PS NPs for the selective sensing of bilirubin in human blood serum among other active interferences such as salts, sugars, haemoglobin, cholestrol *etc.*

The aim of thesis is schematically represented in ***Figure 1.20*** where thorough literature survey clearly demonstrated need for currently synthesized PS nanobeads over other conventional nanoparticles.

And lastly the overall outcome of the research work carried out in the present Ph.D. thesis has been summarized in chapter-6 along with its future perspectives.

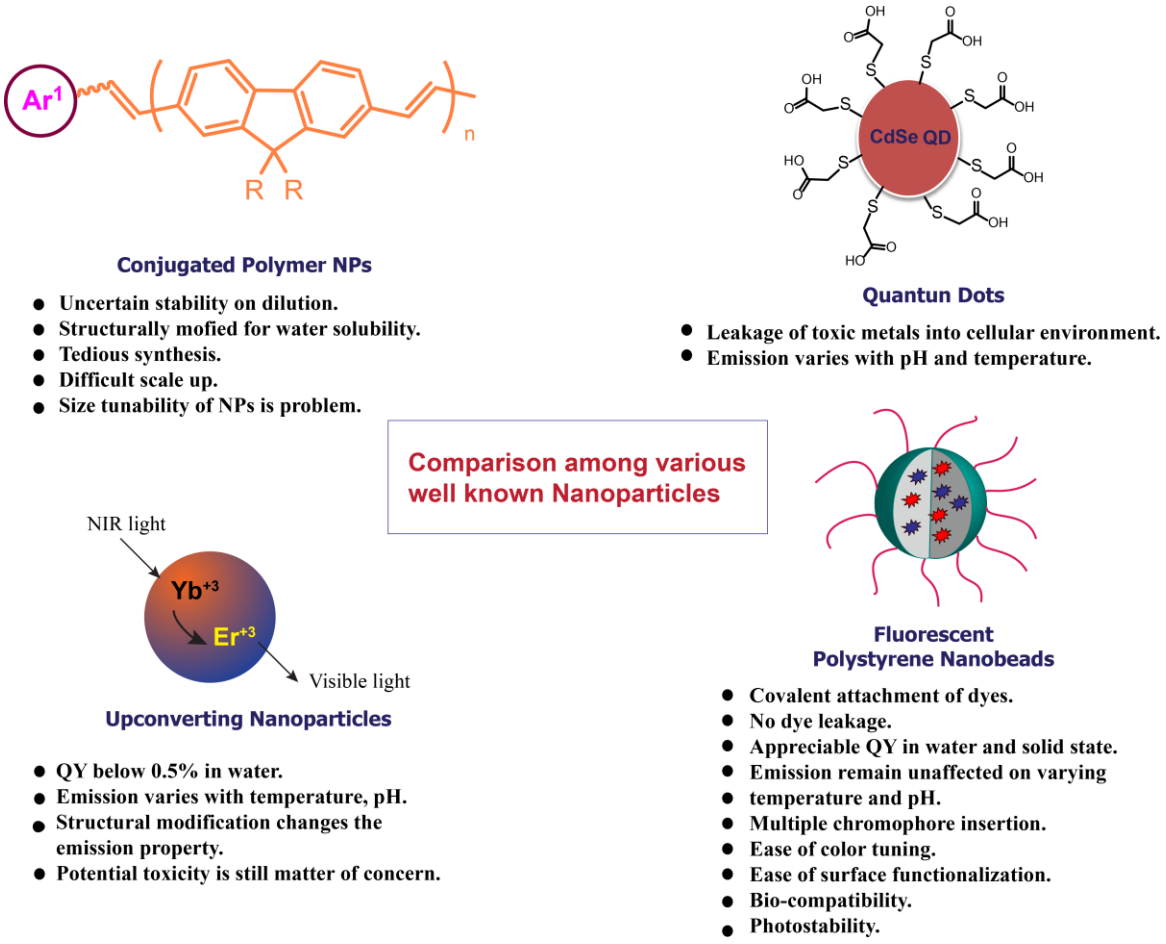

Figure 1.20: Schematics illustrating the superiority of fluorescent PS NPs over the other well known NPs including upconverting NPs, quantum dots, conjugated polymer NPs *etc*.

1.8 References:

1. Chinen, A. B.; Guan, C. M.; Ferrer, J. R.; Barnaby, S. N.; Merkel, T. J.; Mirkin, C. A. *Chem. Rev.* **2015**, *115*, 10530-10574.

2. Tuncel, D.; Demir, H. V. *Nanoscale* **2010**, *2*, 484-494.

3. Rong, Y.; Wu, C.; Yu, J.; Zhang, X.; Ye, F.; Zeigler, M.; Gallina, M. E.; Wu, I. C.; Zhang, Y.; Chan, Y. H.; Sun, W.; Uvdal, K.; Chiu, D. T. *ACS Nano* **2013**, *7*, 376-384.

4. Li, Z.; , Yong Zhang, Y. *Angew. Chem. Int. Ed.* **2006**, *118*, 7896-7899.

5. Hossan, Y.; Hor, A.; Luu, Q.; Smith, S. J.; May, P. S.; Berry, M. T. *J. Phys. Chem. C* **2017**, *121*, 16592-16606.

6. Mai, H.; Zhang, Y.; Sun, L.; Yan, C. *J. Phys. Chem. C* **2007**, *111*, 13721-13729.

7. Saghatelian, A.; Volcker, N. H.; Guckian, K. M.; Lin, V. S. Y.; Ghadin, M. R. *J. Am. Chem. Soc.* **2003**, *125*, 346-347.

8. Bozdemir, O. A.; Guliyev, R.; Buyukcakir, O.; Selcuk, S.; Kolemen, S.; Gulseren, G.; Nalbantoglu, T.; Boyaci, H.; Akkaya, E. U. *J. Am. Chem. Soc.* **2010**, *132*, 8029-8036.

9. Qu, D, H.; Ji , F.Y.; Wang, Q. C.; Tian, H. *Adv. Mater.* **2006**, *18*, 2035-2038.

10. Guo, Z.; Zhu, W.; Tian, H. *Chem. Commun.* **2012**, *48*, 6073-6084.

11. Cao, L.; Wang, X.; Meziani, M. J.; Lu, F.; Wang, H.; Luo, P. G.; Lin, Y.; Harruff, B. A.; Veca, L. M.; Murray, D.; Xie, S.-Y.; Sun, Y.-P. *J. Am. Chem. Soc.* **2007**, *129*, 11318-11319.

12. Shen, J.; Zhu, Y.; Yang, X.; Li, C. *Chem. Commun.* **2012**, *48*, 3686-3699.

13. Pu, K.Y.; Liu, B. *Adv. Mater.* **2011**, *21*, 3408-3423.

14. Song, Y.; Zhu, S.; Yang, B. *RSC Adv.* **2014**, *4*, 27184-27200.

15. Santra, S.; Yang, H.; Holloway, P. H.; Stanley, J. T.; Mericle, R. A. *J. Am. Chem. Soc.* **2005**, *127*, 1656-1657.

16. Schwartz, A.; Marti, G E.; Poon, R.; Gratama, J. W.; Repollet, E. F. *Cytometry* **1998**, *33*, 106-114.

17. Vogt, R. F.; Cross, G. D.; Henderson, L. O.; Phillips. D. L. *Cytometry* **1989**, *10*, 294-302.

18. Ganesh, N., Zhang, W.; Mathias, P. C.; Chow, E.; Soares, J. A. N. T.; Malyarchuk, V.; Smith, A. D.; Cunningham, B. T. *Nat. Nanotech.* **2007**, *2*, 515-520.

19. Müller, M.; Zentel, R.; Maka, T.; Romanov, S. G.; Torres, C. M. S. *Chem. Mater.* **2000**, *12*, 2508-2512.

20. Desmonts, L. B.; Reinhoudt,' D. N.; Crego-Calama, M. C. *Chem. Soc. Rev.* **2007**, *36*, 993-1017.

21. Wolfbeis, O. S. *J. Mater. Chem.* **2005**, *15*, 2657-2669.

22. Wu, J.; Liu, W.; Ge, J.; Zhang, H.; Wang, P. *Chem. Soc. Rev.* **2011**, *40*, 3483-3495.

23. Reppy, M. A.; Pindzola, B. A. *Chem. Commun.* **2007**, 4317-4338.

24. Ding, C.; Zhu, A.; Yang Tian, Y. *Acc. Chem. Res.* **2014**, *47*, 20-30.

25. Li, J.; Zhu, J. J. *Analyst* **2013**, *138*, 2506-251.

26. D'Andrade. B. W.; Forrest, S. R. *Adv. Mater.* **2004**, *16*, 1585-1595.

27. Wei, Y.; Chen, C. T. *J. Am. Chem. Soc.* **2007**, *129*, 7478-7479.

28. Bouffard, J.; Swager, T. M. *Macromolecules* **2008**, *41*, 5559-5562.

29. Wu, C.; Szymanski, C.; McNeill, J. *Langmuir* **2006**, *22*, 2956-2960.

30. Sonawane, S. L.; Asha, S. K. *ACS Appl. Mater. Interfaces* **2013**, *5*, 12205-12214.

31 Sonawane, S. L.; Asha, S. K. *J. Phys. Chem. B* **2014**, *118*, 9467-9475.

32. Grazon, C.; Rieger, J.; Renault, R. M.; Clavier, G.; Charleux, B. *Macromol. Rapid Commun.* **2011**, *32*, 699-705.

33. Chen, J.; Zhong, W.; Tang, Y.; Wu, Z.; Li, Y.; Yi,P.; Jiang, J. *Macromolecules* **2015**, *48*, 3500-3508.

34. Taniguchi, T.; Takeuchi, N.; Kobaru, S.; Nakahira, T. *J. Colloid Interface Sci.* **2008**, *327*, 58-62.

35. Reisch, A.; Klymchenko, A. S. *Small* **2016**, *12*, 1968-1992.

36. Chen, J.; Zhang, P.; Fang, G.; Weng, C.; Hu, J.; Yi, P.; Yua, X.; Lia, X. *Polym. Chem.* **2012**, *3*, 685-693.

37. Vollrath, A.; Schubert, S.; Schubert, U. S. *J. Mater. Chem. B* **2013**, *1*, 1994-2007.

38. Feng, G.; Dinga, D.; Liu, B. *Nanoscale* **2012**, *4*, 6150-6165

39. Ruedas-Rama, M. J.; Walters, J. D.; Orte , A.; Hall, E. A. H. *Anal. Chim. Acta* **2012**, *751*, 1-23.

40. Wolfbeis, O. S. *Chem. Soc. Rev.* **2015**, *44*, 4743-4768.

41. Shipway, A. N.; Katz, E.; Willner, I. *ChemPhysChem,* **2000**, *1*, 18-52.

42. B. K.; Gierschner, J.; Park, S. Y. *Acc. Chem. Res.* **2012**, *45*, 544–554.

43. Choi, H.; Ko, S. J.; Choi, Y.; Joo, P.; Kim, T.; Lee B. R.; Jung, J, W.; Choi, H. J.; Cha, M.; Jeong, J, R.; Hwang, I, W.; Song, M. H.; Kim, B. S.; Kim, J. Y. *Nature Photonics*, **2013,** *7*, 732–738.

44. Deng, W.; Goldys, E. M. *Analyst* **2014**, *139*, 5321-5334.

45. Ng, S. M.; Koneswaran, M.; Narayanaswamy, R. *RSC Adv.* **2016**, *6*, 21624-21661

46. Burns, A.; Sengupta, P.; Zedayko, T.; Baird, B.; Wiesner, U. *Small* **2006**, *2*, 723-726.

47. Ruedas-Rama, M. J.; Walters, J. D.; Orte, A.; Hall, E. A. H. *Anal. Chim. Acta* **2012**, *751*, 1-23.

48. Burns, A.; Owb, H.; Wiesner, U. *Chem. Soc. Rev.* **2006**, *35*, 1028-1042.

49. Sevan, T, S.; Tan, T. T. Y.; Yi, D. K.; Jana, N. R. *Langmuir* 2010, *26*, 11631-11641.

50. Lia, K.; Liu, B. *Chem. Soc. Rev.* **2014**, *43*, 6570-6597.

51. Robin, M. P.; O'Reilly, R. K. *Polym. Int.* **2015**, *64*, 174-182

52. Schork, F, J.; Luo, Y.; Smulders, W.; Russum, J. P.; Butté, A.; Fontenot, K. *Adv. Polym. Sci.* **2005**, *175*, 129-255.

53. Antonietti, M.; Landfester, K. *Prog. Polym. Sci.* **2002**, *27*, 689-757.

54. Capek, I.; Chern C. S. *Adv Polym. Sci.* **2001**, *155*, 101–65.

55. Vivaldo-Lima,E.; Wood, P. E.; Hamielec, A. E. *Ind. Eng. Chem. Res.* **1997**, *36*, 939-965.

56. Barrett, K. E. J. *Br. Polym. J.* **1973**, *5*, 259-271.

57. Asua, J. M. *J Polym Sci Part A: Polym. Chem.* **2004**, *42*, 1025-1041.

58. Chern, C. S. *Prog. Polym. Sci*. **2006**, *31*, 443-486.

59. Landfester, K. *Top Curr. Chem.* **2003**, *227*, 75-123.

60. Mason, T. G.; Wilking, J. N.; Meleson, K.; Chang, C. B.; Graves, S. M. *J. Phys.: Condens. Matter* **2006**, *18*, R635–R666.

61. Landfester, K. *Annu. Rev. Mater. Res.* **2006**, *36*, 231-279.

62. Chou,Y. J.; El-Aasser, M. S.; Vanderhoff, J. W. *J. Dispers. Sci. Technol.* **1980**, *1*, 129-150.

63. Miller, C. M.; Blythe, P. J.; Sudol, E. D.; Silebi, C. A.; El-Aasser, M. S. *J Polym Sci Part A: Polym. Chem.* **1994**, *32*, 2365-2376.

64. Feng, L.; Zhu, C.; Yuan, H.; Liu, L.; Lv, F.; Wang, S. *Chem. Soc. Rev.* 2013, **42**, 6620-6633.

65. Geng, J .; Li , K.; Qin, W.; Ma, L.; Gurzadyan, G. G.; Tang, B. Z.; Liu, B. *Small* **2013**, *9*, 2012-2019.

66. Wu, C.; Schneider, T.; Zeigler, M.; Yu, J.; Schiro, P. G.; Burnham, D. R.; McNeill, J. D.; Chiu, D. T. *J. Am. Chem. Soc.* **2010**, *132*, 15410-15417.

67. Yang, Z.; Yuan, Y.; Jiang, R.; Fu, N.; Lu, X.; Tian, C.; Hu, W.; Fan, Q.; Huang, W. *Polym. Chem.* **2014**, *5*, 1372-1380.

68. Kulkarni, B.; Surnar, B.; Jayakannan, M. *Biomacromolecules* **2016**, *17*, 1004-1016.

69. Zhang, X.; Chen, Z. J.; Wurthner, F. *J. Am. Chem. Soc.* **2007**, *129*, 4886-4887.

70. Bae, Y. H.; Yin, H. *J. Control Release* **2008**, *131*, 2-4.

71 Chen, H. T.; Kim, S. W.; Li, L.; Wang, S. Y.; Park, K.; Cheng, J. X. *P Natl. Acad. Sci. USA*, **2008**, *105*, 6596-6601.

72. Behnke, T.; Wurth, C.; Laux, E. M.; Hoffmann, K.; Resch-Genger, U. *Dyes Pigment* **2012**, *94*, 247-257 .

73. Ma, Y.; Sadoqi, M.; Shao, J. *Int. J. Pharm.* **2012**, *436*, 25-31.

74. Rodriguez, V. B.; Henry, S. M.; Hoffman, A. S.; Stayton, P. S. Li, X. D.; Pun, S. H. *J. Biomed. Optics* **2008**, *13*, 014025

75. Peng, H. Q.; Sun, C. L.; Niu, L. Y.; Chen, Y. Z,; Li-Zhu Wu, L. Z.; Tung, C. H.; Yang, Q. Z. *Adv. Funct. Mater.* **2016**, *26*, 5483-5489.

76. Sauer, R.; Turshatov, A.; Baluschev, S.; Landfester, K. *Macromolecules* **2012**, *45*, 3787−3796.

77. Dossi, M.; Ferrari, R.; Dragoni, L.; Martignoni, C.; Gaetani, P.; D'Incalci, M.; Morbidelli, M.; Moscatelli, D. *Macromol. Mater. Eng.* **2012**, *298*, 771-778.

78. Chen, J.; Zhong, W.; Ying Tang, Y.; Wu, Z.; Li, Y.; Yi, P.; Jiang, J. *Macromolecules* **2015**, *48*, 3500-3508.

79. Tian, Z.; Shallerz, A. D.; Alexander, D. Q. Li. *Chem. Commun.* **2009**, 180-182.

80. Mackiewicz, N.; Nicolas, J.; Handke, N.; Noiray, M.; Mougin, J.; Daveu, C.; Lakkireddy, H. R.; Bazile, D.; Couvreur, P. *Chem. Mater.* **2014**, *26*, 1834-1847.

81. Pengab, H. S.; Chiu, D. T. *Chem. Soc. Rev.* **2015**, *44*, 4699-4722.

82. Sun, H.; Poulsen, A. M. S.; Gu, H.; Almdal, K. *Chem. Mater.* **2006**, *18*, 3381-3384.

83. Holzapfel, V.; Musyanovych, A.; Landfester, K.; Lorenz, M. R.; Mailander, V. *Macromol. Chem. Phys.* **2005**, *206*, 2440-2449.

84. Wu, C.; Jin, Y.; Schneider, T.; Burnham, D. R.; Smith, P. B.; Chiu, D. T. *Angew. Chem. Int. Ed.* **2010**, *49*, 9436-9440.

85. Malik, A. K.; Hussain, S.; Kalita, A.; Iyer, P. K. *ACS Appl. Mater. Interfaces* **2015**, *7*, 26968-26976.

86. Reisch, A.; Didier, P.; Richert, L.; Oncul, S.; Arntz, Y.; ly, M. Y.; Klymchenko, A. S. *Nat. Commun.* **2014**, *5*, 4089-4098.

87. Vollrath, A.; Schallon, A.; Pietsch, C,; Schubert, S.; Nomoto, T.; Matsumoto, Y.; Kataoka, K.; Schubert, U. S. *Soft Matter* **2013**, *9*, 99-108.

88. Dausend, J.; Musyanovych, A.; Dass, M.; Walther, P.; Schrezenmeier, H.; Landfester, K.; Mailander, V. *Macromol. Biosci.* **2008**, *8*, 1135-1143.

89. Holzapfel, V.; Lorenz, M.; Weiss, C. K.; Schrezenmeier, H.; Landfester, K.; Mailander, V. *J. Phys.: Condens. Matter* **2006**, *18*, S2581–S2594.

90. Wu, C.; Bull, B.; Szymanski, C.; Christensen, K.; McNeill, J. *ACS Nano* **2008**, *2*, 2415-2423.

91. Bao, B.; Tao, N.; Yang, D.; Yuwen, L.; Weng, L.; Fan, Q.; Huang, W.; Wang, L. *Chem. Commun.* **2013**, *49*, 10623-10625.

92. Baier, M. C.; Huber, J.; Mecking, S. *J. Am. Chem. Soc.* **2009**, *131*, 14267-14273.

93. Chen,J.; Zhang, P.; Fang, G.; Yi, P.; Zeng, F.; Wu, S. *J. Phys. Chem. B* **2012**, *116*, 4354-4362

94. Kamtekar, K. T.; Monkman, A. P.; Bryce, M. R. *Adv. Mater.* **2010**, *22*, 572-582.

95. Karzazi, Y. *J. Mater. Environ. Sci.* **2014**, *5*, 1-12.

96. Park, E. J.; Erdem, T.; Ibrahimova, V.; Nizamoglu, S.; Demir, H. V.; Tuncel, D. *ACS Nano* **2011**, *5*, 2483–2492.

97. Chang, K.; Liu, Z.; Chen, H.; Lan Sheng, L.; Zhang, S. X. A.; Chiu, D. T.; Yin, S.; Wu, C.; Qin, W. *Small* **2014**, *10*, 4270-4275.

98. Pham, H. H.; Gourevich, I.; Jonkmanb, J. E. N.; Kumacheva, E. *J. Mater. Chem.* **2007**, *17*, 523-526.

99. Zhong, W.; Zeng, X.; Chen, J.; Hong, Y.; Xiao, L.; Zhang, P. *Polym. Chem.* **2017**, *8*, 4849-4855.

100. Childress, E. S.; Roberts, C. A.; Sherwood, D. Y.; LeGuyader, C. L. M.; Harbron, E. J. *Anal. Chem.* **2012**, *84*, 1235-1239.

101. Chan, Y. H.; Wu, C.; Ye, F.; Jin, Y.; Smith, P. B.; Chiu, D. T. *Anal. Chem.* **2011**, *83*, 1448-1455.

102. Zhao, Q.; Zhang, C.; Liu, S.; Liu, Y.; Zhang, K. Y.; Zhou, X.; Jiang, J.; Xu, W.; Yang, T.; Huang, W. *Sci. Rep.* **2015**, *5*, 16420.

103. Chan, Y. H.; Jin, Y.; Wu, C.; Chiu, D. T. *Chem. Commun.* 2011, 47, 2820–2822.

104. Gole, B.; Shanmugaraju, S.; Bar, A. K.; Mukherjee, P. S. *Chem. Commun.* **2011**, *47*, 10046-10048.

105. Gole, B.; Song,W.; Lackinger, M.; Mukherjee, P. S. *Chem. Eur. J.* **2014**, *20*, 13662-13680.

106. Zhang, K.; Zhou, H. B.; Mei, Q. S.; Wang, S. H.; Guan, G. J.; Liu, R. Y.; Zhang, J.; Zhang, Z. P. *J. Am. Chem. Soc.* **2011**, *133*, 8424-8427.

107. Gao, D. M.; Wang, Z. Y.; Liu, B. H.; Ni, L.; Wu, M. H.; Zhang, Z. P. *Anal. Chem.* **2008**, *80*, 8545-8553.

108. Ma, Y.; Li, H.; Peng, S.; Wang, L. *Anal. Chem.* **2012**, *84*, 8415-8421.

109. Oh, W. K.; Jeong, Y. S.; Kim, S.; Jang, J. *ACS Nano* **2012**, *6*, 8516-8524.

110. Pu, K.; Shuhendler, A. J.; Rao, J. *Angew. Chem. Int. Ed.* **2013**, *52*, 10325-10329.

111. Disney, M. D.; Zheng, J.; Swager, T. M.; Seeberger, P. H. *J. Am. Chem. Soc.* **2004**, *126*, 13343-13346.

112. Zhou, S.; Peng, X.; Xu, H.; Qin, Y.; Jiang, D.; Qu, J.; Chen, H. Y. *Anal. Chem.* **2018**, *90*, 7982-7988.

113. Wang, Y.; Chen, J.; Jiao, H.; Chen, Y.; Li, W.; Zhang, Q.; Yu, C. *Chem. Eur. J.* **2013**, *19*, 12846-12852.

114. Sokolova, V.; Epple, M. *Nanoscale* **2011**, *3*, 1957-1962.

115. Gnach, A.; Bednarkiewicz, A. *Nano Today* **2012**, *7*, 532-563.

116. Wilhelm, S.; Kaiser, M.; Würth, C.; Heiland, J.; CarrilloCarrion, C.; Muhr, V.; Wolfbeis, O. S.; Parak, W. J.; ReschGenger, U.; Hirsch, T. *Nanoscale* **2015**, *7*, 1403–1410.

117. Lia, K.; Liu, B. *Chem. Soc. Rev.* **2014**, *43*, 6570-6597.

118. Wilkins, D. J. *Nature (London)* **1964**, *202*, 798.

119. Gibanel, S.; Heroguez, V.; Gnanou, Y.; Aramedia, E.; Bucsi, A.; Forcada, J.; *Polym. Adv. Technol.* **2001**, *12*, 494-499.

120. Ramırez, L. P.; Landfester, K. *Macromol. Chem. Phys.* **2003**, *204*, 22-31.

CHAPTER-2

Covalent Stitching of π-Conjugated Chromophores into PS nanobeads for Multicolor Emission in Water

Abstract: *This chapter presents the synthesis of fluorescent polystyrene nanoparticles for multicolor emission in water. Fluorescent Polystyrene (PS) nanobeads in the size range ~70 – 120 nm covalently incorporating perylene bisimide (PBI-PS) and/or oligo (p-phenylenevinylene) (OPV-PS) were developed by miniemulsion polymerization technique. A dye loading content (DLC) of < 3 % was sufficient to impart high fluorescence emission capability to the PS beads. OPV- PS exhibited emission in the range 400 – 550 nm with peak emission at 446 nm (λ_{ex} = 350 nm; ϕ_{FL} = 26 %); PBI-PS showed emission from 520 – 650 nm with peak emission at 545 nm (λ_{ex} = 490 nm; ϕ_{FL} = 9.7 %) in 1X PBS buffer, while OPV(PBI)-PS nanobeads incorporating both the fluorophores exhibited multicolor emission capabilities (λ_{ex} from 350 nm to 490 nm). The nanoparticles were characterized by Field emission scanning electron microscopy (FESEM), transmission electron microscopy (TEM) and dynamic light scattering (DLS) for size and zeta potential for surface charge.*

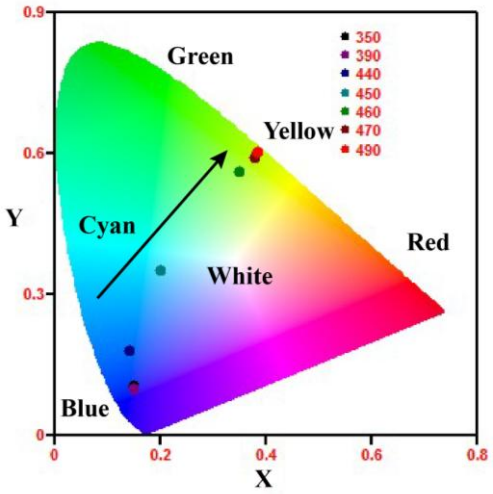

2.1 Introduction:

π-conjugated molecules and polymers are increasingly being explored for their application in fields other than light emitting[1-5]or photovoltaic devices[6-8] like in cellular imaging,[9-13] diagnosis, and biosensing[14-16] (***Figure 2.1***). Their emission color tunability by structural modifications offers a library of molecules to choose from for imaging applications in different wavelength ranges.[17-23] As a pathway to bring in fluorescent moiety into the nanoparticles, different approaches are used by the researchers, as comprised in the previous discussion. Such fluorescent polymeric nanoparticles could be prepared either by post-polymerization techniques with conjugated monomers or encapsulating conjugated dyes into biocompatible polymer matrices.[13,24,25] While these approaches enable the application of π-conjugated molecules and oligomers for cell imaging, there remains some limitations. Like, limited solubility of the π-conjugated molecules makes it difficult for them to get applied into the cellular environment. The difficulty to control the nanoparticle size from the post-polymerization approach and the challenge of avoiding aggregation induced quenching of fluorescence of the π-conjugated fluorophore remains as barrier for such conjugated polymeric nanoparticles.

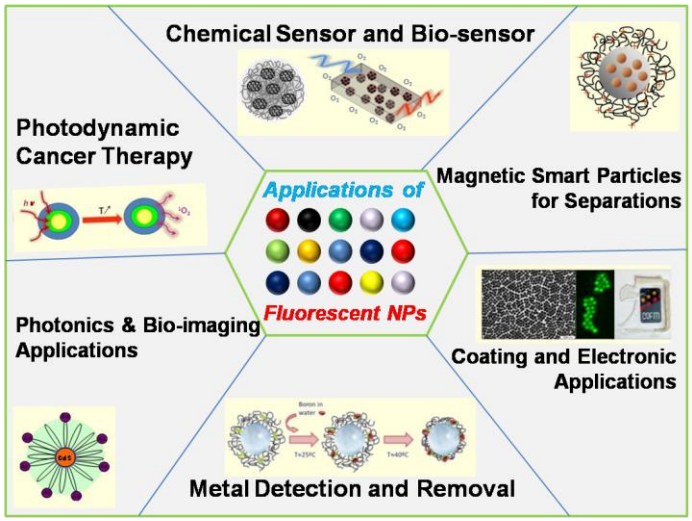

Figure 2.1: Fluorescent properties and applications of few reported polymeric NPs.

In addition, methods involving dye encapsulation into polymeric nanoparticles having weak or non-emissive backbone poses the challenge of dye leakage as well.[17,26,27] Dye leakage into the cell environment not only renders toxicity but also increases background noise thereby weakening the signal to noise ratio. Covalent incorporation of the fluorophores into a carrier polymer backbone could avoid these issues. This approach of covalent linking not only prevents dye leakage but may also enhance the signal to noise ratio for a better imaging output. However, this remains a challenging task because it becomes difficult to get polymeric beads with controlled or narrow particle size

distribution, when the fluorescent conjugated molecules are aimed to be covalently attached to the polymeric backbone. The poor solubility of the rigid aromatic conjugated molecules in the medium of polymerization (generally used like ethanol or water for dispersion or emulsion polymerization) leads to the uncontrollable growth of the beads, resulting in formation of randomly sized beads.

It is synthetically feasible to prepare polymer beads with narrow particle size distribution using polymerization techniques like the emulsion or dispersion polymerization as illustrated through the discussion in ***Chapter 1***. For instance, the group of Katharina Landfester has reported the application of fluorescently labelled polystyrene (PS) particles prepared by miniemulsion polymerization technique as markers for cells.[10] The fluorescent PS particles were prepared by physical entrapment of dyes (***Figure 2.2a***). In this note, dispersion polymerization have been used by Swapnil *et al.* for preparation of fluorescent PS beads with covalently incorporated conjugated molecules *via* dispersion polymerization (***Figure 2.2b***).[28] The rigid π-conjugated fluorophores [based on perylene bisimide (PBI) and oligo (*p*-phenylenevinylene) (OPV)] were incorporated in the form of cross-linkers and they could achieve solid state emitting PS beads in the size range <10 μm. Embedding the fluorophores in the styrene backbone was proven effective in reducing the aggregation induced quenching of fluorescence.

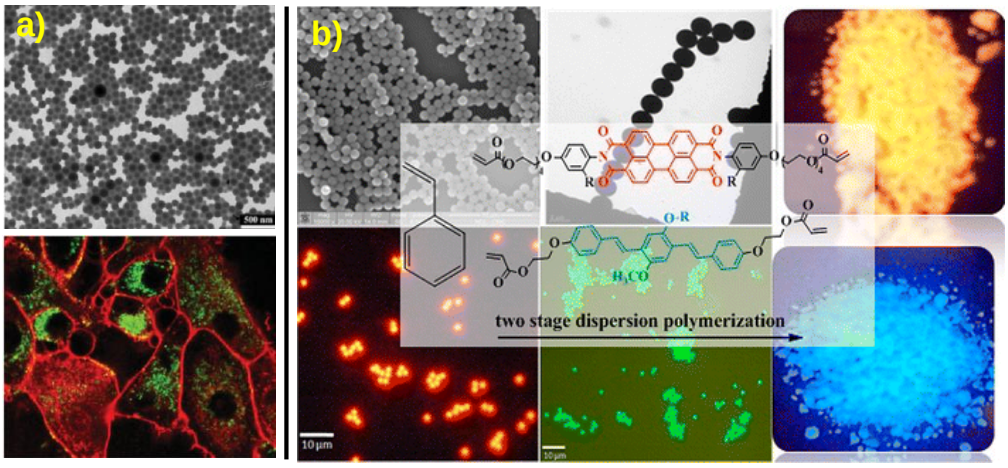

Figure 2.2: a) Polystyrene nanoparticles from miniemulsion polymerization and their uptake observed from confocal fluorescence imaging (Figure is adopted from ***Ref 10***, with permission from Wiley VCH), b) incorporation of different fluorescent dyes in polystyrene nanoparticles for high and tunable emission (Figure is adopted from ***Ref 28***, with permission from ACS Publications).

For tracking the intracellular fate of nanoparticles as well as for cell imaging applications it is required to have some specific characteristics, like (a) The size of PS

beads should fall in the range of 50-150 nm[29], (b) resulting beads must be water dispersible for studying biological applications, (c) quantum yield and brightness in water should have higher value, (d) there should be no dye leakage into the cell environment and (e) their optical properties should not be affected by external trigger, and (f) most importantly the system should be bio-compatible.[30]

Thus in order to achieve the above mentioned requirements, herein we utilized miniemulsion polymerization technique to incorporate OPV and PBI based dyes into polystyrene nanoparticles through covalent attachment. The miniemulsion polymerization is beneficial not only to obtain uniform and monodisperse polystyrene nanobeads in the size range of ~100 nm but also impart water dispersibility to the nanobeads making it suitable for cell imaging application. The miniemulsion polymerization was carried out in presence of water, where an oil-in-water emulsion is formed between the oil (styrene monomer) and water.

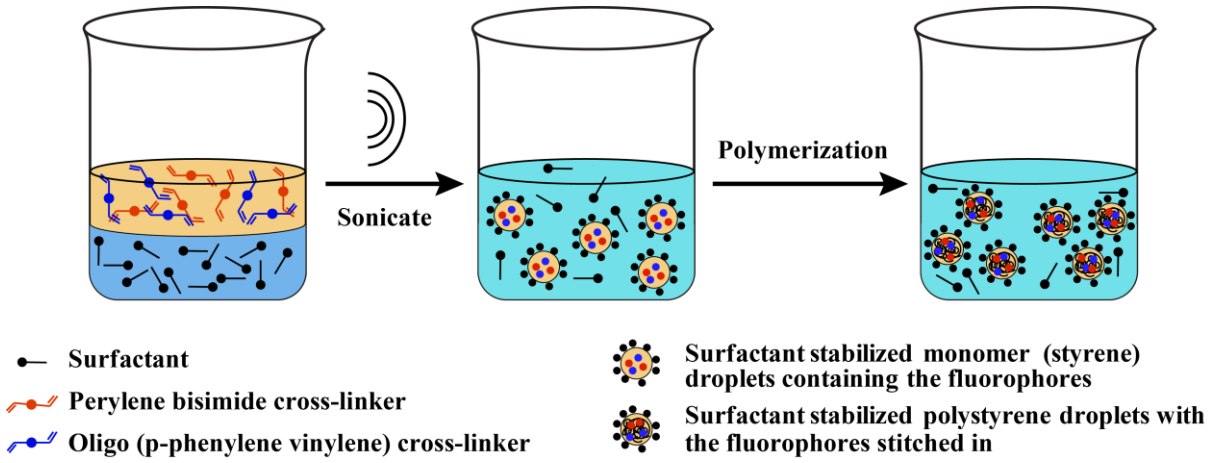

Scheme 2.1: Schematic representation of the synthesis of fluorescent Polystyrene (PS) nanobeads by miniemulsion polymerization, incorporating both OPV and PBI fluorophores for multicolor emission from aqueous medium.

Although the fluorophores are rigid aromatic molecules which are insoluble in water, they have reasonable solubility in the styrene monomer, thereby resolving the previously mentioned solubility issue. OPV and PBI based fluorophores were chosen because of their high emission quantum yield and exceptional photostability. Three different classes of fluorescent PS nanobeads were developed to achieve single and multi-colour emissive PS nanoparticles; (i) PS with OPV based fluorophore *i.e.* OPV-PS-n, (ii) PS with PBI based fluorophore *i.e.* PBI-PS-n and (iii) PS with both the fluorophores (OPV and PBI) together *i.e.* OPV(PBI)-PS. Fluorophores were in form of cross-linkers to

enable their covalent incorporation into PS backbone to prevent any dye leakage into cell microenvironment which is an important yet difficult prerequisite for cell imaging applications. Thus a simple, easy and scalable approach for developing multicolor emitting PS nanoparticles of narrow size distribution suitable for cell imaging application has been presented.

2.2 Results and Discussions:

2.2.1 Synthesis and structural characterization:

The synthesis of the Perylene bisimide (PBI) and oligo (p-phenylenevinylene) (OPV) cross-linkers was reported previously by us.[28,32] ***Scheme 2.2*** and ***Scheme 2.3*** show the structure of the cross-linkers and their incorporation into polystyrene (PS) via miniemulsion polymerization route respectively.

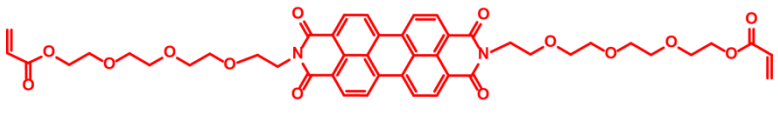

Perylene Bisimide (PBI) based Cross-linker

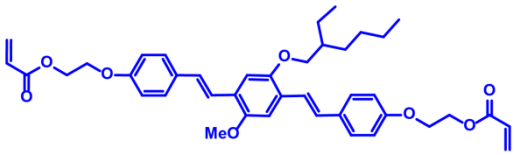

Oligo (p-phenylene vinylene) (OPV) based Cross-linker

Scheme 2.2: Structure of Perylene bisimide (PBI) and Oligo(p-phenylenevinylene) (OPV) based cross-Linkers**.**

Polymerizable fluorophores were synthesized with the aim to covalently stitched the fluorophores into the PS backbone during the polymerization to prevent any dye leakage. The details of the structural characterization of the cross-linkers are given in the ***Section 2.3***.

The miniemulsion polymerization recipe consists of the monomer (styrene with the fluorescent cross-linker dissolved in it), deionized water, surfactant (sodium dodecyl sulfate SDS), water soluble initiator (potassium persulfate (KPS)), and co-stabilizer (hexadecane HD) which are subjected to high shear (by ultrasonication) to obtain small stable droplets. Besides the smaller particle size obtained in miniemulsion polymerization, the other advantages over dispersion polymerization are the higher polymerization rate, higher molecular weights of the resulting polymer as well as the higher incorporation of cross-linkers (both OPV and PBI) into the polystyrene backbone.

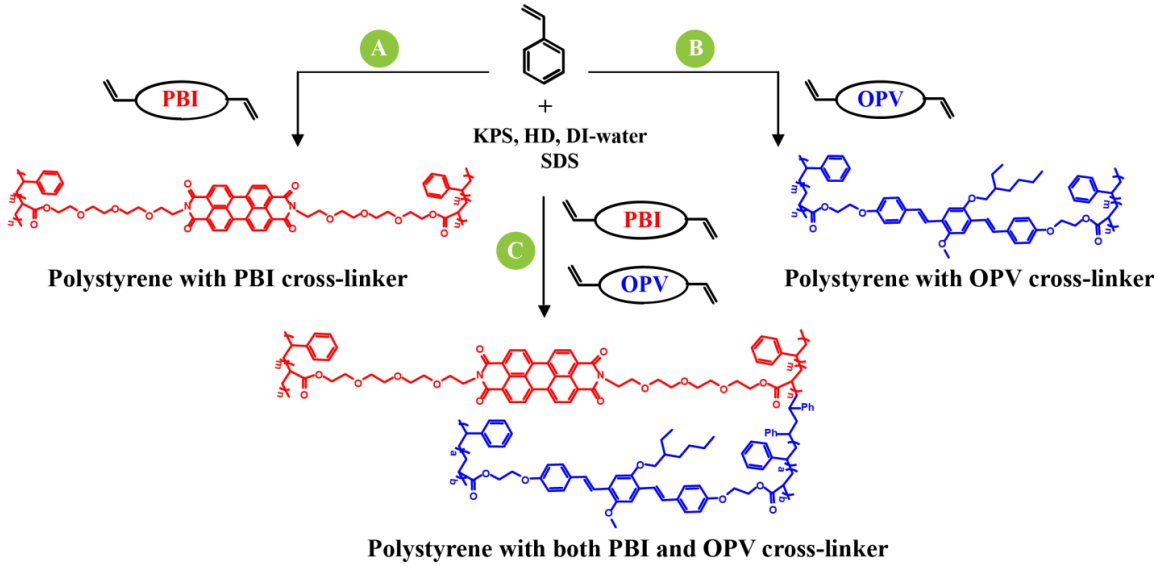

Scheme 2.3: Schematics of miniemulsion polymerization of styrene incorporating (A) PBI (B) OPV (C) Both OPV and PBI based cross-linkers.

Additionally one could also get emission directly through water based latex as this technique does not make use of organic solvent like ethanol which is typically used in dispersion polymerization. This fluorescent PS nanoparticle produced by miniemulsion polymerization are typically negatively charged due to the anionic initiator and unwashed surfactant as confirmed by Zeta potential measured at pH=7 given in ***Table 2.1***. Although positively charged PS NPs are internalized much faster, there are reports that indicated rapid endocytosis of large (~100 nm) negatively charged PS nanoparticles also without much accumulation on the cell membrane.[34] A series of polymers incorporating varying amounts of either PBI or OPV were developed. The OPV in the feed was varied from 0.64 mg/g of styrene to 30 mg/g of styrene and these polymers were labeled as OPV-PS-n. On the other hand, higher amounts of PBI > 10 mg/g of styrene could not be taken in the feed as it remained undissolved in the styrene monomer. Thus, in the PBI-PS-n series, the PBI amount was varied from 0.4–10 mg/g of styrene.

The actual incorporation of the dyes in the PS backbone was determined from their absorption spectra based on their respective coefficient of absorption. The molar extinction coefficient of PBI was 80600 $LM^{-1}cm^{-1}$, and that for OPV was 36315 $LM^{-1}cm^{-1}$.

Table 2.1: Sample designation, Number and Weight Average Molar Mass, Polydispersity indices (Đ), Solid Content (%), Zeta potential (ζ).

Samples	Mn [a]	Mw [a]	PDI [a]	Solid content (%)	ζ-Potential (mV) [b]	TGA (T_d= 5%)
OPV-PS-1	121000	360000	2.9	12.8	-30.5	365
OPV-PS-2	94900	313000	3.3	10.5	-32.1	-
OPV-PS-3	100200	224000	2.2	13.2	-27.1	-
OPV-PS-4	82300	167000	2.0	14.2	-29.0	-
OPV-PS-5	53400	207900	3.8	20.0	-31.8	-
OPV-PS-6	88000	303200	3.4	20.4	-29.7	-
OPV-PS-7	-	-	-	19.8	-33.6	365
PBI-PS-1	74500	207300	2.7	19.3	-30.0	365
PBI-PS-2	97100	280900	2.9	18.6	-27.4	-
PBI-PS-3	152100	651900	4.2	15.3	-35.7	-
PBI-PS-4	117600	358300	3.0	18.0	-34.4	-
PBI-PS-5	126900	360300	2.8	12.7	-30.7	365
OPV(PBI)-PS	59100	242600	4.1	20.5	-31.1	365

a) Measured by Gel Permeation Chromatography (GPC) in tetrahydrofuran (THF) calibrated with linear, narrow molecular weight distribution polystyrene standards.
b) Measured at pH 7 using 0.001 M KCl as background electrolyte.

Figure 2.3 shows the combined plot of feed versus incorporation of both the OPV and PBI dyes in the PS backbone. From the plot, it could be clearly observed that both of them followed a linear trend *i.e.* increasing incorporation with increasing amount of dyes taken in the feed. A polymerization was set up including both OPV and PBI together in the miniemulsion polymerization recipe. Although the fluorophores were cross-linkers their incorporation was much less compared to the styrene (10^{-5} moles of the fluorophore

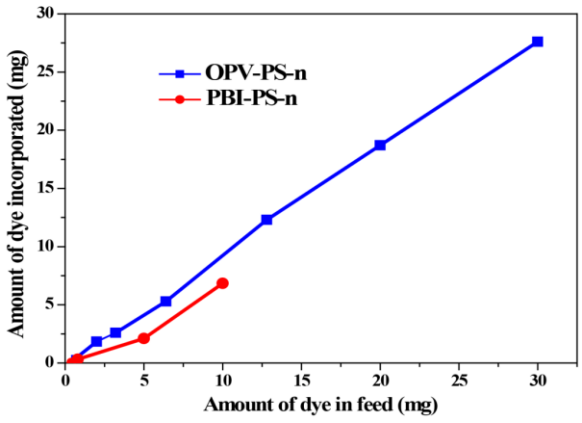

Figure 2.3: Plot of feed versus incorporation of OPV and PBI in the PS backbone.

with respect to styrene). Therefore, almost all the polymers except the ones with the highest fluorophore incorporation remained soluble and could be characterized using size exclusion chromatography (SEC) in THF as eluent. The molecular weights (Mn) were very high ranging from 53,000 to 1,52,000 with polydispersity indices varying from 2.0 to 4.2. The molecular weight of the polymers is provided in ***Table 2.1***. GPC chromatogram in THF are given in ***Figure 2.4A,B*** and the thermal characteristics of selected representative polymers are given in ***Table 2.1*** and their plot in ***Figure 2.4C***.

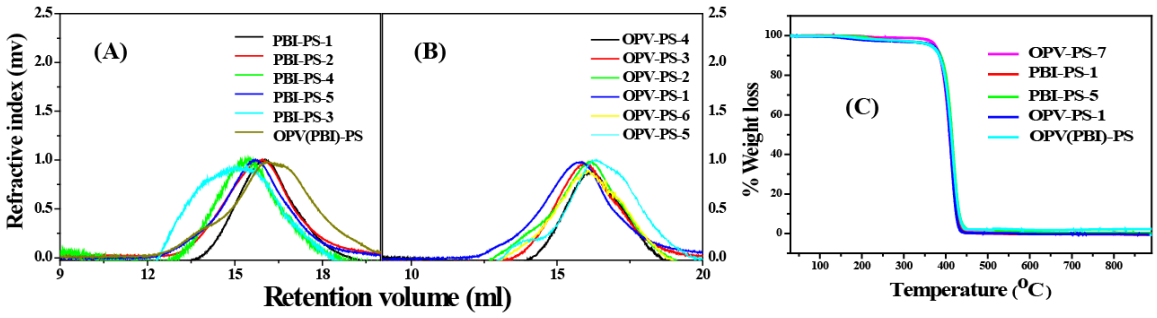

Figure 2.4: GPC Chromatogram of (a) **PBI-PS-n /OPV(PBI)-PS** (left) (b) **OPV-PS-n** polymers (right) in THF with flow rate of 1 ml/min. (c) TGA (Thermogravimetric analysis) of respective polymer samples.

2.2.2 Encapsulation of dyes into nanoparticles:

The signal corresponding to the protons of the fluorophores OPV and PBI could not be detected in the proton NMR spectra of the PS samples even for the highest loading of OPV and PBI as seen in ***Figure 2.5***.

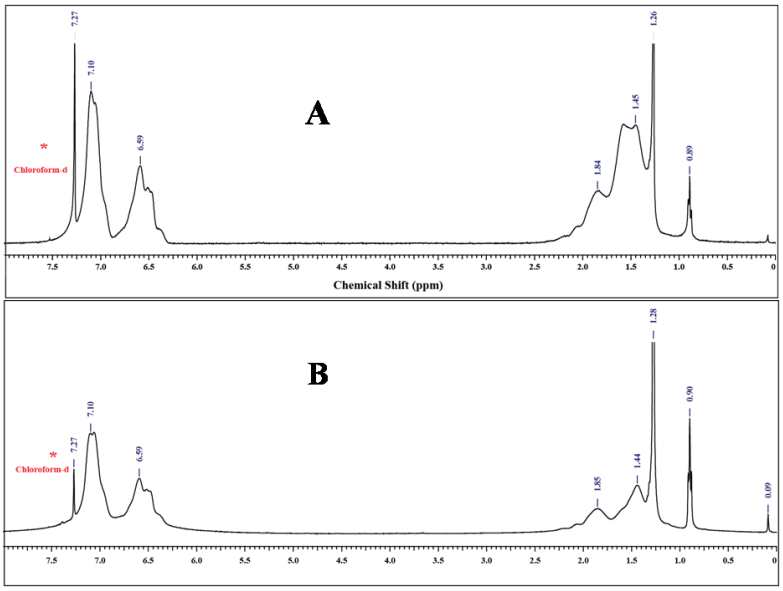

Figure 2.5: ^{1}H-NMR spectra of (a) OPV-PS-7, (b) PBI-PS-5 polymer recorded in $CDCl_3$.

However, their signature could be clearly observed in the absorption spectra recorded in chloroform, from which the dye loading content (DLC) and dye loading efficiency (DLE) could be estimated. The fluorophore incorporation into the PS backbone was expressed as the DLC, which was determined using the absorption spectroscopy. ***Figure 2.6a*** compares a stack plot of the absorption from OPV-PS-n; the inset compares the absorption from pristine PS and OPV cross-linker with that of OPV-PS-7 (all recorded in chloroform). The absorption of OPV exhibited a blue shift upon incorporation into PS backbone from an absorption wavelength maximum of 390 nm in the pristine OPV cross-linker to ~ 365 nm in the polymer. This blue shift is attributed to the π stacking of the aromatic PS units around the OPV chromophores.[28]

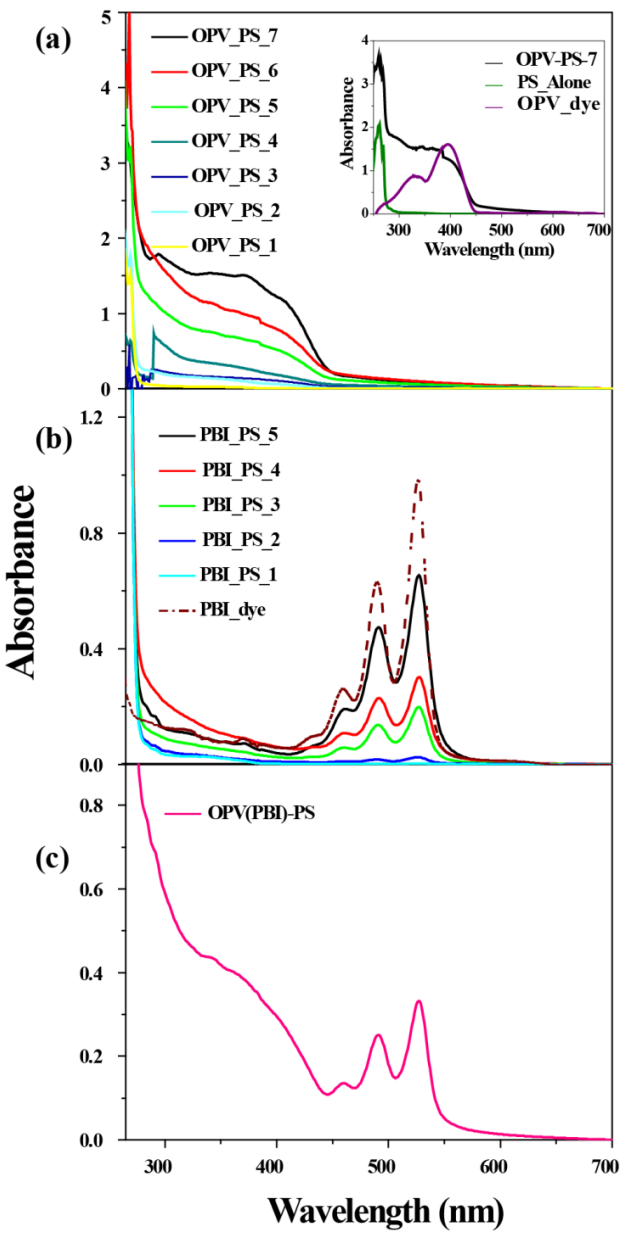

Figure 2.6: Absorption spectra of OPV-PS-n (λ_{max} =365 nm) (a) PBI-PS-n (λ_{max} =527 nm) (b) and OPV(PBI)-PS (c) recorded in chloroform for calculating dye loading content (DLC) (1 mg/ml concentration).

Figure 2.6b shows the absorption spectra of PBI-PS-n recorded in chloroform as the solvent. PBI has a typical absorption with peaks at 475, 490 and 520 nm corresponding to the 0-2, 0-1 and 0-0 transitions respectively. The absorption of the PBI chromophore remained unaffected after its incorporation into the PS backbone, while ***Figure 2.6c*** shows the absorption spectra of OPV(PBI)-PS which showed signature peaks for both OPV and PBI.

The absorption maxima of PBI at 527 nm and that of OPV at 365 nm in the PS sample were used to calculate the DLC and DLE of PBI and OPV respectively.

Calculation details are provided in ***Section 2.3***. The DLC (%) varied from 0.37 to 2.76 for OPV-PS-n, while it ranged from 0.01 to 0.68 for PBI-PS-n and for OPV(PBI)-PS it was 0.74 for OPV and 0.36 for PBI. The DLE for all polymers were also calculated; it varied from 58-96% for OPV-PS-n, 15-68% for PBI-PS-n and in the case of OPV(PBI)-PS where both fluorophores were incorporated, it was 74% for OPV and 72% for PBI. The DLC and DLE values are given in ***Table 2.2***.

Table 2.2: Details of characterization of polymer nanoparticles.

Samples	Amount of dye in feed (mg)	Amount of dye incorporated (mg) [a]	DLC (%) [a]	DLE (%) [a]	Size (nm) [b]	PDI [b]
OPV-PS-1	0.64	0.37	0.04	58	115	0.10
OPV-PS-2	2	1.84	0.18	90	118	0.07
OPV-PS-3	3.2	2.6	0.26	81	111	0.01
OPV-PS-4	6.4	5.3	0.53	83	106	0.12
OPV-PS-5	12.8	12.3	1.23	96	101	0.03
OPV-PS-6	20	18.7	1.87	93	89	0.04
OPV-PS-7	30	27.6	2.76	92	72	0.13
PBI-PS-1	0.4	0.06	0.01	15	100	0.07
PBI-PS-2	0.8	0.32	0.03	40	98	0.04
PBI-PS-3	5	2.1	0.21	42	74	0.15
PBI-PS-4	5	3.2	0.32	64	91	0.04
PBI-PS-5	10	6.85	0.68	68	98	0.11
OPV(PBI)-PS	10 (5)	7.36 (3.6)	0.74 (0.36)	74 (72)	96	0.01

a) Dye Loading content (DLC) and Dye Loading Efficiency (DLE) are calculated by absorption studies in $CHCl_3$.

b) Measured by Dynamic Light Scattering in deionized water.

2.2.3 DLS and Microscopic Analysis of nanoparticles:

The particle size and the particle size distribution of these fluorescent PS samples were determined using dynamic light scattering (DLS) analysis of the polymer particles suspended in deionized water (***Table 2.1***). The particle size varied from 72 nm for the sample with highest OPV incorporation to 118 nm for the sample with lower OPV incorporation. In the PBI series size ranged from 74 nm to 100 nm. The particle size for OPV(PBI)-PS was found to be 96 nm. The PDI values below 0.1 obtained by DLS

indicated monodisperse particles. The combined plot for the intensity average size distribution for all polymers is given in ***Figure 2.7***.

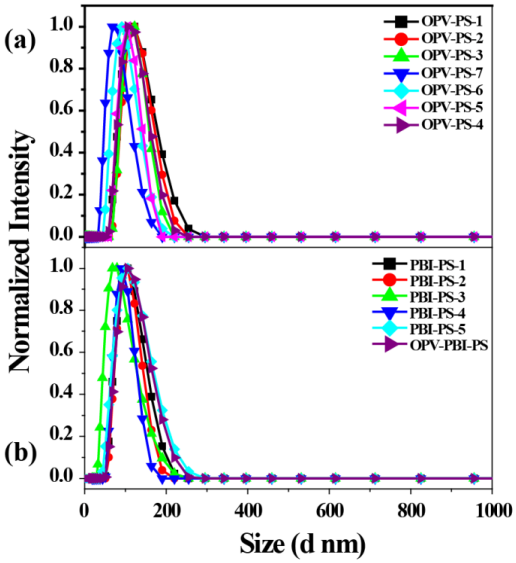

Figure 2.7: Intensity -Average Size distribution of OPV-PS-n (a), PBI/OPV(PBI)-PS (b) polymers in deionized water using Dynamic Light Scattering.

TEM images were also recorded for the samples and ***Figure 2.8*** showed the images for a few representative samples. ***Figure 2.9*** compared the FESEM images of some of the representative fluorescent PS samples. The average particle size observed from the FESEM images was in the range of 75 - 97 nm. The sizes of these fluorescent PS nanobeads from TEM images (72 to 80 nm) were in the similar range as that observed from the FESEM and their values are tabulated in ***Table 2.3***. Particle size obtained from FESEM and TEM was found to be smaller as compared to DLS. This may be due to change in the measurement of particle size between a dried state in FESEM, TEM and hydrated state in DLS. All the three techniques (DLS, TEM, FESEM) confirmed the spherical morphology of polymer nanoparticles in the < 100 nm size range.

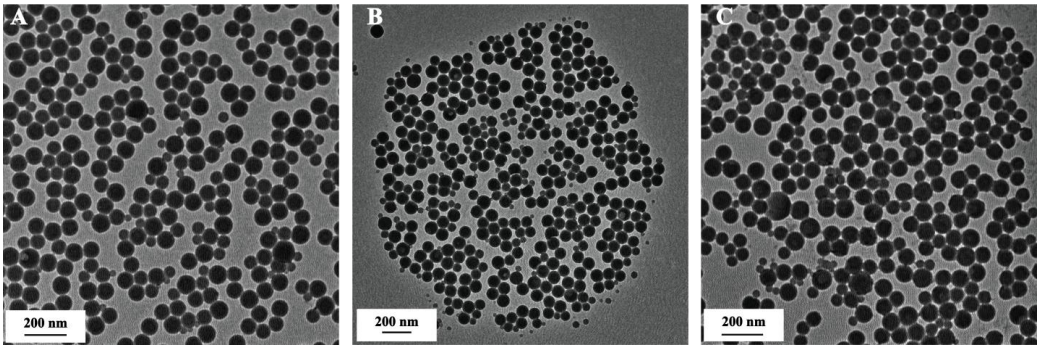

Figure 2.8: TEM image of (A) PBI-PS-4 (B) OPV-PS-6 (C) OPV(PBI)-PS polymers.

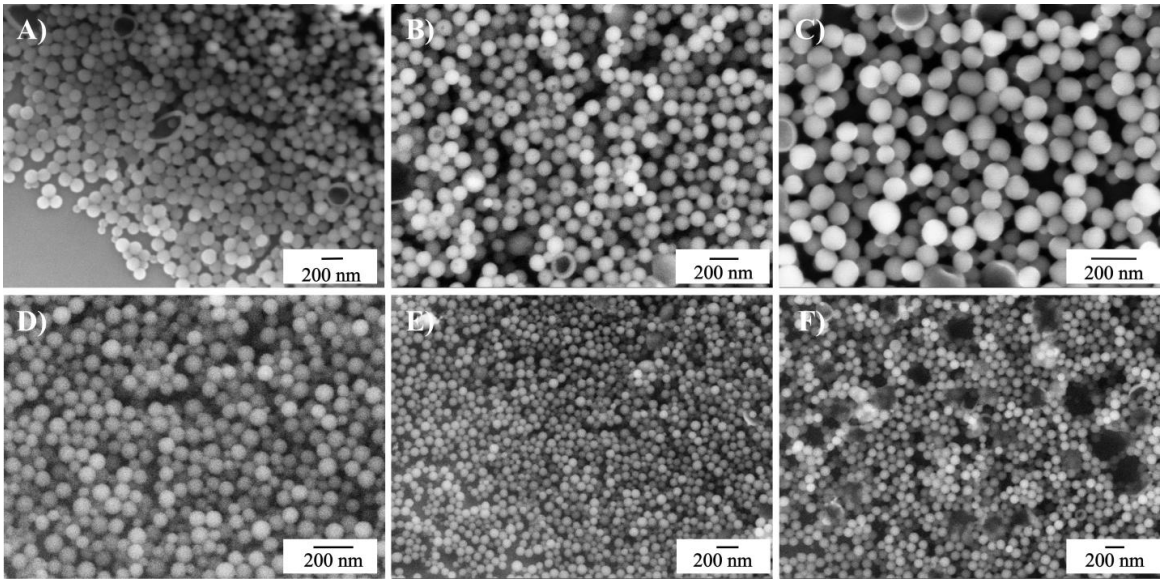

Figure 2.9: FESEM image of (A) OPV-PS-6 (B) OPV-PS-3 (C) OPV-PS-2 and (D, E) PBI-PS-5 (different magnification) (F) OPV(PBI)-PS polymers drop cast on silicon wafer.

Table 2.3: Comparison of average size of particles obtained from TEM and FESEM.

Samples	Average size from TEM (nm)	Average size from FESEM (nm)
OPV-PS-6	75.6±3	76.5±4
OPV-PS-2	-	97.6±9
OPV_PS-3	-	92.9±5
PBI-PS-4	72.4±3	-
PBI-PS-5	-	75.6±6
OPV(PBI)-PS	79.5±5	80.5±4

2.2.4 Photophysical Properties:

Figure 2.10 exhibited the emission as well as excitation spectra of OPV-PS-n polymers (0.1mg/ 3ml) in 1X PBS buffer. The excitation spectra clearly showed the vibronic fine structure with peaks at 345 nm and 365 nm. Increased emission was observed from the OPV-PS-n polymers with increasing incorporation of OPV (see inset). The solution state quantum yield of the OPV-PS-n polymers in 1X PBS buffer was

measured using quinine sulfate in 0.1M H_2SO_4 as standard and the values are given in ***Table 2.3***. The solution state quantum yield also reflected increasing values with increased incorporation of fluo rophore; OPV-PS-7 with the highest OPV incorporation (DLC: 2.76 %) exhibited the highest quantum yield of ϕ_s = 26 % among the OPV-PS-n polymers. ***Figure 2.11*** compared the emission spectra of the PBI-PS-n polymers upon excitation at 490 nm. The solution state quantum yield of the PBI-PS-n polymers in 1X PBS buffer was measured using N,N' bis(hexylheptyl)perylene-3,4:9,10-bis(dicarboximide) in chloroform as standard and the values are given in ***Table 2.2***. In the case of PBI-PS-n polymers, higher incorporation of PBI beyond ~2 mg/g PS resulted in a decrease in emission intensity. Thus, PBI-PS-4 and PBI-PS-5 (DLC: 0.32 and 0.68 % respectively) had lower emission in the 1X PBS buffer solution compared to PBI-PS-3 (DLC: 0.21 %) (Inset). The solution state quantum yield of PBI-PS-3 was the highest (9.7 %) among the PBI-PS-n samples. ***Figure 2.12A*** showed the emission and excitation spectra for OPV/PBI-PS, where the excitation spectrum (collected at 576 nm) clearly showed the features corresponding to both OPV and PBI chromophores. Upon excitation at 350 nm, emission corresponding to OPV in the range 375 – 600 nm was observed, while excitation at 490 nm resulted in perylene emission with a peak at 550 nm. In fact, weak, but clear emission corresponding to perylene could be observed at 550 nm upon exciting at the OPV wavelength of 350 nm also, which is an

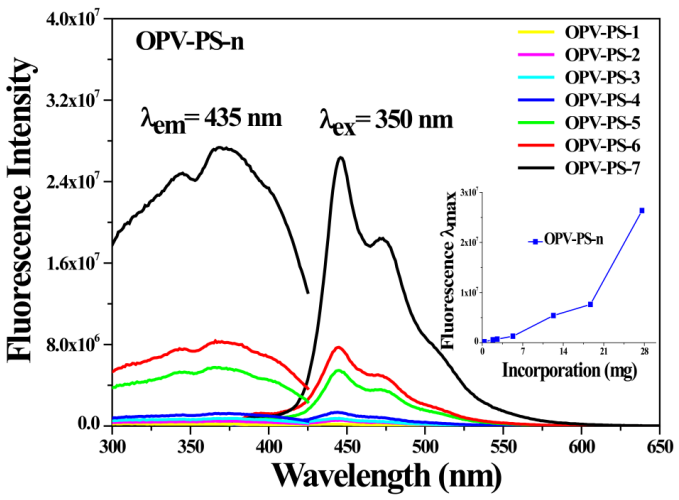

Figure 2.10: Solution state emission and excitation spectra for OPV-PS-n polymers in 1X PBS buffer

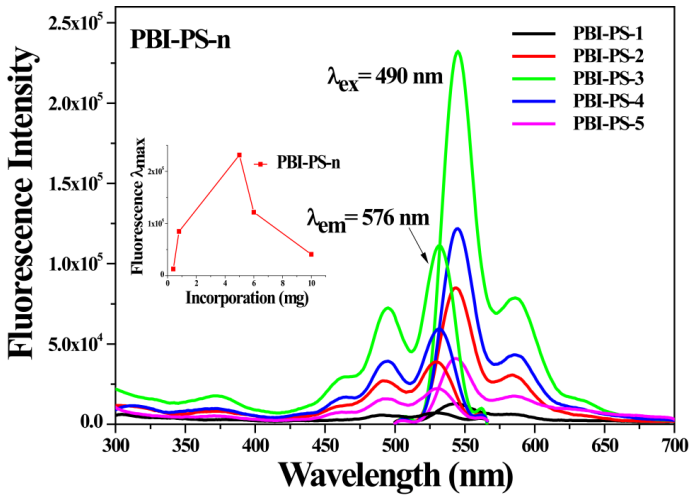

Figure 2.11: Solution state emission and excitation spectra for PBI-PS-n polymers in 1X PBS buffer.

evidence for fluorescence resonance energy transfer (FRET) from the OPV to the PBI donor. This FRET-induced PBI emission appeared stronger than the emission from PBI upon direct excitation at 490 nm. The emission color could also be tuned by mixing the different PS samples incorporating either of the fluorophores. A mixture of OPV-PS-7 and PBI-PS-3 was prepared by mixing each of the two samples at a concentration of 50 µg/ml (named as PS(OPV7+PBI3)). ***Figure 2.12 B*** compared the excitation and emission spectra for this mixture.

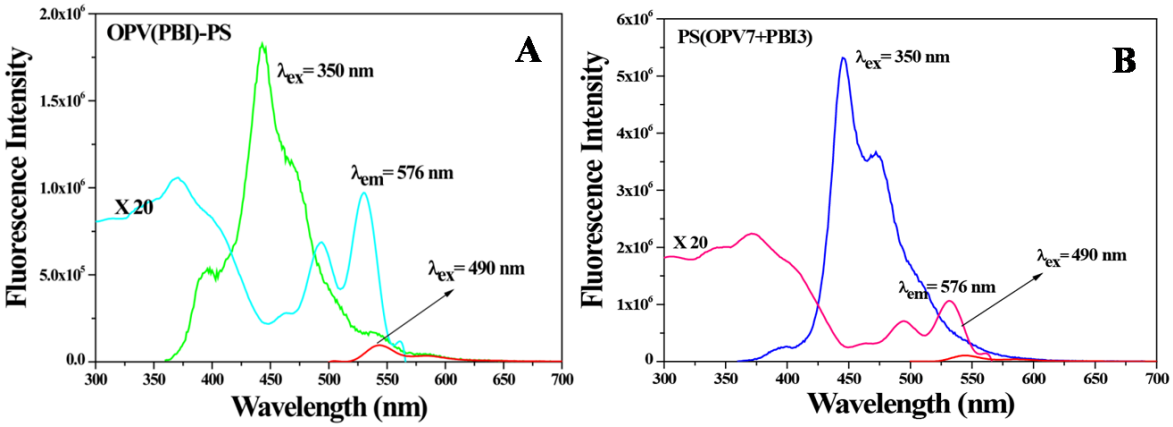

Figure 2.12: Solution state emission and excitation spectra for (a) OPV(PBI)-PS and (b) PS(OPV7+PBI3) in 1X PBS buffer.

A small difference between the PS(OPV7+PBI3) mixture and the PS sample incorporating both OPV and PBI together was the absence of the FRET-induced PBI emission in the former (***Figure 2.13***)

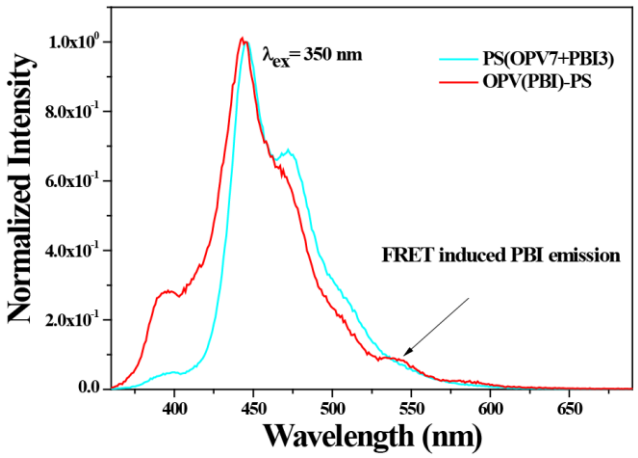

Figure 2.13: Normalized emission spectra upon excitation at 350 nm for PS(OPV7+PBI3) (physical mixture) and OPV(PBI)-PS (covalent) polymer at concentration (0.1 mg/ 3 ml) in 1X PBS buffer showing FRET induced PBI emission in case of covalent OPV(PBI)-PS polymer.

Table 2.4 Emission characteristics of the PS nanoparticles.

Samples	Quantum Yield (%)[a]
OPV-PS-1	0.2
OPV-PS-2	0.8
OPV-PS-3	1.0
OPV-PS-4	2.2
OPV-PS-5	7.2
OPV-PS-6	7.5
OPV-PS-7	26
PBI-PS-1	0.4
PBI-PS-2	1.8
PBI-PS-3	9.7
PBI-PS-4	3.0
PBI-PS-5	0.7
OPV(PBI)-PS	
0.1 OD at 365 nm	3.1 (OPV)
0.1 OD at 532 nm	1.8 (PBI)

(a) Measured in 1X PBS buffer at 0.1 OD.

2.2.5 Multi color emission: The color tunability of these fluorescent PS beads was illustrated using the CIE coordinate diagram. From the diagram, it could be clearly seen that the presence of both the fluorophores in OPV(PBI)-PS polymer afforded a range of excitation wavelength to choose from starting with the blue excitation at 350 nm to the orange yellow wavelength of 490 nm through various shades of cyan and green. (***Figure 2.14a***) Similar CIE coordinate diagrams for the OPV alone (Blue) (***Figure 2.14b***) and PBI alone (yellow) PS samples (***Figure 2.14c***) are also shown to describe their emission color. The CIE values for all the polymers are tabulated in ***Tables 2.5, 2.6***. The polymer samples with the high dye loading content with good emission characteristics (OPV-PS-7 and PBI-PS-3) were taken up for cell uptake studies, along with OPV(PBI)-PS, as stated earlier.

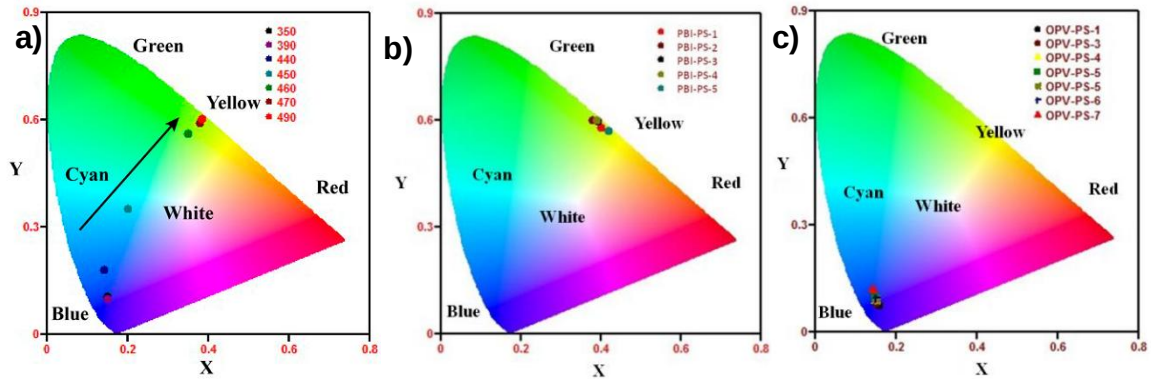

Figure 2.14: a) CIE co-ordinate diagram for OPV(PBI)-PS polymer showing the color tuning by varying the excitation wavelength. CIE coordinate diagrams of b) PBI-PS-n and c) OPV-PS-n nanobeads.

Table 2.5: CIE coordinate values for **OPV(PBI)-PS/ PBI-PS-n .**

Samples	X	Y
OPV-PS-1	0.16	0.12
OPV-PS-2	0.15	0.10
OPV-PS-3	0.16	0.07
OPV-PS-4	0.15	0.09
OPV-PS-5	0.15	0.10
OPV-PS-6	0.15	0.09
OPV-PS-7	0.14	0.12
PBI-PS-1	0.40	0.58
PBI-PS-2	0.38	0.60
PBI-PS-3	0.39	0.60
PBI-PS-4	0.39	0.60
PBI-PS-5	0.42	0.57

Table 2.6: CIE coordinate values for **OPV(PBI)-PS** polymer at different excitation wavelength.

Samples	X	Y
350	0.15	0.11
390	0.15	0.10
440	0.15	0.19
450	0.24	0.39
460	0.37	0.56
470	0.39	0.57
490	0.38	0.60

2.3 Experimental Section:

2.3.1 Materials: Sodium dodecyl sulfate (Reagent plus, 98.5%, Aldrich), hydroquinone (Reagent plus, 99%, Aldrich), zinc acetate (98%, Aldrich), 4-methoxyphenol (Aldrich), 4-hydroxy benzaldehyde (98%, Aldrich), 2-ethylhexylbromide (Aldrich), triethyl phosphite (Aldrich), potassium-tert-butoxide (Aldrich) and Perylene-3, 4, 9, 10-tetracarboxylic dianhydride (PTCDA) (Aldrich) and *n*-Hexadecane (99%, Alfa Aesar) were used as received. Styrene (Aldrich) was first washed with aqueous sodium hydroxide followed by water and then dried for several hours in calcium chloride and distilled under reduced pressure prior to use. Para-formaldehyde, HBr in glacial acetic acid, potassium iodide, potassium carbonate, dimethyl formamide (DMF), dichloromethane (DCM), tetrahydrofuran (THF) and 2-chloroethanol and all the other chemicals were locally purchased and further purified using standard protocols. Potassium peroxodisulfate (ACS reagent, 99%, Aldrich) was recrystallized before use. Deionized water was used throughout the experiments.

2.3.2 Measurements: The instrumentation used for characterization of the fluorescent cross-linkers and the polymers like the NMR, UV and fluorescence spectrophotometer are the same as described in our previous reports.[28] The number-average molar mass (Mn), weight average molar mass (Mw) and polydispersity index (Mw/Mn) of all the polymers were measured by Size exclusion chromatography using Viscotek VE 3580 RI detector in tetrahydrofuran (THF) at a flow rate of 1 $mlmin^{-1}$ and polystyrene standards for calibration. High-resolution mass spectra (ESI) were recorded on ORBITRAP LC-MS/MS mass analyzer (Thermo Scientific, Q Exactive). 20 µg/ml of sample in acetonitrile was injected for recording the spectra. For the miniemulsion polymerizaiton, the emulsion was sonicated using Branson 2510 sonicator. The average size of particles (Z_{avg}) and its polydispersity index (PDI) was measured using Zetasizer ZS 90 apparatus from Malvern instruments at a fixed angle of 90° at 25 °C. Freshly prepared samples were measured thrice in order to check the reproducibility of data. Zeta potential of diluted aqueous dispersions (0.1 mg/ml) were measured by Malvern Zetasizer Nano ZS 90 using 1 mM KCl as background electrolyte at pH= 7. For the fluorescence quantum yield measurement of polymer dispersions in 1X PBS buffer, 0.1 OD of all the polymers were made at their respective absorption maxima and their emission was recorded. The quantum yield of the OPV incorporated polymers were calculated using quinine sulfate in 0.1 M H_2SO_4 as standard while the quantum yield of PBI incorporated polymers was

calculated using N,N'-bis(hexyl heptyl)perylene-3,4:9,10-bis(dicarboximide) in chloroform as standard. Field emission scanning electron microscopy (FESEM) images were taken using Zeiss Ultra plus scanning electron microscope, and the diluted latex samples (3.5 µl/ml) were drop cast onto silicon wafers. Samples were coated with 5 nm thick gold film prior to recording. Transmission Electron microscopic images were taken using FEI-Tecnai^{TM}-F20 electron microscope operating at 200 kV. Diluted samples (3.5µl/ml) drop cast directly on the carbon-coated copper grid and the solvent was allowed to dry at room temperature. Thermogravimetric analyses (TGA) were carried out on SDT Q600 TG-DTA analyzer under N_2 atmosphere at a heating rate of 10 ºC min^{-1} within the temperature range of 30-900 °C.

The Percent Solid content of the latex was determined by the following (eq 1):

$$SC\ (\%) = \frac{W_d}{W_l} \times 100 \quad \text{.....eq 1}$$

where W_d and W_l are the weight of dried polymer and weight of polymer latex respectively. The values for the same are given in ***Table 2.1***

2.3.3 Synthesis of Cross-linkers: The cross-linkers were synthesized using previously reported procedure.[28,32]

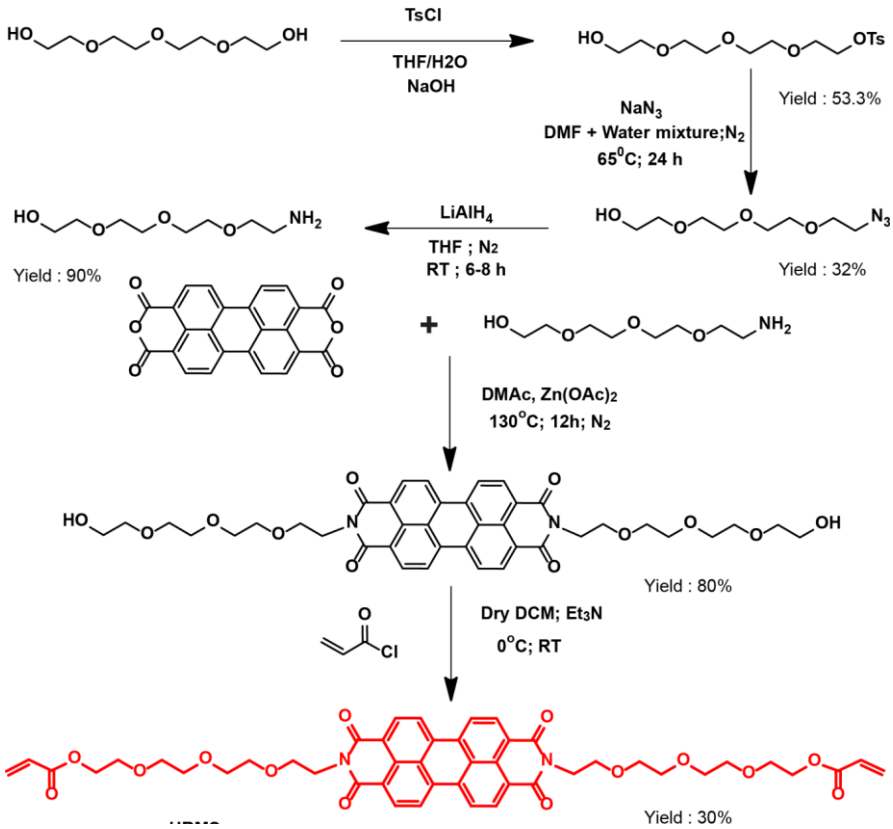

Scheme 2.4 Synthetic Scheme of PBI based Cross-linker.

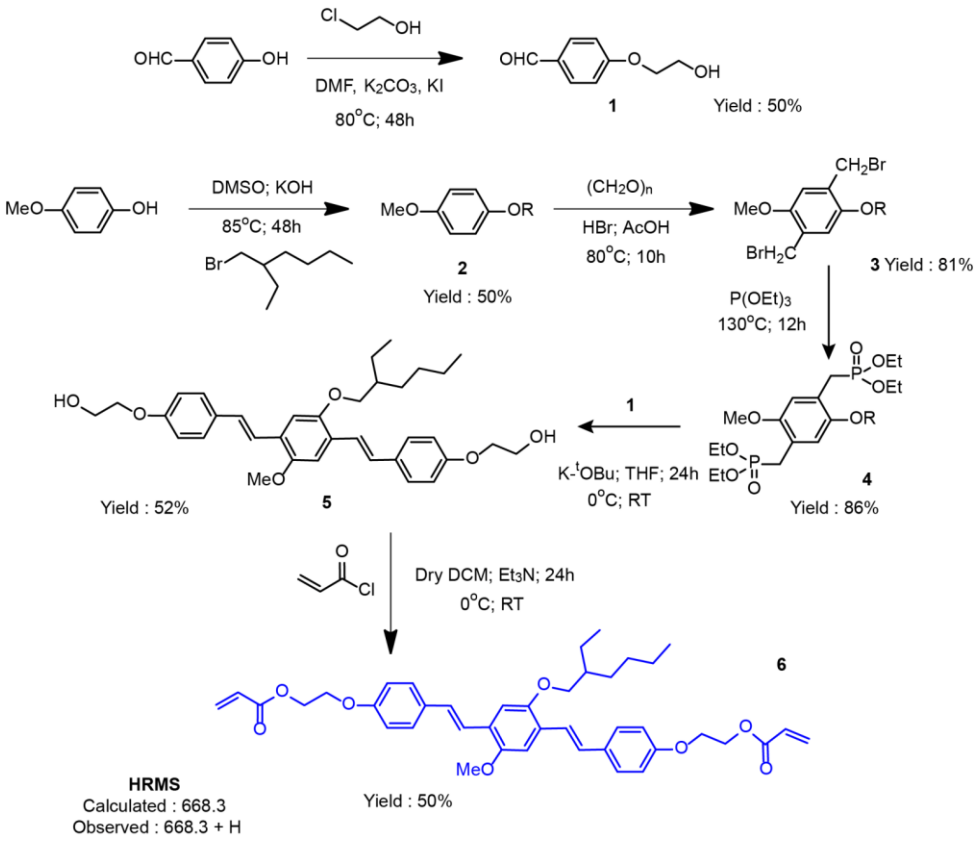

Scheme 2.5 Synthetic Scheme of OPV based Cross-linker.

Synthesis of PBI based cross-linker:

400 mg PBI-TEG diol (5.4×10^{-4} mol) and 0.22 ml triethylamine (2.7×10^{-3} mol) were taken in 250 ml two necked round bottomed flask along with 50 ml dry DCM under nitrogen atmosphere. The flask was kept for stirring under ice cooled condition for 30 min followed by slow addition of acryloyl chloride (0.22 ml, 2.7×10^{-3} mol) over a period of 20 min at 0 °C. After the addition it was brought to room temperature slowly. Then the reaction was allowed to stir for 24 h. The progress of reaction was timely monitored using TLC. The reaction was worked up by washing the organic phase with water and brine and then organic phase was evaporated off. Finally the compound was column purified using DCM/Methanol (1%) as solvent. Yield (30%): 120 mg.

^{1}H-NMR (400 MHz, $CDCl_3$, δ): 8.69 (m, 8H, perylene ring), 6.39 (dd, 2H, acrylic double bond), 6.13 (q, 2H, acrylic double bond), 5.84 (dd, 2H, acrylic double bond), 4.49 (t, 4H, -NCH_2), 4.30 (t, 4H, -NCH_2), 3.89 (t, 4H), 3.62 (m, 20H).

^{13}C-NMR (100 MHz, $CDCl_3$, δ): 165.88, 163.10, 134.32, 131.15, 130.71, 129.09, 128.01, 126.10, 122.83, 77.33, 69.89, 69.83, 67.66, 63.42, 39.07.

LC-MS/MS for $C_{46}H_{46}N_2O_{14}$ (in MeCN): m/z calculated 850.29. Found: 851.30 [M + H], 873.28 [M + Na].

Synthesis of OPV based cross-linker:

In 250 ml two- necked round-bottomed flask, 265 mg OPV diol (4.7×10^{-4} mol) and 0.33 ml of triethylamine (2.4×10^{-3} mol) were dissolved in 50 ml of dry DCM under nitrogen atmosphere. Then it was allowed to stir for 30 min at 0 °C. 0.2 ml (2.4×10^{-3} mol) of acryloyl chloride was taken in DCM and added to the flask for a period of 20 min at 0 °C. Reaction was allowed to stir at room temperature for 24 h and timely monitored by TLC. Crude compound was worked up by washing with water and then organic phase was dried off and it was further purified by column chromatography using Pet ether/ EtOAc (20%) as solvent system. Yield (50%): 132.50 mg.

^{1}H-NMR (400 MHz, $CDCl_3$, δ): 7.49-6.93 (3m, 14H, Ar-H, vinylic H), 6.45 (dd, 2H, acrylic double bond), 6.20 (m, 2H, acrylic double bond), 5.89 (dd, 2H, acrylic double bond), 4.54 (m, 2H, -$ArOCH_2$), 4.27 (m, 2H, -$C(O)OCH_2$), 3.92 (m, 4H), 1.83 (b, 1H, tert), 1.37 (m, 6H), 0.99 (m, 6H).

^{13}C-NMR (100 MHz, $CDCl_3$, δ): 165.85, 163.14, 150.92, 131.10, 127.82, 127.56, 127.41, 121.45.114.6, 71.56, 65.73, 62.86, 56.12, 39.54, 30.89, 30.69, 29.01, 23.98, 22.85, 13.85, 11.07.

LC-MS/MS for $C_{46}H_{46}N_2O_{14}$ (in MeCN): m/z calculated 668.33. Found: 669.34 [M + H], 691.32 [M + Na].

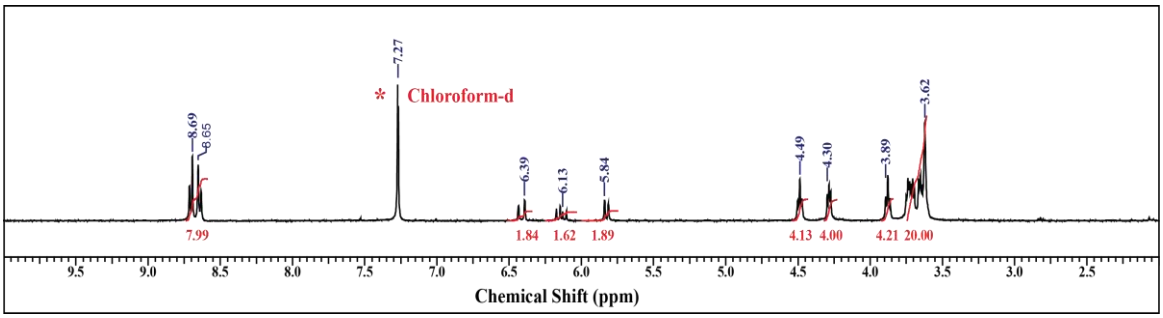

Figure 2.16 ^{1}H-NMR spectra of PBI Cross-linker recorded in $CDCl_3$.

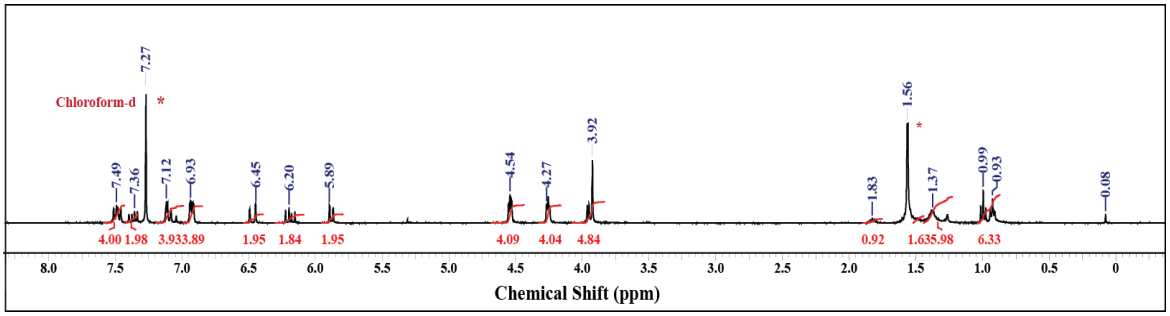

Figure 2.17 ^{1}H-NMR spectra of OPV Cross-linker recorded in $CDCl_3$.

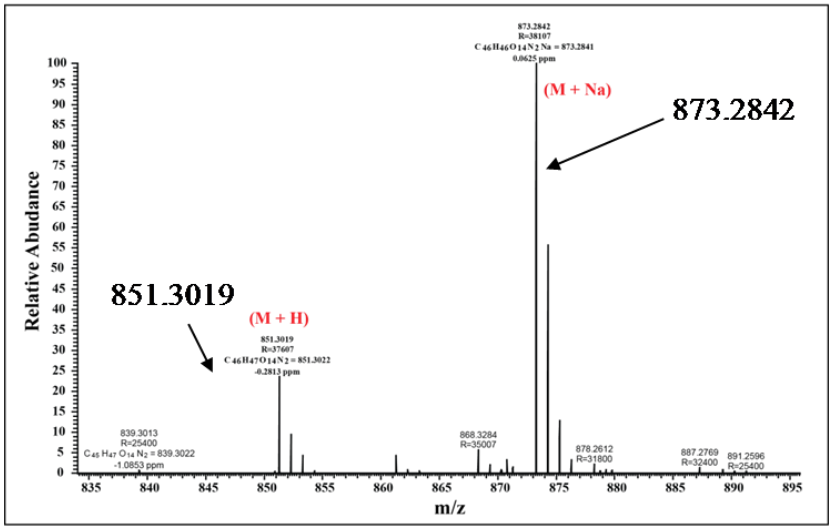

Figure 2.18 LC-MS/MS spectra of PBI Cross-linker recorded in MeCN.

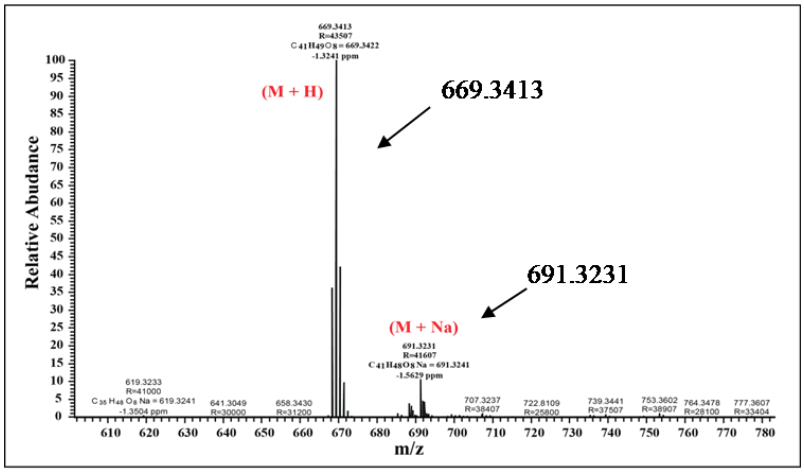

Figure 2.19 LC-MS/MS spectra of PBI Cross-linker recorded in MeCN.

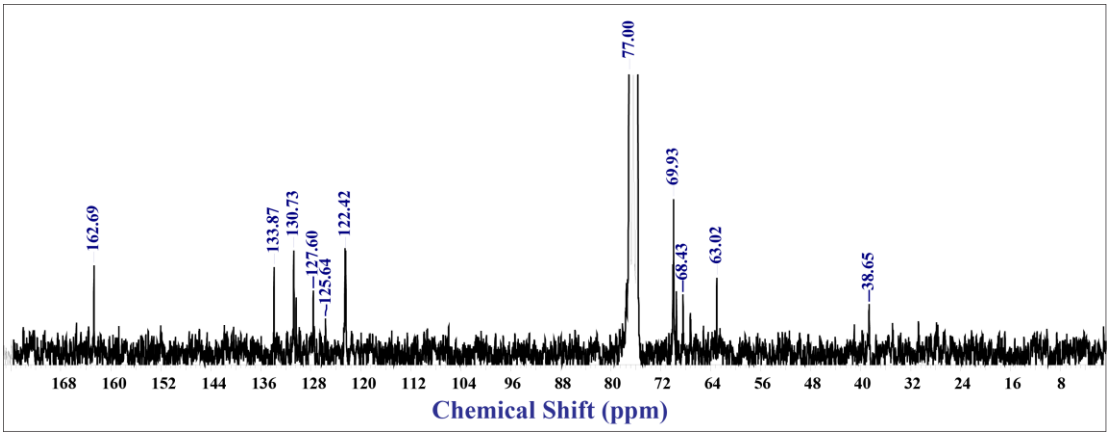

Figure 2.19 ^{13}C-NMR spectra of PBI Cross-linker recorded in $CDCl_3$.

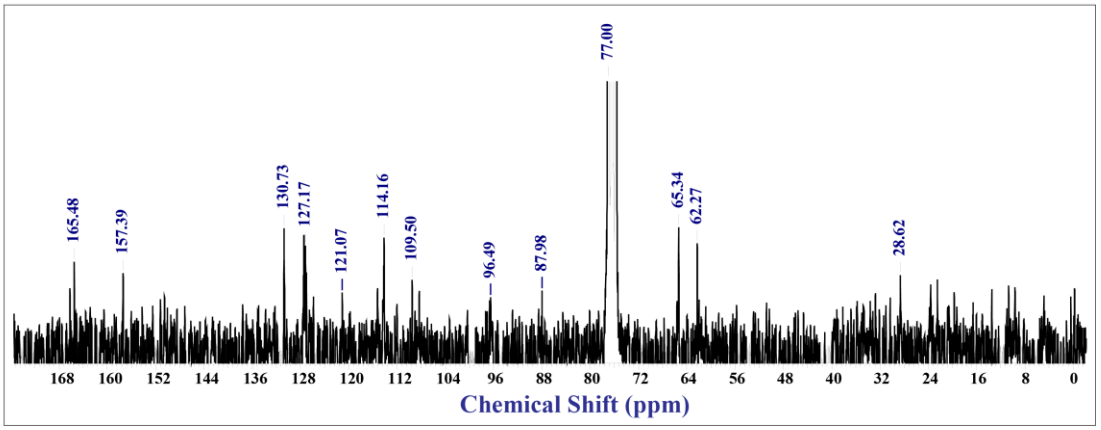

Figure 2.20 ^{13}C-NMR spectra of OPV Cross-linker recorded in $CDCl_3$.

2.3.4 Preparation of Fluorescent Polystyrene nanoparticles: Polystyrene nanoparticles were synthesized by miniemulsion polymerization approach.[31]

The organic phase containing 1 g of styrene, fluorescent cross-linker (varying amount) and 48 mg of hexadecane were mixed and added dropwise into an aqueous phase consisting of 12-36 mg of Sodium Dodecyl Sulfate dissolved in 3.5 g of water. This mixture was stirred at room temperature for 1 h for pre-emulsification. Miniemulsion was obtained by sonicating the mixture for 20 min in an ice cooled bath. To start the polymerization, 3.3 mg of KPS in 0.5 g of water was added and the temperature was increased to 80 ^{0}C for 8 h with stirring (speed fixed at 750 rpm). After 8 h polymerization was stopped using two drops of 1 wt% hydroquinone solution. The recipe is tabulated in ***Table 2.5***. The latex was dialyzed using 6000 kDa cut-off cellulose dialysis bag against deionized water for 4 days to remove excess surfactant.

Table 2.5 Recipe for miniemulsion polymerization.

Components	Amount
Water	4 g
Styrene	1 g
Cross-linker	Varied
Hexadecane	48 mg
SDS	12-36 mg
KPS	3.3 mg

2.3.5 Calculation of DLC and DLE: Dye Loading Content (DLC) and Dye Loading Efficiency (DLE) were determined by absorption spectroscopy. 3 mg of dried polymer was dissolved in 3 ml of Chloroform and the absorbance of the solution was recorded at 365 nm for OPV polymers and at 525 nm for PBI polymers which corresponded to the absorption wavelength maxima for the respective dyes. The amount of dye incorporated into the polymer nanoparticle was then calculated based on the molar extinction coefficient of the respective dyes (PBITEG = 80600 $LM^{-1}cm^{-1}$, OPV = 36315 $LM^{-1}cm^{-1}$).[32] DLC and DLE were determined by using following equation (eq 2, 3)[33]:

$$DLC = \frac{\text{Weight of dye encapsulated in nanoparticle}}{\text{Weight of dye loaded nanoparticle}} \times 100 \quad \text{.....eq 2}$$

$$DLE = \frac{\text{Weight of dye encapsulated in nanoparticle}}{\text{Weight of dye in feed}} \times 100 \quad \text{.....eq 3}$$

2.4 Conclusion:

We have presented a simple method of developing fluorescent nanobeads which could be used for cell imaging applications based on commodity polymers like polystyrene. The miniemulsion polymerization technique enabled the synthesis of fluorescent PS particles with narrow particle size distribution in the ~100 nm range. Multiple fluorophores have been inserted into the single bead without significantly affecting its size. Spherical morphology of nanobeads was confirmed by FESEM as well as TEM. The covalent incorporation of the fluorophores (in the form of cross-linkers) ensured the absence of dye leakage and the PS backbone also reduced aggregation induced self-quenching of fluorescence of the dyes. The fluorophores chosen – OPV and PBI based are known for their high fluorescence quantum yields and excellent

photostability. Adaptation of this technique also led to increased dye loading from 10^{-7} moles (*via* dispersion polymerization)[28,32] to 10^{-5} moles (current work) (almost 100 times more) and the result is higher quantum yield in water. In fact, quantum yield for OPV-PS-7 was found to be 26% in water which is highest for any OPV based system in water. Based on emission properties, Polymers with highest quantum yield and emission in water *i.e.* OPV-PS-7 and PBI-PS-3 were chosen further for bio-imaging application along with one having both OPV and PBI fluorophores *i.e.* OPV(PBI)-PS.

NOTE: The results presented in this chapter are already published as a part of publication in *ACS Biomater. Sci. Eng.* **2017**, *3*, 1788-1798 with the title '*π-Conjugated Chromophore Incorporated Polystyrene Nanobeads as Single Optical Agent for Three-Channel Fluorescent Probe in Bioimaging Application*'.

2.5 References:

1. Ego, C.; Marsitzky, D.; Becker, S.; Zhang, J.; Grimsdale, A. C.; Müllen, K.; MacKenzie, J. D.; Silva, C.; Friend, R. H. *J. Am. Chem. Soc.* **2003**, *125*, 437−443.

2. Hubijar, E.; Papadimitratos, A.; Lee, D.; Zakhidov, A.; Ferraris, J.P. *J. Phys. Chem. B* **2013**, *117*, 4442−4448.

3. Tanaka, H.; Herland, A.; Lindgren, L. J.; Tsutsui, T.; Andersson,M. R.; Inganas, O. *Nano Lett.* **2008**, *8*, 2858−2861.

4. Tu, G.; Mei, C.; Zhou, Q.; Cheng, Y.; Geng, Y.; Wang, L.; Ma,D.; Jing, X.; Wang, F. *Adv. Funct. Mater.* **2006**, *16*, 101−106.

5. Grimsdale, A. C.; Chan, K. L.; Martin, R. E.; Jokisz, P. G.; Holmes, A. B. *Chem. Rev.* **2009**, *109*, 897−1091.

6. Jiang, Y.; McNeill, J. *Chem. Rev*. **2017**, *117*, 838−859.

7. Narasimha, K.; Jayakannan, M. *ACS Appl. Mater. Interfaces* **2014**, *6*, 19385−19396.

8. Sharma, S.; Kolhe, N. P.; Gupta, V.; Bharti, V.; Sharma, A.; Datt, R.; Chand, S.; Asha, S. K. *Macromolecules* **2016**, *49*, 8113−8125.

9. Wu, W. C.; Chen, C. Y.; Tian, Y.; Jang, S. H.; Hong, Y.; Liu, Y.;Hu, R.; Tang, B. Z.; Lee, Y. T.; Chen, C. T.; Chen, W. C.; Jen, A. K. Y. *Adv. Funct. Mater.* **2010**, *20*, 1413−1423.

10. Holzapfel, V.; Musyanovych, A.; Landfester, K.; Lorenz, M. R.; Mailänder, V. *Macromol. Chem. Phys.* **2005**, *206*, 2440−2449.

11. Wolfbeis, O. S. *Chem. Soc. Rev.* **2015**, *44*, 4743−4768.

12. Zaquen, N.; Lu, H.; Chang, T.; Mamdooh, R.; Lutsen, L.;Vanderzande, D.; Stenzel, M.; Junkers, T. *Biomacromolecules* **2016**, *17*, 4086−4094.

13. Reisch, A.; Klymchenko, A. S. *Small* **2016**, *12*, 1968−1992.

14. Pu, K.; Shuhendler, A. J.; Rao, J. *Angew. Chem. Int. Ed.* **2013**, *52*, 10325−10329.

15. Pu, K.; Shuhendler, A. J.; Jokerst, J. V.; Mei, J.; Gambhir, S. S.;Bao, Z.; Rao, J. *Nat. Nanotech.* **2014**, *9*, 233−239.

16. Gao, X.; Feng, G.; Manghnani, P.N.; Hu, F.; Jiang, N.; Liu, J.;Liu, B.; Sun, J. Z.; Tang, B. Z. *Chem. Commun.* **2017**, *53*, 1653−1656.

17. Bao, B.; Tao, N.; Yang, D.; Yuwen, L.; Weng, L.; Fan, Q.;Huang, W.; Wang, L. *Chem. Commun.* **2013**, *49*, 10623−10625.

18. Jiang, K.; Sun, S.; Zhang, L.; Lu, Y.; Wu, A.; Cai, C.; Lin, H. *Angew. Chem. Int. Ed.* **2015**, *54*, 5360−5363.

19. Huang, J.; Liu, Y.; Qian, C. G.; Sun, M. J.; Shen, Q. D. *RSC Adv.* **2014**, *4*, 3924−3928.

20. Feng, X.; Yang, G.; Liu, L.; Lv, F.; Yang, Q.; Wang, S.; Zhu, D. *Adv. Mater.* **2012**, *24*, 637−641.

21. Feng, L.; Liu, L.; Lv, F.; Bazan, G. C.; Wang, S. *Adv. Mater.* **2014**, *26*, 3926−3930.

22. Wu, C. F.; Bull, B.; Szymanski, C.; Christensen, K.; McNeill, J. *ACS Nano* **2008**, *2*, 2415−2423.

23. Pecher, J.; Huber, J.; Winterhalder, M.; Zumbusch, A.; Mecking, S. *Biomacromolecules* **2010**, *11*, 2776−2780.

24. Li, K.; Liu, B. *Chem. Soc. Rev.* **2014**, *43*, 6570−6597.

25. Zhu, C.; Liu, L.; Yang, Q.; Lv, F.; Wang, S. *Chem. Rev.* **2012**, *112*, 4687−4735.

26. Zhang, X.; Yu, J.; Wu, C.; Jin, Y.; Rong, Y.; Ye, F.; Chiu, D. T. *ACS Nano* **2012**, *6*, 5429−5439.

27. Sauer, R.; Turshatov, A.; Baluschev, S.; Landfester, K. *Macromolecules* **2012**, *45*, 3787−3796.

28. Sonawane, S. L.; Asha, S. K. *ACS Appl. Mater. Interfaces* **2013**, *5*, 12205−12214.

29. Win, K. Y.; Feng, S. S. *Biomaterials* **2005**, *26*, 2713−2722.

30. Shang, L.; Nienhaus, K.; Jiang, X.; Yang, L.; Landfester, K.;Mailänder, V.; Simmet, T.; Nienhaus, G. U. *Beilstein J. Nanotechnol.* **2014**, *5*, 2388−2397.

31. Ramírez, L. P.; Landfester, K. *Macromol. Chem. Phys.* **2003**, *204*, 22−31.

32. Sonawane, S. L.; Asha, S. K. *J. Phys. Chem. B* **2014**, *118*, 9467−9475.

33. Kulkarni, B.; Surnar, B.; Jayakannan, M. *Biomacromolecules* **2016**, *17*, 1004−1016.

34. Montalti, M.; Battistelli, G.; Cantelli, A.; Genovese, D. *Chem. Commun.* **2014**, *50*, 5326−5329.

CHAPTER-3

Application of π-Conjugated Chromophores Incorporated PS Nanobeads for Bio-imaging in Cancer Cells

Abstract: *The fluorescent PS nanobeads (synthesized in Chapter-1) incorporating two different chromophores, covalently stitched to the polymeric backbone were used for bio-imaging applications after incubation with HeLa cells, where more than 95% cell viability confirmed the biocompatibility of the PS nanobeads. The cellular uptake of the nanoparticles was confirmed by flow cytometry analysis and confocal laser scanning microscopy (CLSM) images. The sub-cellular localization of the nanoparticles in the cytoplasm could be precisely established by their simultaneous multicolor emission, which ruled out any influence from the background emission. The PS based single optical agent presented here can function as three-channel fluorescent probe to meet the requirements of multicolor bio-imaging materials.*

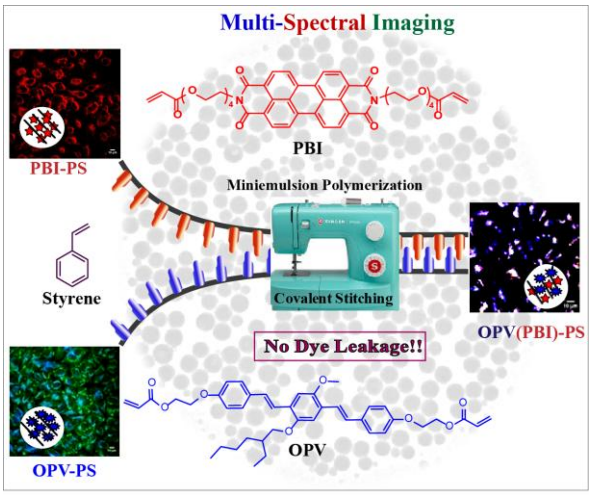

3.1 Introduction:

Interesting properties of π-conjugated molecules and polymers made them increasingly interesting for application in various fields[1-5] and this allowed development of a library of luminescent species as per the requirement for a particular application. As discussed in ***Chapter 1***, fluorescent polymeric nanoparticles are of high interest for various applications including bio-imaging[6-10], where the emission property from suitable fluorophore plays the crucial role. Especially for bio-imaging applications, it is very important to be able to identify the location of the fluorophore inside the cell environment without conflicting background emission. The literature cites the application of near infrared (NIR) emitting fluorophores specifically to address this issue of overcoming the autofluorescence from the cellular components (usually in the blue and green range).[11-13] However, the requirement of specific NIR detecting spectrofluorimeter combined with the challenges of synthesizing the NIR dyes sometimes limits their application. Other tested materials for bio-imaging applications include quantum dots, upconverting nanoparticles *etc*. (***Figure 3.1***) which often suffer from limitations like emission variation with temperature and pH, leaching of the toxic substances into the cell environment etc, making them less useful for the desired purpose.[4,14-18] On the other hand, several of the visible light emitting organic fluorophores could be taken together in a nanoparticle form to attain tuned emission over several wavelengths. The multicolor emission could be applied as a specific method to locate the position of the emitting species within the cellular compartment and to enhance the resolution contrast of the image.

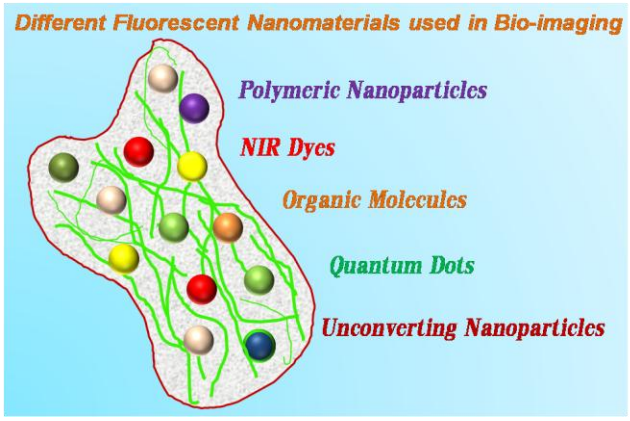

Figure 3.1: illustration of fluorescent materials for bio-imaging application.

π-conjugated fluorescent polymers, in the polyelectrolyte form, which are more soluble in aqueous media, have been utilized for bio-imaging. In fact, in the polyelectrolyte form, they have also been reported to be endowed with biocidal capability against several pathogens.[19,20] Poly (*p*-phenylenevinylene) (PPV) is a π-conjugated fluorescent polymer well studied in photovoltaic applications due to its high emission quantum yields, which have recently found their place in bio-imaging applications as well.[19-22] Bhagyashree *et*

al. reported for the first time the application of the oligo (*p*-phenylenevinylene) (OPV) labeled polycaprolactone (PCL) encapsulated doxorubicin as a dual functional nanocarrier for cellular imaging and anticancer drug delivery to cancer cells (***Figure 3.2A***).[22] Perylene bisimide (PBI) is another π conjugated molecule with very high fluorescence quantum yields and emission in the range > 550 nm, which is preferred for bio-imaging (***Figure 3.2B***).[23,24]

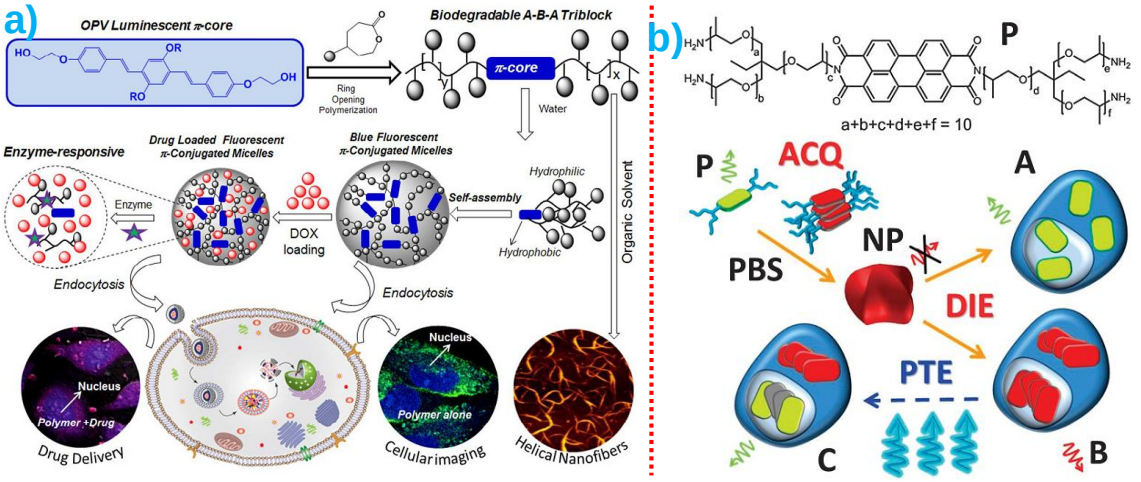

Figure 3.2: a) An oligo (*p*-phenylenevinylene) (OPV) labelled polycaprolactone (PCL) encapsulated doxorubicin, as a dual functional nanocarrier for cellular imaging and anticancer drug delivery to cancer cells [Figure is adapted from ***Ref 22*** with permission from ACS Publications]; b) self-assembly of a PBI based moiety for nanoparticle formation to behave as fluorogenic probes for biological cells under physiological conditions giving a dosage-dependent emission [Figure is adapted from ***Ref 24*** with permission from RSC Publishers]

Polystyrene (PS) nanoparticles are routinely used for cell marker studies due to their proven biocompatibility.[4,25,26] They are internalized by cells following which they are traced using characterization techniques like the flow cytometry, fluorescence microscopy etc. As described in the previous chapter, miniemulsion polymerization technique could be effectively used to incorporate one or multiple fluorophores into the polymeric nanoparticles without much affecting its particle size, together with the advantage of covalent incorporation of the fluorophores into a carrier polymer backbone which could avoid the issues of any dye leakage into cell environment.[14,27]

As observed during the emission studies, the solution state quantum yield in water was observed to be highest for OPV-PS-7 in terms of OPV emission among the PS nanoparticles bearing OPV as the covalently attached dye. Similarly, PBI emission was found to be most efficient for PBI-PS-3 from the family of nanobeads having PBI fluorophore. Thus, these two polymeric nanoparticles were selected for the bio-imaging

studies, along with the nanoparticle having both of the fluorophores (OPV(PBI)-PS). However, for studying possible cytotoxic behavior of the dyes from the nanoparticles, the nanoparticles with highest content of the dye were deliberately chosen. In this chapter, we reported the cell uptake (HeLa and MCF-7 cells) and multicolor imaging using fluorescent polystyrene (PS) nanobeads developed by miniemulsion polymerization.

3.2 Results and Discussions:

3.2.1 Photophysical Properties: As a prerequisite for exact determination of the fluorescent tags after loading into the cell, constant emission under different applied conditions is expected from the imaging substance. Thus, to verify the candidature of the mentioned PS nanobeads as suitable imaging agent, their emission was recorded under different temperature and pH. ***Figure 3.3*** depicted the effect of change in temperature within the range of 0 °C to 60 °C on the emission property of (a) OPV-PBI-PS, (b) OPV-PS-7 and (c) PBI-PS-3. Figure clearly demonstrated that the change in temperature has negligible effect to cause any change in the emission property of the fluorophores attached to the PS nanobeads.

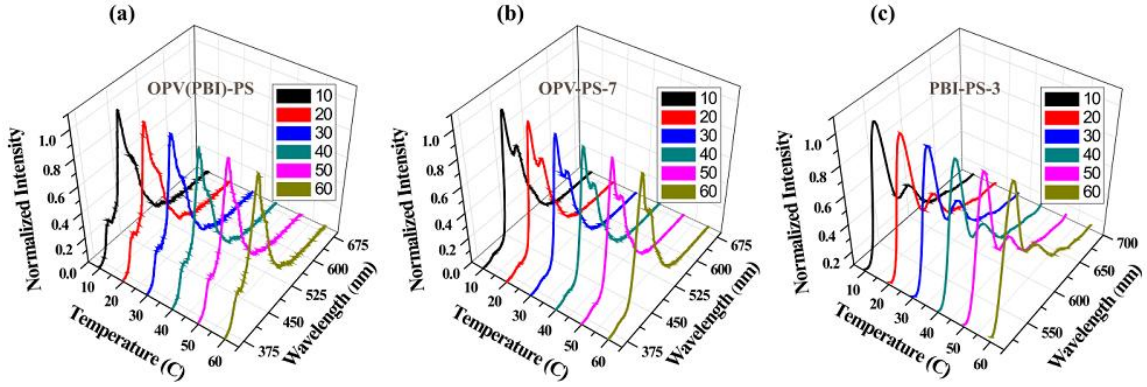

Figure 3.3: Solution state emission spectra showing the dependence of fluorescence intensity on temperature varied from 0 °C to 60 °C for a) OPV(PBI)-PS b) OPV-PS-7 (c) PBI-PS-3 nanobeads (0.1 mg/ 3 ml) in 1X PBS buffer.

When these nanobeads were exposed to different conditions in terms of pH of the medium, their emission was again found to remain unaltered throughout the whole spectrum of pH, as shown in the following ***Figure 3.4***. This further concludes that the change in pH of the external medium does not have any role in bringing out a change to the emissive behaviour of the fluorophores covalently stitched to the polystyrene backbone.

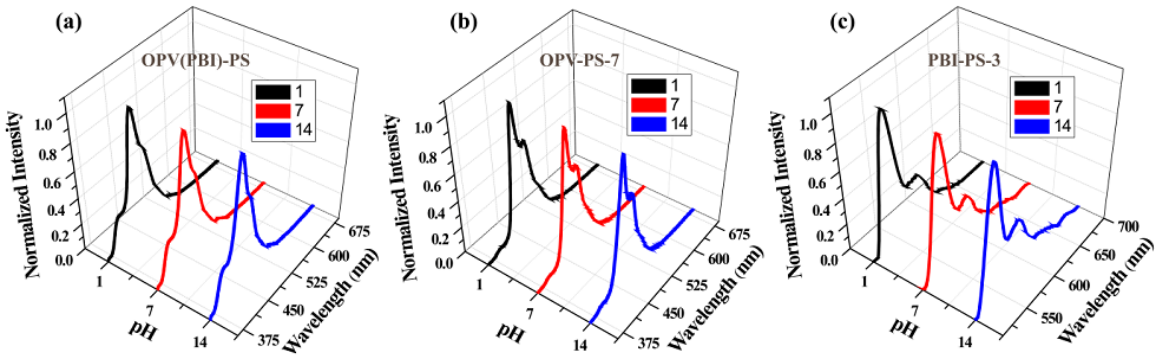

Figure 3.4: Solution state emission spectra showing the dependence of fluorescence intensity on pH varied from 1 to 14 for a) OPV(PBI)-PS b) OPV-PS-7 and (c) PBI-PS-3 nanobeads (0.1 mg/ 3 ml) in 1 X PBS buffer.

Thus results evidently signified that unlike quantum dots and upconverting nanoparticles, the emission from the PS nanoparticles remained steady throughout the entire temperature as well as pH range. The highly hydrophobic nature of polystyrene prevents the contact of the covalently embedded dye molecule with water and thus the fluorescence intensities of the polymer nanoparticles remains stable over a wide range of temperature and pH.

3.2.2 Fluorescence optical microscopic imaging: The Fluorescence optical microscopic images were collected for ethanol dispersion of the samples on glass substrate to once again establish their applicability as multicolor emitting nanoparticles. For imaging OPV, DAPI (Blue, 350-430 nm) filter was used, whereas, for PBI, Rhodamine (Red, 480-580 nm) and Alexa

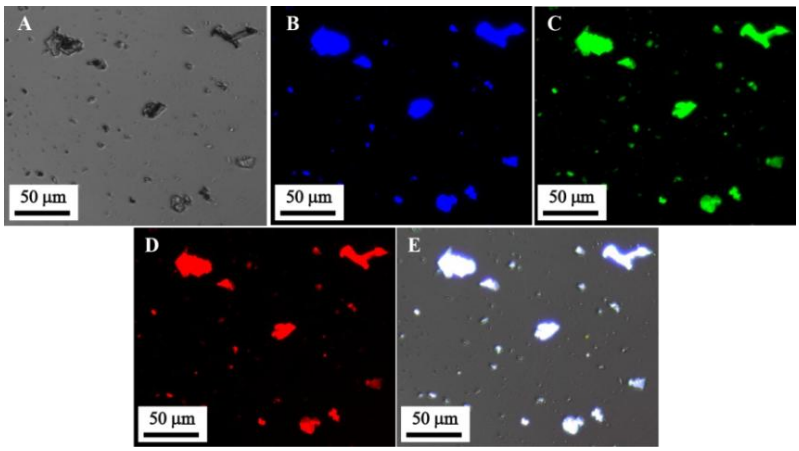

Figure 3.5: Fluorescence optical microscopy images of OPV(PBI)-PS polymer (A) bright field, using (B) using DAPI (blue, 350-430 nm) (C) Alexa (green, 488-520 nm) (D) Rhodamine (red, 480-580 nm) filters and (E) merged image.

(Green, 488-520 nm) filters were used. The OPV(PBI)-PS sample with both the fluorophores incorporated together was imaged using all the three filters – blue, green and red and the corresponding images are shown in ***Figure 3.5***. ***Figure 3.6*** showed the optical images of OPV-PS-7 in the bright field image (A) and showed the blue emission (B) using a blue filter. PBI-PS-3 samples were imaged using both the green and red filters. The images (C), (D), (E) and (F) corresponded to the bright field image, optical image of the green emission using Alexa 488 filter, the red emission obtained using the Rhodamine filter and the merged image respectively. The fluorescent optical images clearly established the potential of the PS nanoparticles for imaging cells in the blue, green and red wavelengths.

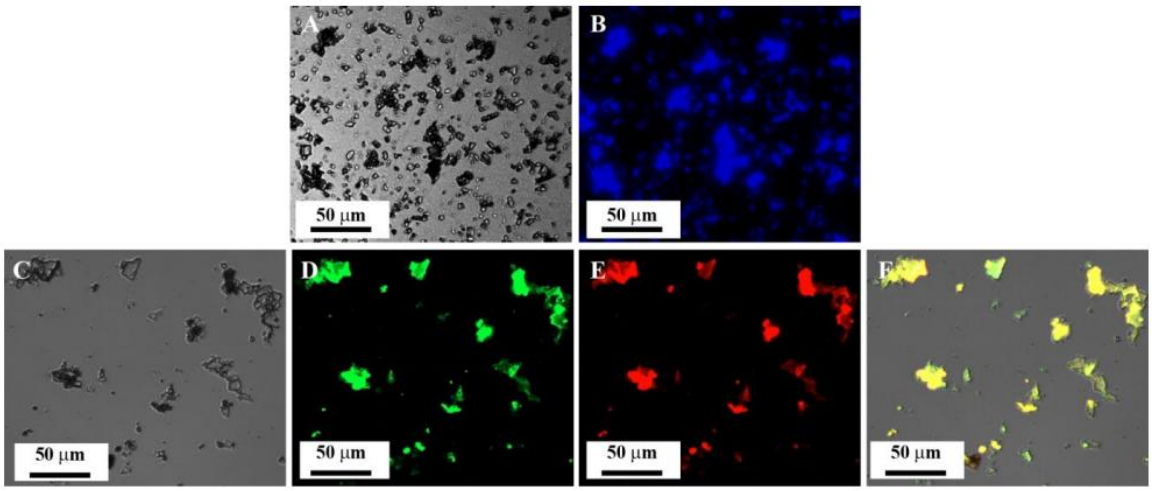

Figure 3.6: Fluorescence optical microscopy images of (a) OPV-PS-7 (A) Bright field (B) using DAPI (Blue, 350-430 nm) filter (Top Row) (b) PBI-PS-3 (C) Bright Field (D) using Alexa (Green, 488-520 nm) (E) Rhodamine (Red, 480-580 nm) filters and (F) Merged Image (Bottom Row).

3.2.3 Cytotoxicity Studies: The cytotoxicity of the fluorescent PS nanobeads was investigated in HeLa cells using the standard MTT assay, which spectrophotometrically quantifies the reduction of MTT into formazan (***Figure 3.7***). The concentration of the PS nanoparticles was varied up to 100 μg/mL. The plot of % cell viability against the concentration of PS supplementation in HeLa cells obtained from MTT assay is shown as a histogram in ***Figure 3.8***. The relative cell viability was determined by considering the viability of the untreated HeLa cells (control) as 100%. The MTT assay results showed that the PS beads with either single fluorophore or with both the fluorophores incorporated had more than 90% cell viability even up

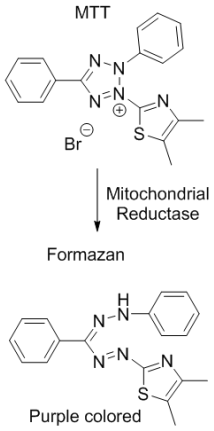

Figure 3.7: Reduction of MTT into formazan using mitochondrial reductase present in living cells.

to 100 μg/mL concentrations. This gave evidence for the excellent biocompatibility of PS nanobeads, which was in confirmation with the literature reports.[4,25,26]

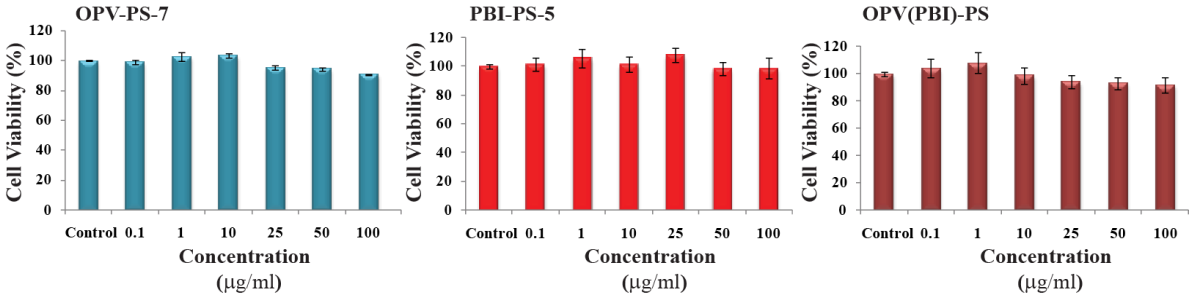

Figure 3.8: Histogram exhibiting Cytotoxicity of polymers in HeLa cells using MTT assay after 48 hrs. Over 95% cell viability indicated that nanoparticles are non-toxic to the cells.

3.2.4 Cellular Uptake Using Flow Cytometry: Flow cytometry analysis were undertaken to have a quantitative estimate of nanoparticle uptake by the cells. Samples with highest emission quantum yields *viz* OPV-PS-7 and PBI-PS-3 were chosen for the studies along with the sample having both fluorophores, namely OPV(PBI)-PS.

Samples at a concentration of 100 μg/mL were incubated for 9 and 24 h. ***Figure 3.9*** showed the fluorescence histogram in HeLa cell lines for the samples incubated for both 9 h (1) and 24 h (2). The fluorescence histogram signified several fold increase in emission from the nanoparticles compared to the control, which clearly demonstrated the internalization of the fluorescent PS nanoparticles by the cells. The enhancement in fluorescent intensity was found to be comparable for both the time period 9 and 24 h. Thus it is appropriate to conclude from ***Figure 3.9*** that 9 h was sufficient for nanoparticle uptake by the cells. While the enhanced fluorescence intensity in the histogram corresponding to both OPV and PBI wavelength for OPV(PBI)-PS, clearly established its multicolor emission capability from blue to red.

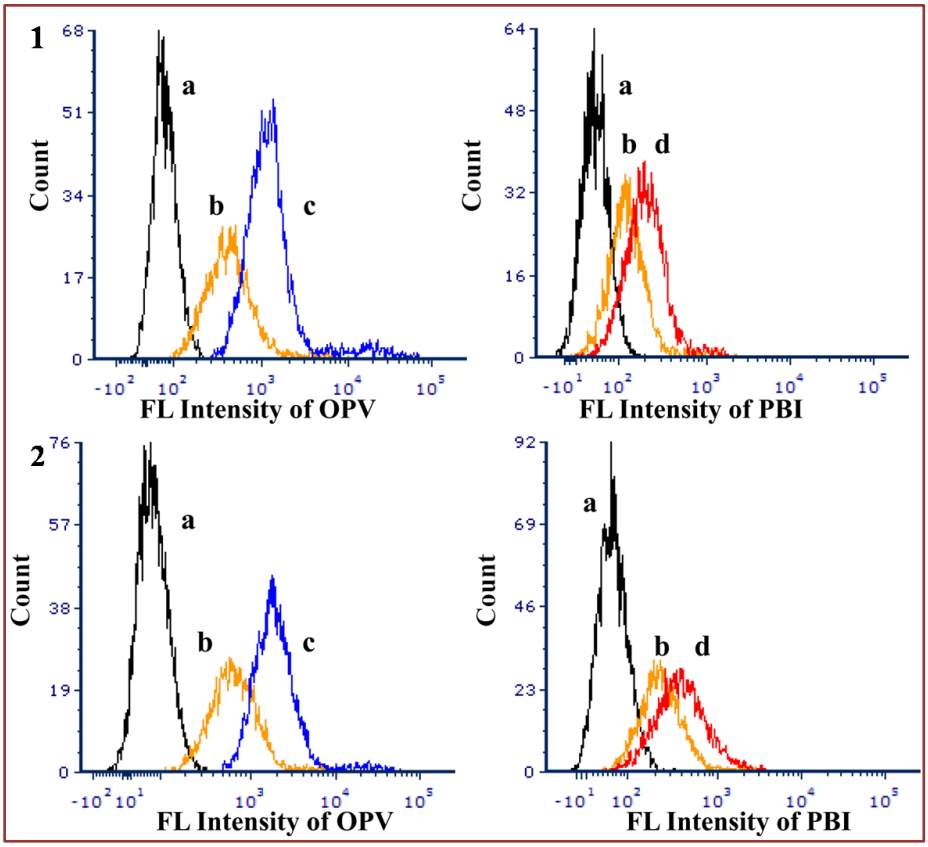

Figure 3.9: Flow cytometry plots for (a) control, (b) OPV(PBI)-PS, (c) OPV-PS-7, and (d) PBI-PS-3 in HeLa cell lines after 9 h (1) and 24 h (2) of incubation.

To further demonstrate that the nanoparticle uptake was not specific to HeLa cells alone, we also used another cell line model, *i.e.* MCF-7, for the flow cytometry studies. MCF-7 is another common cell lines used for *invitro* studies and are breast cancer cells isolated from Caucasian woman. Same concentration of nanoparticles *i.e.* 100 μg/mL (same as used for studies in HeLa cells) were feed to MCF-7 cells for two time periods (9 h and 24 h). The results are provided in ***Figure 3.10***. Similar to previous results with HeLa cells, in this case also, a clear enhancement in fluorescence intensity could be observed from the nanoparticles; once again confirming the nanoparticle uptake by cells.

While for OPV(PBI)-PS, enhacement in emission intensity for both OPV and PBI wavelength reassured its multicolor emission ability.

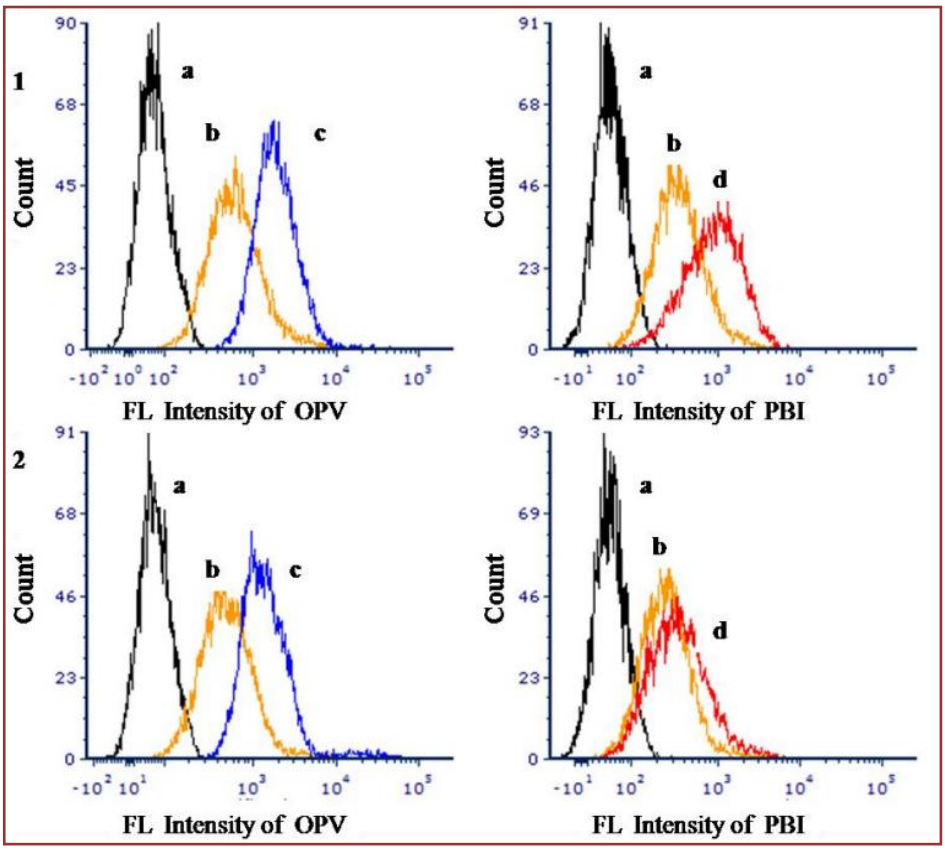

Figure 3.10: Flow cytometry plots for control (a), OPV(PBI)-PS (b), OPV-PS-7 (c) and PBI-PS-3 (d) in MCF-7 cell lines after 24 h (1) and 9 h (2) incubation.

3.2.5 Confocal Microscope Imaging and Cellular Uptake: The cellular uptake of the fluorescent PS nanoparticles in the cells was followed using confocal laser scanning microscopy (CLSM). The same set of samples that were used for the flow cytometry analysis was also used for the confocal imaging studies (OPV-PS-7, PBI-PS-3, and OPV(PBI)-PS) along with PS(OPV7+PBI3) (mixture). An experiment with phalloidin (green) staining was undertaken to confirm the uptake of the PS nanoparticles inside the HeLa cells (***Figure 3.11a−d***). Phalloidin binds with the filamentous actin and the middle panel image in ***Figure 3.11c*** exhibited the bright green emission from phalloidin highlighting the cytoskeleton. The first images on the left-hand side of ***Figure 3.11*** showed the bright-field image (a), the next one (b) exhibited the emission from OPV monitored using the blue channel (λ = 405 nm). The merged image in ***Figure 3.11d*** confirmed the location of the blue emission from OPV in the cytoplasmic region, which in turn supported the fact that the nanoparticles crossed the cell membrane and were internalized by the HeLa cells, were not just adhered to the cell membrane.

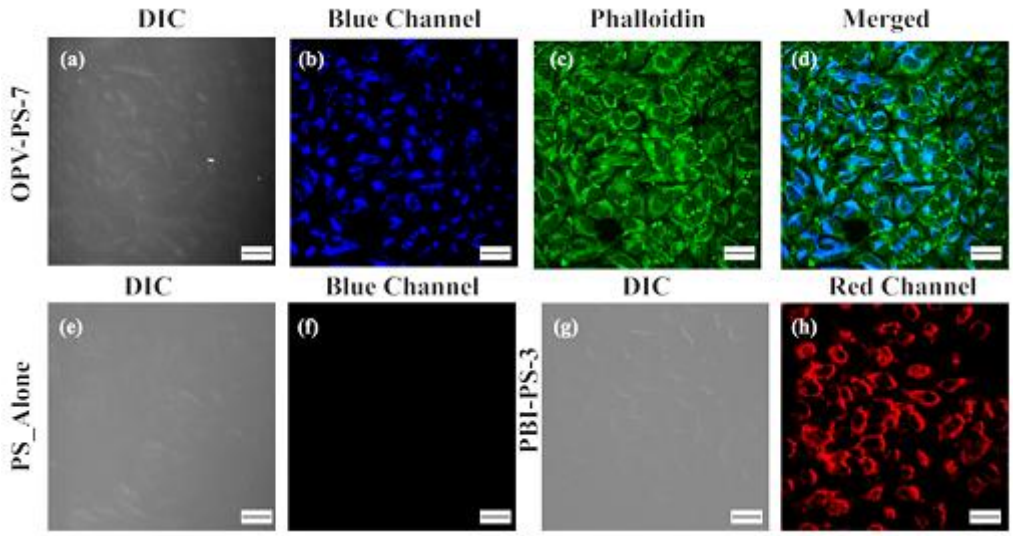

Figure 3.11: CLSM images of HeLa cells incubated with (a–d) OPV-PS-7, (e, f) PS_Alone, (g, h) PBI-PS-3. Scale bar is 30 μm.

Polystyrene is also known to give a faint blue emission due to π–π stacking (***Figure 3.12***), which compares the emission from PS_alone and OPV-PS-7 in 1× PBS buffer.[28] Therefore, PS nanoparticles alone without any fluorophores (PS_alone) were used as a control (***Figure 3.11e, f***). The control experiment clearly established that the

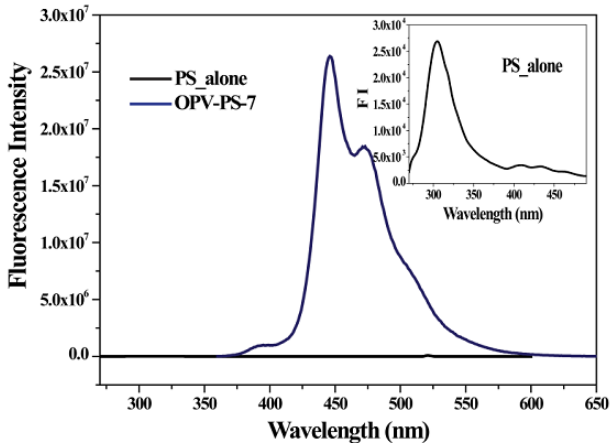

Figure 3.12: Comparision of solution state emission spectra for OPV-PS-7 and PS_alone in 1X PBS buffer (0.1 mg/ 3 ml).

color observed from polystyrene nanoparticles was negligible when compared to that with fluorophore embedded inside it. The image in ***Figure 3.11g, h*** showed the bright-field image and bright red emission from PBI-PS-3 polymer observed using the red channel (λ = 514 nm), respectively. A phalloidin staining experiment was carried out with the PBI-PS-3 sample, provided in ***Figure 3.13***. The merged image unequivocally confirmed the internalization of the PBI-PS nanoparticles by the HeLa cells.

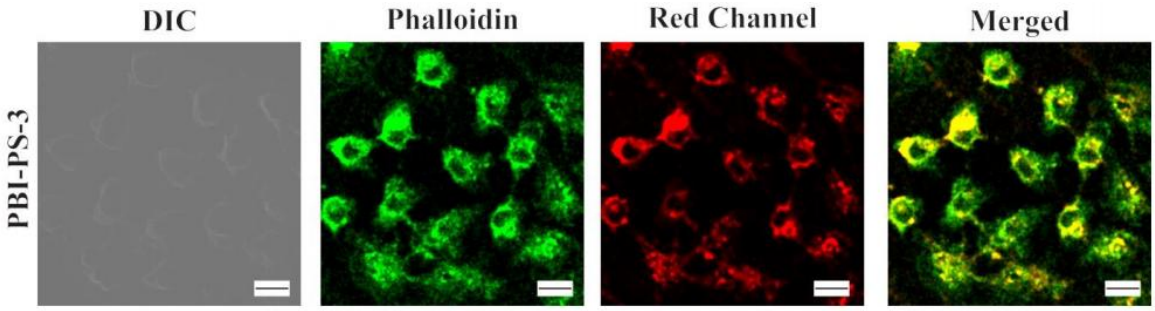

Figure 3.13: CLSM image of Phalloidin staining of PBI-PS-3 in HeLa cells

Similar set of experiments were carried out for MCF-7 cells, which is provided in ***Figure 3.14a−h***. Conclusive evidence for the internalization of the PS nanoparticles in the cytoplasmic region could once again be provided using the phalloidin staining experiment carried out for the PBI-PS-3 sample (***Figure 3.14a−d***). These results were found to be consistent with the flow cytometry analysis.

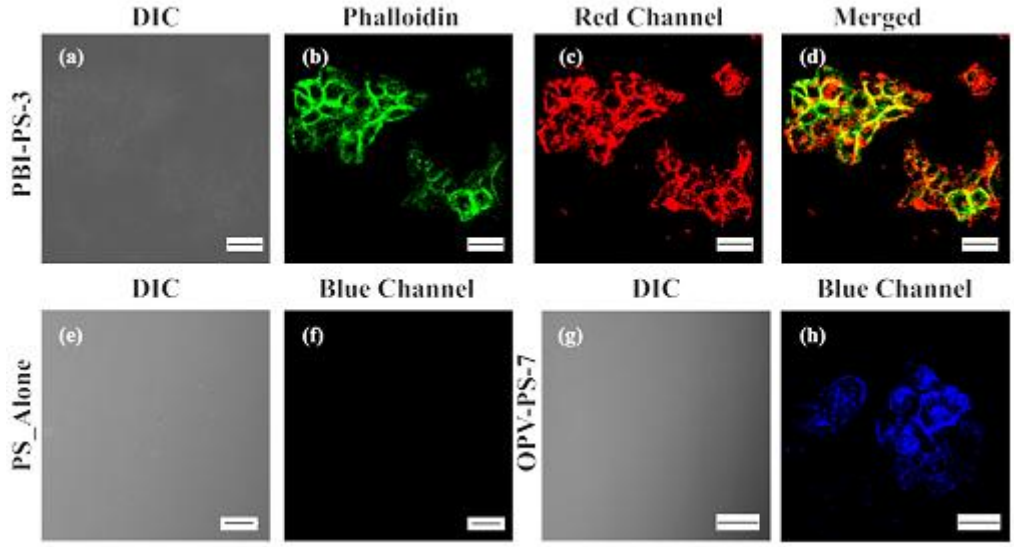

Figure 3.14: CLSM images of MCF-7 cells incubated with (a−d) PBI-PS-3, (e, f) PS_Alone, (g, h) OPV-PS-7. Scale bar is 30 μm.

To demonstrate the multicolor emission ability of OPV-(PBI)-PS, we collected the CLSM images by monitoring the blue (λ = 405 nm), green (λ = 488 nm), and red (λ = 514 nm) channels (***Figure 3.15***). The merged image (***Figure 3.15e***) showed white emission arising from the combination of all the three primary color (Red, Blue, Green). Mixture PS(OPV7+PBI3) was also used for imaging; ***Figure 3.16*** exhibited the cell images collected after incubating cells with PS(OPV7+PBI3). The imaging experiments demonstrated the potential of a single polymer to achieve multicolor cell imaging by simply varying the excitation wavelength.

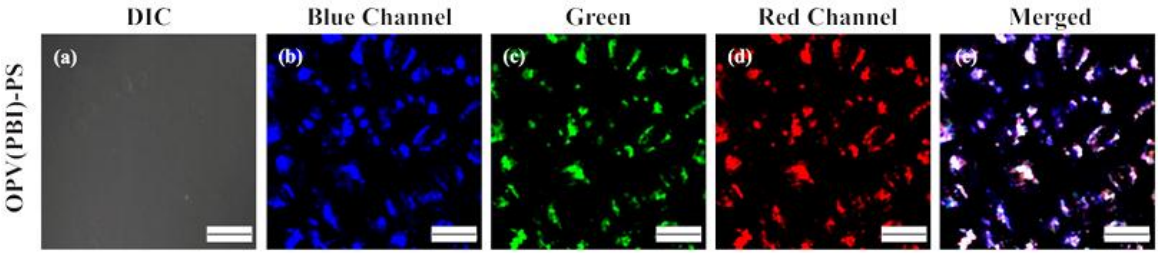

Figure 3.15: CLSM images of HeLa cells incubated with OPV(PBI)-PS polymer. Scale bar is 30 μm.

Thus, the excitation wavelength could be tuned from any wavelength from 350 to 490 nm to tune emission from blue to green to red, thus minimizing errors due to photobleaching or autofluorescence from the cells. To the best of our knowledge, this is the first report showing all the three primary color (Red, Blue, Green) emission from a single polymer (PS nanoparticle) incorporating π-conjugated chromophores for imaging in cells by simply varying the excitation wavelength.

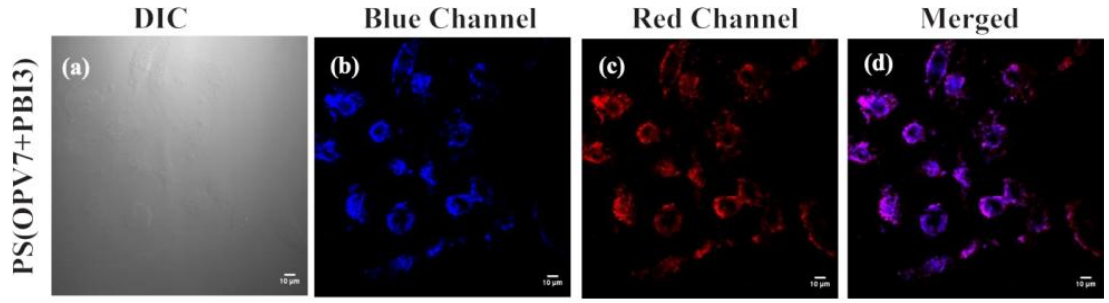

Figure 3.16: CLSM image of HeLa cells incubated with PS(OPV7+PBI3) (physical mixture)

3.3 Experimental Details:

3.3.1 Materials: HeLa cells were incubated at 37 °C under a 5% CO_2 humidified atmosphere as described earlier.[22] Tetrazolium salt, 3,4,5- dimethylthiazol-2,5-diphenyltetrazolium bromide (MTT), DMSO, and 4% paraformaldehyde were bought from Aldrich. Fluoromount was purchased from Southern Biotec. Deionized water was used throughout the experiments.

3.3.2 Details of Analytical Instruments: The Fluorescence microscope images were collected using a Carl Zeiss "Axio Observer Z1" microscope using Rhodamine (480-580 nm, Red), Alexa (488-520 nm, Green) and DAPI (350-430 nm, Blue) filters. The dilute polymer dispersion in ethanol was drop casted onto the glass slide, covered with a

coverslip and observed directly under the microscope. The Cellular uptake images were taken using LSM 710 Confocal Microscope.

3.3.3 Cell Viability Assay (MTT Assay): The cytotoxicity of dye-incorporated polymer nanoparticles was studied using 3-(4,5-dimethylthiazol-2-yl)-2,5-diphenyltetrazolium bromide, a tetrazolium salt (MTT) assay in HeLa cells. Each well in a 96-well plate (Corning, USA) was seeded with 1000 cells in 100 μL of DMEM supplemented with 10% FBS (fetal bovine serum) and were allowed to adhere for 16 h. The media from the cells was then drawn out followed by addition of dye loaded polymer nanoparticles of various concentrations as feed. Cells without any polymer nanoparticles and complete media without cells were taken as blank control and all the wells (treated as well as control) were done in triplicate. After incubating the cells for 72 h, the media containing dye-loaded nanoparticles was aspirated and each well was treated with freshly prepared MTT solution (0.5 mg/mL) and incubated for 4 h. After 4 h, the media from each well were withdrawn and the formazan purple crystals were dissolved in 100 μL of DMSO. The absorbance was immediately recorded from formazan crystals at 570 nm using a 96-well plate reader (Varioskan Flash), which is indicative of number of viable cells per well. The mean of the values from the triplicate run for each of control and polymer-treated cells were then used for calculations.

3.3.4 Cell Uptake Studies Using Flow Cytometry: The cellular uptake of PS nanoparticles was measured using flow cytometry cell analyzer. Cells were seeded in 6-well plate at a density of 1×10^5 cells containing DMEM media. Two cell lines namely HeLa and MCF-7 were treated with desired concentration (100 μg/mL) of PS nanoparticles and incubated for two time periods (9 and 24 h). After the respective time periods, the media were removed and washed once with 1 mL of PBS. The cells were then digested with 500 μLof trypsin immediately followed by incubation for a minute. Afterward, the suspension was centrifuged for 5 min at 1000 rpm and 10 °C and then resuspended in 0.5 mL of PBS buffer. Flow cytometry studies were conducted using a BD LSR Fortessa SORP cell analyzer equipped with five lasers, which is capable of detecting 18 colors. The data collection was done for 10000 counts; 405 and 561 nm lasers were used for the excitation of OPV and PBI, respectively, and the bandpass filters were chosen as 450 ± 50 nm for OPV and 610 ± 20 nm for PBI.

3.3.5 Cell Uptake Studies Using Confocal Microscopy: In the 6-well plate containing DMEM medium supplemented with 10% FBS were placed flame-dried coverslips onto

which HeLa/MCF-7 cells at a density of 1×10^5 cells were seeded. These were then incubated for 16 h at 37 °C. Dye-loaded nanoparticles at the concentration of 100 μg/ mL were then added to the media and incubated for 9 h at 37 °C under a CO_2 environment. After 9 h, the media were aspirated from each well and cells were then washed two times with PBS (1 mL/ wash) for 5 min each and then fixed using 4% paraformaldehyde solution in PBS at room temperature for 10 min and again washed two times with PBS (1 mL/wash) for 5 min. Cells were then stained with Alexa fluor 488 conjugated phalloidin dye (500 μL) for 20 min under dark conditions followed by two washings with 1× PBS for 5 min. Then using a Fluoromount mounting medium (Southern Biotech) the cover slips were mounted on slides and left overnight for drying under dark conditions at room temperature. With a LSM 710 confocal microscope, cells were imaged using the λ 405, 488, 514 for blue, green and red channel lasers and analyzed using ImageJ analysis software and for each channel, image was separated and merged.

3.4 Conclusion:

In conclusion, the synthesized multicolor emitting PS nanobeads covalently incorporating OPV and PBI based fluorophores have been successfully employed for bio-imaging application in cancer cells. Since the fluorophores are embedded well in the PS network, their emission is also not affected by external triggers that may be present in the cellular environment such as pH or temperature. The fluorophores could be taken together in a single bead or PS beads incorporating individual fluorophores could be mixed in order to access multiple excitation wavelengths for imaging applications. As mentioned in the introduction section, the ability for multicolor imaging has the potential to overcome the cellular autofluorescence and to enhance the resolution contrast of the image.

NOTE: The results presented in this chapter are already published as a part of publication in *ACS Biomater. Sci. Eng.* **2017**, *3*, 1788-1798 with the title '*π-Conjugated Chromophore Incorporated Polystyrene Nanobeads as Single Optical Agent for Three-Channel Fluorescent Probe in Bioimaging Application*'.

Acknowledgement: We acknowledge the facilities provided by Professor M. Jayakannan, IISER-Pune and we sincerely thank his students Ms. Mehak Malhotara, Mr. Nilesh Despande, and Ms. Sonashree Saxena for enabling the studies with HeLa and MCF-7 cells.

3.5 References:

1. Grimsdale, A. C.; Chan, K. L.; Martin, R. E.; Jokisz, P. G.; Holmes, A. B. *Chem. Rev.* **2009**, *109*, 897-1091.

2. Jiang, Y.; McNeill, J. *Chem. Rev*. **2017**, *117*, 838-859.

3. Wu, W. C.; Chen, C. Y.; Tian, Y.; Jang, S. H.; Hong, Y.; Liu, Y.;Hu, R.; Tang, B. Z.; Lee, Y. T.; Chen, C. T.; Chen, W. C.; Jen, A. K. Y. *Adv. Funct. Mater.* **2010**, *20*, 1413 - 1423.

4. Wolfbeis, O. S. *Chem. Soc. Rev.* **2015**, *44*, 4743-4768.

5. Pu, K.; Shuhendler, A. J.; Rao, J. *Angew. Chem. Int. Ed.* **2013**, *52*, 10325-10329.

6. Vollrath, A.; Schallon, A.; Pietsch, C.; Schubert, S.; Nomoto, T.; Matsumoto, Y.; Kataoka, K.; Schubert, U. S. *Soft Matter* **2013**, *9*, 99-108.

7. Wu, C.; Bull, B.; Szymanski, C.; Christensen, K.; McNeill, J. *ACS Nano* **2008**, *2*, 2415-2423.

8. Dausend, J.; Musyanovych, A.; Dass, M.; Walther, P.; Schrezenmeier, H.; Landfester, K.; Mailander, V. *Macromol. Biosci.* **2008**, *8*, 1135-1143.

9.Holzapfel, V.; Lorenz, M.; Weiss, C. K.; Schrezenmeier, H.; Landfester, K.; Mailander, V. *J. Phys.: Condens. Matter* **2006**, *18*, S2581-S2594.

10. Bao, B.; Tao, N.; Yang, D.; Yuwen, L.; Weng, L.; Fan, Q.; Huang, W.; Wang, L. *Chem. Commun.* **2013**, *49*, 10623-10625.

11. Sreejith, S.; Divya, K. P.; Ajayaghosh, A. *Angew.Chem. Int. Ed.* **2008**, *120*, 8001-8005.

12. Niu, G.; Liu, W.; Zhou, B.; Xiao, H.; Zhang, H.; Wu, J.; Ge, J.;Wang, P. *J. Org. Chem.* **2016**, *81*, 7393-7399.

13. Zhang, J.; Liu, S.; Hu, X.; Xie, Z.; Jing, X. *ACS Biomater. Sci. Eng.* **2016**, *2*, 1942 - 1950.

14. Reisch, A.; Klymchenko, A. S. *Small* **2016**, *12*, 1968-1992.

15. Feng, G.; Dan Ding, D.; Li, K.; Liua, J.; Liu, B. *Nanoscale* **2014**, *6*, 4141-4147.

16. Sokolova, V.; Epple, M. *Nanoscale* **2011**, *3*, 1957-62.

17. Gnach, A.; Bednarkiewicz, A. *Nano Today* **2012**, *7*, 532-563.

18. Wilhelm, S.; Kaiser, M.; Würth, C.; Heiland, J.; Carrion, C.; Muhr, V.; Wolfbeis, O. S.; Parak, W. J.; Resch-Genger, U.; Hirsch, T. *Nanoscale* **2015**, *7*, 1403-1410.

19. Zhu, C.; Yang, Q.; Liu, L.; Lv, F.; Li, S.; Yang, G.; Wang, S. *Adv. Mater.* **2011**, *23*, 4805-4810.

20. Chong, H.; Nie, C.; Zhu, C.; Yang, Q.; Liu, L.; Lv, F.; Wang, S. *Langmuir* **2012**, *28*, 2091-2098.

21. Zaquen, N.; Lu, H.; Chang, T.; Mamdooh, R.; Lutsen, L.; Vanderzande, D.; Stenzel, M.; Junkers, T. *Biomacromolecules* **2016**, *17*, 4086-4094.

22. Kulkarni, B.; Surnar, B.; Jayakannan, M. *Biomacromolecules* **2016**, *17*, 1004-1016.

23. Holzapfel, V.; Musyanovych, A.; Landfester, K.; Lorenz, M. R.; Mailander, V. *Macromol. Chem. Phys.* **2005**, *206*, 2440-2449.

24. Montalti, M.; Battistelli, G.; Cantelli, A.; Genovese, D. *Chem. Commun.* **2014**, *50*, 5326-5329.

25. Loos, C.; Syrovets, T.; Musyanovych, A.; Mailänder, V.; Landfester, K.; Nienhaus, G. V.; Simmet, T. *Beilstein J. Nanotechnol.* **2014**, *5*, 2403-2412.

26. Ramírez, L. P.; Landfester, K. *Macromol. Chem. Phys.* **2003**, *204*, 22-31.

27. Sauer, R.; Turshatov, A.; Baluschev, S.; Landfester, K. *Macromolecules* **2012**, *45*, 3787-3796.

28. Kuo, A. *CheM* **2011**, *1*, 80-86.

CHAPTER-4A

Remote Functionalized Fluorescent PS Nanobead based Visual Dual Distinct Sensor for the detection of Volatile Organic Compounds

Abstract: *This chapter highlights synthesis and application of dye loaded surface functionalized polystyrene nanoparticles for chemical sensing. Solid state emitting, distinctly dual vapor sensors with high quantum yield was developed using polystyrene incorporating two fluorophores following a miniemulsion polymerization method. Selective functionalization with carboxy and amine functionality was used to decorate the resulting polystyrene nanobeads having both perylenebisimide (PBI) and oligo (p-phenylenevinylene) (OPV) fluorophores. These nanobeads with a size of 70–180 nm showed near white emission under UV light. On contact with vapors of specific electron deficient nitroaromatics OPV emission got selectively quenched to show yellow emission from the nanobeads under UV radiation. Exposure to amine vapor quashed PBI emission selectively resulting in blue emission under UV lamp. Such a vast range of color alteration from white to either blue or yellow from the same sensor makes it a true dual analyte sensor with two distinct outputs. Control of surface functionality (−COOH, $-NH_2$, and neutral) on the nanobeads played a pivotal role in boosting the sensing efficiency; introduction of functionality on the surface facilitated analyte-sensor interaction through hydrogen bonding, prompting their fast responsiveness. Real time, potential device based application was demonstrated with free-standing films which was capable of efficient detection with fast analyte exchange from dilute solutions. Recyclability of the film sensor was demonstrated with 8 cycles of reuse.*

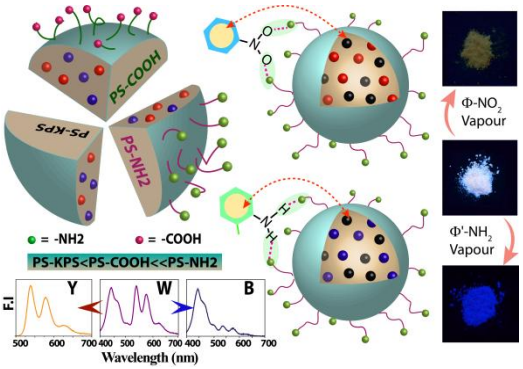

4A.1 Introduction:

The anthropogenic volatile organic compounds (VOCs) including nitroaromatics, organic amines *etc.* have been widely known for their use as important industrial material in chemical synthesis of drugs, dyes, pesticides, synthetic rubber and plastic processing.[1-3] Despite of high industrial importance of such chemicals (*eg.* nitrobenzene, aniline, *o*-toludine, *o*-anisidine *etc.*), they impose negative impact on the environment; because of their proven carcinogenicity and high degree of toxicity.[4,5] Exposure of such chemicals, even in trace amount is responsible for physiological disorders like methemoglobinemia with symptoms of cyanosis, dizziness, fatigue, shortness of breath and even might have fatal consequence on long exposure. Thus a minor spillage of such VOCs has potential to cause a significant impact, owing to their high vapor pressure.[6] As a measure of precaution, prompt and easy detection of these harmful chemicals from trace quantities of vapor is supremely demanded to prevent their exposure at very early stage.

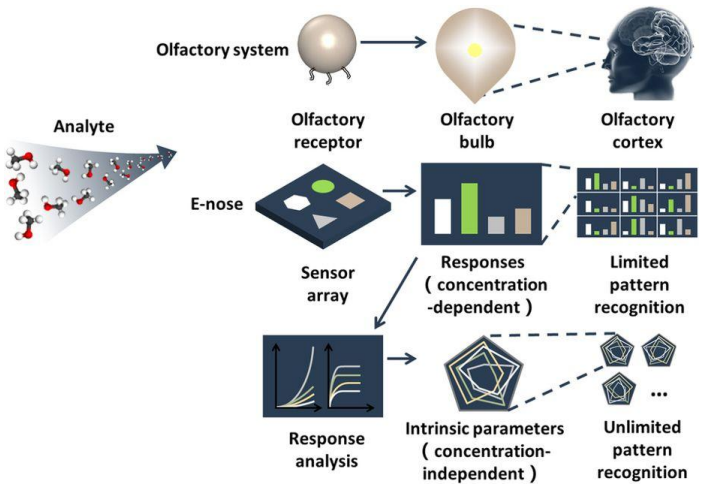

Figure 4A.1: Schematics for detection of VOCs through sensor materials used in E-nose as a bio-mimicking device. Image is adapted from *Sci. Rep.* **2016**, *6*, 23970.

Among the several employed approaches, chemical sensing *via* change in luminescence properties is of great importance particularly being advantageous than other methods in terms of low cost, faster response time, and portability.[7,8] There are several examples in the literature on luminescence based detection on solid supports like silica nanoparticles, quantum dots, gold nanoparticles, molecularly imprinted materials, liposomes, *etc.*[9-14] Of them, solid state polymeric fluorescence based sensor are quite fascinating because of their added advantages of processability to device fabrication, operational simplicity, high sensitivity and selectivity and easy visualization with rapid response time, as discussed thoroughly in ***Chapter-1***. Use of polymer based fluorescent sensor also eliminates any possibility for false signal generation from shifting of

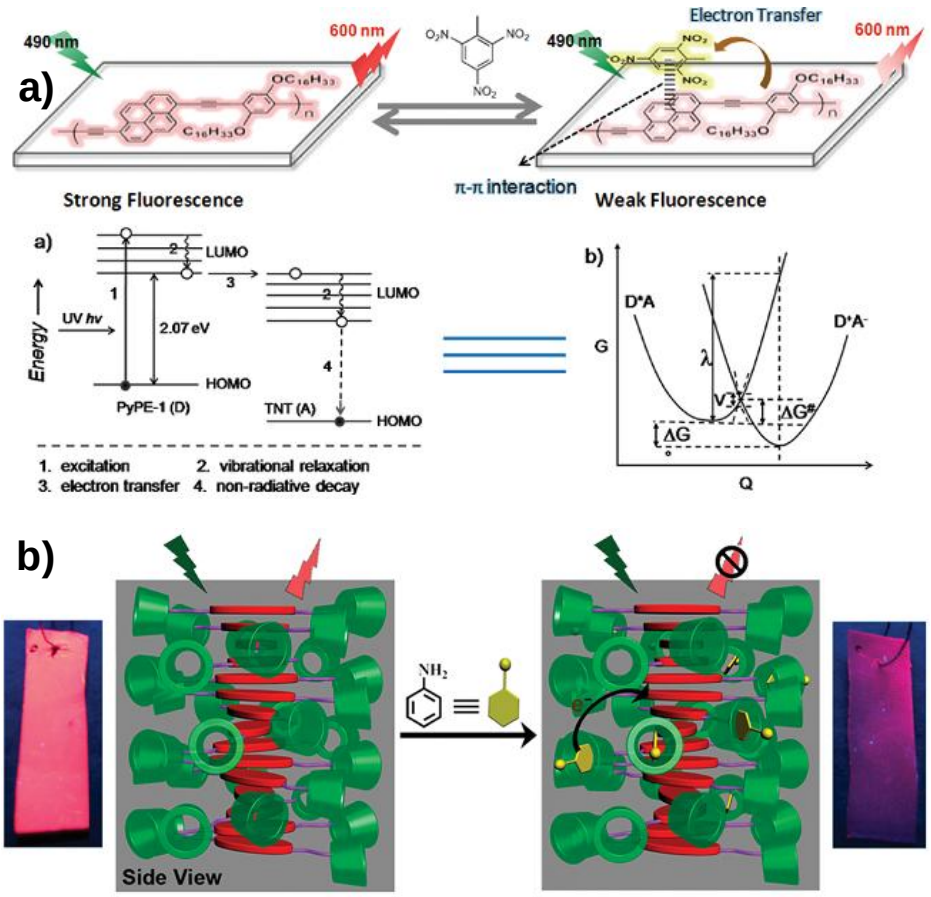

Figure 4A.2: a) Schematic representation and the electron-transfer mechanism for the fluorescence quenching of a conjugated polymer-based fluorescent film by TNT, making a successful detection. [Figure is adapted from ***Ref 28*** with permission from ACS Publishers] b) Schematic illustration of a perylene-bridged bis(cyclodextrins) assembly and its sensing process for aniline. [Figure is adapted from ***Ref 24*** with permission from ACS Publishers]

emission maxima for the fluorophore itself, under different applied concentrations or solvent, making them ideal candidate for on-site applications. Possessing a high solid state quantum yield assures a significant change to be observed during the sensing process; however the promptness of the sensing procedure is determined by the interaction between the sensor and analyte. Thus, a successful solid state sensor should possess (i) high solid state quantum yield[15-18] and (ii) appropriate sites for interaction with analyte.[19-22]

However, reports till date on polymer based sensor contain only either of the criteria where it remained a challenge to meet both of them. Moreover, the developed sensors are effective to a unit or specific class of analytes, thus either selective to amine[23-25] or nitro compounds[26-28] on the particular case of VOCs, owing to the presence of single active moiety. This necessitates the use of different sensors for the successful detection of different classes of analytes. Although dual sensors have been reported, their response

towards the different class of analytes are usually similar -through the attenuation in their emission intensity; *i.e.* emission quenching of sensing

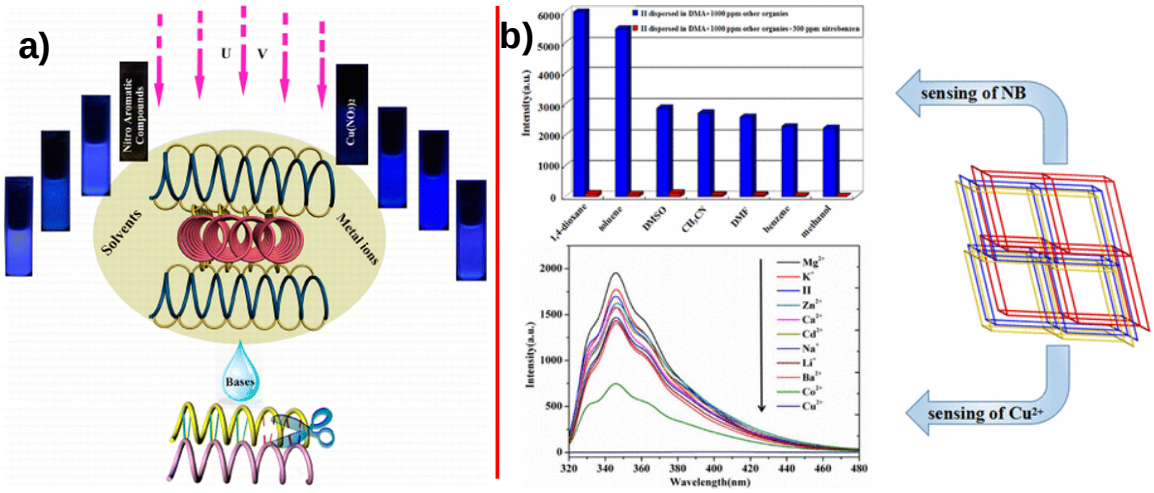

Figure 4A.3: Illustrative example for pairwise detection of a) Cu^{2+} and nitroaromatics, and b) Cu^{2+} and NB through emission quenching in each case. [Figures are reproduces from ***Ref 29*** and 31 respectively, with permission from ACS Publishers]

material in all cases.[29-32] Such dual sensors with dual turn-off feature have been evidenced by Pang *et al.*,[29] Cao *et al.*[30] and Yang *et al.*[31] for multifunctional pairwise detection of nitroaromatic compound (NAC) and Cu(II), explosive and multiple cations in water, NB and Cu(II), respectively. On the same note, from the class of VOCs, dual sensing of NB and aniline through fluorescence quenching has been recently demonstrated by Huang *et al.*[32] In all these examples it is rather difficult to differentiate the class of analyte based on their observed response. A different class of 'supramolecular stack' of sensor was reported from the group of Ajayaghosh *et. al*[33] where two active sensors based on oligo(*p*-phenylenevinylene) (OPV) and perylene bisimide (PBI) were physically mixed to form self-assembled stacks that was responsive towards both nitroorganics as well as organic amines. Our research group had previously reported solid state emitting polystyrene (PS) beads incorporating pyrene and PBI covalently.[34] We had demonstrated selective quenching of pyrene emission, leaving the PBI emission intact upon exposure to vapors of NAC like 4-nitrotoluene but the response time was observed to be rather high. In addition, our synthetic approach of covalent incorporation of the fluorophores also afforded a total absence of dye leakage or leaching in addition to color tunability. Unlike sensors based on physical mixtures of small fluorescent molecules a robust polymer based sensor is amenable to large scale application since it has the scope of casting into free standing films (which is an important prerequisite for on-field use in devices) or enhancing the sensing efficiency by its surface modification.

Thus this type of so called "dual" turn off sensor makes it difficult to distinguish between different classes of analytes which could have easily observed for otherwise distinctly responsive dual sensor. In this aspect there is only one such literature report where two of active sensors are physically mixed to form supramolecular stacks. The resulting mixture thus is capable of sensing the sum of analytes from the individual sensors and the sensing performance remains unaltered. Moreover, the difficulty retained to design, synthesize and purify the two different active moieties each time in order to prepare the final self sorted polymer stack that serves as sensor moiety for the analytes. Also the requirement for large amount of the sensing material makes the approach less appropriate for practical and large scale application, considering the involvement of high procedure and material cost. Additionally being formed with the small molecule system, there is no further scope of casting a free standing film (which is an important prerequisite for on-field use in devices) or enhancing the sensing efficiency by its surface modification.

In the chapter, I have shown that PS based "distinctly-dual sensor" that can sense both nitroaromatic and amino-organic VOCs through distinctly different emission colors. The surface functionalized (-COOH or -NH2) PS nanobeads covalently incorporating both OPV and PBI were developed using the industrial and environmental friendly miniemulsion polymerization approach. OPV and PBI based fluorophores were chosen which represent substantial class of *p*-type and *n*-type organic material with high quantum yield and outstanding photostability which is particularly desirable to enhance sustainability and performance of a sensor.[35-36] Notably, covalent attachment diminished any chance of dye leaching which might hamper reproducibility and performance of sensor.[9,37] Only small amount of fluorophore (dye loading content (DLC) ~0.03%) was sufficient to impart high solid state quantum yield. Remote functionalization of the PS nano beads with -COOH and -NH2 groups proved effective in enhancing the analyte-sensor interaction, resulting in improved sensing efficiency. The sharp visual color change will provide additional advantage for on-site detection of both nitroaromatics and amines with two distinct outputs. Casting of free standing membrane allowed fast exchange of analytes and reusability beyond 8 cycles, without compromising the sensing efficiency. To the best of our knowledge this is the first report on polymer based visual "dual-distinct sensor" to utilize remote functionalization approach for enhancing the sensing efficiency.

4A.2 Results and Discussions:

4A.2.1 Synthesis and structural characterization: The conjugated dyes in the form of OPVand PBI were synthesized and characterized as per previous literature reports and presented in ***Chapter-2***. These dyes were used for miniemulsion co-polymerization with other monomers including styrene and functional monomers. Careful selection of the functional monomers was applied to bring in different functionalities in the resulting polystyrene nanobeads (***Scheme 4A.1***). In a typical miniemulsion synthetic protocol, organic phase (Styrene, OPV and PBI based fluorescent cross-linkers and hexadecane) of

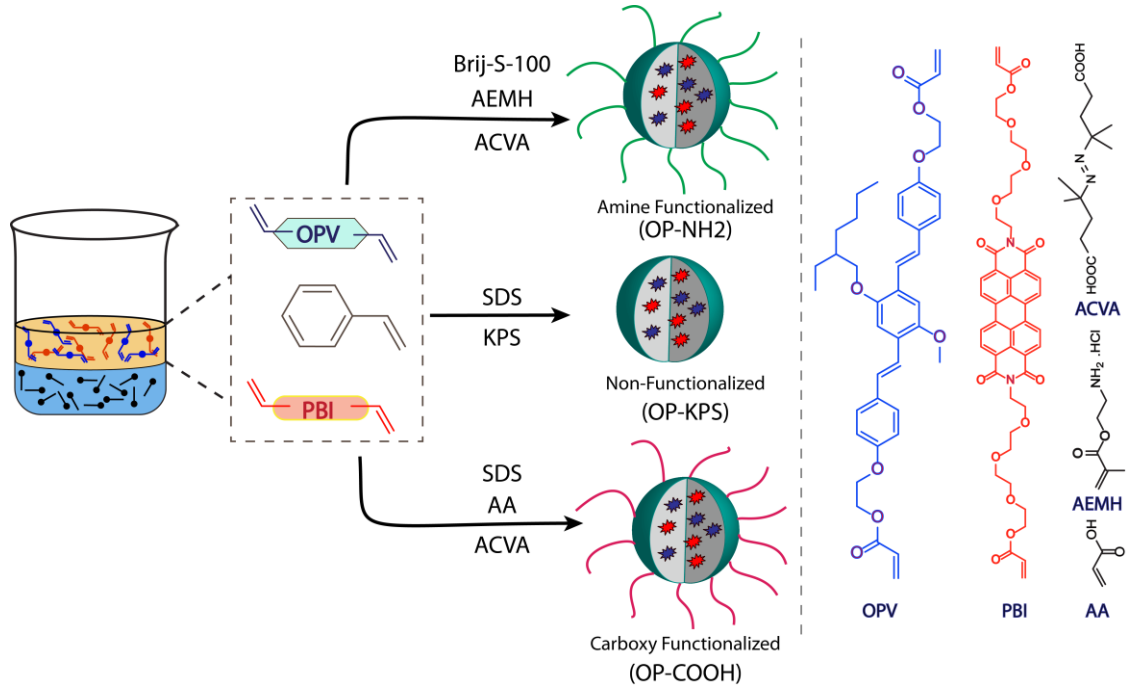

Scheme-4A.1: Schematics of functionalized polystyrene nanobeads synthesis *via* miniemulsion polymerization. ACVA was used as initiator for the synthesis of functionalized nanobeads while KPS was used as initiator for the case of non-functionalized one.

the reaction mixture were added dropwise into the aqueous phase (Surfactant, initiator and respective functional monomers such as acrylic acid, **AA** or aminoethyl methacrylate hydrochloride, **AEMH**) under stirring. This mixture was then allowed to stir at room temperature for another hour for pre-emulsification followed by sonication for 20 min in an ice cooled bath. The polymerization process was carried out by stirring with a speed of 750 rpm for 20 h at 70 ^{0}C. The detailed reactant amount and reaction condition for both functionalized and non-functionalized nanoparticles has been tabulated in ***Table 4A.1***. The obtained latex from this step was dialyzed (MW Cutoff 6 kD), dried and washed several times with methanol to remove excess surfactant, oligomers and unreacted

monomers and the percent solid content for all the polymers were calculated using the following equation (***eq 1***):

$$SC\ (\%) = \frac{W_d}{W_l} \times 100 \quad \text{.....eq 1}$$

where W_d and W_l are the weight of dried polymer and weight of polymer latex respectively. The values for the same are given in ***Table 4A.3***.

Table 4A.1: Reagents used in miniemulsion copolymerization of a) PS-KPS, b) PS-COOH and c) PS-NH2.

Components	Amount
Water	4 g
Styrene	1 g
Cross-linker (OPV and PBI)	Varied
Hexadecane	48 mg
SDS [a,b]	12 mg
KPS [a]	3.3 mg
Acrylic acid [b]	100 mg
AEMH [c]	100 mg
ACVA [b,c]	16 mg
Brij S-100 [c]	33 mg

4A.2.2 Estimation for Encapsulation of dyes into nanoparticles: For calculating Dye Loading Content (DLC) and Dye Encapsulation Efficiency (DLE) of the polymers, tetrahydrofuran (THF) solutions having 1 mg/mL concentration of the polymer were taken and their absorbance were recorded (***Figure 4A.4***) at individual absorption maxima (395 nm for OPV and at 520 nm for PBI dye). Based on their molar extinction coefficients (PBI, 81092 $Lmol^{-1}cm^{-1}$; OPV, 40360 $Lmol^{-1}cm^{-1}$) the amount of dye incorporated into the polymer has been calculated and subsequently their DLC and DLE have been estimated using the regular equations. (***eq 2 and 3***)

$$DLC = \frac{\text{Weight of dye encapsulated in nanoparticle}}{\text{Weight of dye loaded nanoparticle}} \times 100 \quad \text{.....eq 2}$$

$$DLE = \frac{\text{Weight of dye encapsulated in nanoparticle}}{\text{Weight of dye in feed}} \times 100 \quad \text{.....eq 3}$$

Although the concentration of dyes in the feed was same for synthesis of the three nanoparticles, actual incorporation of the dye was found to be different in each case. DLC for OPV was found to be highest for PS-NH2 (0.04%) followed by PS-KPS (0.02%) and PS-COOH (0.02%). For PBI the highest DLC was observed for PS-KPS (0.05%) followed by PS-COOH (0.04%) and PS-NH2 (0.03%). DLE values for all the polymers were found to vary from 26-57 % for OPV and 15-26.5 % for PBI. A comprehensive detail of DLC and DLE values for all the polymers was observed as follows (***Table 4A.2***).

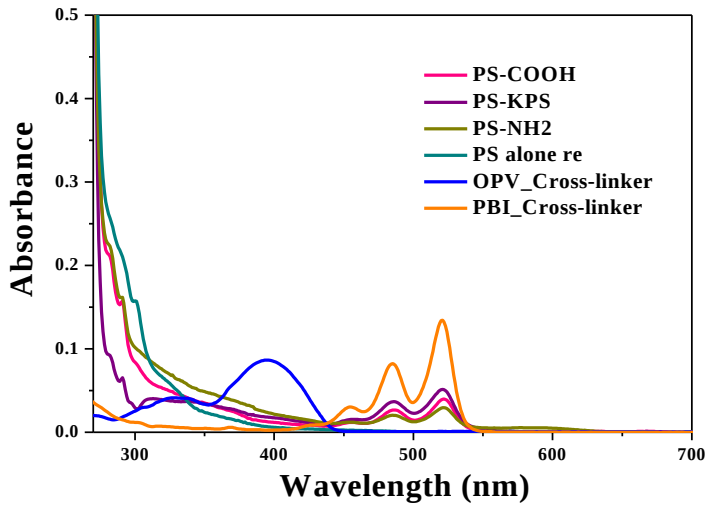

Figure 4A.4: Absorption spectra of the polymers in THF (1 mg/ml) for DLC and DLE calculation.

Table 4A.2: Sample designation, DLC, DLE, and the Quantum Yield of the nanobeads.

Samples	Amount of OPV in feed (actual incorporation)[a] (mg/g of styrene)	Amount of PBI in feed (actual incorporation)[a] (mg /g of styrene)	DLC (%) [a] OPV (PBI)	DLE (%) [a] OPV (PBI)	Quantum Yield (%)[b] OPV (PBI)
PS-KPS	0.7 (0.18)	2 (0.53)	0.02 (0.05)	26 (26.5)	26 (42)
PS-COOH	0.7 (0.16)	2 (0.42)	0.02 (0.04)	23 (21)	32 (65)
PS-NH2	0.7 (0.40)	2 (0.30)	0.04 (0.03)	57 (15)	39 (78)

a) DLC and DLE are calculated by absorption studies in THF.

b) Quantum Yield: determined in solid state using integrating sphere setup.

4A.2.3 Surface Funtionalization of the Polystyrene Nanoparticles: Use of KPS as initiator and SDS as surfactant without any functional monomer for the miniemulsion polymerization resulted in the formation of non-functionalized fluorescent polystyrene nanobeads, referred to as PS-KPS. For the synthesis of functionalized polystyrene nanobeads, AA or AEMH was made use of as functional monomers to facilitate the

introduction of the required functionalities -COOH and -NH_2 in polymers, PS-COOH and PS-NH2 respectively.[38] SDS was used as the surfactant for the synthesis of -COOH functionalized polystyrene nanobeads PS-COOH, for the amino functionalized PS-NH2, Brij S-100 was used as the surfactant as AEMH being opposite in charge to SDS, restricted its use as the surfactant. ACVA was used as initiator in both the polymerizations (***Scheme 4A.1***). Surface charge of the polystyrene nanoparticles, observed from zeta potential measurement at pH = 7 using KCl as background electrolyte has been used to interpret the different functionalities on the nanoparticles. PS-COOH showed a net negative zeta potential of -38 mV, indicating the presence of carboxy functionality on the surface of the nanoparticles (along with few sulfate groups from surfactant). The presence of -NH2 group on the surface of PS-NH2 nanoparticles created a positively charged environment, imparting a net positive zeta potential of +39 mV. In the case of the non-functionalized PS-KPS, use of anionic surfactant and initiator resulted in some anionic groups retained on the surface of the synthesized nanoparticles, creating a slight negative zeta potential of -19 mV (***Table 4A.3***). It has to be noted that no carboxy group from the surfactant or initiatorwas responsible for the slight negative potential observed for PS-KPS, keeping it deprived of -COOH or -NH2 functionality.

Table 4A.3 Number and Weight Average Molar Mass, Polydispersity indice (Đ), Solid content, Zeta potential, Particle size and its PDI.

Samples	Mn[a]	Mw[a]	PDI[a]	Solid content (%)	Zeta Potential	Particle size (nm)[b]	PDI[b]
PS-KPS	157600	464500	2.9	14	-19	129	0.07
PS-COOH	122200	379900	3.1	15.8	-38	72	0.12
PS-NH2	114600	264090	2.3	13.4	+39	184	0.09

a) Measured by Gel Permeation Chromatography (GPC) in THF calibrated with linear, narrow molecular weight distribution polystyrene standards.

b) Measured by Dynamic Light Scattering (DLS) in water.

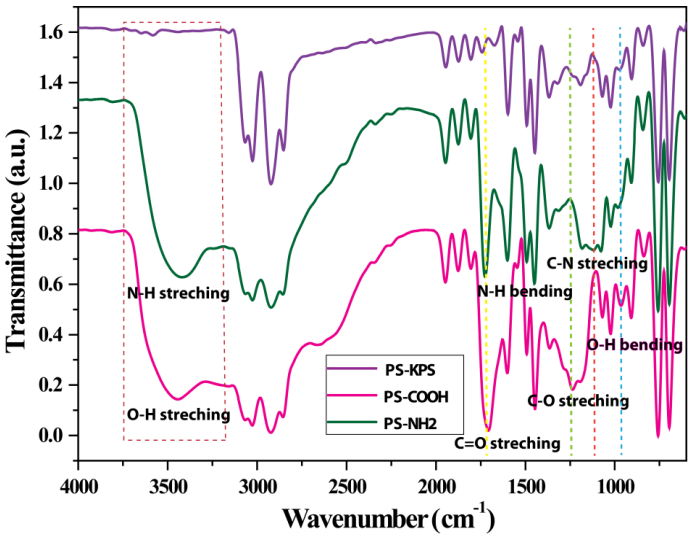

Figure 4A.5: FTIR plot of the polystyrene nanoparticles

Further confirmation for presence of functional groups was observed from FTIR spectroscopic analysis[39] (***Figure 4A.5***) which clearly showed characteristic peaks for respective functional groups. For PS-COOH, broad peak at 3444-2500 cm^{-1} accounted for combination of carboxylic O-H and C-H stretching. Peak at 1709 cm^{-1} corresponded to C=O stretching of acid while peak at 1204 cm^{-1} and 971 cm^{-1} corresponded to C-O and O-H bending of the acid functionality. For PS-NH2, characteristic peak for N-H stretching and bending (in-plane) appeared at 3425 cm^{-1} and 1604 cm^{-1} respectively while broad peak corresponding to C-N stretching appeared at 1129 cm^{-1}. It is important to note that none of the characteristic peaks for -COOH or -NH2 functionality was observed in the case of PS-KPS. The PS nanobeads were soluble in common organic solvents like tetrahydrofuran (THF), in which the molecular weight was determined. It should be mentioned here that although both the fluorophores were cross-linkers; their feed intake was so less compared to styrene that the polymers remained completely soluble after their incorporation. All the polymers were found to possess high molecular weight in the range of 114600 to 157600 Da with PDI varying from 2.3 to 3.1. The observed values for molecular weight are tabulated in ***Table 4A.3*** and their corresponding GPC chromatograms are given in ***Figure 4A.6a***.

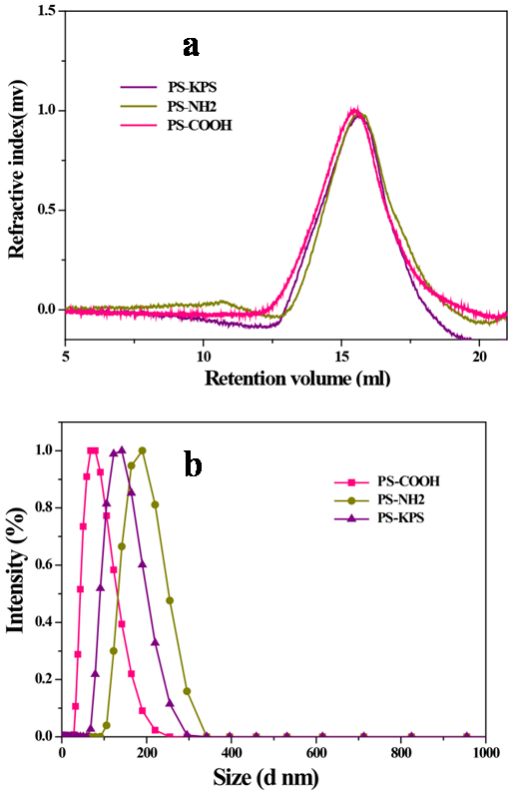

Figure 4A.6: a) GPC plot of polymers in THF with flow rate of 1 ml/min, b) Intensity-average size distribution of polymers in deionized water using DLS

Being synthesized through miniemulsion polymerization, the polystyrene nanobeads were found to have a uniform profile for size distribution. DLS particle size analysis (***Figure 4A.6b***) showed that effective diameter of the synthesized nanoparticles were comparable for all the cases (***Table 4A.3***), with an average value of 72 nm for PS-COOH, 129 nm for PS-KPS and 184 nm for PS-NH2. TEM analysis confirmed the spherical morphology of both functionalized (PS-NH2, PS-COOH) and non-functionalized (PS-KPS) nanobeads and the images for the same were shown in ***Figure 4A.7***.

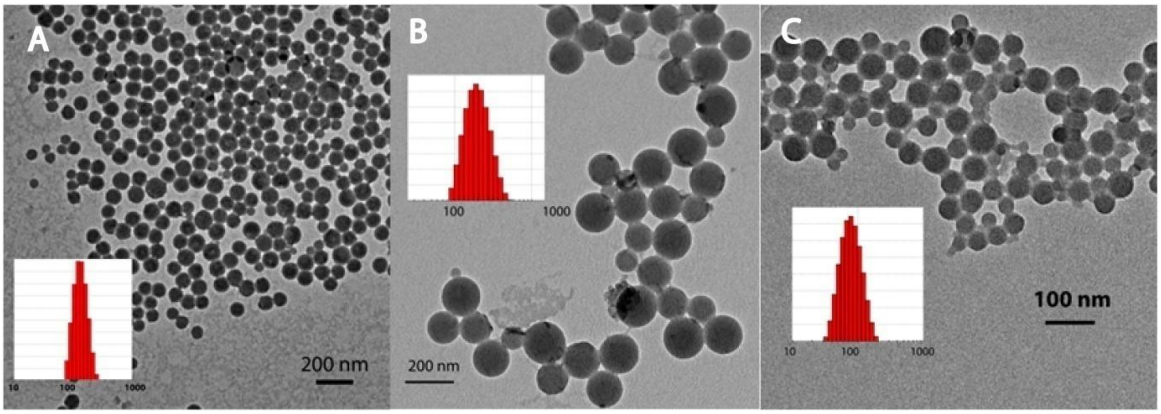

Figure 4A.7: TEM images of the synthesized polystyrene nanobeads, (A) PS-KPS (B) PS-NH2 (C) PS-COOH. Inset figures show the bar chart for size distribution profile for the nanobeads.

Both functionalized and non-functionalized polystyrene nanoparticles were found to have appreciably high thermal stability with 5 wt% loss observed at 351°C and 365 °C respectively (***Figure 4A.8***). The presence of the fluorophores could not be detected *via* NMR spectroscopy as their incorporation was low. However, their existence could be easily observed in the absorption spectra, which was also used for their quantification. Absorption spectra of the polymers from THF solution showed the presence of two characteristic peaks corresponding to both the fluorophores, *i.e.* OPV and PBI (***Figure 4A.4***). A comparative study with the individual absorption peaks for all the three nanobeads with that of pristine fluorophores revealed a blue shift by 30 nm for absorption maxima of OPV (as observed in ***Chapter 2***) while absorption maxima of PBI remained unaffected by the polymerization into polystyrene backbone.

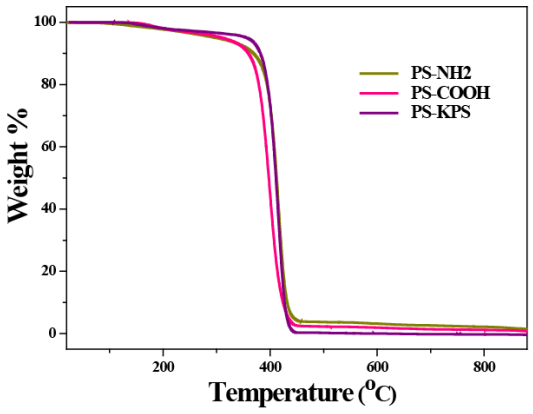

Figure 4A.8: TGA plot of the polymers, showing their thermal stability.

4A.2.4 Photophysical Properties: Solid state emission as well as excitation spectra were recorded for the polymers in powder form on a paper strip (sample applied on transparent adhesive tape supported on cardboard frame). ***Figure 4A.9*** shows the solid state emission spectra collected at (a) 390 nm and (b) at 490 nm for the polymers and their respective excitation spectra collected at (c) 445 nm and (d) 576 nm. Since the synthesized polystyrene nanoparticles contained two differently emitting fluorophores, the resulting emission was a combination of their relative intensities.

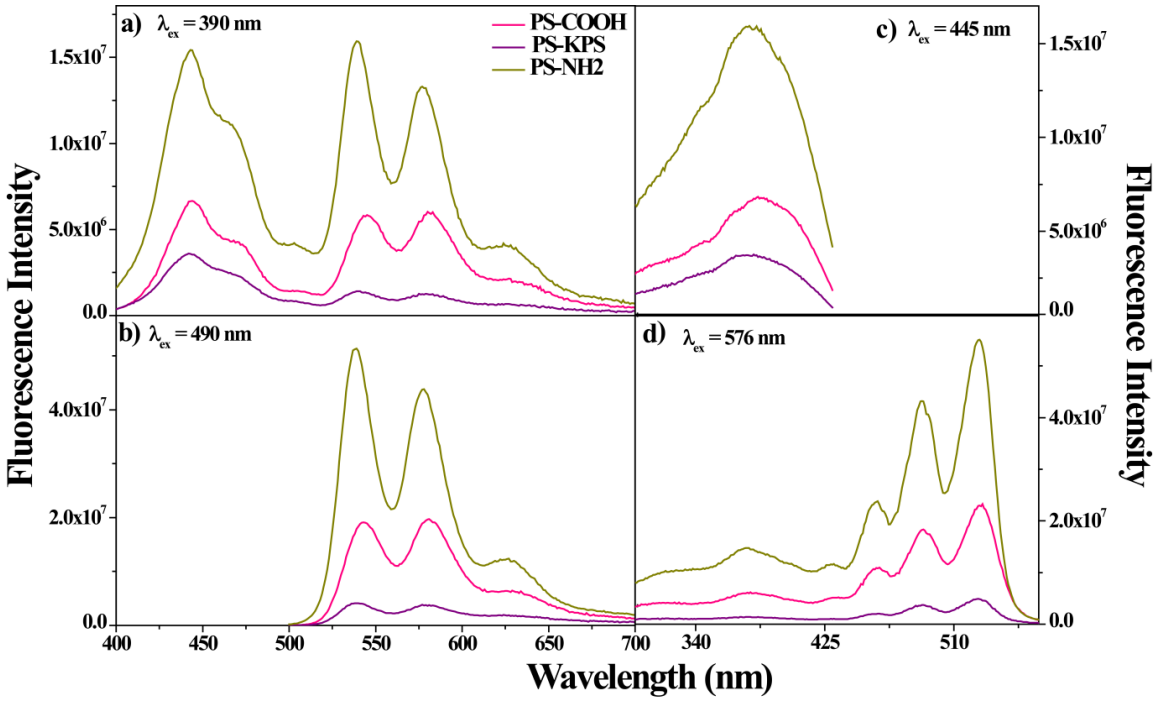

Figure 4A.9: Solid state (powder) emission spectra of the polymers upon excitation at (a) 390 nm and (b) 490 nm. Solid state excitation spectra of the polymers collected at (c) 445 nm and (d) 576 nm.

Both the functionalized nanoparticles (PS-COOH and PS-NH2) showed near-white emission under UV lamp while the non-functionalized PS-KPS nanoparticles showed a light purple emission in the bulk powder (***Figure 4A.10***). The emission spectra collected at 390 nm showed the characteristic emission peak for both OPV (400-510 nm) and PBI (500-700 nm) in all the polymers (***Figure 4A.9***). This indicated evidence for fluorescence resonance energy transfer (FRET) from the OPV to the PBI. Similar experimental condition was applied to measure the solid state quantum yield for each of

Figure 4A.10: Optical images showing emission from (A) PS-NH2 and (B) PS-KPS (C) PS-COOH observed under UV lamp.

the polymers, using the integrating sphere set up attached with excitation source at 390 nm for OPV and 490 nm for PBI respectively. The emission intensity of OPV was highest from PS-NH2, which was in line with its highest DLC (0.04 %). Although the DLC values were similar (0.02 %) for the other two polymers, emission intensity for PS-COOH was found to be slightly higher as compared to PS-KPS. This trend of emission data was found to be consistent with the experimentally obtained quantum yield values, *i.e.* highest for PS-NH2 (39 %) followed by PS-COOH (32 %) and PS-KPS (29 %) (***Table 4A.2***).

In the case of PBI, the emission intensity from the polymer followed a reverse trend; highest emission was observed for PS-NH2, having the lowest PBI incorporation (DLC = 0.03%) while PS-KPS having highest incorporation (DLC = 0.05 %) showed the lowest emission. PS-COOH being moderately incorporated with PBI dye (DLC = 0.04 %), showed an intermediate emission under similar condition. A similar trend was also observed for solid state quantum yield values, *i.e.* highest for PS-NH2 (78 %), then PS-COOH (65 %) and PS-KPS (42 %) (***Table 4A.2***). Despite the difference in emission intensity for individual fluorophores, their resulting combined emission remained same for both PS-COOH and PS-NH2, producing very similar near-white emission under UV lamp. CIE co-ordinate diagram for these two functionalized polymers (co-ordinates for PS-NH2 and PS-COOH were (0.29, 0.31) and

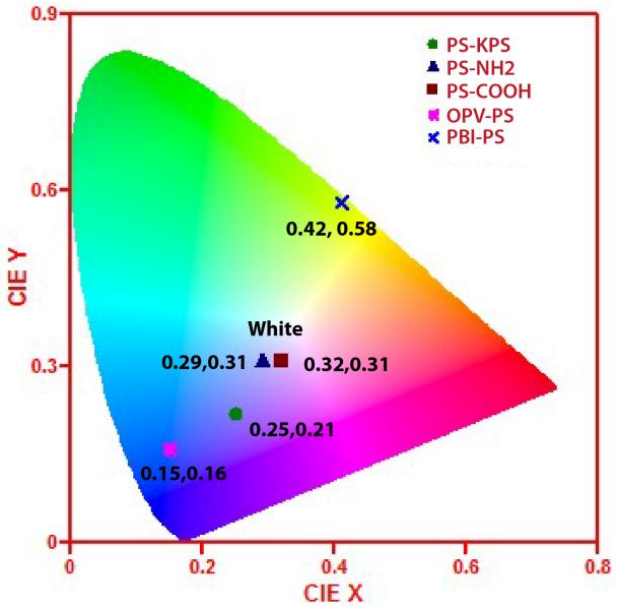

Figure 4A.11: CIE co-ordinate diagram for the polymers.

(0.32, 0.31) respectively) showcased their white light emitting nature. The emission was minutely different for non-functionalized polymer (PS-KPS), which showed light purple emission with CIE co-ordinate of (0.25, 0.21) while OPV-PS and PBI-PS polymers showed blue and red emission respectively (***Figure 4A.11***).

4A.2.5 Sensing Studies with Polymer Powder: The high solid state emissive nature of the polymers makes them attractive candidate for application in chemical sensors where change in their luminescence property can be utilized to detect the presence of an analyte. OPV being an electron rich moiety preferably interacts with electron deficit species whereas the electron deficient nature of the PBI moiety makes it suitable for interaction with electron rich species. This highlights the applicability of OPV based polymers for detection of compounds such as nitroaromatics while PBI moieties are useful to detect the presence of harmful organic amines. Polystyrene nanobeads incorporating OPV alone (OPV-PS) or PBI alone (PBI-PS) were taken to demonstrate the selective application of OPV and PBI fluorophores for the detection of nitroaromatics and organic amines respectively (***Figure 4A.12a,b***). Solid powders of OPV-PS nanoparticles in the form of strip prepared by applying sample on adhesive tape supported on cardboard frame was exposed to vapor of NB as an illustrative example of a member of the nitroaromatic family for a period of 30 minutes. ***Figure 4A.12a*** shows more than 95% quenching of OPV emission from OPV-PS upon exposure to vapor of NB for 30 minutes. In a similar manner, PBI-PS samples were exposed to vapor of *o*-TD as an illustrative example for a member belonging to the organic amine family. ***Figure 4A.12b*** shows 93% quenching of PBI emission upon exposure to vapor of *o*-TD for 30 minutes. The reverse *i.e.* exposure of OPV-PS to vapor of *o*-TD or exposure of PBI-PS to NB for 30 minutes did not lead to

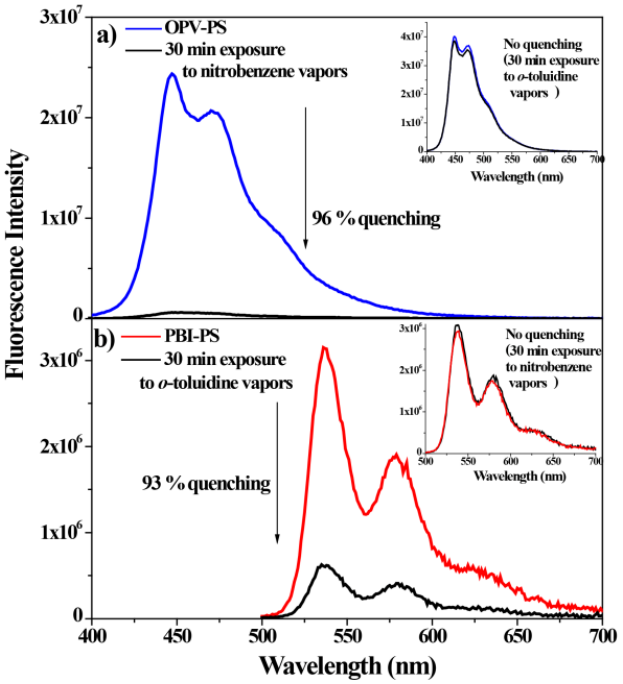

Figure 4A.12: (a) Quenching of OPV emission in OPV-PS upon exposure to NB vapor (Inset: emission after exposure to *o*-TD vapor). (b) Quenching of PBI emission in PBI-PS upon exposure to *o*-TD vapor. (Inset: emission after exposure to NB vapor).

any appreciable changes in their respective emission characteristics as shown in inset in ***Figure 4A.12a, b*** respectively. This clearly demonstrated the selectivity of interaction of electron rich OPV with nitroaromatics and the electron deficient PBI with organic amines.

The polymers incorporating both fluorophores exhibited near white emission, and any change in the electronic states of the fluorophores (arising from selective interaction with analytes) is expected to be reflected as a substantial change in the emission color of the polymer. Additionally, the white light emission had the added advantage of enhanced sensitivity in that even a slight change in emission color could be easily and efficiently detected and quantified. The combined presence of the OPV and PBI fluorophores is thus

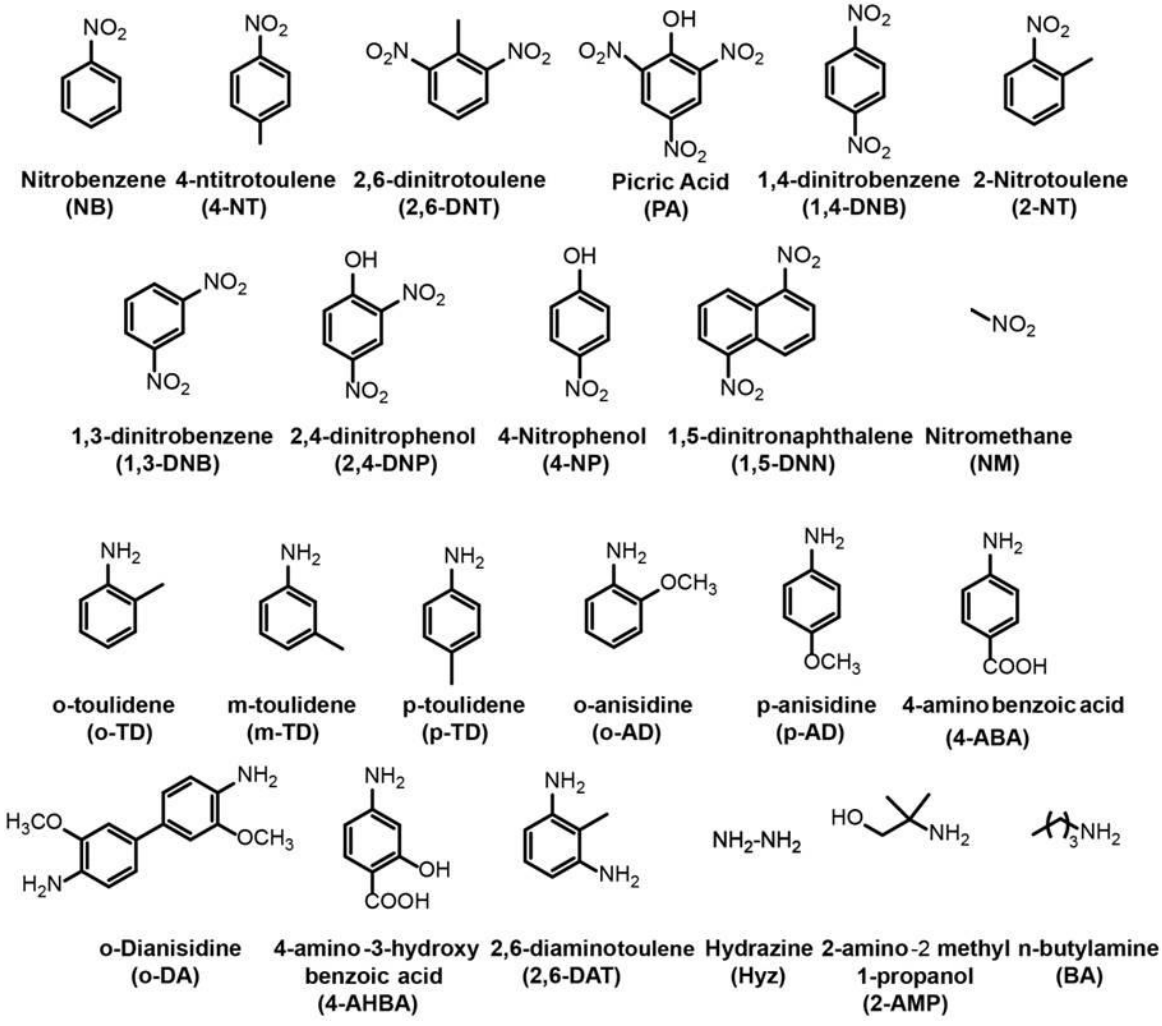

Figure 4A.13: Structures of organic amines and nitro-organic compounds used in this study

expected to impart dual sensing ability to the polystyrene nanoparticle incorporating them. Further, the surface functionalization of the PS beads with -COOH or -NH2 groups

as in PS-COOH and PS-NH2, is expected to boost the sensing efficiency by enhancing the interaction with the analytes. The sensing ability of the three polymers (PS-KPS, PS-COOH and PS-NH2) towards various analytes (***Figure 4A.13***) were checked by exposing the polymer in powder form on the adhesive strip to vapors of the various analytes for a period of 15 minutes.

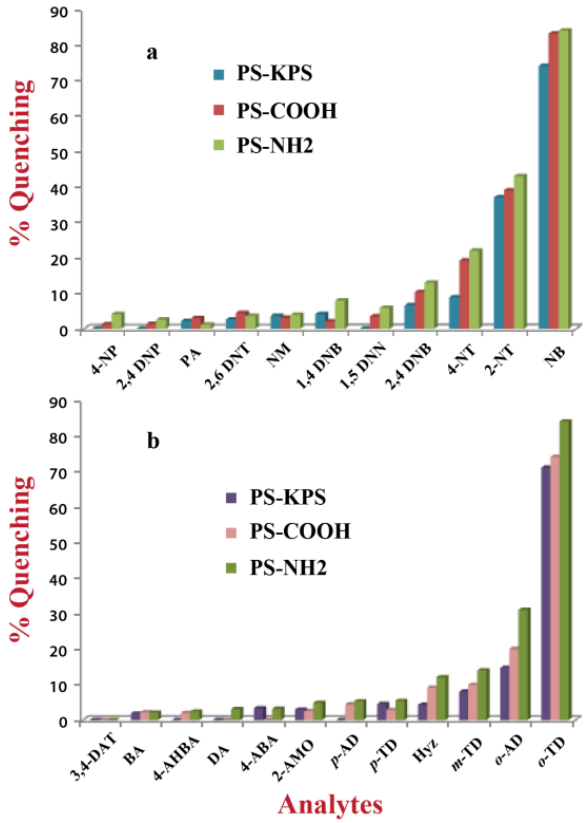

Figure 4A.14: Percentage OPV emission quenching upon exposure to different volatile nitro compounds for 15 minutes. Emission was collected at 400 nm (λex = 390 nm). b) Comparative plot for percentage PBI emission quenching upon exposure to different volatile organic amines for 15 min. Emission was collected at 500 nm (λex = 490 nm).

When the nanobeads were exposed to the vapor of nitroaromatics, a gradual quenching of emission of the OPV moieties occurred due to its interaction with the electron deficient nitroaromatic molecules. This resulted in the emission from PBI fluorophore to become prominent leading to a striking, visible emission color change from white to yellow indicating the presence of nitroaromatics. Similarly when vapor of suitably electron rich analytes such as organic amine were exposed to the polystyrene nanobeads, the PBI emission was quenched, keeping the blue emission from OPV unaffected (change of emission color from white to blue). ***Figure 4A.14a,b*** compiles the percentage emission quenching of OPV and PBI emission for the three polymers upon exposure to vapors of various nitroaromatics and organic amines respectively. NB was found to result in the highest quenching from OPV emission whereas *o*-TD quenched the PBI emission most effectively.

This selectivity from among the library of the analytes arose from two major factors, (a) electron donation/acceptance ability of the analyte and (b) their vapor pressure. Vapor pressure of the analyte controlled the concentration of analyte in the resulting vapor, which in turn determined the possibility of effective interaction between

electron rich and electron deficient fluorophore systems. Although 2-NT had higher vapor pressure, its electron accepting ability was comparatively less than that of NB resulting in reduced sensitivity of interaction of OPV with 2-NT. [4A.33] In the case of *o*-AD, although electron donating ability was higher compared to *o*-TD, the vapor pressure was lower resulting in reduced sensitivity of interaction with PBI. The same is reflected in their quenching efficiency (***Figure 4A.15a***).

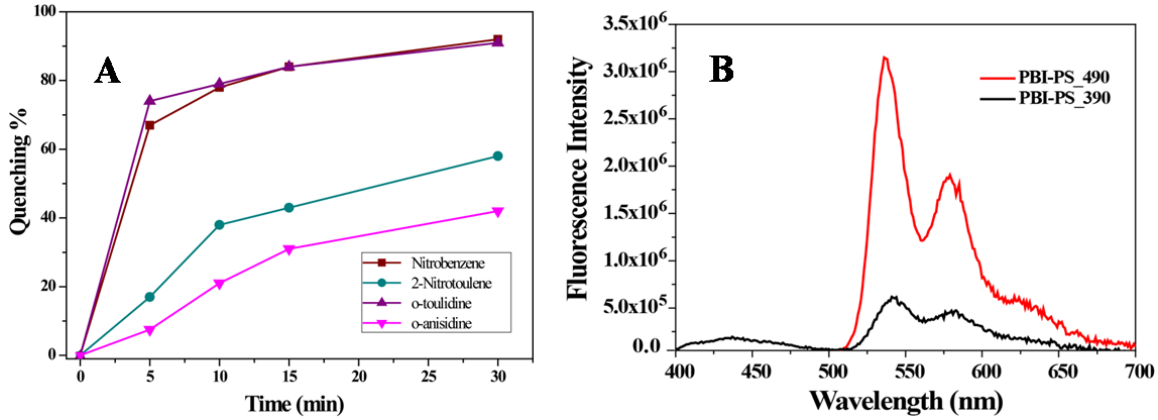

Figure 4A.15: a) Comparative plots for PS-NH2 nanobeads upon exposure to the vapors of NB (wine red), 2-nitrotoulene (cyan) *o*-TD (purple), and *o*-anisidine (magenta) as a function of time. b) Emission spectra of PBI-PS at 490 nm and 390 nm excitation wavelength.

To probe the improvement of sensing ability of the functionalized PS nanoparticles (PS-COOH and PS-NH2) over the non-functionalized nanoparticles (PS-KPS), time dependent studies involving quenching of emission upon interaction of OPV with NB and PBI with *o*-TD was carried out. ***Figure 4A.16a-c*** compares the quenching of OPV emission for the three polymer samples – PS-KPS, PS-COOH and PS-NH2 upon exposure to vapor of NB for varying periods of time. A decrease in the OPV as well as PBI emission intensities was observed as a function of exposure time. As PBI was insensitive to the NB vapors, the reduction in PBI emission could be attributed to reduction in FRET from OPV to PBI due to the gradual reduction in OPV emission. It must be pointed out here that since PBI exhibited absorption at 390 nm, direct excitation of PBI also occurs upon excitation at the OPV wavelength of 390 nm. ***Figure 4A.15b*** compares the emission observed in a PBI alone system (PBI-PS) upon excitation at both 390 and 490 nm. If only FRET was the basis of the observed PBI emission upon excitation at 390 nm, it would have also got quenched upon reduction of OPV emission on exposure to the NB vapor. Since PBI also exhibited some extent of direct excitation at

390 nm, the yellow emission from PBI was retained even after quenching of OPV emission. This was further supported by the emission spectra of PS-NH2 collected by

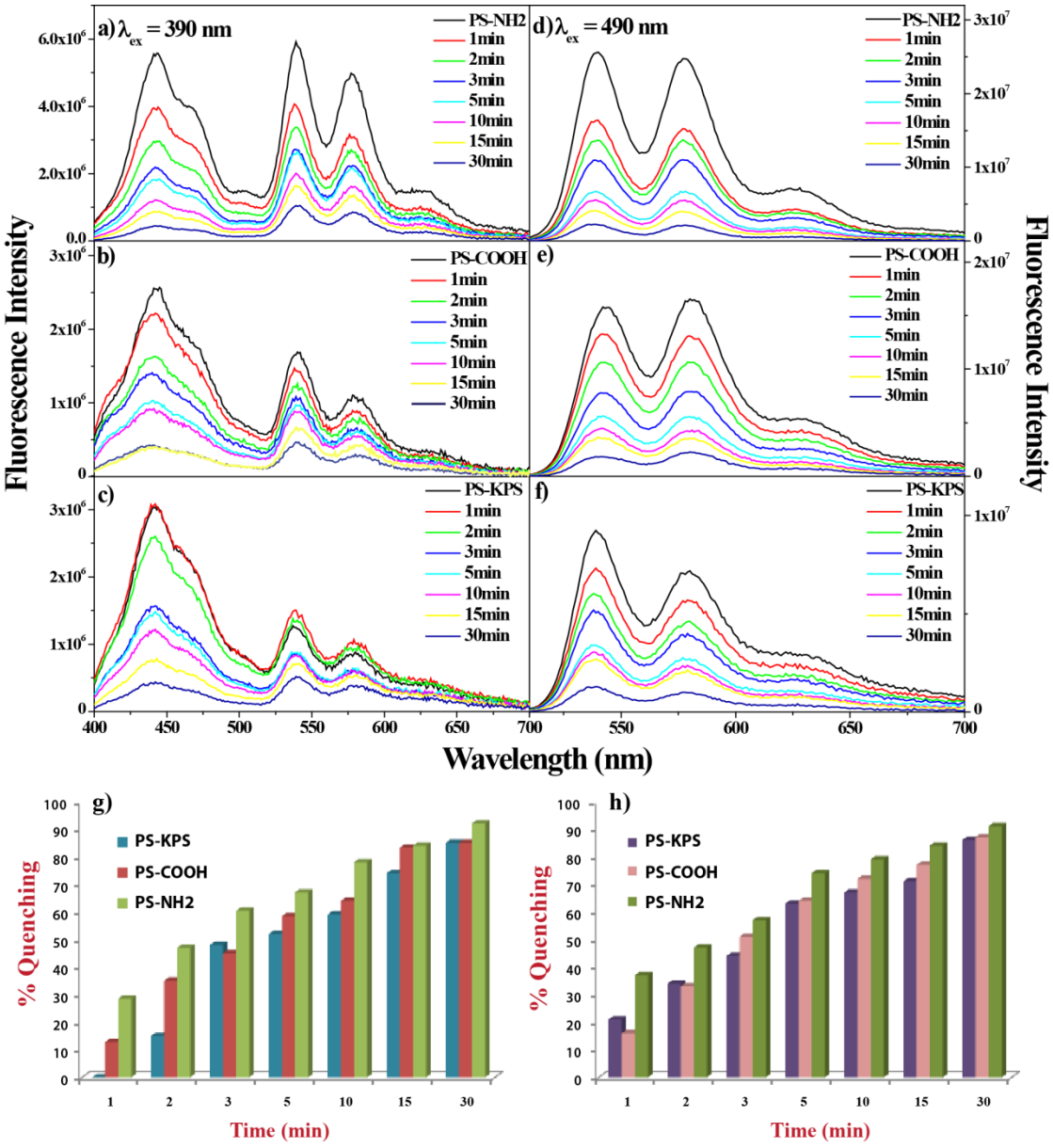

Figure 4A.16: Quenching of OPV emission upon exposure to NB vapor over time (0 to 30 min) for a) PS-NH2, b) PS-COOH and c) PS-KPS and g) their quenching percentage. Quenching of PBI emission upon exposure to vapor of *o*-TD over time (0 to 30 min) for d) PS-NH2, e) PS-COOH and f) PS-KPS and h) their quenching percentage.

exciting at PBI wavelength (490 nm) after the exposure to NB vapor, where no quenching of PBI emission was observed even after 30 minutes of exposure (***Figure 4A.17a***).

A similar experiment depicting the quenching of PBI emission upon exposure to vapors of *o*-TD is compiled for the three polymers in ***Figure 4A.16d-f***. ***Figure 4A.17b*** shows that the OPV emission (for PS-NH2) at 390 nm remained unaltered on exposure to *o*-TD vapor for 0 to 30 minutes, while the PBI emission exhibited reduction in intensity

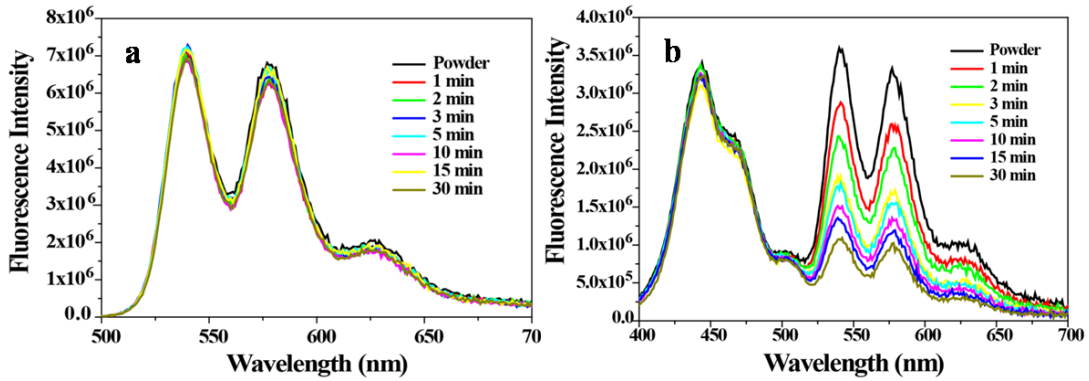

Figure 4A.17: a) Effect of NB vapor on the solid state emission of PBI in PS-NH2 as a function of time (0 to 30 min) at 490 nm. b) Effect of *o*-TD vapor on the solid state emission of OPV in PS-NH2 as a function of time (0 to 30 min) at 390 nm.

as a function of exposure time. The quantification of the percentage quenching of both OPV and PBI emission from these sets of experiments is summarized up in ***Figure 4A.16g-h***. It could be seen from the figure that among the three sets of polymers, the PS-NH2 had a faster response as it exhibited 50 % quenching of OPV / PBI emission within 2 minutes of exposure to the vapors of NB and *o*-TD respectively. PS-COOH also showed faster response compared to PS-KPS, especially for OPV emission quenching by interaction with NB.

Visual observation of the sharp emission color change from white to blue or yellow upon exposure of PS-NH2 powder to *o*-TD or NB vapor respectively is provided from digital images in ***Figure 4A.18(a-c)***. ***Figure 4A.18d*** demonstrates the clear and distinct changes captured for the same through CIE diagram, where the co-ordinates shift from (0.29, 0.31; white) to (0.43, 0.56; yellow) upon exposure with NB vapor (due to the direct excitation of PBI at 390 nm left after quenching of OPV emission) and to (0.19, 0.16; blue) upon exposure to *o*-TD vapor (due of PBI quenching).

When the surfaces of the nanoparticles are functionalized with carboxy or amine groups, sites are generated for formation of H-bonding between these groups and the analyte molecules. Hydrogen bonding facilitates the analyte molecules to approach the appropriate fluorophore and orient themselves in a proper orientation thereby effecting sensing at lesser time.[22,40,41] The slow kinetics for the case of PS-KPS was observed because of the higher time required for the analytes to establish electronic interaction with the fluorophore. Of the two differently functionalized nanoparticles, PS-NH2 having the surface functionalized with amine groups was more efficient for enhancing the sensing

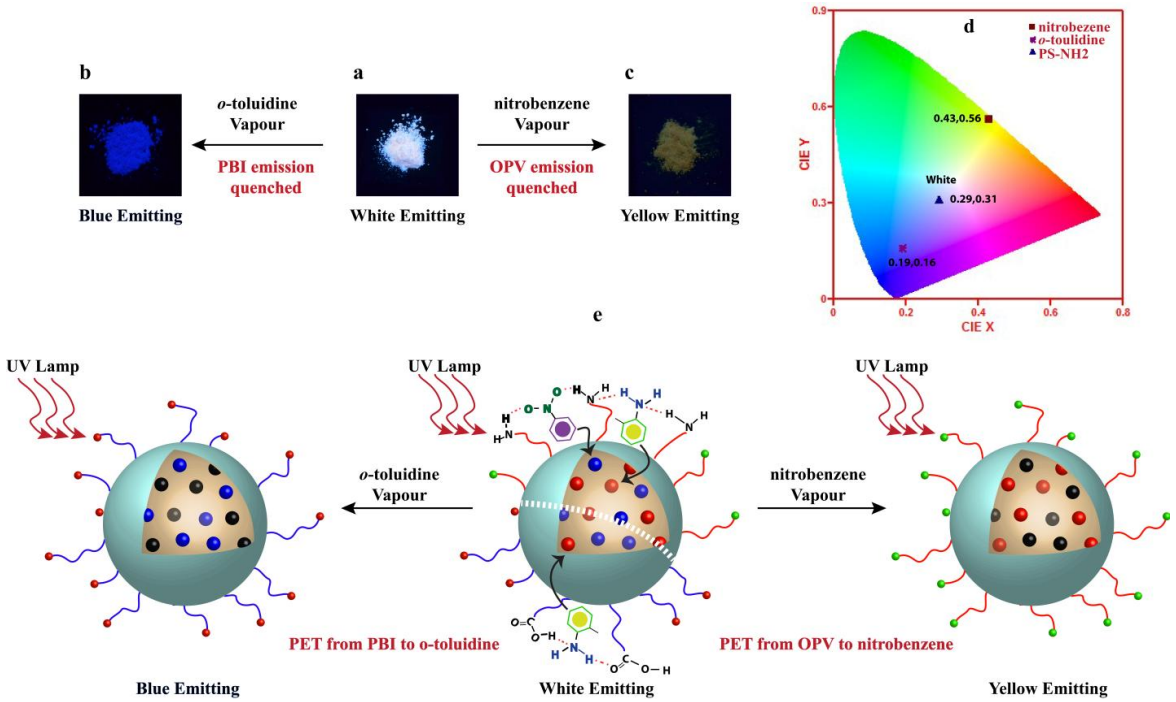

Figure 4A.18: PS-NH2 nanobeads under UV lamp a) pristine form b) after exposure to *o*-TD vapor c) after exposure to NB vapor. d) CIE co-ordinate diagram for PS-NH2 polymer demonstrating the color tuning and sensing of both *o*-TD and NB vapor. e) Possible mechanism of quenching by the nitro-organics and amine-organics vapor.

performance over the carboxy functionalized PS-COOH. The same was confirmed by dipping the PS-NH2 and PS-COOH pellet in KBr into the respective analyte solution for 1 min and their FTIR was recorded. The shift to lower wavenumber was more pronounced in case of PS-NH2 as compared to PS-COOH (***Figure 4A.19***).

A possible mechanism for the enhancement of sensing performance through surface functionalization of the nanoparticles is presented in ***Figure 4A.18e***. The values of quenching efficiency for all analytes were tabulated in the following tables (***Table 4A.4-4A.7)***.

Table 4A.4: Percentage quenching of OPV emission after exposure to various nitro compound vapors for 15 min.

Nitro compounds	PS-NH2	PS -COOH	PS -KPS
NB	**84**	**83.2**	**74**
2-NT	**43**	**39**	**37**
4 NT	**22**	**19.2**	**8.9**
PA	**1.2**	**3**	**2.2**
2,6-DNT	**3.6**	**4.4**	**2.6**
1,4-DNB	**7.9**	**2.1**	**4.1**
2,4-DNB	**13**	**10.3**	**6.6**
2,4-DNP	**2.6**	**1.4**	**0**
4-NP	**4.1**	**1.3**	**0**
NM	**3.9**	**3.1**	**3.6**
1,5 DNN	**5.9**	**3.5**	**0**

Table 4A.5: Percentage quenching of PBI emission after the exposure to various amine vapors for 15 min.

Amines compounds	PS -NH2	PS -COOH	PS -KPS
2-AMP	**4.8**	**2.5**	**2.9**
4-ABA	**3.2**	**0**	**3.3**
4-AHBA	**2.4**	**2**	**0**
BA	**2.1**	**2.2**	**1.8**
DA	**3.1**	**0**	**0**
Hyz	**12**	**9.1**	**4.3**
m-TD	**14**	**9.9**	**8**
p-TD	**5.4**	**2.8**	**4.5**
p-AD	**5.3**	**4.4**	**0**
3,4 DAT	**0**	**0**	**0**
o-AD	**31**	**20**	**14.7**
o-TD	**84**	**77**	**71**

Table 4A.6: Time dependent quenching of OPV emission after the exposure to vapor of NB.

Time (min)	PS -NH2	PS -COOH	PS -KPS
1	**28.5**	**12.8**	**0**
2	**47**	**35**	**15.2**
3	**60.4**	**44.6**	**48.3**
5	**67**	**58.4**	**52.6**
10	**78**	**64**	**59**
15	**84**	**83.2**	**74.8**
30	**92**	**85**	**85**

Table 4A.7: Time dependent quenching of PBI emission after the exposure to vapor of *o*-TD.

Time (min)	PS -NH2	PS -COOH	PS -KPS
1	**36.6**	**16**	**21.2**
2	**47**	**33**	**34.6**
3	**57.2**	**50.5**	**44.1**
5	**74**	**64.6**	**63**
10	**79**	**72**	**67**
15	**84.2**	**77.5**	**71**
30	**91**	**86.7**	**86.3**

Further to test the potential of the polystyrene nanoparticles for real time device based application, the polymer having highest efficiency *i.e.* PS-NH2 was selected for detailed analysis. A free standing film (thickness 0.07±0.01mm) was prepared by dropcasting THF solution of the polymer and exposing it to NB as most responsive nitroaromatics and *o*-TD as most responsive amine from their individual methanolic solutions (100 µL in 30 mL methanol). As observed from its powder form, the film showed white emission from the dry state or on exposure to pure methanol. When the film was dipped in the methanolic solution of NB for a minute, the emission changed to

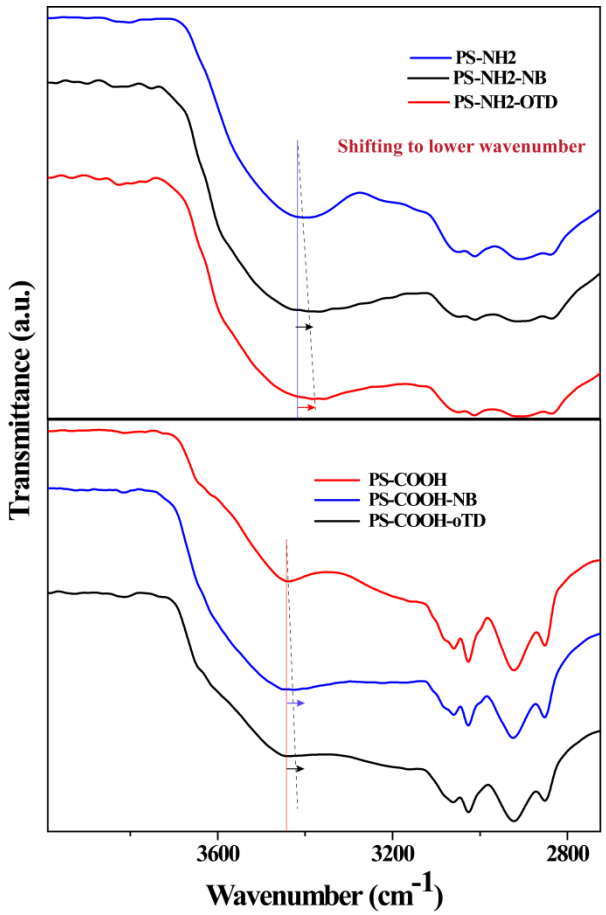

Figure 4A.19: FTIR spectrum comparing the shift in case of PS-NH2 and PS-COOH before and after dipping in the respective analyte solution for 1 min

yellow (***Figure 4A.20a-f***) similar to that observed from powder upon vapor exposure. Submerging the film in *o*-TD solution produced blue emission. Thus the prepared film was found to show similar efficient and quick response towards the incoming analytes, making it a good candidate for application in real life based devices. Furthermore, when the film used for NB detection was directly dipped in *o*-TD solution, it showed exactly similar emission property *i.e.* blue emission and vice versa. At any point of time the film could be made to regain its white emission by simply washing with few drops of methanol. This sensing could be repeated multiple times quickly and reversibly without much loss in sensing efficiency.

Figure 4A.20g depicts 8 consecutive cycles of alternating analyte sensing highlighting the advantages of film based sensing, thus making the film a highly suitable candidate for application in device fabricationto detect analytes in less than a minute.

The vapor phase limit of detection (LOD) for the analytes was also determined from emission quenching of the corresponding fluorophore by different concentrations of the analyte. The sensitivity of the sensor has been determined by considering signal to noise (S/N) ratio of 3 as the limit of detection.[42,43] The emission quenching performance was measured by exposing the prepared strip of PS-NH2 to vapor having different concentrations of the analyte. The saturated vapor of the analyte (prepared to required volume inside air tight syringes over 24 h) was diluted to various concentration by mixing with requisite volume of dry air. The prepared strip was exposed to the diluted vapor of the analyte from inside a pre-evacuated and air tight plastic bag. After 10 min of

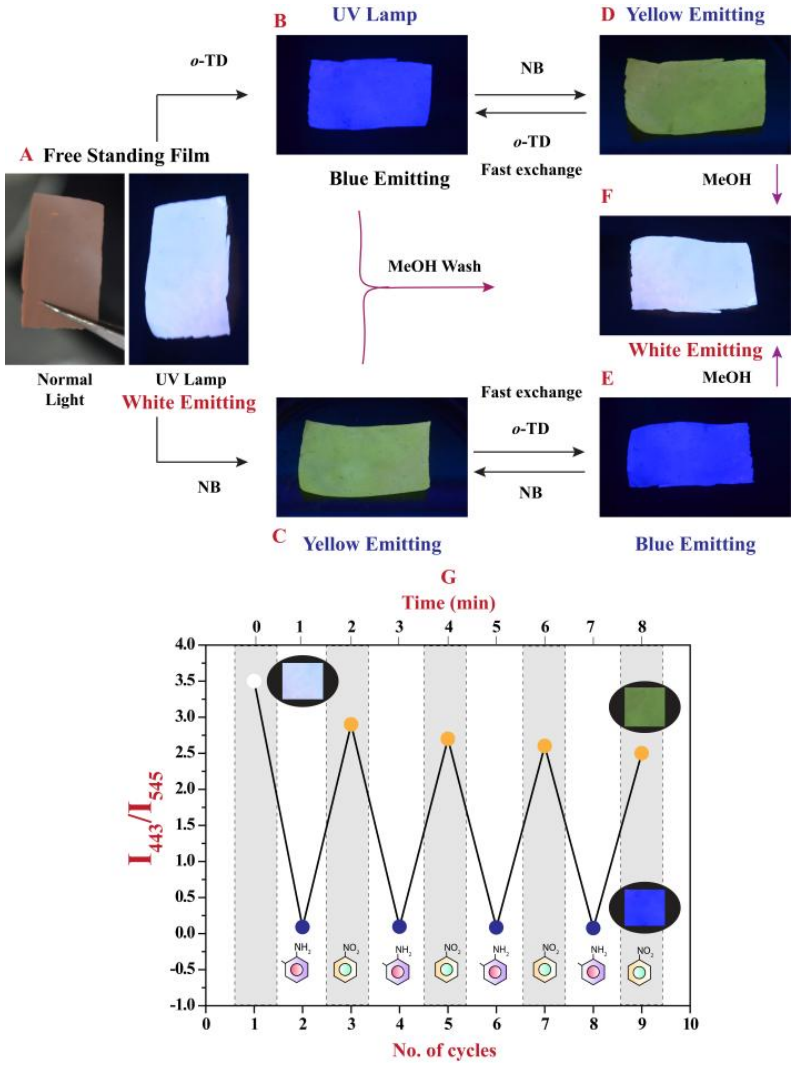

Figure 4A.20: Optical images of A) free standing film of PS-NH2 under normal and UV light (B) after dipping into *o*-TD solution and (C) NB solution (D,E) Fast exchange on dipping into *o*-TD or NB solution and vice versa. (F) Regain of white emission after methanol wash. (G) Multi-analyte detection on alternatively dipping the free standing film of PS-NH2 into NB and *o*-TD solution. Emission spectra were collected every minute after dipping into the respective analyte solution.

exposure, the emission intensity of the nanobeads from the strip was recorded and corresponding quenching was calculated. A thorough comparison with other NB and *o*-TD sensors reported in the literature is synopsized in ***Table 4A.8, 4A.9*** from which we found that our sensors could overcome several inadequacies in type of material, response, fast exchange of analyte and reusability *etc.* with appreciable LOD values when compared to other literatures for both the analytes. The LOD determined by 3S/N ratio was found to be 5.6 ppm for NB and 6.9 ppm for *o*-TD vapor. To the best of our knowledge, this is first report on highest LOD reported for *o*-TD in the literature so far.

Table 4A.8: Comparison of reported sensors for detection of NB.

Name of the Sensor (Type of Material)	Type of Response	LOD (ppm)	Phase of Sensor	Analyte Detection Medium	Dual Distinct Response	Fast exchange of analyte	Recyclability (Cycles)	Ref
MOF	Quenching	0.2	Solution/ Powder	Solvent/ Vapor	No	No	Yes (-)	44
MOF	Current Change	0.62	Solution	Solvent (Water)	No	No	Yes (3)	45
Conjugated Polymers	Quenching	2.6	Solution	Solvent (Water)	No	No	NA	46
MOF	Quenching	NA	Solution	Solvent (DMF)	No	No	Yes (5)	47
MWCT	Current Change	0.04	Solution	Solvent (Water)	No	No	Yes (5)	48
MOF	Quenching for both	60	Solution	Solvent (MeOH)	Non-distinct dual	No	NA	49
MOF	Quenching	160	Solution	Solvent (Acetone)	No	No	Yes (5)	50
MOF	Quenching	NA	Solution	Solvent (DMA)	No	No	Yes (8)	51
Conjugated Polymers	Quenching	NA	Film	Vapor	No	No	Yes (20)	52
Porous Si	Quenching	0.5	Film	Vapor	No	No	Yes (6)	53
Conjugated PAH		NA	Free standing Film	Vapor	No	No	NA	54
Small molecule	Color tuning	NA	Film	Vapor	Yes	No	NA	55
PS nanobeads	Color tuning	5.6	Free standing Film / Powder	Vapor	Yes NB(Yellow) *o*-TD (Blue)	Yes	Yes (8)	This work

Table 4A.9: Comparison of reported sensors for detection of *o*-TD.

Name of the Sensor (Type of Material)	Type of Response	LOD (ppm)	Phase of Sensor	Analyte Detection Medium	Dual Distinct Response	Fast exchange of analyte	Recyclability (Cycles)	Ref
Small molecule	Quenching	NA	Solution/ Powder	Solvent	No	No	Yes (-)	56
Small molecule	Color tuning	NA	Film	Vapor	Yes	No	Not available	55
PS nanoparticle	Color tuning	6.9	Free standing Film / Powder	Vapor	Yes NB(Yellow) *o*-TD (Blue)	Yes	Yes (8)	This work

4A.3 Experimental Details:

4A.3.1 Materials: Sodium dodecyl sulfate (SDS), Brij S-100, 4,4'-Azobis(4-cyanovaleric acid) (ACVA), Potassium persulfate (KPS), Aminoethyl methacrylate hydrochloride (AEMH) were purchased from Aldrich, *n*-Hexadecane (HD) from Alfa Aesar and were used as received. Acrylic acid (AA), styrene bought from Aldrich was purified prior to use as per the standard protocol. All the analytes used for sensing studies were purchased from commercially available sources and used as received. Solvents and other reagents were purchased from local suppliers and purified using standard procedures. Demineralized water was used throughout the whole scheme of work.

4A.3.2 Details of Analytical Instruments: The instrumentation used for characterization of the polymers like the GPC, TEM, DLS (for size and zeta potential), Sonicator, TGA, NMR, absorption and fluorescence spectrophotometer are same as described in the ***Chapter 2***. The polymer powders were mixed with KBr to make pellets and their infrared spectra was recorded using Bruker α–T spectrophotometer in the range of 4000-600 cm^{-1}. The Solid State Quantum yield was determined using F-3029 Quanta-Phi 6″ Integrating Sphere connected to Horiba JobinYvon Fluorolog 3 spectrophotometer. GC-MS analyses were performed with Agilent make 7890B GC coupled with 5977A MD detector.

4A.3.3 Preparation of Sample for Sensing Studies: For carrying out the vapor sensing analysis, the polymer powders were directly exposed to the analyte vapor. In one such process, transparent adhesive tape was secured on a thin cardboard frame as a support and then polymer powder was adhered on it. This sample strip was then exposed to the analyte vapor and PL measurement was performed to check for its sensing property. In another case, a free standing film was prepared from THF solution containing 20 mg of polymer per ml of solvent. The solution was poured into a petridish and the solvent was allowed to evaporate at room temperature. The film (thickness 0.07 ± 0.01 mm) was then peeled off, cut into desired size and used directly for sensing studies in the similar way.

4A.3.4 Study of the chemical sensing: For studying the polymers towards sensing of the analytes from vapor phase, saturated vapor chambers were prepared by placing analytes inside a closed 50 mL falcon for 24 h at room temperature (25 °C). After 24 h, powder samples in the form of prepared stripes described above was placed inside the falcon, avoiding any direct contact of the analyte with the sample and the chamber was closed. The sample was then removed from the vapor chamber after the mentioned residence time and emission spectra were recorded immediately.

For sensing studies with free standing film (thickness 0.07 ± 0.01 mm), the prepared film was directly dipped into methanolic solution of the analyte (100 µL in 30 mL methanol) for 1 min and then removed to soak off the excess liquid from the film surface. The emission spectra were recorded with the dried film, without any further delay.

For checking the emission from the OPV moiety of the polymers, the samples were excited at $\lambda_{excitation}$ = 390 nm and the emission spectra were collected in the range of 400 to 700 nm. While, for PBI, emission spectra was recorded in the range of 500 to 700 nm using $\lambda_{excitation}$ = 490 nm. The percentage quenching was calculated using following equation (***eq 4***):

$$\% \text{ Quenching} = \frac{I_0 - I}{I_0} \times 100 \quad \text{.....eq 4}$$

Where I_0 and I are the intensities at their respective emission maxima, before and after exposure to the analyte.

4A.3.5 Detailed calculation for measurement of analyte concentration from vapor phase:

For knowing the concentration of analyte in saturated vapor identical vapor chamber was generated inside an air tight syringe containing 1.5 mL of the analyte and 20 mL air. The analyte was allowed to gain equilibrium between vapor and liquid phase in next 24 hrs. The collected vapor was then directly bubbled into 1 mL acetonitrile taken in a GC vial. The obtained solution was then analyzed using GC-MS and the area of the corresponding peak was compared to that of a standard known solution (2 µL of analyte in 10 mL acetonitrile) to determine the analyte concentration in vapor phase using the following equation (***eq 5***) (details of calculation is provided below):

$$C_{ana} = C_{std} \times \frac{A_{ana}}{A_{std}} \times 112.25 \times 10^4 \text{ ppm} \quad \text{.....eq 5}$$

where C_{ana} = concentration of analyte in vapor, C_{std} = concentration of analyte in stock solution, A_{ana}= area corresponding to vapor, A_{std}= area corresponding to stock solution.

An acetonitrile solution having 20 mL analyte vapor dissolved in was injected to GC-MS for determination of area under chromatogram and subsequent comparison with standard

sample solution. Since area under the chromatogram is directly proportional to the concentration of the analyte solution,

$$C_{sample} = \frac{A_{sample}}{A_{standard}} \times C_{standard}$$

The concentration of the analyte in the solution was used to determine the concentration in vapor phase as follows:

No. of moles of the analyte present in 1 mL acetonitrile solution (calculated conc. of C_{sample} M) is (C_{sample} x 10^{-3})

This mole number originated from 20 mL of the saturated vapor, hence 10^6 mL of such vapor would contain (C_{sample} x 10^{-3} x 10^6 / 20, or 50 x C_{sample}) moles of the analyte.

Now, as per ideal gas equation, volume of (50 x C_{sample}) moles of the anlayte under NTP is (22400 x 50 x C_{sample}), or (C_{sample} x 1.12 x 10^6) ml.

Thus the saturated vapor contains (C_{sample} x 1.12 x 10^6) ml of the analyte per 10^6 ml of total volume, i.e. (C_{sample} x 1.12 x 10^6) parts of analyte per million parts.

Therefore the concentration of the analyte in the vapor phase is calculated as (C_{sample} x 1.12 x 10^6) ppm *.i.e.*

$$C_{ana} = C_{std} \times \frac{A_{ana}}{A_{std}} \times 112.25 \times 10^4 \text{ ppm} \quad \text{.....eq 5}$$

While measuring LOD for analyte vapor, concentration of the analyte in the diluted vapor was calculated using the equation: $C_1V_1 = C_2V_2$

From GC analysis concentration for nitrobenzene and *o*-toulidine inside the vapor chamber were calculated using the above mentioned formula and were found to be 186 and 232 ppm respectively. In order to further determine their limit of detection (LOD), paper strip placed in air tight plastic bag was exposed to different concentration of analyte vapors (0.5 mL, 1 mL, 1.5 mL, 2 mL) which were syringed into the bag and diluted with dry air (9.5 mL, 9 mL, 8.5 mL, 8 mL) and subsequently their emission were recorded.

4A.4 Conclusion:

We have developed distinctly dual vapor based solid state emitting polystyrene nanobeads sensor having OPV and PBI incorporated together in the polymer backbone.

The chromophores were incorporated into the polystyrene nanobeads in a suitable proportion as to obtain near white emission under UV light. The surface of nanobeads was selectively functionalized with amine (PS-NH2) or carboxy (PS-COOH)

functionality and their sensing efficiency was compared with the one having no functionalization (PS-KPS). Exposure of the polymer beads to the vapors of electron deficient nitrocompounds quenched the emission from OPV moiety selectively retaining the emission from PBI resulting in yellow emission from nanobeads under UV lamp. On the other hand, PBI emission was quenched on exposure to amine vapors resulting in blue emission from nanobeads. The functionality on the surface of the nanobeads assisted in better analyte sensor interaction through solid-state hydrogen bonding resulting in enhanced quenching of the respective chromophores when compared to non-functionalized nanobeads. The nanobead with surface amine functionality (PS-NH2) exhibited the highest sensing efficiency for both electron deficient and rich analytes. Device applicability was demonstrated by free standing film (thickness 0.07±0.01mm) of PS-NH2 polymer which underwent fast exchange of analytes observable under UV lamp and reusability of film was checked upto 8 cycles.

NOTE: The results presented in this chapter are already published in *Anal. Chem.* **2018**, *90*, 7434–7441 with the title '*Surface Functionalized Fluorescent PS Nanobead Based Dual-Distinct Solid State Sensor for Detection of Volatile Organic Compounds*'.

4A.5 References:

1. Che, Y.; Yang, X.; Loser, S.; Zang, L. *Nano Lett.* **2008**, *8*, 2219-2223.

2. Wu, P.; He, Q.; Zhu, D.; Jiang, H.; Jiao, Z.; Zhang, Y.; Xu, W.; Fu, Y.; Cao, H.; Cheng, J. *Anal. Methods* **2017**, *9*, 3804–3809.

3. Chen, D. M; Tian, J. Y; Chen, M.; Liu, C. S.; Du, M. *ACS Appl. Mater. Interfaces* **2016**, *8*, 18043−18050.

4. Riedel, K.; Scherer, G.; Engl, J.; Hagedorn H.W.; Tricker, A. R. *J. Anal. Toxicol.* **2006**, *30*, 187–195.

5. Swager , T . M.; Wosnick , J . H . *Mater. Res. Soc. Bull.* **2002**, 27, 446-450.

6. Zhang, X.; Liu, X.; Lu, R.; Zhang, H.; Gong, P. *J. Mater. Chem.* **2012**, *22*, 1167-1172.

7. Kim, H. N.; Guo, Z.; Zhu, W.; Yoon, J.; Tian, H. *Chem. Soc. Rev.* **2011**, *40*, 79–93

8. Yi, F. Y.; Li, J. P.; Wu, D.; Sun, Z. M. *Chem. Eur. J.* **2015**, *21*, 11475 – 11482.

9. Desmonts, L. B.; Reinhoudt, D. N.; Calama, M. C. *Chem. Soc. Rev.* **2007**, *36*, 993–1017.

10. Arduini, M.; Marcuz, S.; Montolli, M.; Rampazzo, E.; Mancin, F.; Gross, S.; Armelao, L.; Tecilla, P.; Tonellato, U. *Langmuir* **2005**, *21*, 9314-9321.

11. Asfura, K. M. G.; Leblanc, R. M. *Chem. Commun.* **2003**, *0*, 2684–2685.

12. Phillips, R. L.; Miranda, O. R.; You, C. C.; Rotello, V. M.; Bunz, U. H. F. *Angew. Chem. Int. Ed.* **2008**, *47*, 2590-2594.

13. Ng, S. M.; Narayanaswamy, R. *Anal. Bioanal. Chem.* **2006**, *386*, 1235-1244.

14. McNamara, K. P.; Rosenzweig, Z. *Anal. Chem.* **1998**, *70*, 4853-4859.

15. Liu, Y.; Wang, K. R.; Guo, D. S.; Jiang, B. P. *Adv. Funct. Mater.* **2009**, *19*, 2230–2235.

16. Zhao, D.; Swager, T. M. *Macromolecules* **2005**, *38*, 9377-9384.

17. Sreejith, S.; Divya, K. P.; Ajayaghosh, *Chem. Commun*. **2008**, 2903-2905.

18. Levitus, M.; Schmieder, K.; Ricks, H.; Shimizu, K. D.; Bunz, U. H. F.; Garcia-Garibay, M. A. *J. Am. Chem. Soc.* **2001**, *123*, 4259-4265.

19. Thomas, S. W.; Joly, G. D.; Swager, T. M. *Chem. Rev.* **2007**, *107*, 1339−1386.

20. Bai, M.; Huang, S.; Xu, S.; Hu, G.; Wang, L. *Anal. Chem.* **2015**, *87*, 2383−2388.

21. Huang, S.; He, Q.; Xu, S.; Wang, L. *Anal. Chem.* **2015**, *87*, 5451−5456.

22. Gole, B.; Shanmugaraju, S.; Bar, A. K.; Mukherjee, P. S. *Chem. Commun.* **2011**, *47*, 10046–10048.

23. Han, T.; Lam, J. W. Y.; Zhao, N.; Gao, M.; Yang, Z.; Zhao, E.; Dong, Y.; Tang, B. Z. *Chem. Commun.* **2013**, *49*, 4848-4850.

24. Jiang, B. P. Guo, D. S.; Liu, Y. *J. Org. Chem.* **2011**, *76*, 6101–6107.

25. Jiang, B. P. Guo, D. S.; Liu, Y. *J. Org. Chem.* **2010**, *75*, 7258–7264.

26. Yan, K; Yang, Y; Zhu, Y; Zhang, J. *Anal. Chem*. **2017**, *89*, 8599−8603.

27. Kartha, K. K.; Babu, S. S.; Srinivasan, S.; Ajayaghosh, A. *J. Am. Chem. Soc.* **2012**, *134*, 4834−4841.

28. He, G.; Yan, N.; Yang, J.; Wang, H.; Ding, L.; Yin, S.; Fang, Y. *Macromolecules* **2011**, *44*, 4759–4766.

29. Pang, L.Y.; Yang, G. P.; Jin, J. C. Kang, M.; Fu, A.Y.; Wang, Y. Y.; Shi, Q. Z. *Cryst.Growth Des.* **2014**, *14*, 2954−2961.

30. Cao, L. H.; Shi, F.; Zhang, W. M.; Zang, S. Q.; Mak, T. C. W. *Chem. Eur. J.* **2015**, *21*, 15705 – 15712.

31. Yang, L.; Lian, C.; Li, X.; Han, Y.; Yang, L.; Cai, T.; Shao, C. *ACS Appl. Mater. Interfaces* **2017**, *9*, 17208−17217.

32. Huang, X. L.; Liu, L.; Gao, M. L.; Han, Z. B. *RSC Adv.* **2016**, *6*, 87945-87949.

33. Sandeep, A.; Praveen, V. K.; Kartha, K. K.; Karunakaran, V.; Ajayaghosh, A. *Chem. Sci.* **2016**, *7*, 4460–4467.

34. Sonawane, S. L.; Asha, S. K. *ACS Appl. Mater. Interfaces* **2016**, *8*, 10590−10599.

35. Würthner, F. *Chem. Commun*. **2004**, *0*, 1564–1579.

36. Singh, H.; Balamurugan, A.; Jayakannan, M. *ACS Appl. Mater. Interfaces* **2013**, *5*, 5578−5591.

37. Hu, J.; Li, C.; Liu, S. *Langmuir* **2010**, *26*, 724-729.

38. Holzapfel, V.; Musyanovych, A.; Landfester, K.; Lorenz, M. R.; Mailänder, V. *Macromol. Chem. Phys.* **2005**, *206*, 2440–2449.

39. Ramanathan, T.; Fisher, F. T.; Ruoff, R. S.; Brinson, L. C. *Chem. Mater.* **2005**, *17*, 1290-1295.

40. Gole, B.; Song, W.; Lackinger, M.; Mukherjee, P. S. *Chem. Eur. J.* **2014**, *20*, 13662 – 13680.

41. Long, Y.; Du, X.; Wang, Y.; Zhao, J.; Tai, H.; Tang, X.; Jiang, Y. *RSC Adv.* **2014**, *4*, 59643-59649.

42. Shrivastava, A.; Gupta, V. B. *Chronicles of Young Scientists* **2011**, *2*, 21−25.

43. Liu, S. G.; Luo, D.; Li, N.; Zhang, W.; Lei, J. L.; Li, N. B.; Luo, H. Q. *ACS Appl. Mater. Interfaces* **2016**, *8*, 21700−21709.

44. Tian, D.; Chen, R. Y.; Xu, J.; Li, Y. W.; Bu, X. H. *APL Materials* **2014**, *2*, 124111-124112.

45. Liu, L. L.; Chen, J.; Yu, C. X.; Lv, W. X.; Yu, H. Y.; Xiao-Qing Cui, X. Q.; Liu, L. *Dalton Trans.***2017**, *46*, 178-185.

46. Huang, W.; Smarsly, E.; Han, J.; Bender, M.; Seehafer, K.; Wacker, I.; Schröder, R. R.; Bunz, U. H. F. *ACS Appl. Mater. Interfaces* **2017**, *9*, 3068−3074.

47. Parshamoni, S.; Telangae, J.; Konar, S. *Dalton Trans.* **2015**, *44*, 20926-20935.

48. Govindasamy, M.; Mani1, V.; Chen, S. M.; Subramani, B.; Devasenathipathy, R.; Tamilarasan, S. *Int. J. Electrochem. Sci.* **2016**, *11*, 10837 – 10846.

49. Huang, X. L.; Liu, L.; Gao, M. L.; Han, Z. B. *RSC Adv*. **2016**, *6*, 87945-87949.

50. Zhao, S.; Lv, X. X,; Shi, L. L.; Li, B. L.; Wu, B. *RSC Adv.* **2016**, *6*, 56035-56041.

51. Zhang, S. R.; Du, D. Y.; Qin, J. S.; Li, S. L.; He, W. W.; Lan, Y. Q.; Su, Z. M. *Inorg. Chem*. **2014**, *53*, 8105−8113.

52. Wu, X.; Li, H.; Xu, Y.; Xu, B.; Tong, H.; Wang, L. *Nanoscale* **2014**, *6*, 2375-2380.

53. Content, S.; Trogler, W. C.; Sailor, M. J.; *Chem. Eur. J.* **2000**, *6*, 2205-2213.

54. *Liao,Y. Z.; Strong, V.; Wang, Y.; Li, X. G.; Wang, X.; Kaner, R. B. Adv. Funct. Mater.* **2012**, *22*, 726–735.

55. Sandeep, A.; Praveen, V. K.; Kartha, K. K.; Karunakaran, V.; Ajayaghosh, A. *Chem. Sci.* **2016**, *7*, 4460–4467.

56. Shang, C.; Wang, G.; He, M.; Chang, X.; Fan, J.; Liu, K.; Peng, H.; Fang, Y. *Sensors and Actuators B* **2017**, *241*, 1316–1323.

CHAPTER-4B

Amine decorated Polystyrene Nanobeads with π-Conjugated OPV Chromophore For Picric acid Sensing in Water

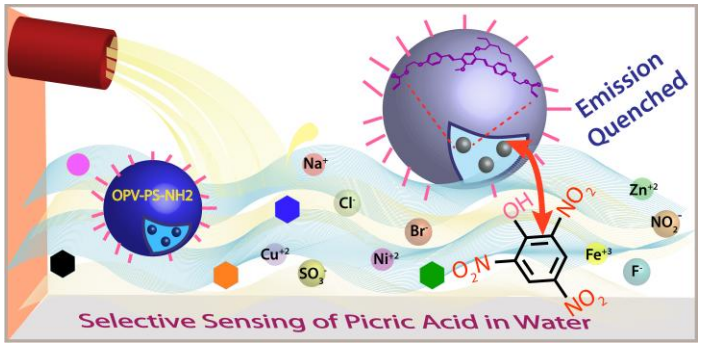

Abstract: *This chapter deals with synthesis of amine functionalized fluorescent polystyrene nanobeads for selective detection of Picric acid (PA) in water among other interferences such as metal ions, anions and other nitroexplosives. Amine functionalized oligo (p-phenylenevinylene) (OPV) incorporated polystyrene nanobeads (PS-OPV-NH2) was synthesized using miniemulsion polymerization in the size range of 182 nm. The amine (-NH2) functionalization was performed to enhance the selectivity of sensor from among the library of other nitro-organics. The combined effect of energy transfer, inner filter effect and electron transfer mechanism resulted in outstanding selectivity of sensor. To check the applicability of sensor in the real water sample interference from large number of cations and anions were checked. Finally device based on-site application and reusability of sensor was examined by free standing film of polymer. Thus rapid and efficient sensor could be developed for visual detection of PA in aqueous medium with detection limit as low as 58 nM.*

4B.1 Introduction:

The sensitive and selective sensing of nitroexplosives is seeking immense consideration due to security reasons and environmental protection.[1] Among the nitro explosives, picric acid (PA) is highly explosive material due to its high denotation velocity and low safety coefficient. Additionally, unlike other nitroexplosive, it is also widely used in dye and drug industries, antiseptic and pesticide manufacturing *etc*.[2] This makes it easier to enter the environment and pollute soil and natural water owing to its excellent water solubility. Any such environmental pollution leads to severe health concerns including anemia, cancer, male impotency and other respiratory problems.[3-5] Such an important aspect has thus dragged the focus of researchers from around the globe and various sensor has been developed through time. To name a few, very recent approaches to detect the presence of picric acid consists of various luminescent materials like quantum dots (QD)[6], polymers[7], upconverting nanoparticles (UCNP)[8], metal-organic frameworks (MOF)[9], small molecules[10] *etc* (***Figure 4B.1***). One such example of MOF based sensor has been reported by Shi *et al.*[11] for highly efficient detection of PA in DMA. This sensor is based on the luminescence quenching of a fluorescent MOF. Likewise Sang *et al.*[12] and Venkatramaiah *et al.*[10] reported covalent organic framework (COF) and small molecule based PA sensor in methanol and ethanol respectively. Based on the similar working principle, Wang *et al.* has recently developed a QD based sensor[9], where exploitation of emission property for carbon QD has been used for selective detection of PA from water. In another study with UCNP, presence of PA has been detected from mixed aqueous solvent through quenching of its inherent emission property.[8] But most of these sensors suffered from major limitations such as poor selectivity,[10,13-15] poor water dispersibility, aggregation induced emission quenching in aqueous medium, *etc*.[10-16]

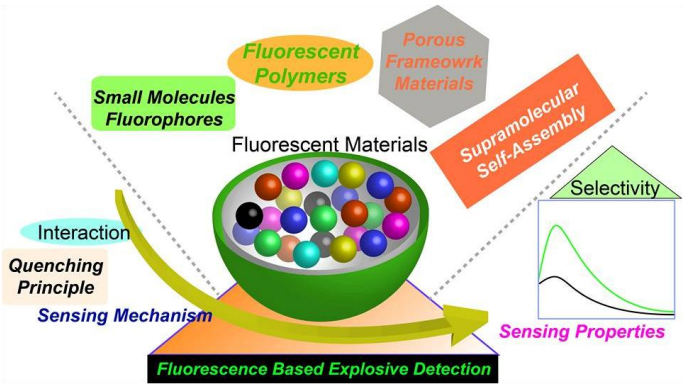

Figure 4B.1: Illustration of fluorescence based materials for sensing nitroexplosives.

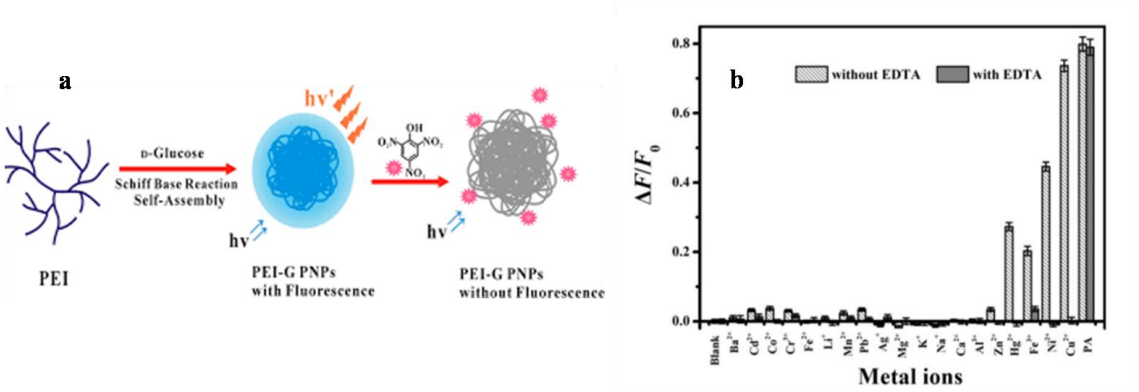

Figure 4B.2: a) Preparation of poly(ethylenimine) (PEI)-D-glucose polymeric NPs and detection of PA. (b) Its emission response to metal ions in presence and absence of EDTA. (Figure is adapted from ***Ref 26*** with permission from ACS Publishers)

Additional factors such as release of toxic metals in case of MOF, UCNP and QD, instability of MOF in water limits their practical applicability.[16-18] Also the varying emission of UCNPs and QDs on exposure to varying temperature and pH makes it really difficult for a conclusive remark on the observed sensing.[17,18] This leads to a continuous stretch to the search for a fluorescent based sensor for picric acid to check and prevent any possible harm in terms of environmental pollution and detecting buried explosives.

In the context of fluorescent based sensors, conjugated polymers always hold the superiority in terms of high QE, tunable emission, *etc*. Thus, applications of conjugated polymers are expected to produce effective outcome for analyte sensing. However, in such reported sensors, the lack of specific binding site for the interaction with analytes[19-21] along with multistep tedious synthesis,[19,21,22] sometime limits their application. Other common drawback lies in the scope of application, where the interference of other nitro explosives[22-25] or some heavy metal ion[20,25,26] *eg.* Cu(II), Ni(II), Fe(III), Zn(II) (that are present in water) are significant (***Figure 4B.2***) and hence their removal is required prior to the sensing of PA.[26]

In an attempt to overcome the above limitations without compromising the selectivity as well as sensitivity of the sensor, we are presenting two approaches *i.e.* surface functionalization and covalent stitching of fluorophore. In this work we have prepared amine (-NH2) functionalized polystyrene (PS) based sensor for the visual detection of PA using green and environmentally benign miniemulsion polymerization method (***Scheme 4B.1***). We have chosen oligo (*p*-phenylenevinylene) (OPV) based chromophore because of its appreciable quantum yield, excellent thermal and photo stability; polystyrene as backbone to reduce aggregation induced quenching of

fluorophore emission. However keeping our previous knowledge of covalent stitching in mind, OPV was covalently stitched to the polymer backbone to prevent any dye leaching which might hamper the sensor performance during application cycles. Amine functionalization on the surface of the nanobeads was performed with the view to provide specific binding sites for the analytes and to improve its selectivity by boosting

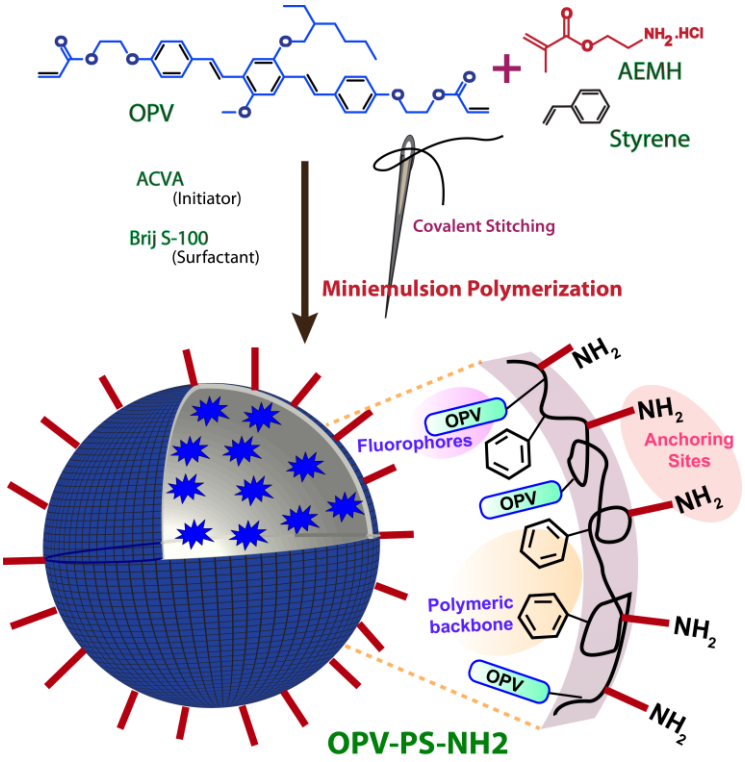

Scheme-4B.1: Schematics for synthesis of amine decorated polystyrene nanobeads *via* miniemulsion polymerization.

analyte-sensor interaction. Furthermore, interference from almost 16 cations including Ni(II), Cu(II), Zn(II), Fe(III) that are commonly present in water were checked to test their effect on sensor performance. Device applicability and reusability of sensor was checked further by casting free standing film from polymer. Hence efficient, prompt and highly selective on-site sensing of PA can be achieved in 100% aqueous medium.

4B.2 Results and Discussions:

4B.2.1 Synthesis and structural characterization: π-conjugated OPV based dye was synthesized and characterized as per the previously described procedure. The dye was then covalently incorporated into polystyrene backbone through miniemulsion co-polymerization, using non-ionic Brij S-100 as surfactant and 4,4'-Azobis(4-cyanovaleric acid) (ACVA) as initiator. Aminoethyl methacrylate hydrochloride (AEMH) was used as functional monomer to functionalize the surface of the resulting nanobeads (PS-OPV-

NH2) with -NH2 group, creating favorable sites for interaction with electron deficient compounds as incoming analyte. Such amine functionalized OPV incorporated polystyrene nanobeads was prepared following the protocol described in the previous section of the ***Chapter 4A*** (***Section 4A.2.1)***. In such a typical reaction process, the organic phase containing 1 g of styrene, 30 mg OPV and 48 mg of hexadecane was dropwise added to a aqueous phase (4 mL) 100 mg of AEMH, 16 mg of ACVA and 33 mg of Brij S-100. This mixture was then pre-emulsified for an hour at room temperature. The emulsion thus obtained was then sonicated for another 20 min in an ice-cooled bath.

Table 4B.1: Number and weight average molar mass, polydispersity indices (PDI), solid content, zeta potential of PS-OPV-NH2.

Sample	**Mn[a]**	**Mw[a]**	**PDI[a](Đ)**	**Solid content (%)**	**Zeta Potential[b]**
PS-OPV-NH2	56700	151000	2.6	21	+36.6

a) Measured by Gel Permeation Chromatography (GPC) in Chloroform ($CHCl_3$) calibrated with linear, narrow molecular weight distribution polystyrene standards.
b) Measured by Dynamic Light Scattering in water.

Finally, the polymerization was carried out for 20 h at 70 ^{0}C with a constant stirring at 750 rpm. Then obtained latex was dialyzed using a dialysis membrane (molecular weight cutoff = 6 kD) against deionised water for 3 days, with water change in every six hours. The percentage solid content of the polymer was calculated using standard equation. The solid content value of PS-OPV-NH2 is tabulated in ***Table 4B.1***.

The surface charge of the resulting nanobeads was confirmed by a net elevated positive zeta potential of +36.6 mV, indicating presence of -NH2 groups on the surface (***Table 4B.1***). FTIR analysis further confirmed the presence of -NH2 group, from the presence of characteristic peaks (***Figure 4B.3a***). Broad peak centered at 3408 cm^{-1} accounted for N-H stretching while the in-plane bending resulted a sharp peak at 1604 cm^{-1}. Another broad peak at 1100 cm^{-1} accounted for C-N stretching. The relative

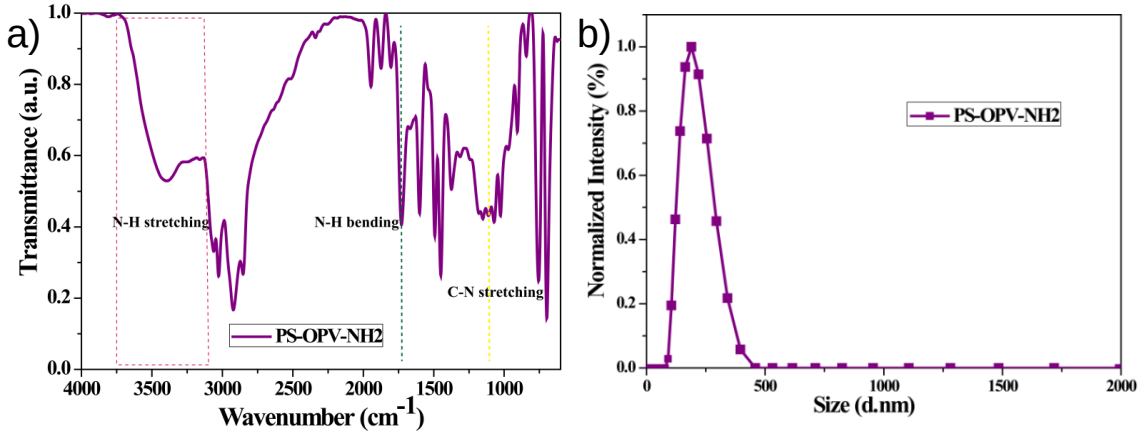

Figure 4B.3: a) FTIR plot of polymer on KBr pellet, b) Normalized intensity-average size distribution of polymer in demineralized water using Dynamic Light Scattering

molecular weight was determined by gel permeation chromatography (GPC) in tetrahydrofuran (THF). It was found to possess high molecular weight in the range of 151 KDa (Mw) with PDI value of 2.6 and the values are tabulated in ***Table 4B.1***. The size of the nanobeads, as observed from particle size analysis with dynamic light scattering lied in the range of 182 nm with PDI value of 0.08, signified uniform size distribution profile as obtained by miniemulsion polymerization approach (***Figure 4B.3b***, ***Table 4B.2***).

Table 4B.2: Dye loading content (DLC), Dye loading efficiency (DLE), polydispersity index (Đ).

Sample	Amount of OPV in feed (mg)	Amount of OPV incorporated (mg)[a]	DLC (%)[a] For OPV	DLE (%)[a] For OPV	Size (nm)[b]	PDI[b]
PS-OPV-NH2	30	16.1	1.6	53.6	182	0.08

a) Dye Loading content (DLC) and Dye Loading Efficiency (DLE)are calculated by absorption studies in THF.
b) Measured by Dynamic Light Scattering in water.

TEM imaging further confirmed spherical morphology of the nanobeads, with monomodal distribution of nanoparticle size, as obtained by DLS (***Figure 4B.4a***).

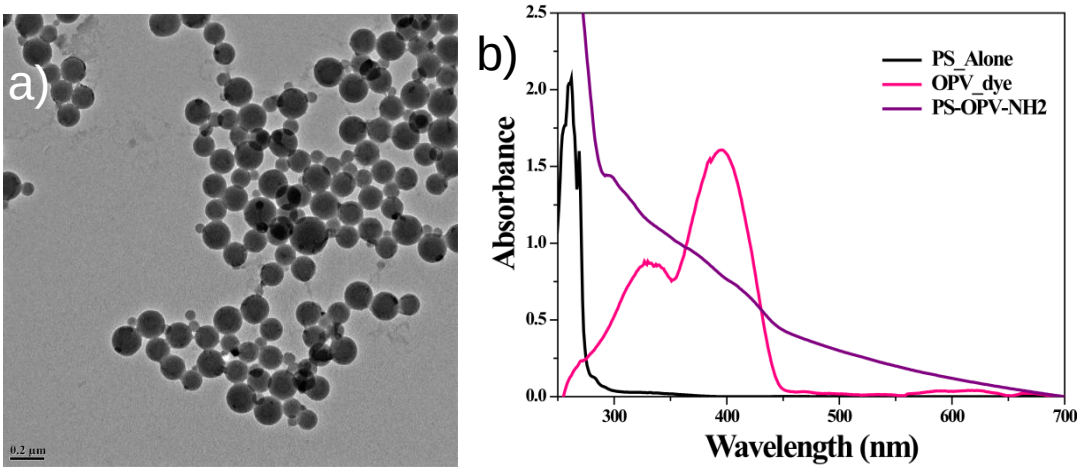

Figure 4B.4: a) TEM image of PS-OPV-NH2 polymer, showing the spherical morphology with uniform size distribution, b) Absorption spectra of the polymer in THF (1 mg/ml) for DLC and DLE calculation.

Lower incorporation of the OPV dye into polymer backbone prevented the detection of its characteristic signals by NMR spectroscopy. However, its presence has easily been identified and quantified from the absorption spectrum recorded in THF (***Figure 4B.4b***). The nanobeads showed an absorption maximum at 365 nm, corresponding to the incorporated OPV moieties, with a blue shift of 30 nm compared to pristine dye. The amount of dye incorporated into polymer backbone could easily be quantified based on its molar absorptivity value (40360 $Lmol^{-1}cm^{-1}$, THF), following the standard equations of DLC and DLE calculation. Its DLC value was found to be 1.6 % while its DLE was 53.6 % (***Table 4B.2***), showing an efficient insertion of the OPV dyes into the polystyrene core.

4B.2.2 Photophysical Properties: ***Figure 4B.5a, b*** display the emission and excitation spectra of PS-OPV-NH2 in water at excitation wavelength of (a) 390 nm and (b) 445 nm respectively. Polymer showed bright blue emission in water under UV lamp which was further confirmed by its CIE co-ordinate diagram with CIE co-ordinate value of (0.15, 0.14) (***Figure 4B.5c***). Its excitation spectra distinctly exhibited two vibrational bands at 345 nm and 365 nm. Further the effect of pH and temperature variation was studied on the emission properties of polymer. The results clearly showed that the emission remained unaffected for a wide range of temperature and pH. This highlighted the advantage of polystyrene nanobeads, where a constant emission is possible under different conditions, unlike QDs and UCNPs which might hampers the sensing efficiency of sensor (***Figure 4B.5d, e***).

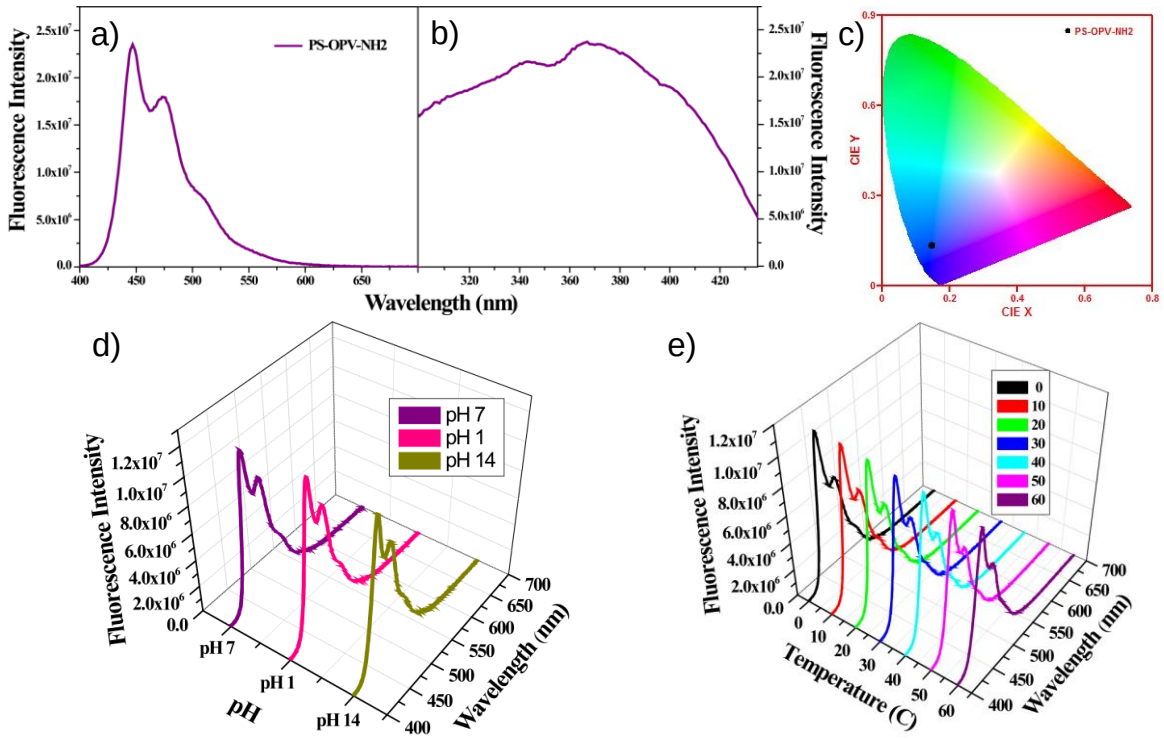

Figure 4B.5: a) Solution state (a) emission (at 390 nm) and (b) excitation spectra (collected at 445 nm) of the polymer PS-OPV-NH2 in demineralized water, c) CIE co-ordinate diagram of PS-OPV-NH2. d) Emission spectra for PS-OPV-NH2 depicting non-quenching of OPV emission on varying pH from 1 to 14 and e) Emission spectra for PS-OPV-NH2 depicting non-quenching of OPV emission on varying temperature from 0 °C to 60 °C.

The high and constant emission of PS-OPV-NH2 in water, added with its good water dispersibility, excellent thermal and photostability, indicates its proper candidature for a fluorescence based chemosensor in aqueous medium. During our previous investigation, we have seen that electron-rich nature of OPV fluorophore helps it to interact with electron-deficient analyte such as nitrobenzene. Emission quenching by nitrobenzene vapour and its ethanolic solution prompted us to explore the usability of OPV containing fluorescent nanoparticles for detection of nitro explosives in contaminated water. Furthermore, we have also functionalized the nanoparticle surface with –NH2 groups to increase the interaction between OPV dye core and the incoming nitro explosives, thereby increasing the overall sensing performance. We have already demonstrated the possibility of the OPV dyes for developing sensors to selectively detect nitro organics from organic solutions. Thus the electron rich nature of OPV prompted us to explore its sensing behaviour toward electron deficient nitro explosives in water.

4B.2.3 Sensing Studies with PS-OPV-NH2: To check the selectivity of sensor toward picric acid (PA) from among other organic analytes, fluorescence titration experiments were conducted by addition of fixed concentration of various analytes (10^{-4} M) listed in

Figure 4B.6 into the water dispersion of PS-OPV-NH2 (Details of experiment are provided in experimental section, ***4B.3***). ***Figure 4B.7 (A, B)*** compares the effect of

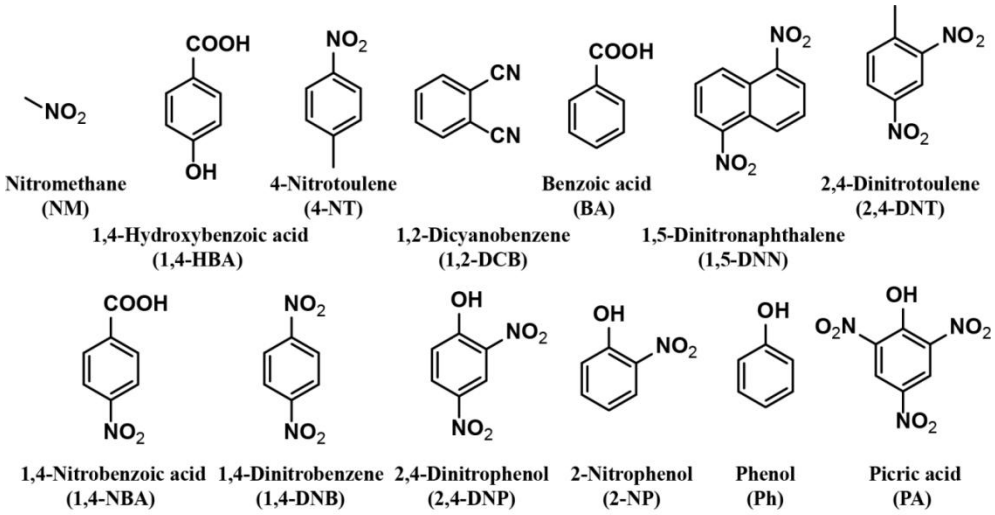

Figure 4B.6: Chemical structures of nitro organic compounds used in this study

various analytes on the % quenching of sensor. The results clearly demonstrated the selectivity of sensor towards nitrophenols (PA, 2, 4-DNP, 2-NP) while no remarkable change in fluorescence intensity was observed on the addition of other analytes. ***Figure 4B.7C*** shows the gradual increase in % quenching on increasing concentration of PA with instant fluorescence quenching of ~29% at $1x10^{-5}$ M concentration which reached ~92% at $1x10^{-4}$ M concentration. The inset in ***Figure 4B.7C*** shows the marked disappearance of the blue emission from polymer on addition of PA to it, upon observation under a UV lamp. ***Figure 4B.7D*** shows the simultaneous decrease in the excitation spectra on addition of PA. This showed rapid and prompt sensing of PA useful for on-site detection of explosives.

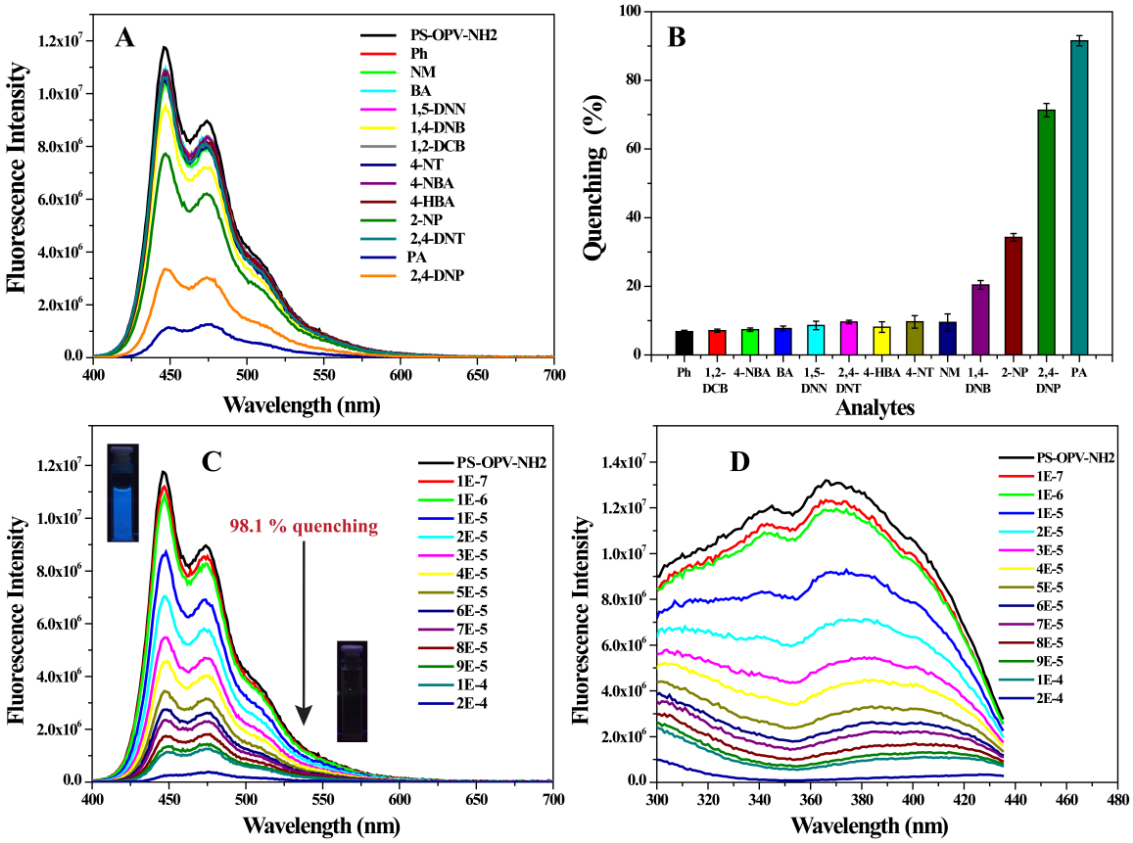

Figure 4B.7: A) Emission spectra of PS-OPV-NH2 and B) its quenching percentage upon addition of different nitro-organic compounds (1x 10^{-4} M) in water. C) Emission and D) excitation spectra of PS-OPV-NH2 polymer collected after the addition of varying concentration of PA (1x10^{-7} to 2x10^{-4} M). Emission and excitation spectra was collected at λex = 390 nm and λem = 445 respectively.

To analyse the reason behind the selective sensing of PA among the library of other nitro-organics and its mechanism, the quenching efficiency was further studied using Stern-Volmer equation .[21] ***Figure 4B.8*** shows the correlation between fluorescence intensity of PS-OPV-NH2 and PA concentration. The linear fitting of plot (Inset of ***Figure 4B.8A***) displayed two clear linear range of Io/I *vs* PA concentration which ranged from 0 to 30 µM (R^2= 0.982) and 40 to 70 µM (R^2= 0.998). The limit of detection was calculated based on signal to noise ratio of 3[21] and it was estimated to be 58 nM which indicate appreciably high sensitivity of the sensor towards PA.The non-linearity in the S-V plot indicated amplified quenching thereby suggesting the involvement of more than one quenching mechanism which may include (a) ground state complex formation between polymer and PA, (b) energy transfer, (c) inner filter effect (IFE) and (d) photoinduced electron transfer (PET) from PS-OPV-NH2 to PA.

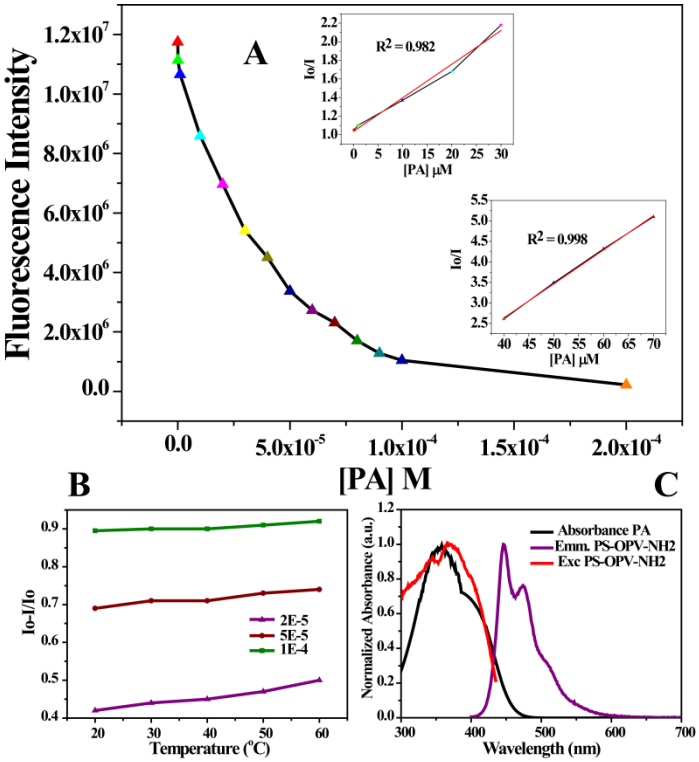

Figure 4B.8: A) Plot of changes in fluorescence intensity of PS-OPV-NH2 *vs* concentration of PA and their linear range using Stern-Volmer equation. B) Temperature dependent quenching of polymer emission after PA addition. C) Spectral overlap of excitation/emission spectra of PS-OPV-NH2 with that of absorption spectra of PA.

To get a deeper understanding, the absorption spectra of polymer with varying concentration of PA were recorded (***Figure 4B.9***) and no obvious shift or appearance of new peak in the absorption spectra was observed in presence of PA. This ruled out the possibility of quenching by ground state complex formation between PA and polymer. Furthermore, ***Figure 4B.10*** shows evident spectral overlap between emission spectra of polymer and absorption spectra of nitrophenols while inefficient overlap was observed for the rest of the analytes. This result supported the involvement of long range energy transfer in the quenching process. Also, emission quenching efficiency of PA recorded at different temperature confirmed the nature of quenching to be static type. ***Figure 4B.8B*** showed no appreciable change in quenching of polymer after PA addition (2E-5 to 1E-4 M) as a function of temperature (20 °C to 60 ^{o}C); confirming static quenching which further verifies energy transfer from polymer to PA.[21,27] Additionally, complete overlap of the absorption spectra of PA (λ_{max} = 360 nm) with excitation spectra of

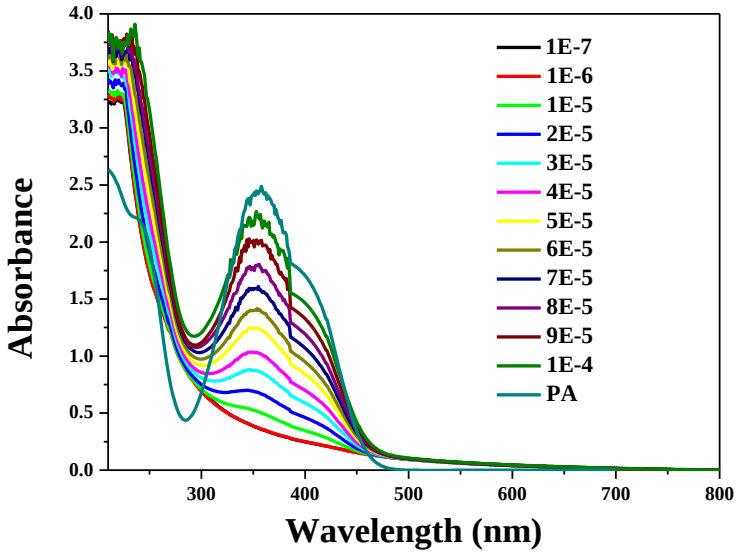

Figure 4B.9: Plot of absorption spectra of PS-OPV-NH2 on varying concentration of PA

polymer (λ_{max} = 365 nm) also indicated possibility of inner filter effect which reduces the fluorescence intensity of fluorophore due to competitive absorption by PA resulting in non-linearity between concentration of analyte and observed fluorescence intensity of fluorophore (***Figure 4B.8C***). But it is to be noted that spectral overlap between emission/excitation spectra of polymer to that of absorption spectra of PA or 2,4-DNP was almost same (***Figure 4B.10***), however % quenching by these compounds followed the order : PA> 2,4-DNP> 2-NP. This can be attributed to PET via acid base interaction since they all contained one hydroxyl (-OH) group with varying nitro group that governed their acidity. To further verify the role of functional group in sensing, effect of compounds with only -OH group (Ph, 4-HBA) or only -NO_2 group (1,4-NBA, 4-NT, 2,4-DNT, 1,2-DCB, 1,5-

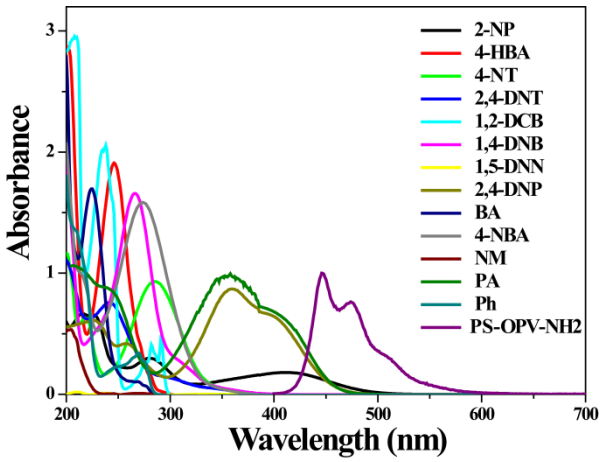

Figure 4B.10: Mechanism of quenching depicting the overlap of absorption spectra of nitrophenols to that of OPV emission.

DNN) on % quenching of polymer was checked. As shown in ***Figure 4B.7 (A, B)*** no obvious effect on the emission spectra of polymer was observed by their addition which reassured the requirement of both -OH as well as -NO_2 group in the sensing mechanism.

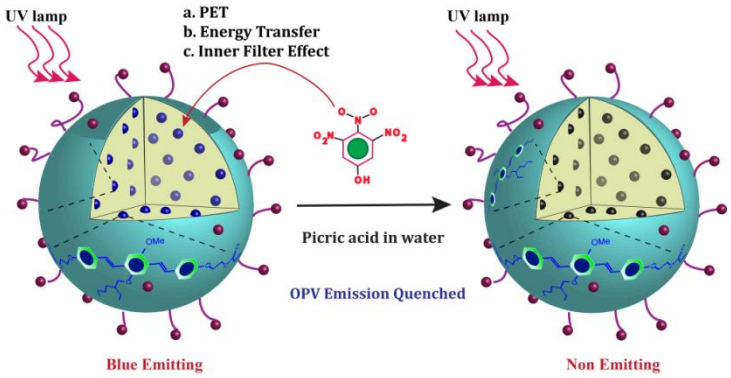

Figure 4B.11: Schematics for the mechanism of quenching of OPV emission by PA in water

Hence on the basis of above discussion, it is quite clear that outstanding selectivity and sensitivity of polymer toward PA sensing in water is due to the combined effect of three mechanisms namely, energy transfer, PET and IFE (***Figure 4B.11***).

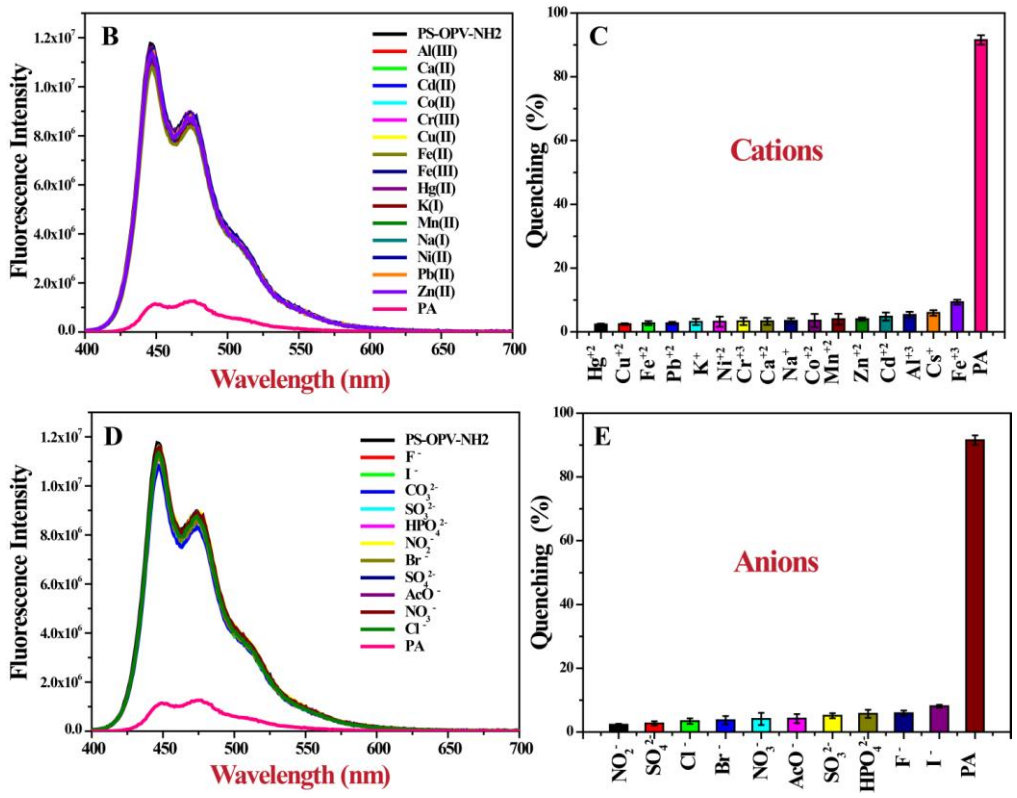

Figure 4B.12: A) Emission spectra of PS-OPV-NH2, B) its comparative quenching percentage upon addition of different cations *vs* PA (1 x 10^{-4} M) in water. C) Emission spectra of PS-OPV-NH2 and D) its comparative quenching percentage upon addition of different anions *vs* PA (1 x 10^{-4} M) in water. Error bar indicates standard deviations of three measurements.

As sensing studies was performed in aqueous medium, it was extremely crucial to check for possible interference from cations and anions that might be present in the contaminated water sample. Almost 16 different cations were chosen including both hard and soft metal ions and as shown in ***Figure 4B.12A, B*** none of the metal ions exhibited any obvious quenching of the emission spectra of PS-OPV-NH2 unlike other sensors[26] where hard metal ions have to be first complexed with EDTA before carrying out PA sensing. This clearly establishes an advantage in terms of ready to use nature of the sensor, without requirement for metal removal through complexation.

Similarly a library of anions was also checked (***Figure 4B.12C, D***) and none were found to affect the emission intensity of polymer. We also explored effect of ionic strength on the sensing efficiency of PA. To demonstrate the same the emission spectra of polymer before and after the addition of 1 M NaCl was collected and no change in its emission intensity was observed (***Figure 4B.13***). Also fluorescence quenching efficiency of PA remained similar even after the addition of 1 M NaCl indicating that sensor had the capability to withstand the complex environment and could be used for PA sensing even in sea water.

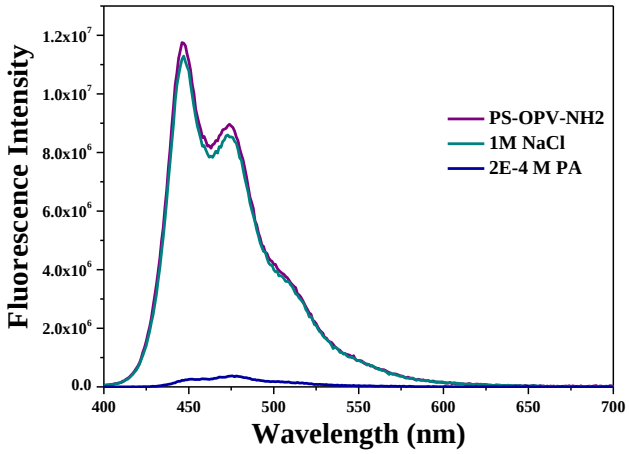

Figure 4B.13: Emission spectra of PS-OPV-NH2 after the addition of 1 M NaCl, showing its potential to detect PA from salty seawater.

Scope of PS-OPV-NH2 for real time device based application was tested using a free-standing membrane (λ_{max}= 477 nm), prepared from evaporating the THF solution of the polymer on a glass surface. When the film was dipped in PA contaminated water (PA conc. of $2x10^{-4}$ M) for 1 min, an instant drop in the emission was observed, measuring 53% quenching of the original intensity (***Figure 4B.14***). This demonstrated the high potential of OPV-PS-NH2 towards device based application for detection of PA from aqueous medium, in the form of self-standing film.

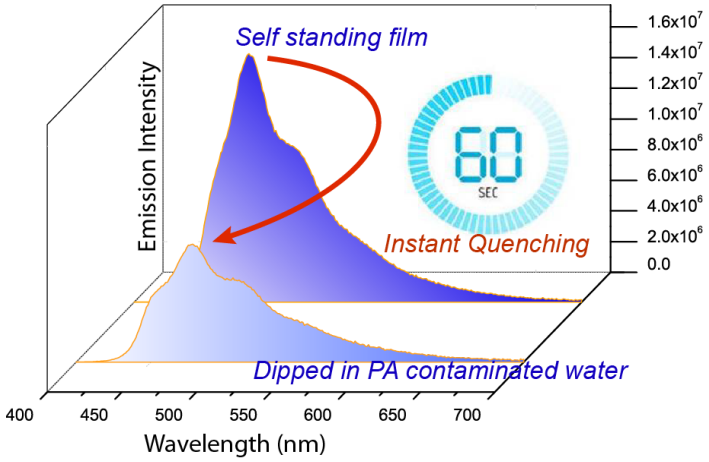

Figure 4B.14: Quenching observed on dipping free standing film into PA in water

4B.3 Experimental Details:

4B.3.1 Materials: 4,4'-Azobis(4-cyanovaleric acid) (ACVA), Brij S-100, (KPS), Aminoethyl methacrylate hydrochloride (AEMH) were purchased from Aldrich and *n*-Hexadecane (HD) from Alfa Aesar and were used without any further purification. Styrene was purchased from Aldrich and was purified as per the standard protocol. All the analytes used for sensing studies including nitro organics and inorganic salts were purchased from commercially available sources and used as received. Solvents and other reagents were purchased from local suppliers and further purified using standard procedures. Deionized water was used throughout the studies.

4B.3.2 Details of Analytical Instruments: The details of instrumental techniques used for characterization of polymer such as DLS (for size and zeta potential), GPC, TEM, Sonicator, NMR, absorption and fluorescence spectrophotometer are same as described in the previous chapters.

For pH dependent studies was carried out using 100 µg of polymer was taken in various mentioned pH (3 mL) followed by recording its emission spectra. For temperature dependent studies, a suspension of 100 µg of the polymer in 3 mL deionized water was taken and emission spectra were recorded using Peltier sample compartment with a thermoelectric temperature controller and autotone PID. The temperature was set manually (with a fixed tolerance range of 0.5 °C) with the equilibration time of 10 min before each reading. For TEM imaging, aqueous suspension of the polymer sample was drop casted onto carbon coated copper grid and solvent was allowed to dry at room temperature. For quantum yield measurement, the emission spectra of 0.1 OD of polymer at absorption maxima were recorded and its quantum yield was calculated using Quinine

sulfate as standard. All the emission experiments were performed in deionized water and slit width of 1 nm and "S1c/R1" mode was maintained throughout the studies.

4B.3.3 Estimation for Dye Incorporation into nanobeads: Dye Loading Content (DLC) and Dye Loading Efficiency (DLE) were calculated by taking 1 mg/mL of the polymer in Tetrahydrofuran (THF) and its absorbance was measured subsequently at its absorption maxima at 365 nm. The amount of dye incorporated into polymer backbone was calculated based on its absorption coefficient (40360 $Lmol^{-1}cm^{-1}$) in THF. Further its DLC and DLE values were calculated using standard equations mentioned in the previous section of the chapter.

4B.3.4 Preparation of Sample for Sensing Studies and Study of the Chemical Sensing: For sensing studies of nitro-organics in water 100 µg of OPV-PS-NH2 was dispersed into 3 mL of deionized water. And to the same was added fixed concentration (10^{-4} M) of various analytes listed in ***Figure 4B.6***. The suspension was then subjected to thorough mixing followed by immediate recording of the emission spectra. All the experiments were repeated thrice to avoid any discrepancy and average of the three values was plotted as bar graph alongwith with their standard error. For sensing of PA in water, various concentration of PA was added to the fixed volume of OPV-PS-NH2 suspension as mentioned above and its emission as well as excitation spectra were recorded. Interference from various anions and cations in water was checked using same concentration (10^{-4} M) for each of the analytes. For free standing film, 20 mg of polymer in 1 mL THF was poured in petridish. After drying the film (thickness 0.07 ±0.01 mm) was peeled off and used directly for sensing studies.

For sensing studies with free standing film, the prepared film was directly dipped into methanolic solution of the analyte (100 µL in 30 mL methanol) for 1 min and then removed to soak off the excess liquid from the film surface. The emission spectra were recorded with the dried film, without any further delay.

For measuring the emission from OPV, the polymer sample was excited at $\lambda_{excitation}$ = 390 nm and subsequently its emission spectra was collected in the range of 400-700 nm.

The equations for calculation of percentage quenching (***eq 1***) and Stern-Volmer coefficient (***eq 2***) are given below:

$$\% \text{ Quenching} = \frac{I_0 - I}{I_0} \times 100 \quad \text{.....eq 1}$$

$$\frac{I_0}{I} = K[Q] + 1 \quad \text{.....eq 2}$$

Where I_0 and I is the initial and final emission intensity of OPV (at its emission maxima, 446 nm), on addition of the analyte.

Table 4B.3: Average quenching percentage of OPV emission and quenching ± error (%) after the addition of the respective nitro compounds in water.

Nitro compounds	Average Quenching (%)	Quenching ± Error (%)
Ph	**6.8**	**0.4**
1,2-DCB	**7.1**	**0.5**
4-NBA	**7.4**	**0.5**
BA	**7.7**	**0.7**
1,5-DNN	**8.6**	**1.2**
2,4-DNT	**9.6**	**0.5**
4-HBA	**8.1**	**1.5**
4-NT	**9.6**	**1.8**
NM	**9.5**	**2.5**
1,4-DNB	**20.4**	**1.2**
2-NP	**34.3**	**1.1**
2,4-DNP	**71.3**	**1.9**
PA	**91.5**	**1.5**

Table 4B.4: Average quenching percentage of OPV emission and quenching ± error (%) after the addition of the anions in water.

Nitro compounds	Average Quenching (%)	Quenching ± Error (%)
NO_2^-	**2.3**	**0.3**
SO_4^{2-}	**2.7**	**0.6**
Cl^-	**3.4**	**0.8**
Br^-	**3.7**	**1.3**
NO_3^-	**4.1**	**1.9**
AcO^-	**4.2**	**1.4**
SO_3^{2-}	**5.1**	**0.8**
HPO_4^-	**5.7**	**1.3**

F^-	**5.9**	**0.8**
I^-	**8.1**	**0.4**
PA	**91.5**	**1.5**

Table 4B.5: Average quenching percentage of OPV emission and quenching ± error (%) after the addition of the cations in water

Nitro compounds	Average Quenching (%)	Quenching ± Error (%)
Hg(II)	**2.3**	**0.3**
Cu(II)	**2.4**	**0.3**
Fe(II)	**2.7**	**0.6**
Pb(II)	**2.7**	**0.5**
K(I)	**3.1**	**0.9**
Ni(II)	**3.2**	**1.6**
Cr(III)	**3.3**	**1.2**
Ca(II)	**3.3**	**1.1**
Na(I)	**3.4**	**0.8**
Co(II)	**3.5**	**2.1**
Mn(II)	**3.9**	**1.7**
Zn(II)	**4.0**	**0.5**
Cd(II)	**4.8**	**1.3**
Al(III)	**5.4**	**0.9**
Cs(I)	**5.9**	**0.8**
Fe(III)	**9.3**	**0.7**
PA	**91.5**	**1.5**

Table 4B.6: Comparison table for fluorescent sensors of PA reported in literatures.

Material	Linear Range (μM)	LOD	Medium Used	Interference from cations and anions	Effect of pH	Selectivity	Ref.
MOF	-	-	Acetonitrile	Not Checked	-	Yes	2
Organic Cage	-	0.06 μM	Dichloromethane (DCM)	Not Checked	-	Yes	28
Small molecules	0-10	0.5 μM	Ethanol	Not Checked	-	Poor	10
Small molecules	2-16	2 μM	DMSO-Chloroform	Not Checked	-	Poor	14
Small molecules	0-20	0.35 μM	Toulene-DCM	Not Checked	-	Poor	15
Metal organic framework	0-50	2.5 μM	Dimethyl acetamide (DMA)	Not Checked	-	Yes	11
Covalent organic polymer	-	4.37 μM	Methanol	Not Checked	-	Yes	12
Small molecules	0-1	.28 μM	Water/ THF (7:3)	No interference	-	Yes	29
Tetraphenyl ethelene Nanosphere	-	0.005 μM	Water/ THF (9:1)	Not Checked		Yes	30
Iridium complex	-	-	Water/acetone (9:1)	Slightly for Hg(II)	No effect	Yes	31
Conjugated polyelectrolytes	0-51	0.72 μM	Water/ THF (9:1)	Not Checked	-	Not studied	25
Inorganic polymer	-	(54 μg/mL) 1ppm	Water/ THF (9:1)	Not Checked	-	Not studied	32
Hyperbranched polymer	-	1 μg/mL	Water/ THF (9:1)	Not Checked	-	Not studied	33
Functional polymer		1 μM	Water/ THF (9:1)	Not Checked	-	Non-selective	19
MoS_2 Quantum dots	0.99-36.5	0.095	Water	Moderate interference from Fe(III), Ni(II), Hg(II), Co (II)	-	Yes	34
Conjugated polyelectrolytes	0-20	128 ppt	Water	Not Checked	-	Yes	20
Graphene oxide	-	0.55 μM	Water	Not Checked	-	Yes	35
Small molecules	0.01-0.07	0.013 μM	Water	No interference	-	Yes	36
Carbon dots	-	0.10 μM	Water	Moderate interference observed	pH dependent quenching	Yes	37
Carbon dots	-	1 μM	Water	Not Checked	pH dependent quenching	Yes	38
Non conjugated polymer NPs	0.05-70	0.026 μM	Water	Appreciable interference from Cu(II), Ni(II), Fe(III), Zn(II)	pH dependent quenching	Yes	26
PS nanobeads	0-30; 40-70	0.058 μM	Water	No interference at all	No dependence	Yes	This work

4B.4 Conclusion:

In conclusion, we have developed both solution and solid state PS sensor for the selective sensing of nitroexplosives in aqueous medium. The surface of nanobeads was decorated with -NH_2 group with the aim to enhance analyte-sensor interaction thereby improving selectivity of sensor. The outstanding selectivity of the sensor among the library of other nitro-organics was attributed to combined effect of energy transfer, inner filter effect and electron transfer. PA concentration in 100 % water medium, as low as 58 nM could have been efficiently detected by the sensor. Additionally, no interference from large number of cations and anions was observed making the sensor highly efficient for real water analysis. Also, its emission remained independent of external triggers; making it applicable over wide range of temperature and pH. For device based application free standing film was made. Thus rapid, efficient, sensitive sensor was developed for the selective detection of PA in water.

4B.5 References:

1. Salinas, Y.; Martínez-Máñez, R.; Marcos, M. D.; Sancenón, F.; Costero, A. M.; Parra, M.; Gil, S. *Chem. Soc. Rev.* **2012**, *41*, 1261–1296.

2. Nagarkar, S. S.; Desai, A. V.; Ghosh, S. K. *Chem. Commun.* **2014**, *50*, 8915-8918.

3. Malik, A. H.; Hussain, S.; Kalita, A.; Iyer, P. K. *ACS Appl. Mater. Interfaces* **2015**, *7*, 26968−26976.

4. Toal, S. J.; Trogler, W. C. *J. Mater. Chem.* **2006**, *16*, 2871−2883.

5. Ye, J.; Zhao, L.; Bogale, R. F.; Gao, Y.; Wang, X.; Qian, X.; Guo, S.; Zhao, J.; Ning, G. *Chem. Eur. J.* **2015**, *21*, 2029-2037.

6. Bai, M.; Huang, S.; Xu, S.; Hu, G.; Wang, L. *Anal. Chem.* **2015**, *87*, 2383-2388.

7. Tanwar, A. S.; Hussain, S.; Malik, A. H.; Afroz, M. A.; Iyer, P. K. *ACS Sens.* **2016**, *1*, 1070-1077.

8. Ma, Y.; Huang, S.; Deng, M.; Wang, L. *ACS Appl. Mater. Interfaces* **2014**, *6*, 7790-7796.

9. Wang, Y.; Chang, X.; Jing, N.; Zhang, Y. *Anal. Methods* **2018**, *10*, 2775-2784.

10. Venkatramaiah, N.; Kumar, S.; Patil, S. *Chem. Commun.* **2012**, *48*, 5007-5009.

11. Shi, Z. Q.; Guoa, Z. J.; Zheng, H. G. *Chem. Commun.* **2015**, *51*, 8300-8303.

12. Sang, N.; Zhan, C.; Cao, D. *J. Mater. Chem. A* **2015**, *3*, 92-96.

13. Gole, B.; Bar, A. K.; Mukherjee, P. S. *Chem. Eur. J.* **2014**, *20*, 1332-13336.

14. Roy, B.; Bar, A. K.; Gole, B.; Mukherjee, P. S. *J. Org. Chem.* **2013**, *78*, 1306-1310.

15. Bhalla, V.; Gupta, A.; Kumar, M.; Rao, D. S. S.; Prasad, S. K. *ACS Appl. Mater. Interfaces* **2013**, *5*, 672-679.

16. Nagarkar, S. S.; Joarder, B.; Chaudhari, A. K.; Mukherjee, S.; Ghosh, S. K. *Angew. Chem. Int. Ed.* **2013**, *52*, 2881.

17. Wolfbeis, O. S. *Chem. Soc. Rev.* **2015**, *44*, 4743-4768.

18. Reisch, A.; Klymchenko, A. S. *Small* **2016**, *12*, 1968–1992.

19. Liu, Y.; Gao, M.; Lam, J. W. K.; Hu, R.; Tang, B. Z. *Macromolecules* **2014**, *47*, 4908-4919.

20. Hussain, S.; Malik, A. H.; Afroz, M. A.; Iyer, P. K. *Chem. Commun.* **2015**, *51*, 7207-7210.

21. Qin, A.; Lam, J. W. Y.; Tang, L.; Jim, C. K. W.; Zhao, H.; Sun, J.; Tang, B. Z. *Macromolecules* **2009**, *42*, 1421-1424.

22. Wang, T.; Zhang, N.; Bai, R.; Bao, Y. *J. Mater. Chem. C* **2018**, 6, 266-270.

23. Wang, J.; Mei, J.; Yuan, W.; Lu, P.; Qin, A.; Sun, J.; Mac, Y.; Tang, B. Z. *J. Mater. Chem.* **2011**, *21*, 4056-4059.

24. Zhou, H.; Li, J.; Chua, M. H.; Yan, H.; Tang, B. Z.; Xu, J. *Polym. Chem.* **2014**, *5*, 5628-5637.

25. Yuan, W. Z.; Zhao, H.; Shen, X. Y.; Mahtab, F.; Lam, J. W. Y.; Sun, J. Z.; Tang, B. Z. *Macromolecules* **2009**, *42*, 9400-9411.

26. Liu, S. G.; Luo, D.; Li, N.; Zhang, W.; Lei, J. L.; Li, N. B.; Luo, H. Q. *ACS Appl. Mater. Interfaces* **2016**, *8*, 21700-21709.

27. Lakowicz, J. R. Principles of Fluorescence Spectroscopy, 3rd ed. Springer: New York **2006**; DOI: 10.1007/978-0-387-46312-4.

28. Acharyya, K.; Mukherjee, P. S. *Chem. Commun*. **2014**, *50*, 15788-15791.

29. Ding, A.; Yang, L.; Zhang, Y.; Zhang, G.; Kong, L.; Zhang, X.; Tian, Y.; Tao, X.; Yang, J. *Chem. Eur. J.* **2014**, *20*, 12215-12222.

30. Feng, H. T.; Zheng. Y. S. *Chem. Eur. J.* **2014**, 20, 195-201.

31. Hou, X. G.; Wu, Y.; Cao, H. T.; Sun, H. Z.; Li, H. B.; Shan, G. G.; Su, Z. M. *Chem. Commun.* **2014**, *50*, 6031-6034.

32. Lu, P.; Lam, J. W. Y.; Liu, J.; Jim, C. K. W.; Yuan, W.; Chan, C. Y. K.; Xie, N.; Hu, Q.; Cheuk, K. K. L.; Tang, B. Z. *Macromolecules* **2011**, *44*, 5977–5986.

33. Li, H.; Wu, H.; Zhao, E.; Li, J.; Sun, J. Z.; Qin, A.; Tang, B. Z. *Macromolecules* **2013**, *46*, 3907−3914.

34. Wang, Y.; Ni, Y. *Anal. Chem.* **2014**, *86*, 7463-7470.

35. Dinda, D.; Gupta, A.; Shaw, B. K.; Sadhu, S.; Saha, S. K. *ACS Appl. Mater. Interfaces* **2014**, *6*, 10722-10728.

36. Gogoi, B.; Sen Sarma, N. *ACS Appl. Mater. Interfaces* **2015**, *7*, 11195-11202.

37. Sadhanala, H. K.; Nanda, *J. Phys. Chem. C* **2015**, *119*, 13138-13143.

38. Niu, Q.; Gao, K.; Lin, Z.; Wu, W. *Anal. Methods* **2013**, *5*, 6228.

CHAPTER-5

Tailor-made Amphiphilic Polymer as Surfactant for Miniemulsion Polymerization of Oligo(p-phenylene vinylene) incorporated Polystyrene Nanobeads and Visual Detection of Bilirubin in Human Serum

Abstract: *This chapter presents the synthesis and application of glucuronic acid bearing polystyrene nanoparticles for bilirubin sensing in human serum. Glucuronic acid functionalized, water dispersible fluorescent PS nanobeads (PSG-OPV-n) were developed for the selective detection of free bilirubin in clinically applicable range (<25 to >50 µmol/L) in human serum. Polystyrene backbone having pendant glucuronic acid (PS-DGlu) functionalities was designed and systematically synthesized to be used as stabilizing agent in styrene miniemulsion polymerization; covalently incorporating oligo(p-phylenevinylene) (OPV) based fluorophore to prepare PSG-OPV-n. This OPV fluorophore was incorporated with an aim to work as signal transducer while glucuronic acid on surface of PS nanobeads would serve as interaction site for free bilirubin to facilitate non-covalent interaction via hydrogen bonding. Efficient FRET from OPV to bilirubin was observed owing to appreciable spectral overlap between emission of OPV and absorption of bilirubin. Visual color change from blue to bluish green was observed under UV lamp after addition of bilirubin into polymer. Selectivity of the sensor was checked among the pool of other interferences such as glucose, sucrose, metal ions, cholesterol and biliverdin. The limit of detection was found to be as low as 20 nM which is far less than clinical range for causing jaundice. Moreover, the developed sensor shows its effectiveness towards real time monitoring of free bilirubin in human serum.*

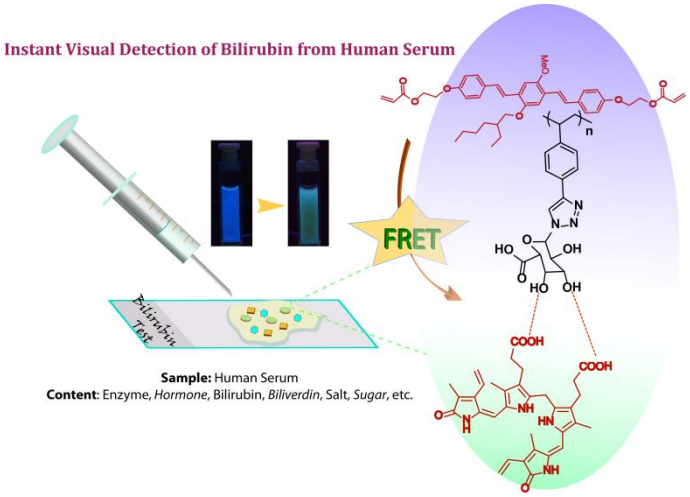

5.1 Introduction:

Bilirubin is produced as a breakdown byproduct of red blood cells (RBCs) which gets metabolized in liver and finally excreted form the body in the form of bile (***Figure 5.1a***).[1] However any disruption to this normal metabolic pathway due to any reason including viral or bacterial infection causing excess breakdown of RBCs leads to excess production of free bilirubin in the body.[2,3] Free bilirubin is extremely fatal and its excess accumulation above the normal level *i.e.* <25 to >50 µmol/L in human serum is directly related to liver malfunctioning.[4,5] (***Figure 5.1b***). Thus, it is extremely crucial to determine accurately the concentration of free bilirubin in human serum in order to diagnose liver disorders and jaundice.[5,6] Researchers across the globe have been looking at alternative approaches for a quick and accurate bilirubin assay.

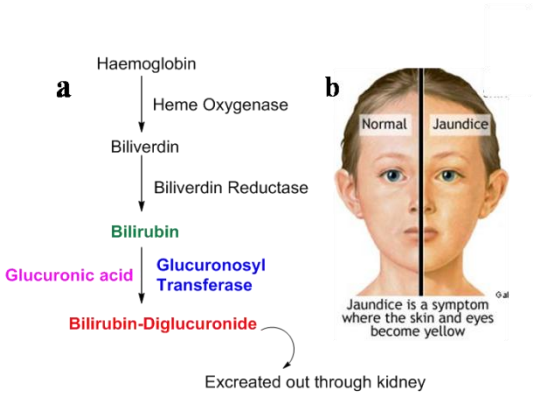

Figure 5.1: (a) Illustration of haemoglobin breakdown. and (b) deposition of free bilirubin signifying jaundice.

The currently practiced method of its clinical estimation is based on a colorimetric test known as the 'total van den Bergh reaction' which is chemical reaction between bilirubin and sulphanilic acid but is often pH dependent and time consuming; takes 30-45 min for achieving maximum coloration.[2,7] Fluorescence based biosensor are highly preferable because of added advantage like, high selectivity, promptness, efficiency along with wide range of analyte concentration.[8-10] There exists a handful literature reports on the fluorometric detection of free bilirubin in human serum. Some of the pioneer work in this area have been addressed by Santhosh *et al.*, Ellairaja *et al.*, Du *et al.*[11-13] For example, Santhosh *et al.* reported protein labelled fluorescent biomolecules for monitoring of free bilirubin in serum.[11] Ellairaja *et al.* reported picomolar detection of free bilirubin in human biofluids using imine based fluorescent small molecule.[12] Very recently, metal-organic framework (MOF) based highly efficient bilirubin sensor was reported by Du *et al.* with faster response time, lower detection limit (picomolar), and wide range of analyte concentration. [13] However, most of these sensors are accompanied by attenuation in their fluorescence intensity *i.e.* emission quenching on adding analyte.

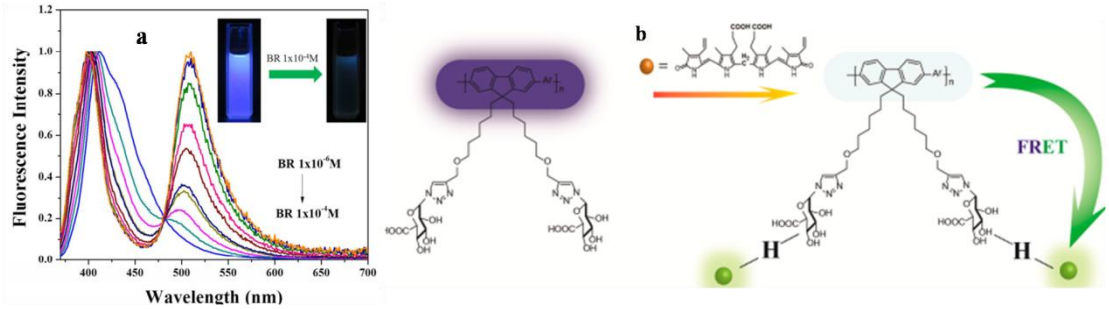

Figure 5.2 Polyfluorene based sensor depicting FRET between polymer and bilirubin resulting in color tuning to (a) green emission after analyte addition and (b) its schematics. Figure is adopted from ***Ref 15***, with permission from ACS Publications).

Polymer based sensors are particularly demanding because of their high sensitivity, easy color tunability and operational simplicity. Until now, there are only two reports on such polymer based bilirubin sensor with color tuning of emission after the addition of analyte.[14,15] One of report deals with conjugated polyfluorene backbone based monitoring of free bilirubin in THF/water mixture.[14] While in the other report, the glucuronic acid moiety was attached to such polyfluorene backbone for imparting water solubility to carry out the studies in human blood serum.[15] However, for practical applications, a conjugated polymer based biosensor is not feasible due to the difficulties in the reproducible scale up of the synthesis as well as the cost involved in procuring the raw materials. On the other hand, polystyrene (PS) and poly (methyl methacrylate) (PMMA) are relatively low cost commercial polymers that are produced and consumed in large quantities. Compared to a conjugated polymer based substrate that is more expensive and synthetically more challenging, a design based on commercially available and easily scalable PS or PMMA are more attractive as sensor substrates for quick and accurate estimation of free bilirubin. It would be more desirable if PS or PMMA could be used to develop biocompatible polymeric nanobeads based fluorimetric sensing and estimation protocol for bilirubin since the process would be fast and much more sensitive besides being easy to synthesize and scale up. As an alternative, these polymeric nanobeads could be developed using water soluble polymeric surfactant.[16-19] Polymeric surfactant imparts interesting properties to the final latex as compared to lower molecular weight conventional surfactant such as low critical micellar concentration (CMC), lower foaming and additionally modifying the surface of nanobeads with specific functional polymers.[20] In this context, we have designed and developed novel water soluble polystyrene with pendant glucuronic acid to act as surfactant in the styrene miniemulsion

polymerization incorporating fluorophore as sensing moiety to synthesize glucuronic acid surface functionalized fluorescent PS nanobeads. Mimicking the biological process used by our body to remove toxic bilirubin,[2,21] glucuronic acid was chosen with an aim to serve two main functions. The first is imparting water solubility to the polystyrene polymer to enable it to act as surfactant in miniemulsion polymerization. Secondly, it can provide interaction sites for bilirubin to enhance sensor-analyte synergy via hydrogen bonding. Additionally, it being the non-receptor of serum protein would provide receptor free biosensing platform. OPV was chosen as sensing material because of its nice spectral overlap with bilirubin thus favouring energy transfer process.

Thus these water dispersible functionalized fluorescent PS nanobeads could be successfully applied for the detection of bilirubin in human serum among pool of other competitive interference such as proteins, metal ions, cholestrol, sugars, biliverdin *etc.* Henceforth, it is anticipated that functionalization of the polymer beads with receptors specific for different analytes would enable these functionalized PS beads to function as efficient fluorescent sensors. This will open up new avenues of exploration of fluorescence based sensing for other biologically relevant analytes also. To the best of our knowledge, this would be the first report of quantifying free bilirubin in human serum using materials which are easy to synthesize and scale up and using a method which is more sensitive and fast compared to the current clinically practiced method.

5.2 Results and Discussions:

5.2.1 Synthesis and structural characterization: Styrene based monomer with pendant protected glucuronic acid (5) was synthesized by azide alkyne click reaction (***Scheme 5.1***). 4-ethynyl styrene (3) was synthesized from 4-bromostyrene (1) *via* Sonogashira coupling followed by its deprotection while 2,3,4 tri-*o*-acetyl 1-azido 1-deoxy D-glucuronic acid methyl ester (4) was synthesized using three steps procedure as shown in ***Scheme 5.1*** These were thoroughly structurally characterized by proton NMR spectroscopy along with mass spectrometry and FTIR (Details provided in ***Section 5.3***). Appearance of new peak for triazole H in proton NMR at 8.06 ppm (***Figure 5.33***), confirmed the 'click' reaction, which was further supported from its LC-MS/MS spectra ***(Figure 5.34)*** (Details provided in ***Section 5.3***).

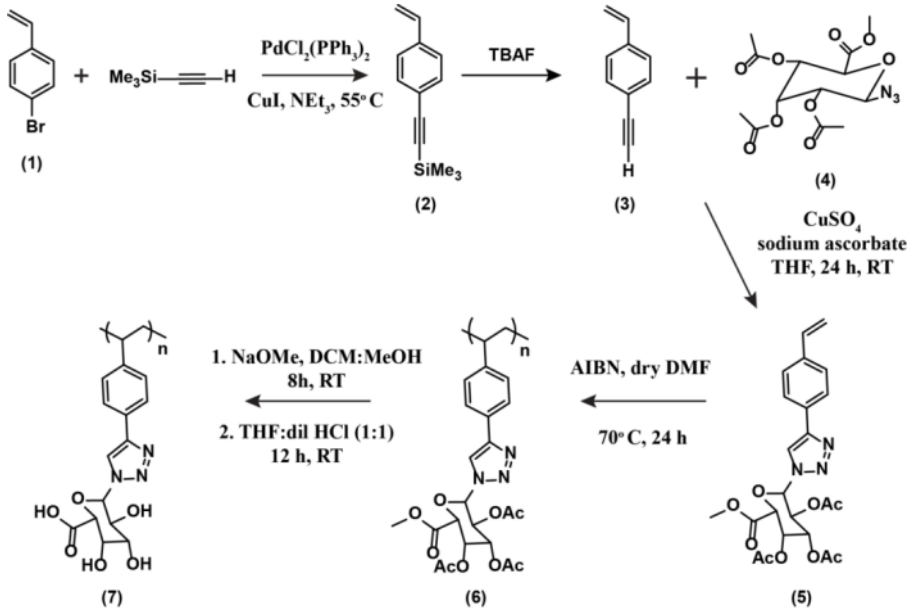

Scheme 5.1: Schematics of synthesis of glucuronic acid functionalized polystyrene nanobeads synthesis *via* miniemulsion polymerization.

This monomer was polymerized *via* free radical polymerization using AIBN as an initiator to give protected D-glucuronic acid PS polymer, PS-PGlu (6) (***Scheme 5.1***). The structural characterization with ^{1}H NMR spectroscopy (***Figure 5.3***) showed the backbone to be comprised of the monomeric unit exclusively.

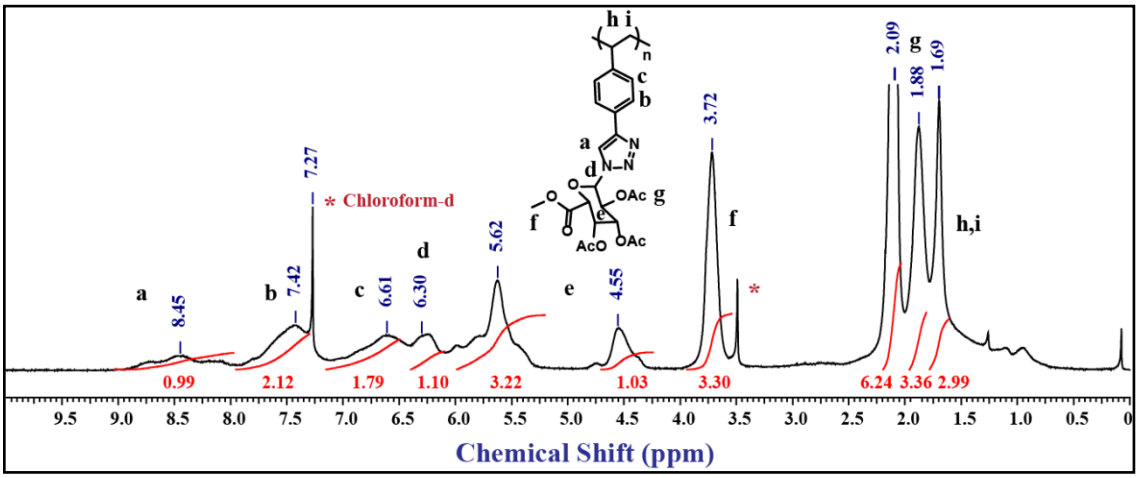

Figure 5.3: ^{1}H-NMR spectrum of polystyrene with protected D-glucuronic acid (PS-PGlu) in $CDCl_3$.

^{1}H-^{1}H COSY spectra of (6) depicted the coupling among its protons (***Figure 5.4 A***). The molecular weight, determined by Gel Permeation Chromatography (GPC) showed a high molecular weight of polymer (***Figure 5.4 B***), which accounted for the broadening of peaks in ^{1}H NMR.

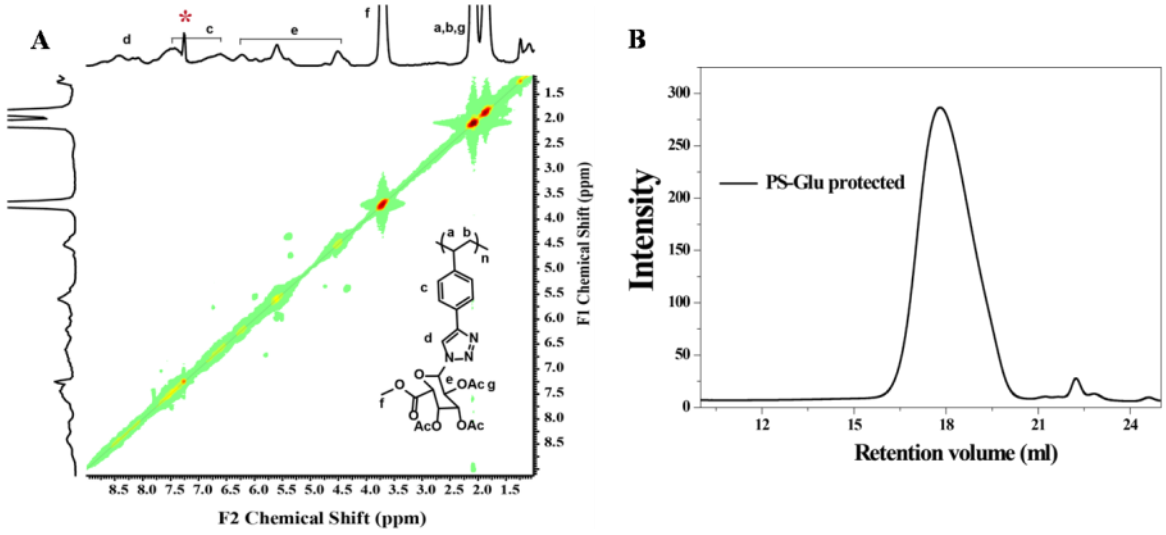

Figure 5.4: (A) ^{1}H-^{1}H COSY NMR spectrum of PS-PGlu in $CDCl_3$. (B) GPC of PS-PGlu in $CHCl_3$.

FTIR spectra of (6) showed an intense peak at 1765 cm^{-1}, corresponding to the C=O stretching frequency from acetate groups (***Figure 5.5A***). PS-PGlu (6) was then deprotected following previously used protocol to give water soluble polymer consisting of polystyrene bearing D-glucuronic acid (PS-DGlu, 7) (***Scheme 5.1***). This PS-DGlu polymer (7) was found to be soluble in water and MeOH, in contrast to its protected polymer (PS-PGlu, 6) indicating the deprotection of acetate and methyl ester groups to free -COOH and -OH groups. The deprotection of these functionalities was further confirmed from its FTIR spectra[22] and contact angle measurement. FTIR showed appearance of a broad peak at 3573-2595 cm^{-1} for combined O-H and C-H stretching frequencies while peak at 1765 cm^{-1} for C=O stretching of acetyl groups is shifted to 1727 cm^{-1}, accounting for the C=O stretching of the deprotected carboxylic acid group.

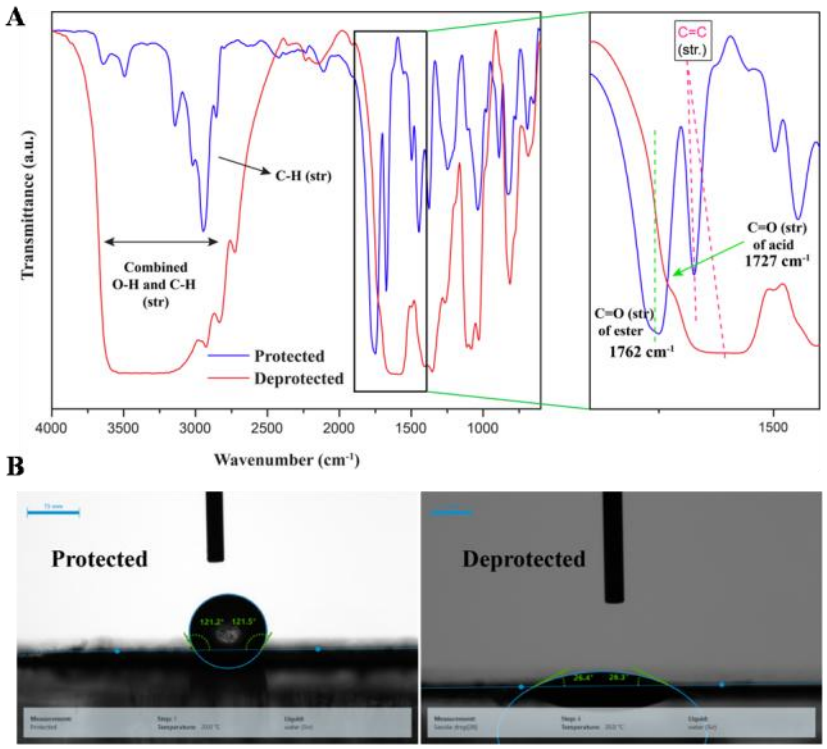

Figure 5.5: Comparison between protected (PS-PGlu) *vs*deprotected (PS-DGlu) polymers using (A) FTIR and (B) contact angle measurement.

Furthermore, contact angle was drastically changed from 121⁰ for PS-PGlu to 26.4⁰ for PS-DGlu polymer because of transition from hydrophobic to hydrophilic environment resulting in the drop of its contact angle (***Figure 5.5 B***).

The surfactant property of PS-DGlu was explored for stabilizing styrene miniemulsion polymerization incorporating oligo(*p*-phenylenevinylene) (OPV) based fluorophore to prepare D-glucuronic acid functionalized fluorescent PS nanobeads (PSG-OPV-n).To evaluate the surfactant property of PS-DGlu, its hydrophilic to lipophilic balance (HLB value) was evaluated using Griffin's method[23,24] according to following equation (1).

$$\mathbf{HLB = (W_H / W_H + W_L) \times 20} \quad \mathbf{.....(1)}$$

where W_H and W_L are weight fraction of hydrophilic and lipophilic blocks present in the polymer, respectively.[25,26] Using this formula, the HLB value for PS-DGlu polymer was calculated to be 14.06 (***Figure 5.6A***). On this note, a typical surfactant having HLB value in range of 8-18 has potential to stabilize oil in water emulsion.[27] This prompted the appropriateness of the polymer (PS-DGlu, 7) to act as a surfactant to stabilize styrene miniemulsion in water. To validate its surfactant nature, its critical micelle concentration

(CMC) was calculated using dynamic light scattering (DLS) where scattering intensity was plotted against concentration of PS-DGlu in water[20] (***Figure 5.6B***). With the formation of micelle in the solution, a sudden change in the scattering intensity is highly expected, thus the minimum concentration of polymer at which scattered intensity sharply increase was used to evaluate CMC. The point of intersection of two linear regression lines was considered as CMC of polymer and it was found to be 0.2 mg/mL. This low value of the CMC further justified for its ability to act as surfactant and thereby stabilized the miniemulsion.

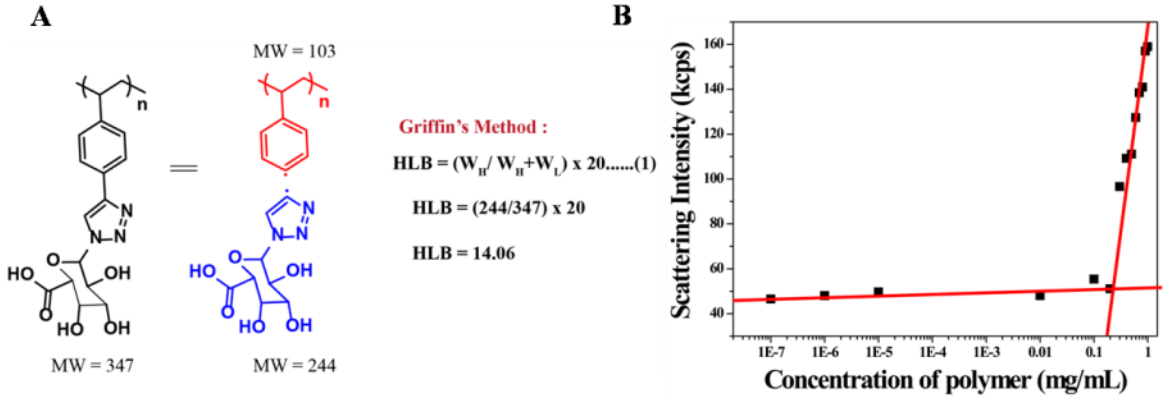

Figure 5.6: (A) Calculation of HLB value of deprotected polymer (PS-DGlu) for investigating its surfactant property. (B) Determination of critical micellar concentration (CMC) of PS-DGlu polymer by DLS.

To test the actual fate of (7) as a surfactant, it was introduced to stabilize styrene miniemulsion having polymerizable OPV to yield D-glucuronic acid functionalized OPV incorporated PS nanobeads in water. Different amounts of PS-DGlu, with fixed amount of styrene and OPV were used to prepare series of functionalized PS nanobeads (PSG-OPV-1 to PSG-OPV-5) using 4-4' azobis(4-cyanovaleric acid) (ACVA) and hexadecane (HD) as initiator and hydrophobe respectively (***Scheme 5.2*** and ***Table 5.1***).

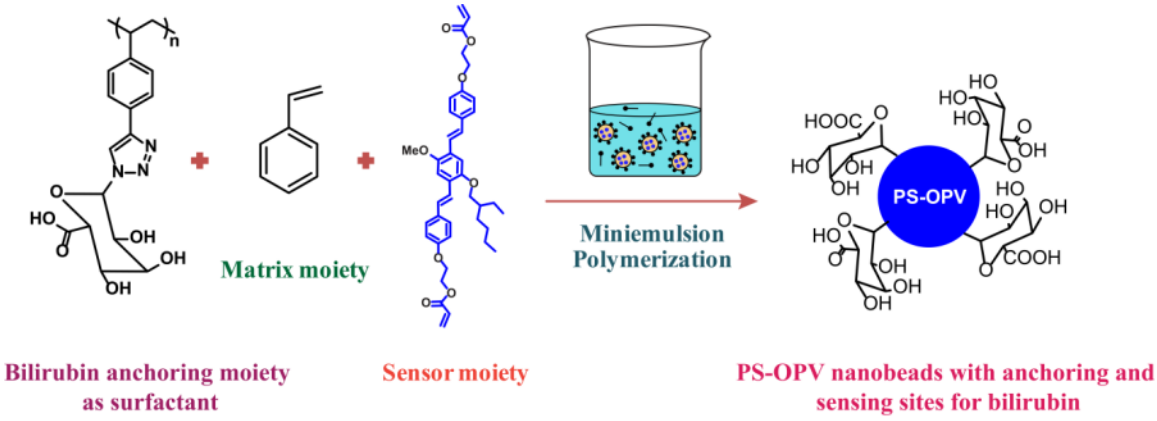

Scheme 5.2: Synthesis of glucuronic acid functionalized PS nanobeads incorporating OPV (PSG-OPV-n) via miniemulsion polymerization.

The size and stability of the obtained PS nanobeads was analyzed by DLS measurement in water (***Figure 5.7***). Size of all the PS nanobeads (PSG-OPV-1 to PSG-OPV-5) were found well within nanometer range, varying from 163 to 328 nm and PDI values remained below 0.1 showing monodisperse particles. The spherical morphology, size uniformity of the nanobeads were further confirmed by microscopic analysis using FESEM.

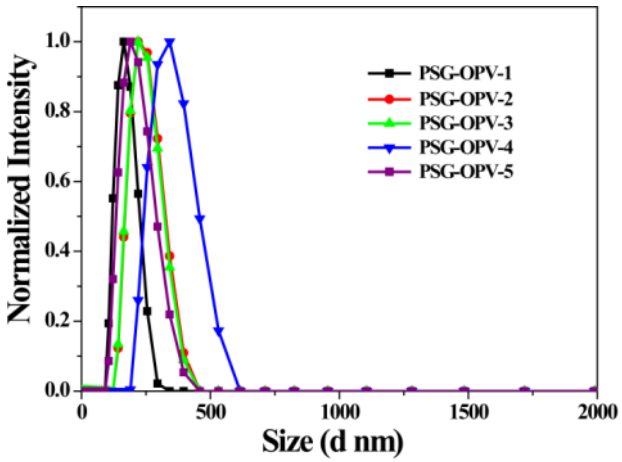

Figure 5.7: Dynamic light scattering (DLS) of PS-OPV-n polymers in ches buffer at pH 10.

Figure 5.8 showed FESEM images of some of representative polymers which pointed out that increasing amount of macrosurfactant (PS-DGlu) leads to more uniformity in size of nanobeads. The stability as well as negative surface charge of nanobeads in water was assured by their zeta potential values which varied from -35 mV to -55 mV (***Table 5.1***). The highly negative zeta potential values of all nanobeads were attributed to presence of -OH and -COOH groups from the macrosurfactant and few -COOH from ACVA.

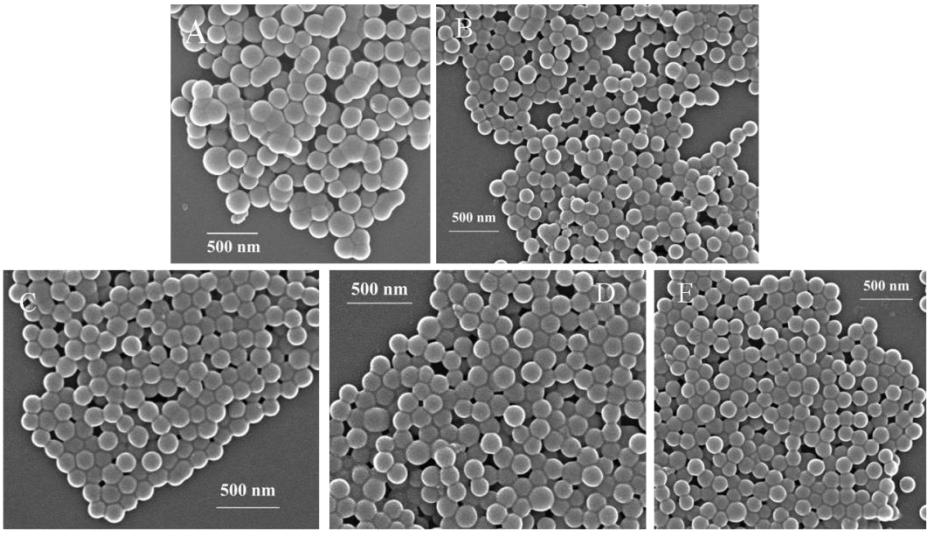

Figure 5.8: FESEM of representative PS-OPV-n polymer beads. (A) PS-OPV-1. (B) PS-OPV-3. (C,D,E) PS-OPV-5.

Surface functionalization with glucuronic acid was further confirmed using FTIR spectra which showed broad peaks at 3406 and 2506 cm^{-1} corresponding to -OH stretching of corresponding to and -OH and -COOH groups while peak around 1718 belonged to C=O stretching of free acid (***Figure 5.9***). The % solid content is measure of percent dry weight of polymer in 1 mL latex and was found to be in range of 6-20% (***Table 5.1***). The polymer was found to be soluble in chloroform ($CHCl_3$) in which their molecular weight was determined. They were found to have appreciable high molecular weight with Mw ranging from 37500 to 272000 Da and PDI value within 2.5 (***Table 5.2***).

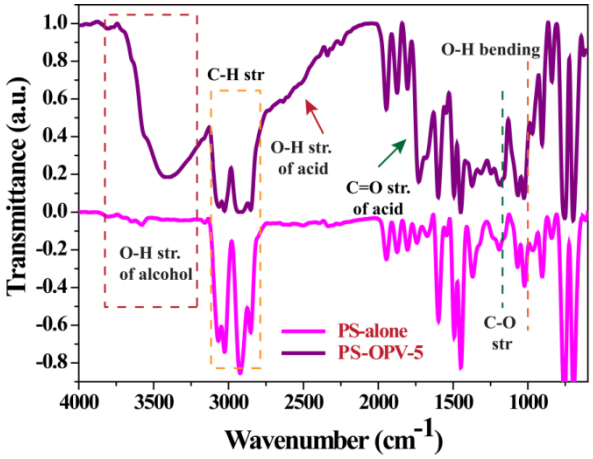

Figure 5.9: FTIR spectrum comparing PS-OPV-5 *vs* PS-alone.

The amount of dye in feed was very less when compared to amount of monomer and thus signal corresponding to fluorophore could not be traced via NMR spectroscopy. However, its presence could easily be seen in absorption spectroscopy from which dye loading content (DLC) could be estimated using its molar absorptivity in THF (40,360 $Lmol^{-1}cm^{-1}$) as described in our previous chapters.

Their DLC values are given in ***Table 5.1*** and it varied within the range of 0.07-0.11% (***Figure 5.10***). Although all the polymer nanobeads contained OPV dye and are surface functionalized with D-glucuronic acid and thus all could be utilized for bilirubin sensing but among them the one (PSG-OPV-5) with highest value of zeta potential, dye incorporation, solid content and molecular weight was finally chosen for bilirubin detection studies. OPV moieties from the polymer were the active fluorophore units and therefore would serve as sensor to signal the presence of analyte through change in emission property. While, the glucuronic acid moieties on the nanobeads surface was introduced to serve two purpose. Firstly, it would act as water solubilizing moiety for the polystyrene polymer to enable it to act as surfactant. Secondly, it would serve as interaction sites to bilirubin *via* non-covalent interaction such as hydrogen bonding and thereby facilitate efficient energy transfer from the fluorophore (OPV) to bilirubin, resulting in quick and efficient sensing.

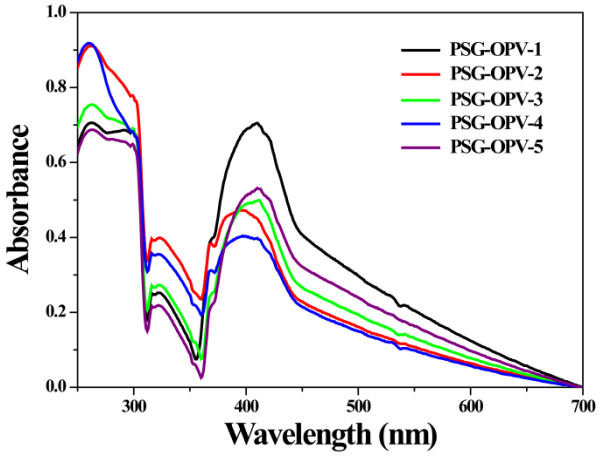

Figure 5.10: Absorption spectra of PSG-OPV-n polymers in THF.

Table 5.1 Sample designation, Dye Loading Content (DLC), Size and its polydispersity index (PDI), solid content, zeta potential (ζ).

Samples	PS-DGlu (mg)	Dye in feed (mg)	Dye incorporated (mg)	DLC (%)	Size (nm)	PDI	Solid Content (%)	ζ-potential (mV)
PS-OPV-1	10	30	11.4	0.11	163.4	0.06	6	-35.4
PS-OPV-2	20	30	7.8	0.08	221.6	0.05	10	-52.1
PS-OPV-3	30	30	8.2	0.08	224.1	0.05	6	-36.0
PS-OPV-4	40	30	6.7	0.07	328.0	0.07	8	-47.5
PS-OPV-5	50	30	8.8	0.09	192.2	0.06	20	-55

5.2.2 Photophysical Studies: Although PS alone have some weak blue emission due to π-π stacking[28] but this emission is negligible and thus a suitable fluorophore needs to be incorporated to impart emission from PS backbone and thus OPV based polymerizable fluorophore is incorporated into PS backbone to impart blue emission from the resulting nanobeads.

Selection of OPV as the suitable fluorophore was done by studying the possibility of its spectral overlap with that of bilirubin. OPV moiety has a characteristic emission in the range of 400 to 550 nm (λem= 446 nm) and thus showed a fair chance of spectral

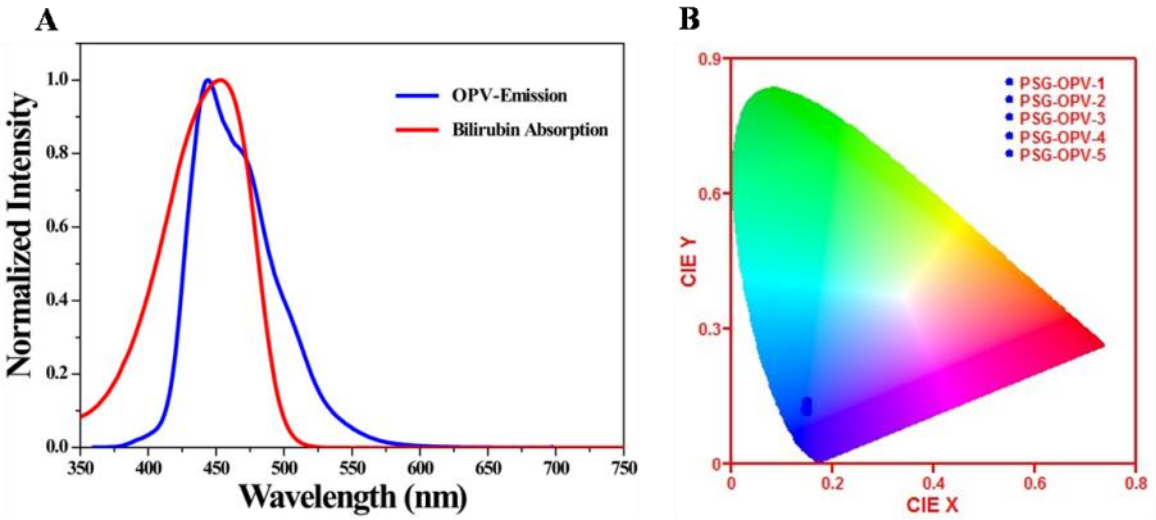

Figure 5.11: (A) Spectral overlap between emission spectra of PSG-OPV-5 and absorption spectra of bilirubin. (B) CIE co-ordinate diagram of all PSG-OPV-n polymers showing their emission in blue region.

overlap with the absorption spectra of bilirubin; which lies in the range of 350-500 nm (λabs=455 nm). ***Figure 5.11A*** showed spectral overlap between normalized emission of OPV and normalized absorption of bilirubin. Therefore, efficient Förster resonance energy transfer (FRET) from OPV to bilirubin was highly expected. All of the glucuronic acid functionalized PS nanobeads (PSG-OPV-n) contained OPV and are blue emitting as confirmed by their CIE co-ordinate diagram (***Figure 5.11B***), although only PSG-OPV-5 was selected for further sensing studies, as per the criteria mentioned earlier. ***Figure 5.12*** showed the photographs of PSG-OPV-5 in (a) water and (b) after addition of human blood serum in visible light; which showed complete absence of aggregation of polymer even after the addition of human blood serum. When the emission and excitation spectra of PSG-OPV-5 were recorded in ches buffer, the corresponding maximums were observed at 390 nm and 445 nm respectively. Both these spectra showed characteristic OPV peak for emission from 400 to 550 nm and excitation from 300 to 435 nm Also, the emission spectra recorded in human serum at pH 10 showed only slight difference in the emission intensity as compared to that in ches buffer at same pH (***Figure 5.13 A, B***).

Figure 5.12: Photograph of PSG-OPV-5 in ches buffer and human serum.

Additionally, in accordance with our previous observations (***Chapter 1 and 4B***), the emission of OPV from PS nanobeads remained unaffected by change in pH and temperature over wide range.

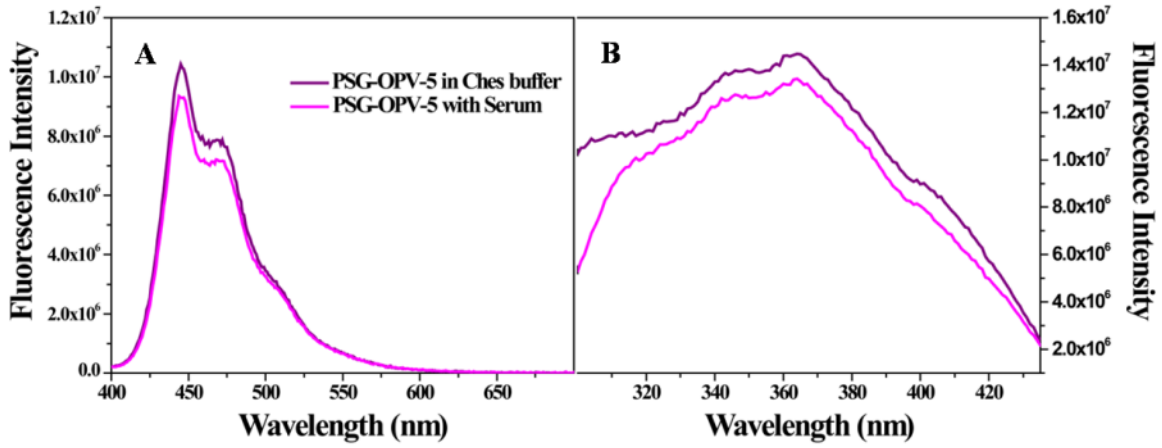

Figure 5.13: Comparison of (A) emission and (B) excitation spectra of PSG-OPV-5 in ches buffer and human blood serum showing no significant difference in their intensity.

5.2.3 Sensing Study of Free Bilirubin in ches buffer: Bilirubin consist of open chain structure of four pyrrole molecules having two pendant carboxylic acid which are known to possess several intramolecular hydrogen bonds and thus reported to have low water solubility at pH 7.4 (cellular pH). However, it is established that pH 10 is sufficient to break these intramolecular hydrogen bonds and to impart water solubility to it.[15,29] Therefore, studies conducted for sensing of bilirubin in literature are usually reported at pH= 10. To check the effectiveness of PSG-OPV-5 for detection of free bilirubin at pH= 10, preliminary studies are carried out using stock solution of polymer and bilirubin in ches buffer at this pH. The details of polymer and bilirubin sample preparations are given in Experimental Section. (All the experiments were conducted in dark; bilirubin being light sensitive).

For carrying out the sensing studies in ches buffer, fixed concentration of PSG-OPV-5 (0.03 mg/mL) was added to the varying concentrations of bilirubin [ranging from $1x10^{-6}$ M to $3x10^{-5}$ M in ches buffer at pH= 10] under dark and their emission, excitation and absorption spectra were recorded immediately. From the emission spectra (***Figure 5.14 A***), it could be seen that with the increase in bilirubin concentration, OPV emission at λmax= 446 nm gradually decreases. The same was further supported by decreasing intensity in excitation spectra with increase in the concentration of bilirubin (***Figure 5.14 B***).

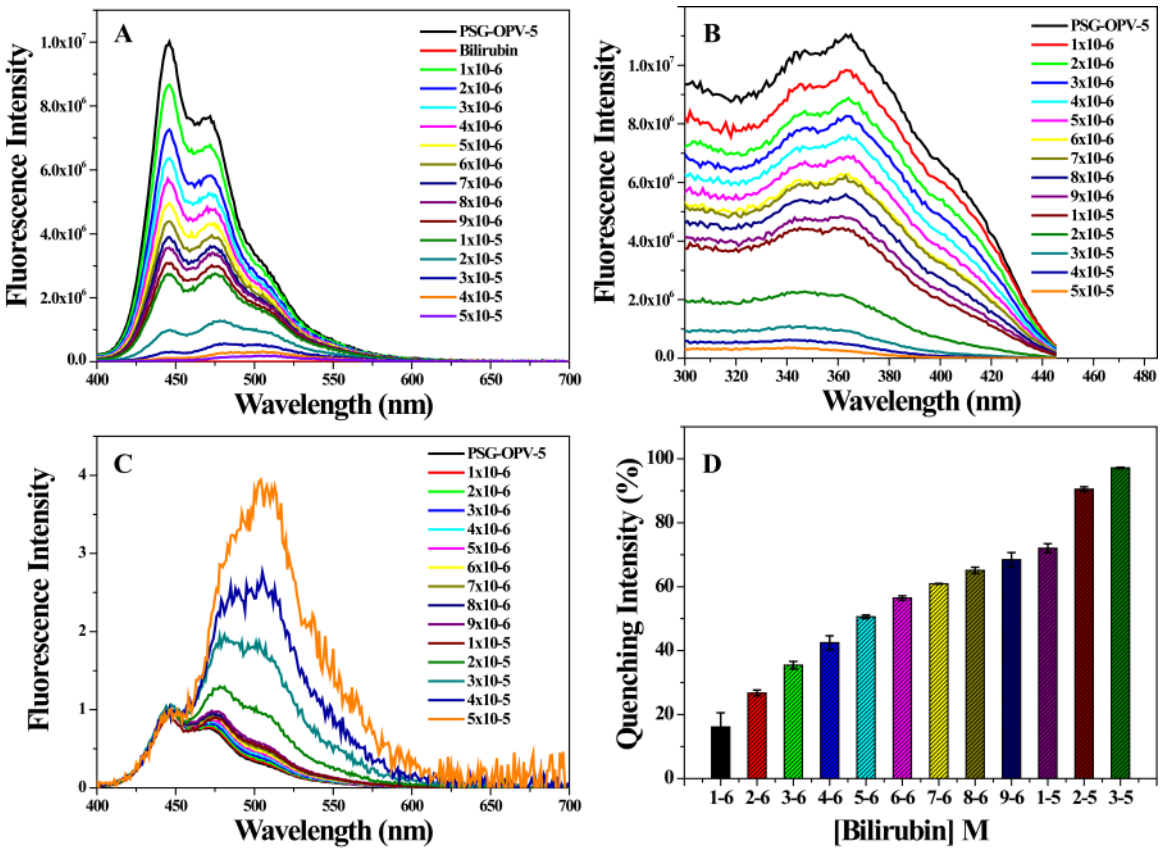

Figure 5.14: (A) Emission and (B) excitation spectra of PSG-OPV-5 recorded after the addition of varying amount of bilirubin (1x 10^{-6} M to 5 x 10^{-5} M). (C) normalized emission spectra of PSG-OPV-5 recorded after the addition of varying amount of bilirubin (1x 10^{-6} M to 5 x 10^{-5} M) at 446 nm. (D) bar graph comparing the quenching intensity *vs* bilirubin concentration. Each measurement was done twice and their average was plotted along with their respective standard deviation.

One could easily observe the enhancement in green emission region after the addition of bilirubin on normalizing the spectra at 446 nm (***Figure 5.14 C***). An instant quenching of ≈36% was observed at concentration of 3x10^{-6} M which finally reached to >50% quenching at 5x10^{-6} M and almost 97% quenching at 3x10^{-5} M (***Figure 5.14 D***).

As shown earlier, PS-OPV-5 was blue emitting polymer (***Figure 5.15 A***). Bilirubin is non emissive species and thus doesn't emit due to its poor quantum yield in any solvent including water (***Figure 5.15 B***). However, upon the gradual addition of bilirubin to the PSG-OPV-5 as shown in ***Figure 5.15 C***, blue emission of OPV quenched while the green emission of bilirubin enhanced in presence of OPV which unambiguously supported FRET between OPV and bilirubin. The visible color change from blue to bluish green under UV lamp was observed.

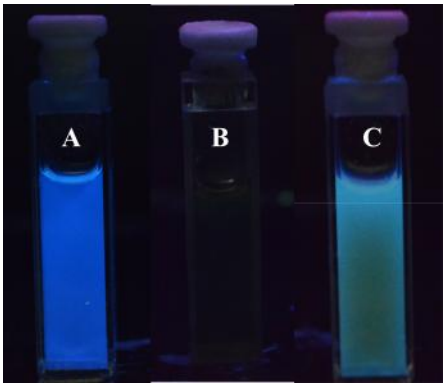

Figure 5.15: Photograph showing (A) PSG-OPV-5 (Blue emission) (B) Bilirubin (no emission) (C) PSG-OPV-5 after bilirubin addition (bluish green emission) in ches buffer at pH 10.

The gradual shift of the emission maxima is further confirmed by their CIE co-ordinate diagram, which showed distinct shift of x and y co-ordinates from (0.15,0.12, blue) for PSG-OPV-5 without bilirubin to (0.19,0.42, bluish green) after addition of 5x 10^{-5} M of bilirubin to polymer (***Figure 5.16***). Bluish green color at higher bilirubin concentration may be due to combined contribution of enhanced green emission from bilirubin (due to FRET) and some unquenched emission from OPV.

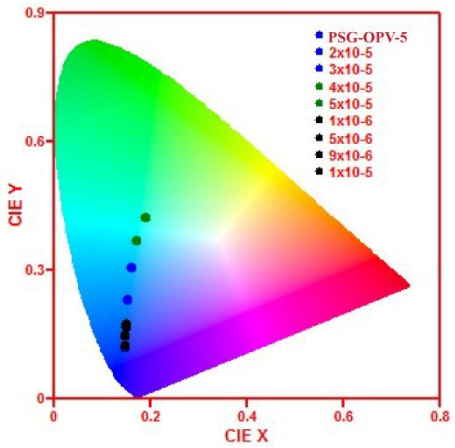

Figure 5.16: CIE co-ordinate diagram of PSG-OPV-5 without and with varying bilirubin concentrations.

5.2.4 Mechanism of Sensing: In order to examine the possibility for existence of different sensing mechanisms for the quenching of OPV emission on interaction with bilirubin, emission quenching of OPV was further analyzed using Stern-Volmer equation. ***Figure 5.17A*** showed the relation between emission intensity of OPV with respect to concentration of bilirubin. Inset showed linear range of Io/I *vs* bilirubin concentration from to 1 x 10^{-7} M to 1 x 10^{-5} M. It can be inferred from figure that only one prominent mechanism is involved upto 1 x 10^{-5} M bilirubin concentration. The linearity of the plot was further checked by linear fitting of data which gave R^2 value of 0.976 showing perfect linear fit (Inset ***Figure 5.17 A***). Additionally from the slope of linear fit, the value of Stern-Volmer constant (K_{sv}) was found to be 262008 M^{-1} which caused the high selectivity of PSG-OPV-5 sensor towards bilirubin. To the best of our knowledge, it is

highest quenching constant value among other reported bilirubin sensors in literature to date.

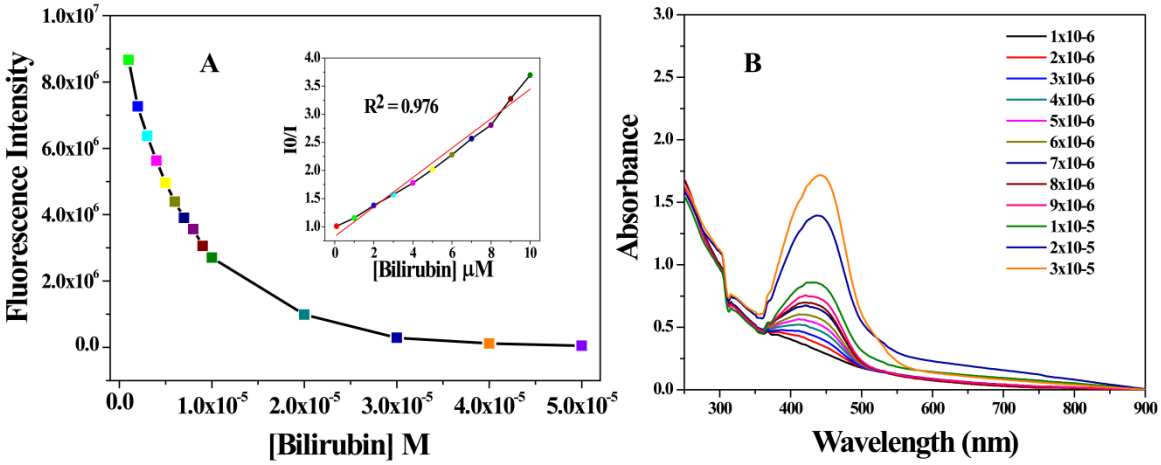

Figure 5.17: (A) Plot of changes in emission intensity of PSG-OPV-5 *vs* concentration of bilirubin and their linear range using Stern-Volmer equation. (B) Absorption spectrum of PSG-OPV-5 after addition of bilirubin in ches buffer.

However, non-linearity beyond 1 x 10^{-5} M concentration, in S-V plot indicated the possibility of more than one sensing mechanism which may include formation of ground state complex between OPV and bilirubin and/or inner filter effect (IFE) other than FRET. The absorption spectra of polymer recorded on varying the analyte concentration did not show any shift or appearance of new peak in presence of bilirubin (***Figure 5.17 B***), and thus excluded any possibility of formation of ground state complex between the two. However, small spectral overlap between excitation spectra of OPV and absorption spectra of bilirubin as shown in ***Figure 5.18*** also indicated the possibility of some extent of IFE between the two, thereby reducing the emission intensity of OPV due to competitive absorption at higher bilirubin concentration beyond 1 x 10^{-5} M. Although, it has to be noted that since possibility of IFE is little, major mechanism involved in the sensing of bilirubin even at higher bilirubin concentration undoubtedly is FRET between OPV and bilirubin (***Figure 5.19***).

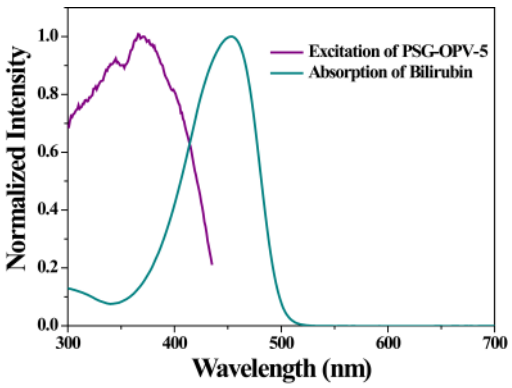

Figure 5.18: Spectral overlap between excitation spectrum of PSG-OPV-5 and absorption spectrum of bilirubin in ches buffer.

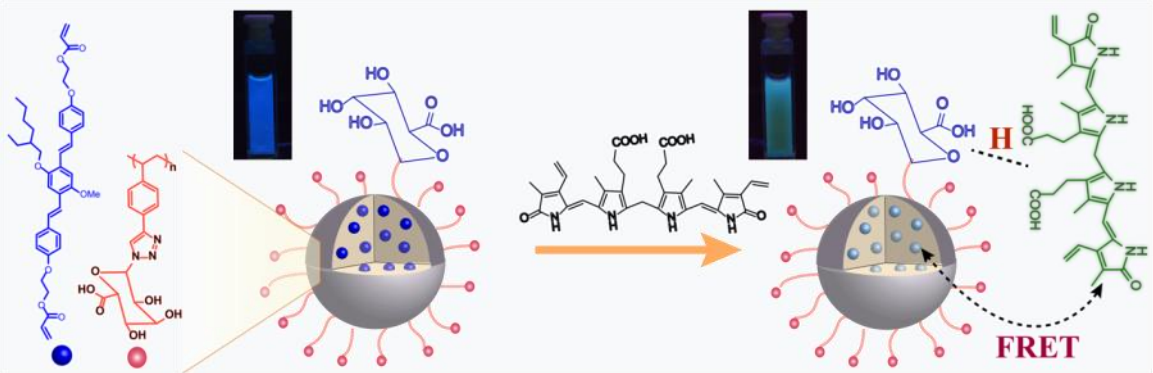

Figure 5.19: Schematics depicting the mechanism of bilirubin sensing.

As bilirubin is biomolecule, the selectivity of PSG-OPV-5 was checked from among the library of other biomolecules such as NaCl, KCl, glucose, sucrose, cholesterol *etc*. which might interfere with emission of polymer. In order to check the same, to the fixed concentration of polymer (0.1 mg/3 mL) was added the fixed concentration of each of the analytes (3x 10^{-5} M) and their emission spectra was recorded (***Figure 5.20 A***), average of three such measurements were plotted in ***Figure 5.20 B***. From the figure, it could surely be inferred that no appreciable quenching was observed upon addition of analytes at concentration of 3 x10^{-5} M other than bilirubin which exhibited almost 97% quenching at same concentration. This together with high quenching constant value signifies the high selectivity of polymer towards bilirubin.

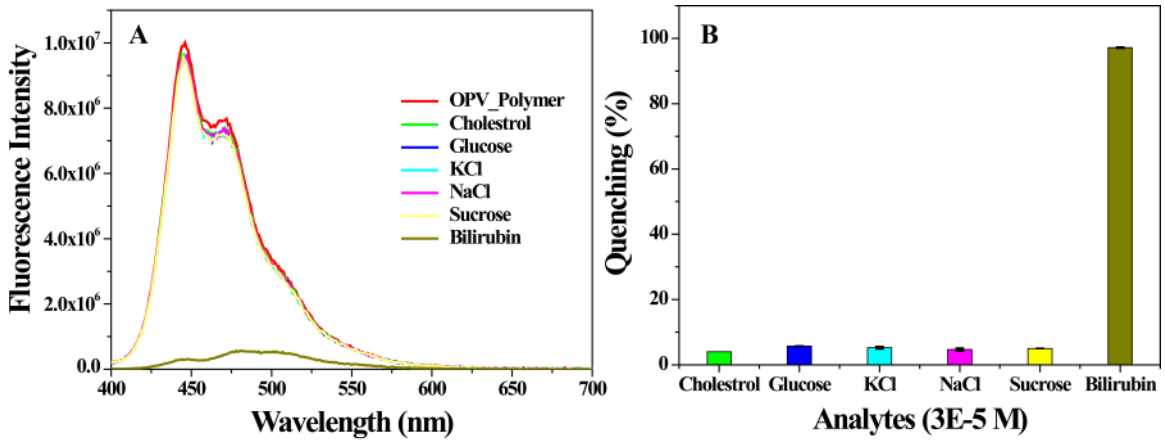

Figure 5.20: (A) Emission spectra showing the selectivity against other interferences in ches buffer, (B) bar graph showing the selectivity against other interferences in ches buffer. Each measurement was done twice and their average was plotted along with their standard deviation.

5.2.5 Sensing studies of free bilirubin in Human Serum: As shown in previous section, the sensor could be successfully applied in water for bilirubin detection with limit of detection as low as 20 nM. Now, to verify the sensor for real time biosensing application, the sensor was further applied for bilirubin detection in human blood serum which contains dissolved proteins, metal ions, triglycerides, glucose, hormones and water. In short, it is blood plasma without any clotting factor. In order to explore further, 100 µL of human blood serum was added to each of vial containing 1 x 10^{-6} M to 3 x 10^{-5} M bilirubin concentration. This mixture was then added to fixed polymer concentration (0.1 mg/3mL) in ches buffer at pH= 10 under dark followed by recording its emission, excitation and absorption spectra almost immediately. Emission spectra showed marked decrease in OPV emission with the increasing concentration of bilirubin similar to studies done in water (***Figure 5.21 A***).

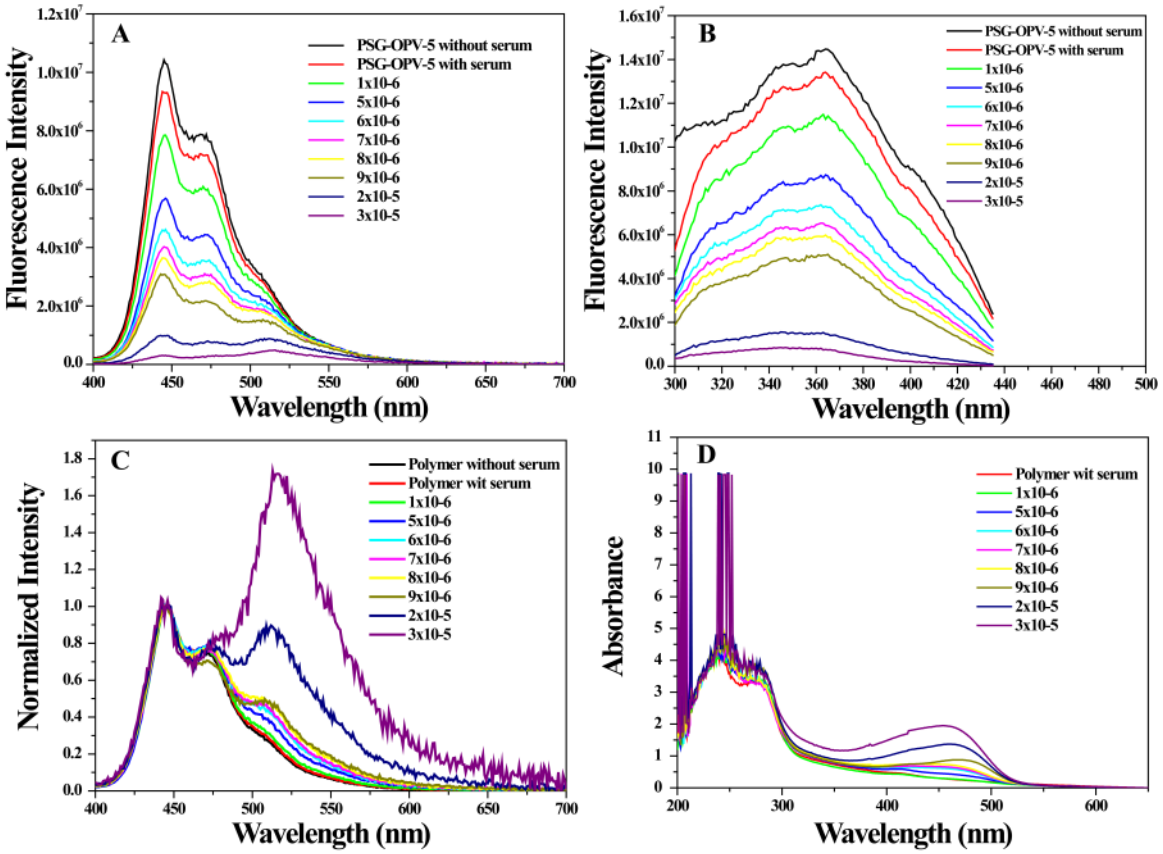

Figure 5.21: (A) Emission, (B) excitation, (C) Normalized emission spectra, (D) absorption spectra of PSG-OPV-5 recorded after the addition of varying concentrations of bilirubin (1x 10^{-6} M to 3 x 10^{-5} M) in human blood serum.

Instant quenching of ≈24% was observed with 1x 10^{-6} M bilirubin concentration which enhanced to more than 55% for 6 x 10^{-6} M and finally complete quenching was observed with concentration of 3 x 10^{-5} M. The same was further confirmed by its excitation spectra which also exhibited marked decrease in the intensity upon gradual addition of bilirubin in human blood serum (***Figure 5.21 B***). Normalizing emission spectra at 446 nm clearly showed enhancement in green emission region after the addition of bilirubin (***Figure 5.21 C***).

Strong absorption below 300 nm in the absorption spectra of samples in human serum (***Figure 5.21 D***) indicated the presence of other analytes such as proteins, cholesterol *etc*. which tend to absorb in this region. Finally the interference was checked from structure homologue of bilirubin *i.e.* biliverdin. Biliverdin closely resembles bilirubin in structure, differing by the presence of one additional double bond at C10 position making the dipyrromethene units in conjugation. ***Figure 5.22*** clearly signified the drastic drop in emission of OPV upon addition of bilirubin while less appreciable change was observed in case of biliverdin. This proved good selectivity of sensor toward bilirubin over other structural homologue even in human blood serum.

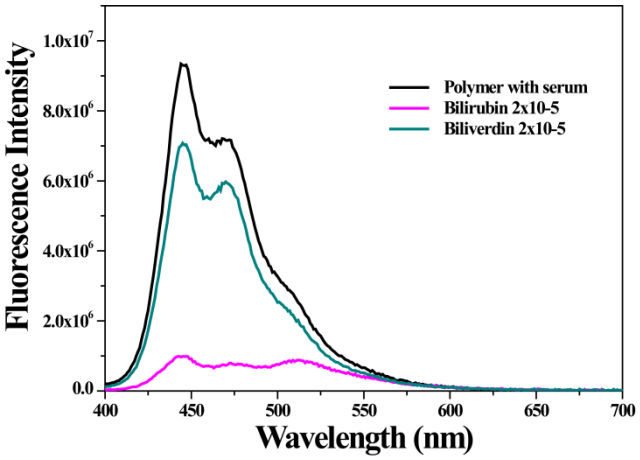

Figure 5.22: Emission spectra of PSG-OPV-5 recorded after the addition of same concentration of bilirubin *vs* bliverdin (2 x 10^{-5} M) in human blood serum.

5.3 Experimental Section:

5.3.1 Materials: 4-bromostyrene, D-glucuronic acid, azidotrimethylsilane (TMS-N_3), Tin(IV) chloride, , bis(triphenylphosphine) palladium(II) dichloride [$Pd(PPh_3)_2Cl_2$], copper(I) iodide (CuI), 4-ethynyl trimethylsilane, tetrabutylammoniumfluoride (TBAF, 1M in THF), azobisisobutyronitrile (AIBN), styrene, hexadecane (HD), potassium persulfate (KPS) were purchased from Aldrich and used without further purifications. Other reagents and solvents such as tetrahydrofuran (THF), dichloromethane (DCM), triethylamine (Et_3N), acetic anhydride, iodine, copper sulfate ($CuSO_4$), sodium ascorbate, sodium thiosulfate pentahydrate, sodium bicarbonate *etc* were purchased locally. All the

solvents were dried using standard procedures. Polymerizable fluorophore [oligo-*p(*phenylenevinylene), OPV] was synthesized according to previously reported procedure.

5.3.2 Measurements: The instruments techniques used for characterization of monomers and polymers such as DLS (for size and zeta potential), FTIR, sonicator, NMR, GC-MS analysis, absorption and fluorescence spectrophotometer are same as described in our previous report. For solid sample, powders were mixed with KBr to make pellets while for liquid sample, their dilute solution is directly drop casted on attenuated reflectance reflectance (ATR) and their infrared spectra were recorded in the range of 4000-600 cm^{-1}. Molecular weight was determined using PL-220 GPC instrument in choloroform and flow rate was maintained as 1 mL/min. For DLS, average of three consecutive readings of freshly prepared samples was taken in order to minimize error.

5.3.3 Synthesis of monomers and polymers:

Monomers (1-5) were synthesized using reported procedures.[30,31]

1. Synthesis of penta-acetate glucuronic acid (Glu-1):

To 5 g of D-glucuronic acid was added 75 mL of acetic anhydride and the solution was kept for stirring under ice cooled condition. Then iodine was slowly added and color of the solution became red. This is allowed to stir for 2 h at 0 ^{o}C and further 3 h at room temperature.

The excess of acetic anhydride was distilled off and rest of the mixture was dissolved in DCM. The organic layer was then washed three times with sodium thiosulfate pentahydrate to remove iodine and concentrate to dryness to give white solid.

Yield: 80%.

^{1}H NMR (200 MHz, $CDCl_3$): δ in ppm 5.80 (d, 1H), 5.36 (t, 1H), 5.28 (t, 1H), 5.11 (t, 1H), 4.32 (d, 1H), 2.26 (s, 3H), 2.12 (s, 3H), 2.03 (m, 9H). LC-MS/MS (in MeCN) m/z calculated - 404.02; observed M+Na - 427.08, M+K - 443.06.

2. Synthesis of 1, 2, 3, 4-Tetra-O-Acetyl-methyl-β-D-Glucuronide (Glu-2):

To the above pentacetate product was added dry methanol and allowed to reflux for 24 h. The excess methanol is distilled off under vacuum. The product was purified by recrystallization from methanol.

Yield: 60%.

^{1}H NMR (200 MHz, $CDCl_3$): δ in ppm 5.26 (m, 2H), 4.97 (t, 1H), 4.71 (d, 1H), 4.14 (d, 1H), 3.78 (s, 3H), 2.08 (s, 3H), 2.04 (s, 6H).

LC-MS/MS (in MeCN) m/z calculated - 376.13; found M+Na 399.08, M+K 415.06.

3. Synthesis of 2, 3, 4-tri-O-acetyl-1-azido-1-deoxy-β-D-glucuronic acid methyl ester (Glu-3, 4):

To 2 g of 1, 2, 3, 4-Tetra-O-Acetyl-methyl-β-D-Glucuronide was added 35 mL of dry DCM under argon atmosphere. TMS-N_3 (1.6 ml) and tin (IV) chloride (0.2 ml) was then added to it and was allowed to stir for additional 15 h at room temperature. After the mentioned time, reaction mixture was diluted with DCM and saturated with sodium bicarbonate solution to quench excess of tin(IV) chloride and stirred vigorously for 30 min. The mixture was then poured in water and the product was extracted with DCM, dried over sodium sulfate and is used without any further purification.

Yield: 92%.

^{1}H NMR (200 MHz, $CDCl_3$): δ in ppm 5.24 (apt t, 2H), 4.95 (t, 1H), 4.72 (d, 1H), 4.13 (d, 1H), 3.77 (s, 3H), 2.07 (s, 3H), 2.03 (s, 3H), 2.01 (s, 3H). LC-MS/MS (in MeCN) m/z calculated - 359.29; observed M+Na - 382.35.

FTIR(cm^{-1}): 2121 (-N_3).

4. Synthesis of 4-(Trimethylsilane)ethynylstyrene (2) from 4-bromostyrene:

To 1.86 g of 4-bromostyrene, 2.28 g of ethynyltrimethylsilane, 30 mg of copper (I) iodide was added 40 ml dry Et_3N. The reaction mixture was heated at 50 ºC. After 5 min, 150 mg of bis(triphenylphosphine) palladium (II) dichloride was added to the above mixture and allowed to stir for 16 h at the same temperature. Afterwards trimethylamine salt was filtered off followed by distillation under vacuum. The crude product was column purified using pet ether.

Yield: 59%.

^{1}H NMR: δ in ppm 7.21 (d, o-Ar, 2H), 7.16 (d, m-Ar, 2H), 6.48 (dd, 1H), 5.61 (d,1H), 5.12 (d,1H), 0.28 (s, Si(Me)3), 9H).

FTIR (cm^{-1}) : 2157 (triple bond C-Si).

5. Synthesis of 4-ethynylstyrene (3):

The silyl protected styrene (1 g) was dissolved in 5 ml dry THF and to it 1.0 M solution of tetra-*n*-butyl ammonium fluoride (7.5 ml) was added dropwise. The reaction mixture was stirred at room temperature for one hour and then THF was evaporated off under vacuum. The crude product was partitioned with DCM and water and the water layer was extracted twice with DCM and the combined layer was evaporated to dryness. The product is column purified using pet ether.

Yield: 90%.

^{1}H NMR: δ in ppm 7.36 (*o*-Ar, 2H), 7.31 (d, *m*-Ar, 2H), 6.64 (dd, 1H), 5.75 (d,1H), 5.26 (d,1H), 3.04 (s,1H).

FTIR (cm^{-1}): 3295 (free Alkyne C-H).

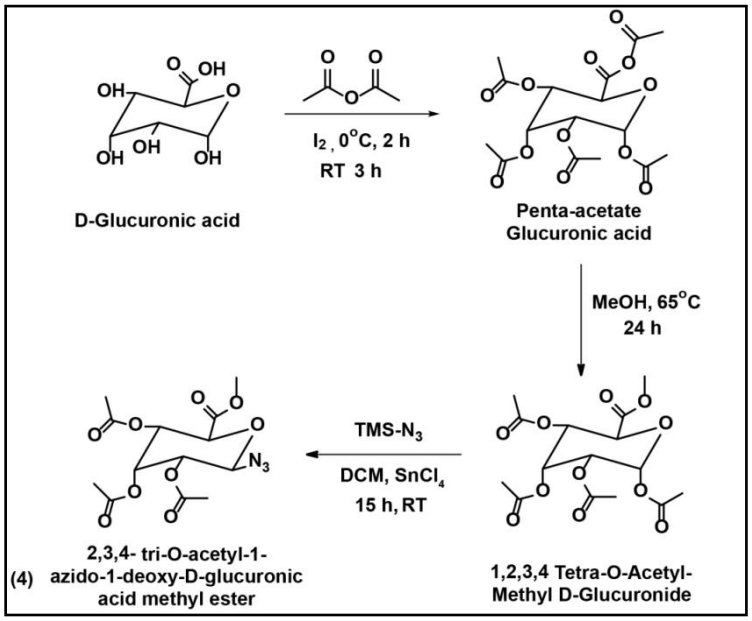

Scheme 5.3: Synthesis of 2, 3, 4-tri-O-acetyl-1-azido-1-deoxy-β-D-glucuronic acid methyl ester (4).

6. Click reaction to synthesize (5):

In two neck round bottom flask was added 1 g of 4-ethynylstyrene (2) and 2.4 g of 2, 3, 4-tri-O-acetyl-1-azido-1-deoxy-β-D-glucuronic acid methyl ester (4) in dry THF and the mixture was then subjected to three freeze/thaw cycle. Then 480 mg of copper sulfate and 620 mg of sodium ascorbate in minimum quantity of water was then added to the mixture. The mixture was allowed to stir for 24 h under argon atmosphere. The progress of reaction was monitored using FTIR analysis. Once FTIR showed complete absence of free alkyne C-H peak, the reaction mixture was stopped and subjected to dryness under vacuum. The product was purified using pet ether/ ethyl acetate (40/60) to afford (2R, 3S, 4R, 5S, 6R)-2-(methoxycarbonyl)-6-(4-(4-vinylphenyl)-1H-1,2,3-triazol-1-yl)tetrahydro-2H-pyran-3,4,5-triyl triacetate.

Yield: 80%.

^{1}H NMR (200 MHz, $CDCl_3$): δ in ppm 8.06 (s, 1H), 7.79 (d, 2H), 7.51 (d, 2H), 6.73 (q, 1H), 6.01 (d, 1H), 5.85 (d, 1H), 5.51-5.33 (m, 4H), 4.37 (d, 1H), 3.77 (s, 3H), 2.09 (s, 6H), 1.90 (s, 3H).

LC-MS/MS (in MeCN) m/z calculated - 487.16; observed M+H - 488.16, M+Na - 510.15, M+K 526.12.

7. Polymerization to synthesize PS-PGlu (6) :

(2R, 3S, 4R, 5S, 6R)-2-(methoxycarbonyl)-6-(4-(4-vinylphenyl)-1H-1,2,3-triazol-1-yl)tetrahydro-2H-pyran-3,4,5-triyl triacetate (1 g), AIBN (50 mg) were taken in together in schlenk tube. To it 10 ml dry DMF was added. This mixture was degassed using three freeze/thaw cycle. The schlenk tube was then placed in oil bath at 80 ^{0}C for 24 h while stirring at 750 rpm. After 24 h, the reaction mixture was cooled and further diluted with minimum amount of THF. The polymer was then precipitated by pouring the solution in excess methanol. And oligomers were removed by repeating three precipitation/filtration cycles.

Yield: 55%.

^{1}H NMR (400 MHz, $CDCl_3$): δ in ppm 8.45 (t, 1H), 7.42 (b, 2H), 6.61 (b, 2H), 6.30 (b, 1H), 5.62 (m, 3H), 4.55 (m, 1H), 3.72 (s, 6H), 2.09 (s, 6H), 1.88 (s, 3H), 1.69 (s, 3H).

8. Deprotection of protected glucuronic acid bearing polystyrene polymer (PS-DGlu, 7):

100 mg of the polymer was dissoved in 5 ml dichloromethane and 2 ml methanol mixture. To it 0.7 ml 25 weight% sodium methoxide in methanol was added. This mixture was allowed to stir for 8 h. After rotary evaporation, polymer was washed with acetone and dissolve in 1:1 THF: water mixture. Then dilute HCl (0.025 M) was added and the reaction was stirred for additional 12 h. Then the excess solvent was removed and polymer was dissolved in minimum amount of water followed by dialyzing it against deionized water using 1 kD molecular weight cutoff dialysis membrane for 3 days, changing water thrice. Final polymer was obtained as white powder after freeze drying the dialyzed solution.

FTIR (cm^{-1}): 3354 (broad peak), 1727, 1611, 1411, 1335, 1100, 1024, 818, 687.

9. Preparation of PSG-OPV-n using PS-DGlu (7) as surfactant:

PS-DGlu polymer was used as surfactant in the miniemulsion polymerization process for synthesizing novel D-glucuronic acid functionalized fluorescent PS nanobeads. The organic phase consist of styrene (1 g), HD (48 mg), polymerizable OPV dye (30 mg) while the aqueous phase consist of water (4 g), initiator (ACVA) (16 mg) and varying amount of PS-DGlu polymer (values are mentioned in ***Table 5.1***). The organic phase was then added dropwise to the aqueous phase and kept for pre-emulsification at room

temperature for another one hour followed by sonication under ice cooled condition for 20 min. The miniemulsion was then allowed to polymerize at 70 ºC for 20 h with a stirring speed of 750 rpm. After quenching the polymerization with two drops of 1 wt% hydroquinone, the obtained latex was purified by dialysis using 6 kD MW cut-off membrane for three days.

5.3.4 Calculation of dye loading content (DLC): Three mg of dried polymer was taken in 3 mL of THF and its absorbance was recorded using absorption spectroscopy. This absorbance was used to calculate the dye loading from the molar absorptivity of OPV in THF (40,360 $Lmol^{-1}cm^{-1}$) at its absorption maxima.

5.3.5 Sensing of free bilirubin in aqueous medium: The stock solution of polymer was prepared at concentration of 0.1 mg/3 mL using ches buffer at pH 10. Varying concentration of bilirubin solution ranging from $1x10^{-6}$ to $5x10^{-5}$ M in ches buffer at pH= 10 were prepared and kept in dark. All the solution were kept in dark at 18 ºC. The change in emission and absorption intensity of polymer after the addition of different concentrations of bilirubin were recorded at 18 ºC with slit width of 1 nm.

5.3.6 Sensing of free bilirubin in human serum: Human blood serum was taken from Dr. Mahesh Kulkarni's laboratory from CSIR-National chemical laboratory as contribution for carrying out scientific research and was used as received without any further treatment. Fixed amount of 100 µL of human blood serum was added to the varying concentration of bilirubin in range of $1x10^{-6}$ M to $3x10^{-5}$ M. And these solutions were then added to fixed concentration of polymer (0.1 mg/3 mL) in ches buffer at pH= 10 to make the final volume of 3 mL. The change in emission and absorption intensity of polymer after the addition of different concentrations of bilirubin were recorded at 18 ºC with slit width of 1 nm. One separate experiment was conducted using same volume (3 mL) of polymer and serum without adding bilirubin at pH= 10.

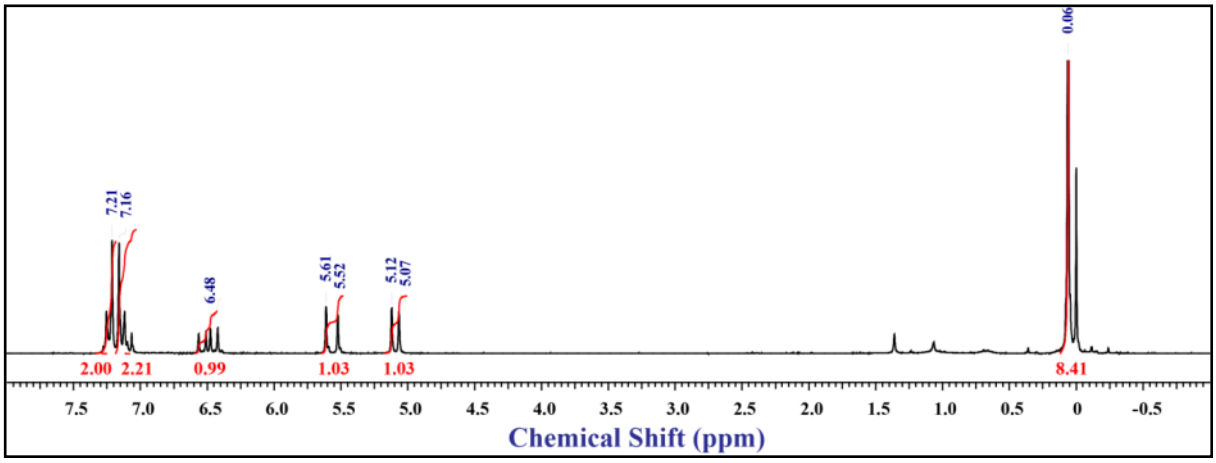

Figure 5.23. ^{1}H-NMR spectrum of (4-trimethylsilyl)ethynylstyrene in $CDCl_3$

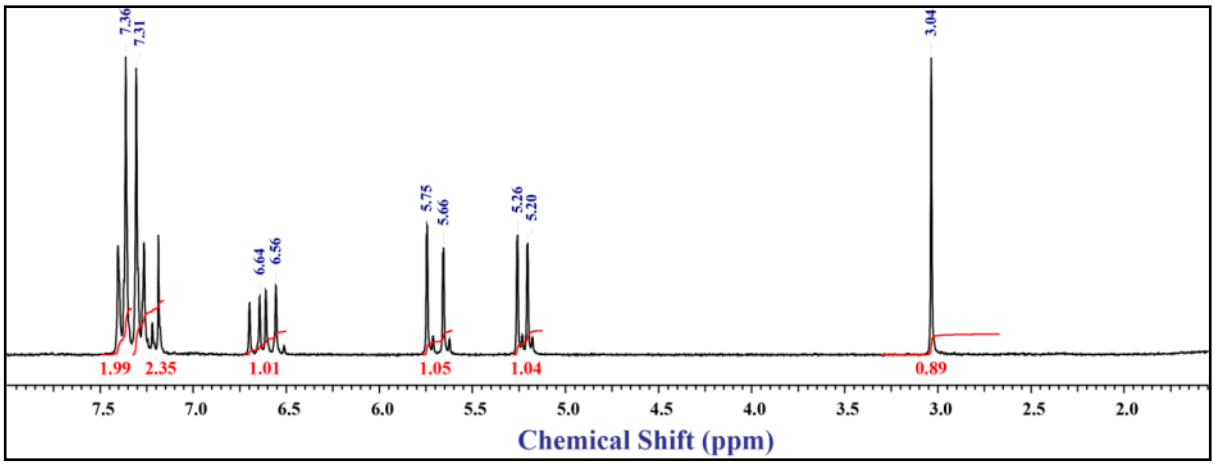

Figure 5.24: ^{1}H-NMR spectrum of 4-ethynylstyrene in $CDCl_3$

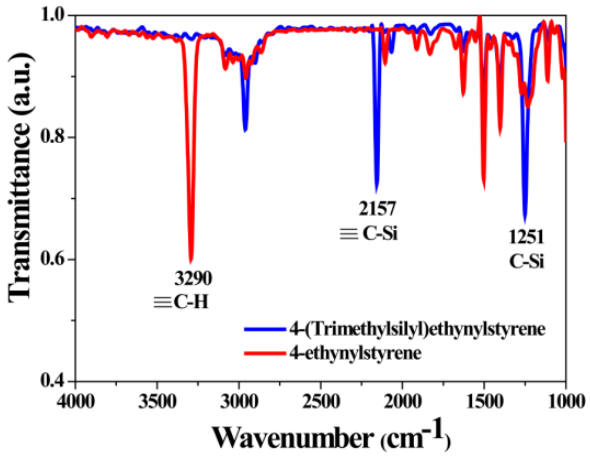

Figure 5.25: FTIR spectrum of comparing (4-trimethylsilyl)ethynylstyrene and 4-ethynylstyrene on KBr pellet.

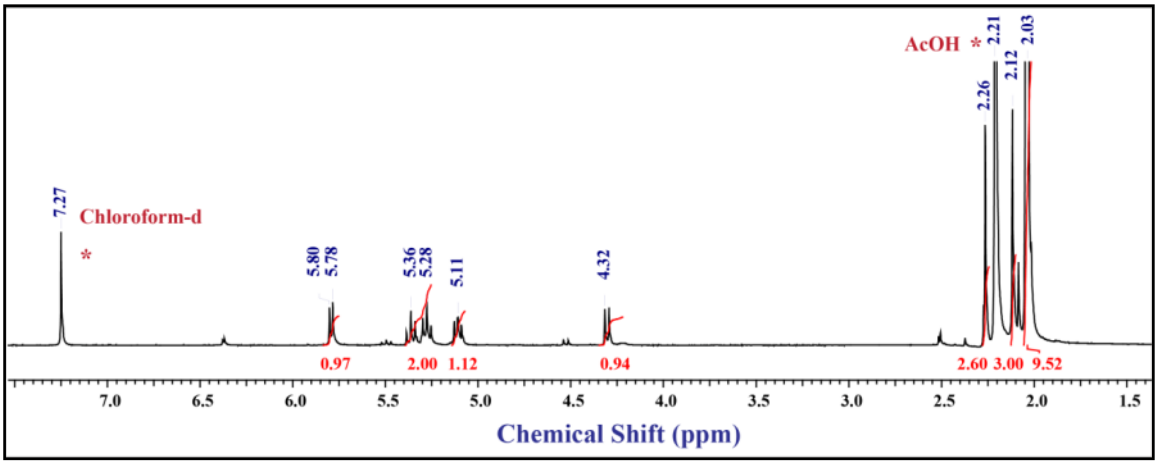

Figure 5.26: ^{1}H-NMR spectrum of Penta-acetate D-Glucuronic acid in $CDCl_3$.

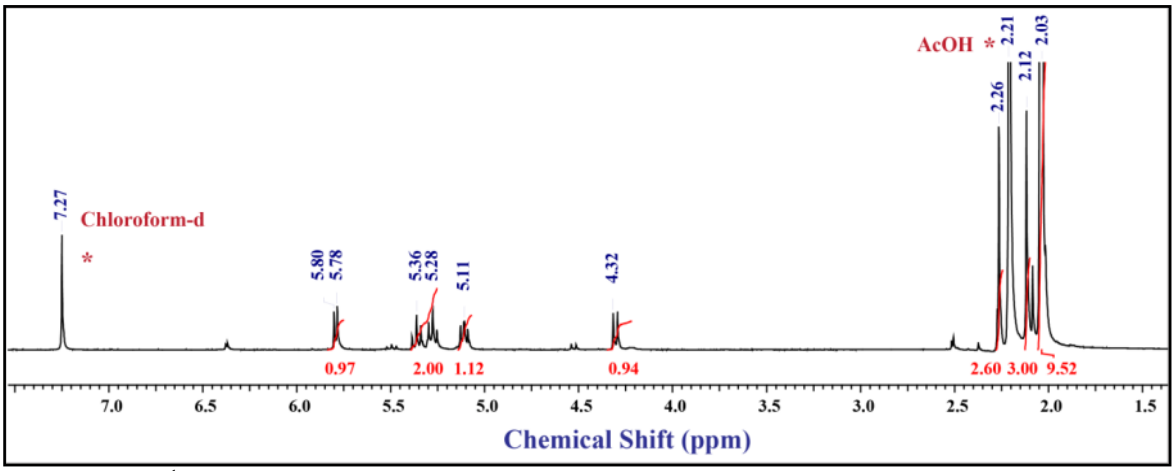

Figure 5.27: ^{1}H-NMR spectrum of Tetra-O-acetyl-methyl D-glucuronide in $CDCl_3$.

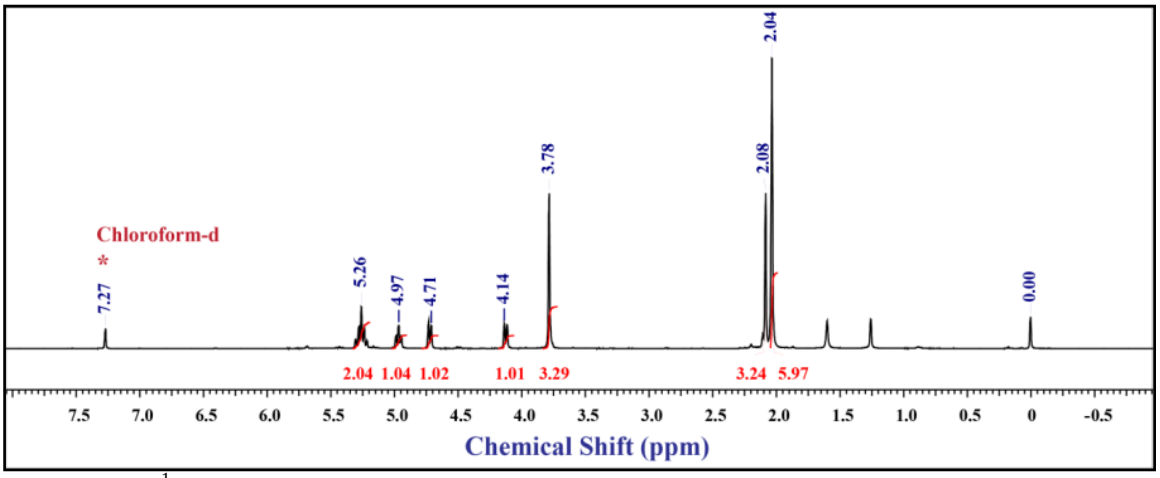

Figure 5.28: ^{1}H-NMR spectrum of tri-O-acetyl-1-azido-1-deoxy-D-glucuronic acid methyl ester in $CDCl_3$.

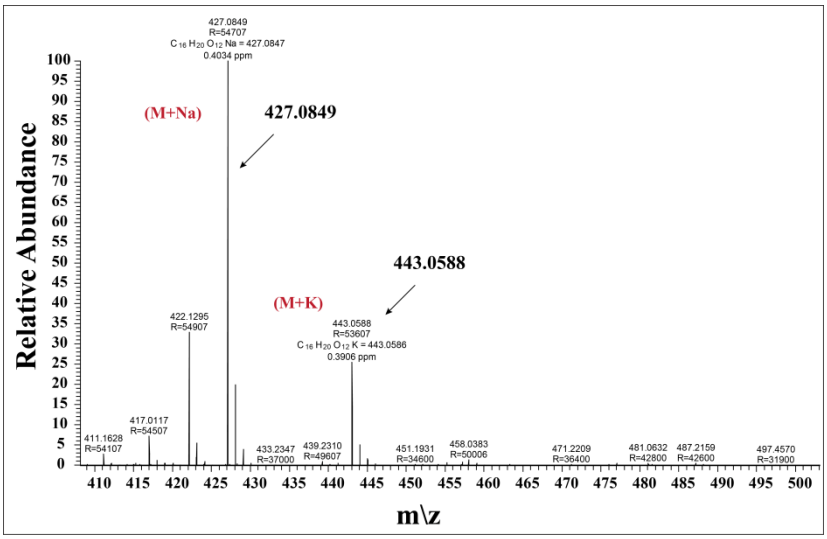

Figure 5.29: LC-MS/MS spectrum of Penta-acetate D-glucuronic acid in MeCN.

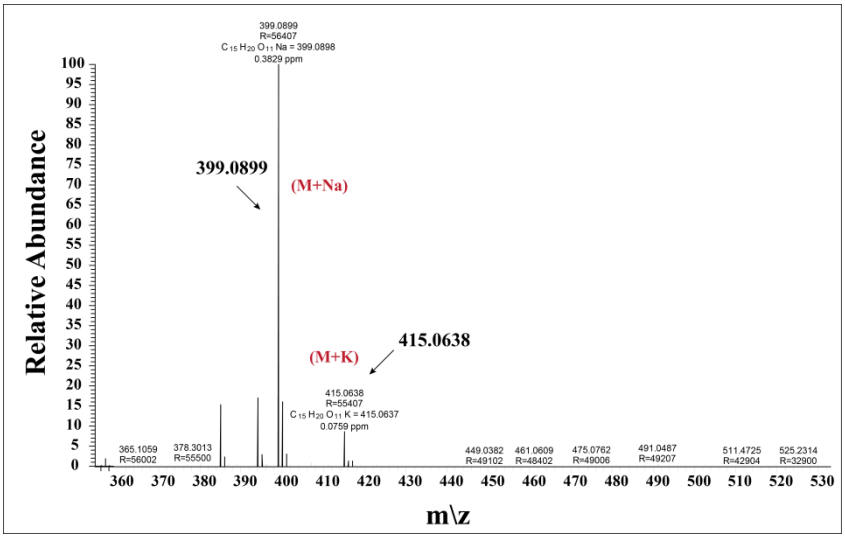

Figure 5.30:. LC-MS/MS spectrum of Tetra-O-acetyl-methyl D-glucuronide in MeCN.

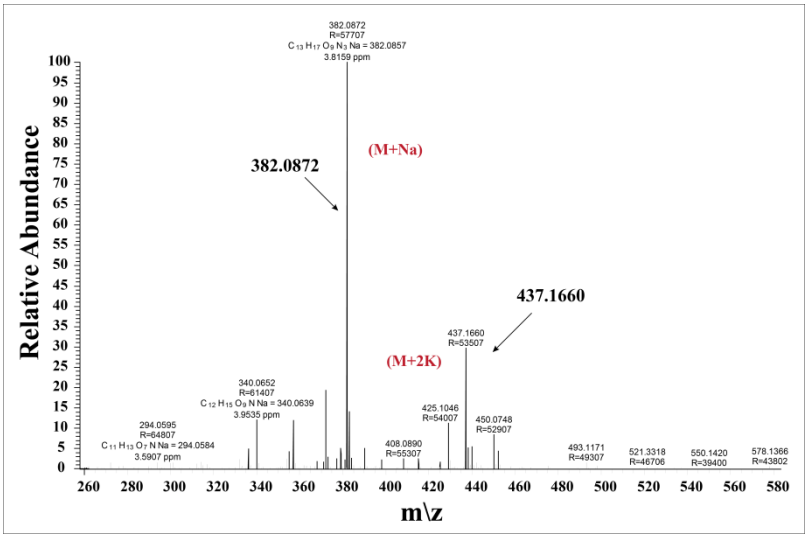

Figure 5.31: LC-MS/MS spectrum of tri-O-acetyl-1-azido-1-deoxy-D-glucuronic acid methyl ester in MeCN.

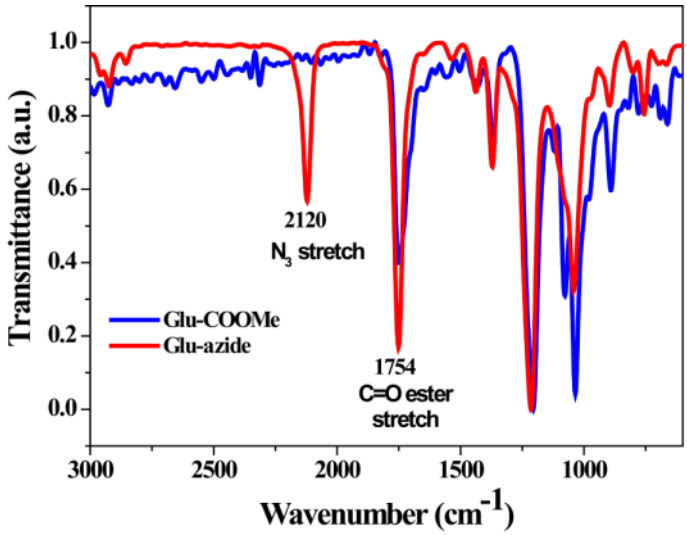

Figure 5.32: FTIR spectrum comparing tetra-O-acetyl-methyl D-glucuronide (Glu-COOMe) and tri-O-acetyl-1-azido-1-deoxy-D-glucuronic acid methyl ester (4) on KBr pellet.

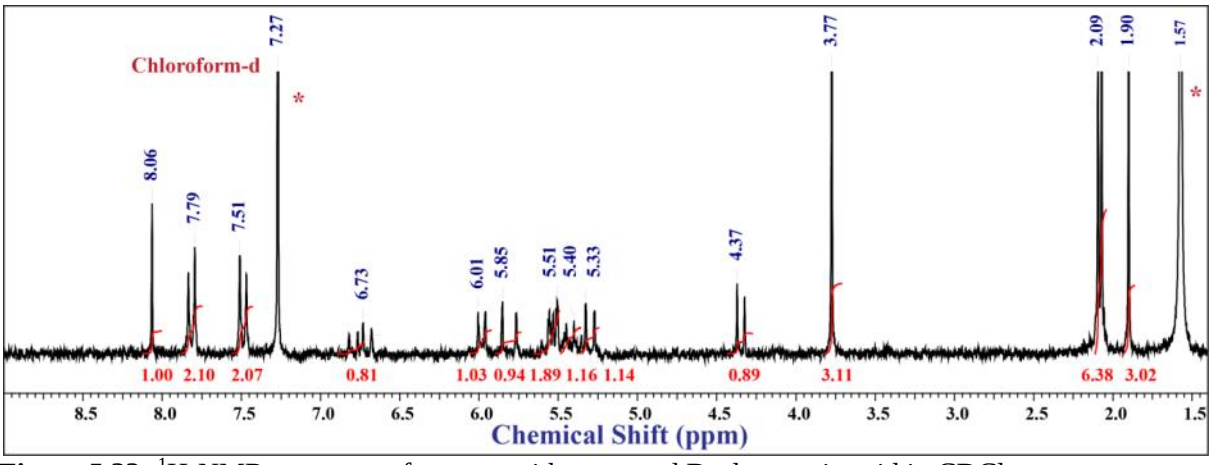

Figure 5.33: ^{1}H-NMR spectrum of styrene with protected D-glucuronic acid in $CDCl_3$.

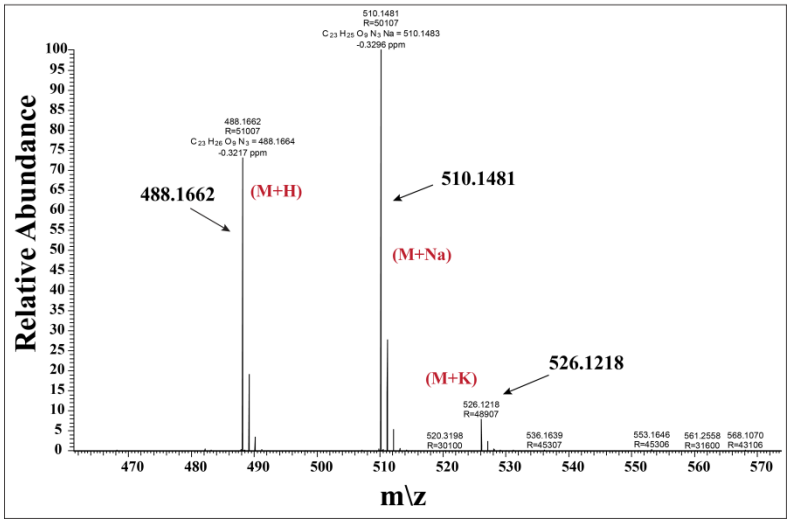

Figure 5.34: LC-MS/MS spectrum of styrene with protected D-glucuronic acid in MeCN.

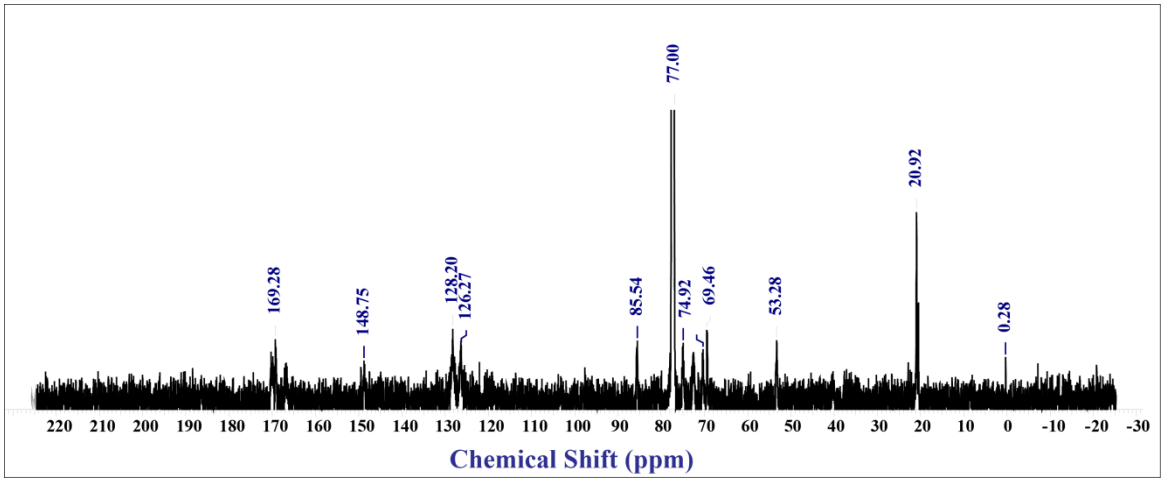

Figure 5.33: ^{13}C-NMR spectrum of PS-PGlu in $CDCl_3$.

Table 5.2: Sample designation, weight average molecular weight (Mw) and its polydispersity index (PDI) in $CHCl_3$.

Samples	Mw (Da)	PDI
PS-OPV-1	155000	1.7
PS-OPV-2	54500	2.4
PS-OPV-3	37500	2.4
PS-OPV-4	272000	2.3
PS-OPV-5	110000	2.1

5.4 Conclusion:

A tailor made water soluble glucuronic acid bearing polystyrene polymer (PS-DGlu) was synthesized which not only stabilized the PS nanobeads in the size range of 160-328 nm, but also surface functionalize the nanobeads with glucuronic acid together with successful covalent incorporation of OPV as fluorophore in styrene miniemulsion polymerization. To the best of our knowledge, it is the first report on glucuronic acid functionalized PS nanobeads (PSG-OPV-n) mentioned in the literature so far. The glucuronic acid would impart water solubility to PS-DGlu polymer to enable it to act as surfactant in miniemulsion polymerization which is also reported for the first time in literature. Additionally, the glucuronic acid on the PS nanobeads, served as interaction site for the selective detection of bilirubin via non-covalent interaction. Due to its excellent water dispersibility and good spectral overlap between emission of OPV and absorption of bilirubin; detection of free bilirubin was first targeted in water. Among series of PSG-OPV-n, PSG-OPV-5 was chosen because of its higher zeta potential, solid content, molecular weight and OPV incorporation in comparison to other nanobeads. Instant visual detection of bilirubin under UV lamp could be possible where blue emission of polymer turned bluish green instantly after bilirubin addition. This could be explained on the basis of energy transfer from OPV to bilirubin which is further supported by its emission spectra as well as CIE co-ordinate diagram. The interference from other biomolecules such as glucose, sucrose, metal ions, cholesterol *etc*. was checked. The limit of detection was found to be as low as 20 nM which is found to be in clinically applicable range of <25 to >50 µmol/L. Finally, the polymer nanobeads were checked for real time monitoring of bilirubin in human blood serum where PSG-OPV-5 was found to be selective against its structural homologue *i.e.* biliverdin. Thus highly selective and sensitive visual sensor for bilirubin in human blood serum could be developed using combined strategy of FRET and hydrogen bonding interactions.

5.5 References:

1. Bonnett, R.; Davies, J. E.; Hursthouse, M. B. *Nature* **1976**, *262*, 326-328.

2. Fevery, J. *Liver International* **2008**, 592-605.

3. Koolman, J.; Roehm, K. H. Color Atlas of Biochemistry, 2nd ed.; Thieme: Stuttgart, Germany, and New York, **2005**.

4. Silbernagl, S.; Despopoulos, A. Color Atlas of Physiology, 6th ed.; Thieme: Stuttgart, **2009**; 252.

5. Boyer, T. D.; Manns, P. P.; Sanyal, A. J. Hepatology: *A Textbook of Liver Disease*, 6th ed.; Saunders: London, **2011**; p 1079.

6. Feng, Q.; Du, Y.; Zhang, C.; Zheng, Z.; Hu, F.; Wang, Z.; Wang, C. *Sens. Actuators B* **2013**, *185*, 337-344.

7. Rand, R. N.; di Pasqua, A. *Clin. Chem.* **1962**, *8*, 570-578.

8. Xia, N.; Zhou, B.; Huang, N.; Jiang, M.; Zhang, J.; Liu, L. *Biosens. Bioelectron.* **2016**, *85*, 625-632.

9. Santos Figueroa, L. E.; Moragues, M. E.; Climent, E.; Agostini, A.; Martinez Manez, R.; Sancenon, F. *Chem. Soc. Rev.* **2013**, *42*, 3489-3613.

10. Chen, H.; Xie, Y.; Kirillov, A. M.; Liu, L.; Yu, M.; Liu, W.; Tang, Y. *Chem. Commun.* **2015**, *51*, 5036-5039.

11. Santhosh, M.; Chinnadayyala, S. R.; Kakoti, A.; Goswami, P. *Biosens. Bioelectron.* **2014**, *59*, 370-376.

12. Ellairaja, S.; Shenbagavalli, K.; Ponmariappan, S.; Vasantha, V. S. *Biosens. Bioelectron.* **2017**, *91*, 82-88.

13. Du, Y.; Li, X.; Lv, X.; Jia, Q. *ACS Appl. Mater. Interfaces* **2017**, *9*, 30925-30932.

14. Senthilkumar, T.; Asha, S. K. *Macromolecules* **2013**, *46*, 2159-2171.

15. Senthilkumar, T.; Asha, S. K. *Macromolecules* **2015**, *48*, 3449-3461.

16. Stoffelbach, F.; Belardi, B.; Santos, J. M. R. C. A.; Tessier, L.; Matyjaszewski, K.; Charleux, B. *Macromolecules* **2007**, *40*, 8813-8816.

17. Save, M.; Manguian, M.; Chassenieux, C.; Charleux, B. *Macromolecules* **2005**, *38*, 280-289.

18. Riess, G.; Labbe, C. *Macromol. Rapid Commun.* **2004**, *25*, 401-435.

19. Liu, S.; Armes, S. P. *Angew. Chem. Int. Ed.* **2001**, *41*, 1413-1416.

20. Munoz-Bonilla, A.; Herk, A. M. V; Heuts, J. P. A. *Macromolecules* **2010**, *43*, 2721-2731.

21. Zheng, Z.; Fang, J. L.; Lazarus, P. *Drug Metab. Dispos.* **2002**, *30*, 397-403.

22. Ramanathan, T.; Fisher, F. T.; Ruoff, R. S.; Brinson, L. C. *Chem. Mater.* **2005**, *17*, 1290-1295.

23. Griffin, W. C. *J. Soc. Cosmet. Chem.* **1954**, *5*, 259.

24. Zhang, J.; Dubay, M. R.; Houtman, C. J.; Severtson, S. J. *Macromolecules* **2009**, *42*, 5080-5090.

25. Tan, B.; Grijpma, D. W.; Nabuurs, T.; Feijen, J. *Polymer* **2005**, *46*, 1347-1357.

26. Garnier, S.; Laschewsky, A. *Langmuir* **2006**, *22*, 4044-4053.

27. Tadros, T. F. In Applied Surfactants: Principles and Applications;Wiley-VCH Verlag: Weinheim, Germany, **2005**.

28. Kuo, A. *CheM*, **2011**, *1*, 80−86.

29. Brodersen, R. *J. Biol. Chem.* **1979**, *254*, 2364−2369.

30. Tosin, M.; Murphy, P. V. *Org. Lett.* **2002**, *4*, 3675-3678.

31. Malkoch, M.; Thibault, R. J.; Drockenmuller, E.; Messerschmidt, M.; Voit, B.; Russell, T. P.; Hawker, C. J. *J. Am. Chem. Soc.* **2005**, *127*, 14942–14949.

CHAPTER-6

Conclusion and Future Perspective

6.1 Conclusion:

The thesis entitled "**Functionalized Fluorescent Polystyrene Nanobeads For Sensing And Bio-imaging Applications**" mainly highlights the design and development of fluorescent polystyrene nanobeads using miniemulsion polymerization method. Besides the smaller particle size obtained from miniemulsion polymerization, the other advantages include higher molecular weight, higher polymerization rate and higher incorporation of dyes into PS backbone. Polymerizable oligo (*p*-phenylene vinylene) (OPV) and perylenebisimide (PBI) based fluorophores were covalently stitched into PS nanobeads to prevent any dye leakage. OPV and PBI were specifically chosen as suitable fluorophores because of their strong absorption, high emission quantum yield and excellent thermal, chemical and photostability. These nanobeads were surface functionalized with various functional groups depending on the requirement. And these nanobeads showcased excellent and constant emission under different applied conditions like wide range of temperature and pH. Such an excellent fluorescence made them potential candidate for various applications such as bio-imaging, chemical sensing and bio-sensing.

In the first working chapter, we have presented a simple method of developing fluorescent nanobeads in the size range (50 -150 nm) suitable for cell imaging applications based on commodity polymers like polystyrene. The miniemulsion polymerization technique was chosen to enable the synthesis of fluorescent PS particles with narrow particle size distribution in the ~100 nm range. Multiple fluorophores were inserted into the single bead without significantly affecting its size to obtain multicolor emission from beads. Spherical morphology and the size of nanobeads were confirmed by FESEM, TEM and DLS. The covalent incorporation of the fluorophores (in the form of cross-linkers) ensured the absence of dye leakage and the PS backbone also reduced aggregation induced self-quenching of fluorescence of the dyes. The chosen fluorophores (OPV and PBI) are known for their high fluorescence quantum yields and excellent photostability and this results in outstanding emission profile. In fact, quantum yield for OPV-PS-7 was found to be 26% in water which is highest for any OPV reported system

in water. Based on emission properties, polymers with highest quantum yield and emission in water *i.e.* OPV-PS-7 and PBI-PS-3 were chosen further for bio-imaging application along with one having both OPV and PBI fluorophores *i.e.* OPV(PBI)-PS.

In the second working chapter, the currently synthesized multicolor emitting fluorescent PS nanobeads as described in the previous chapter, have been successfully employed for bio-imaging application in cancer cells. Since the fluorophores were embedded well in the PS network, their emission was also not affected by external triggers that may be present in the cellular environment such as pH or temperature. Presence of two different fluorophores inside a single bead made it possible to access multiple excitation wavelengths for multi spectral imaging applications. The ability for such multicolor imaging were successfully able to overcome the cellular autofluorescence and to enhance the resolution contrast of the image, thereby overcoming the common limitation.

In the third working chapter, we have developed distinctly dual vapor based solid state emitting polystyrene nanobeads sensor having OPV and PBI incorporated together in the polymer backbone. The chromophores were incorporated into the polystyrene nanobeads in a suitable proportion as to obtain near white emission under UV light. The surface of nanobeads was selectively functionalized with amine (PS-NH2) or carboxy (PS-COOH) functionality and their sensing efficiency was compared with the one having no functionalization (PS-KPS). Exposure of the polymer beads to the vapors of electron deficient nitro compounds quenched the emission from OPV moiety selectively retaining the emission from PBI resulting in yellow emission from nanobeads under UV lamp. On the other hand, PBI emission was quenched on exposure to amine vapors resulting in blue emission from nanobeads. The functionality on the surface of the nanobeads assisted in better analyte-sensor interaction through solid-state hydrogen bonding resulting in enhanced quenching of the respective chromophores when compared to non-functionalized nanobeads. The nanobead with surface amine functionality (PS-NH2) exhibited the highest sensing efficiency for both electron deficient and rich analytes. Device applicability was demonstrated by free standing film (thickness 0.07±0.01 mm) of PS-NH2 polymer which underwent fast exchange of analytes observable under UV lamp and reusability of film was checked upto 8 cycles.

Along this line, taking the idea from this currently developed methodology, amine functionalized, OPV incorporated PS nanobeads was applied to promptly detect the

presence of picric acid in water. The surface of nanobeads was decorated with -NH_2 group with the aim to enhance analyte-sensor interaction thereby improving selectivity of sensor. The outstanding selectivity of the sensor among the library of other nitro-organics was attributed to combined effect of energy transfer, inner filter effect and electron transfer. PA concentration in 100 % aqueous medium, as low as 58 nM could be efficiently detected by the sensor. Additionally, no interference from large number of cations and anions was observed making the sensor highly efficient for real water analysis. Also, its emission remained independent of external triggers; making it applicable over wide range of temperature and pH. For device based application free standing film was made. Thus rapid, efficient, sensitive sensor was developed from fluorescent dye containing polystyrene nanobeads for the selective detection of PA in water.

In the final working chapter, a tailor made water soluble glucuronic acid bearing polystyrene polymer (PS-DGlu) was synthesized which not only stabilized the PS nanobeads in the size range of 160-328 nm, but also surface functionalized these nanobeads with glucuronic acid together with successful covalent incorporation of OPV as fluorophore in styrene miniemulsion polymerization. To the best of our knowledge, it is the first report on glucuronic acid functionalized PS nanobeads (PSG-OPV-n) mentioned in the literature so far. The D-glucuronic acid functionalization rendered the polystyrene water soluble, thereby enabling it to function successfully as a polymeric surfactant in the miniemulsion polymerization which is also reported for the first time in literature. Additionally, the glucuronic acid on the PS nanobeads, served as interaction site for the selective detection of bilirubin *via* non-covalent interaction. Due to its excellent water dispersibility and good spectral overlap between emission of OPV and absorption of bilirubin; detection of free bilirubin was first targeted in water. Among series of PSG-OPV-n, PSG-OPV-5 was chosen because of its higher zeta potential, solid content, molecular weight and OPV incorporation in comparison to other nanobeads. Instant visual detection of bilirubin under UV lamp could be possible where blue emission of polymer turned bluish green instantly after bilirubin addition. This could be explained on the basis of energy transfer from OPV to bilirubin which is further supported by its emission spectra as well as CIE co-ordinate diagram. The interference from other biomolecules such as glucose, sucrose, metal ions, cholesterol *etc*. was checked. The limit of detection was found to be as low as 20 nM which is found to be in

clinically applicable range of <25 to >50 μmol/L. Finally, the polymer nanobeads were checked for real time monitoring of bilirubin in human blood serum where PSG-OPV-5 was found to be selective against its structural homologue *i.e.* biliverdin. Thus highly selective and sensitive visual sensor for bilirubin in human blood serum has been shown to be developed using combined strategy of FRET and hydrogen bonding interactions.

To conclude, we have established simple, easy and scalable approach for developing multicolor emitting, covalently stitched, surface functionalized fluorescent PS nanobeads with high quantum yield (both solid as well as solution state) for imaging and sensing based applications.

6.2 Future Perspective:

Thiol-Michael addition reactions have been explored half a century ago, however recently it has gained recognition in polymer sciences as "click" polyaddition reactions. Being included in "click" chemistry these has been known to be effective tool for wide areas of its usuage. One of them includes synthesis of thiol-ester particles to obtain functional materials. On the other hand, miniemulsion polymerization is known to produce the nanoparticles (NPs) in the size range of 50-500 nm. However, combining thiol-Michael reaction together with miniemulsion polymerization could result in the preparation of thiol-ester polymeric NPs. Additionally, using acrylate based fluorescent cross-linker would act as both fluorophore as well as substrate for thio-Michael reaction. Thus, fluorescent thiol-ester NPs can be obtained in single step without any further modification of tagging fluorescent moiety. Such a fluorescent thiol-ester NPs can be used as cell markers in imaging studies where their intracellular fate will be governed by fluorophores *i.e.* dye directive cellular imaging would be possible.

As shown in ***Scheme 6.1***, thiol-ester miniemulsion can be prepared using oligo (p-phenylene vinylene) (OPV) or/and perylenebisimide (PBI) based cross-linkers in butyl acetate which act as organic diluent. To this organic phase, hexadecane is to be added as hydrophobe. And this mixture then would be added to the aqueous phase containing tri(ethylene glycol)dithiol (TEGDT) and sodium dodecyl sulfate (surfactant). This would be then subjected to ultrasonication followed by addition of potassium persulfate (initiator) to start polymerization to obtain fluorescent OPV or PBI or OPV(PBI) based thiol-ester NPs.

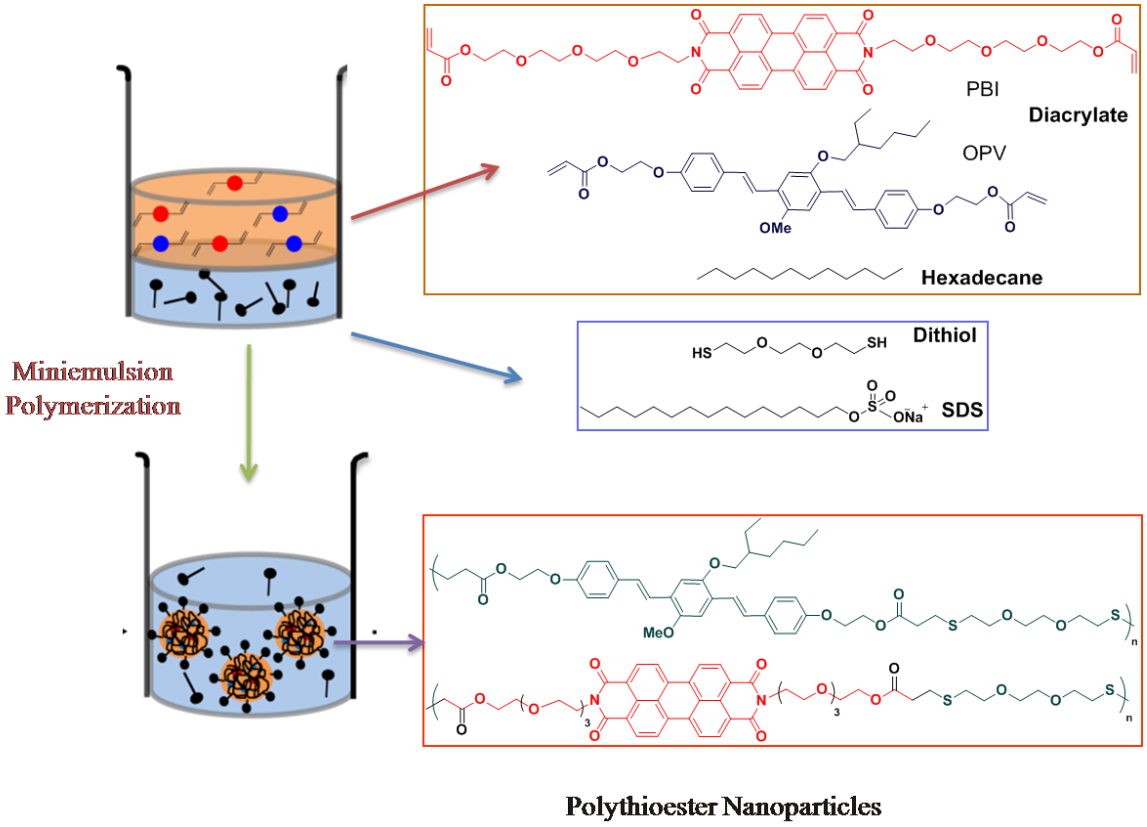

Scheme 6.1: Synthesis of polythioester NPs *via* thiol-Michael miniemulsion polymerization.

ABOUT THE AUTHOR

Ms. Sarabjot Kaur was born to Dr. Balbir Singh and Dr. Manmeet Kaur in 1989 at Bilaspur, Chattisgarh, India. She completed her schooling and higher secondary education from Ujjain Public School, Ujjain (2007). She finished her graduation from Govt. Holkar (Autonomous) Science College, Indore (2010) and moved to School of Chemical Sciences, DAVV University, Indore, Madhya Pradesh to pursue her M.Sc. in chemistry (2012). After qualifying all India CSIR-UGC National Eligibility Test (NET-JRF) examination with AIR 8th, she joined Polymer Science and Engineering (PSE) Division, CSIR-National Chemical Laboratory, Pune, India as Shyama Prasad Mukherjee (SPM) fellow to pursue her Ph.D. degree in January, 2014 under the supervision of Prof. Dr. Asha Syamakumari. She has received the research fellowship (JRF and SRF) from Council of Scientific and Industrial Research (CSIR), New Delhi, India since January, 2014 to carry out the Ph.D. thesis work.

Publications in International Journals and Patents

1. Makkad S.K., Asha S.K. π-Conjugated Chromophore Incorporated Polystyrene Nanobeads as Single Optical Agent for Three Channel Fluorescent Probe in Bioimaging Application. *ACS Biomater. Sci. Eng.* **2017**, *3*, 1788-1798.

2. Makkad S. K., Asha S. K. Surface Functionalized Fluorescent PS Nanobead based Visual Dual Distinct Sensor for the detection of Volatile Organic Compounds. *Anal. Chem.* **2018**, *90*, 7434-7441.

3. Makkad S. K., Asha S. K. Amine decorated Polystyrene Nanobeads incorporating π-Conjugated OPV Chromophore for Picric acid Sensing in Water. (*Manuscript Communicated*)

4. Makkad S. K., Asha S. K. Tailor-made Amphiphilic polymer as surfactant for Miniemulsion Polymerization of Oligo (p-phenylene vinylene) Incorporated Polystyrene Nanobeads for Water Based Visual Detection of Bilirubin. (*Manuscript Prepared*)

5. Makkad S. K., Asha S. K. Multicolour Emitting Polymer Beads And Applications Thereof. Patent number Appl. no –2994/DEL/2015.(Complete Specification filed)

6. Makkad S. K., Asha S. K. Glucuronic acid functionalized fluorescent polystyrene nanobeads for biosensing application. Patent Filed.

7. Makkad S. K., Asha S. K. Easy, Affordable And Efficient Turn On Detection of Fluoride and Arsenate ions in water by Carbon dots obtained from Tea. (NF no.- 2018-NF-0013).

8. Makkad S. K., Asha S. K. Functionalized Polystyrene Nanobeads And their Application in Sensing thereof. Patent number Appl. no – 201811006753.

9. Makkad S. K., Asha S. K. Fluorescent Polymer For Visual Solid State Sensing of Volatile Organic Compounds.

Participation in Conferences

1. **Sarabjot Kaur** and Asha S. K. "Multicolour emitting Polystyrene nanoparticles with л-conjugated dyes for Bioimaging in Cancer cells" **Macro 2017** Thrivananthapuram, Kerala.

2. **Sarabjot Kaur** and Asha S. K. "Multicolour emitting Polystyrene nanoparticles with л-conjugated dyes for Bioimaging in Cancer cells" **National Science Day** at CSIR-NCL, Pune, 2017.